EFFECT OF LASER TEXTURED DLC COATED AISI 52100 STEEL ON THE TRIBOLOGICAL BEHAVIOR FOR ENGINE APPLICATIONS

ARSLAN AHMED

FACULTY OF ENGINEERING
UNIVERSITY OF MALAYA
KUALA LUMPUR

2017

EFFECT OF LASER TEXTURED DLC COATED AISI 52100 STEEL ON THE TRIBOLOGICAL BEHAVIOR FOR ENGINE APPLICATIONS

ARSLAN AHMED

THESIS SUBMITTED IN FULFILMENT OF THE REQUIREMENTS FOR THE DEGREE OF DOCTOR OF PHILOSOPHY

FACULTY OF ENGINEERING
UNIVERSITY OF MALAYA
KUALA LUMPUR

2017

UNIVERSITY OF MALAYA

ORIGINAL LITERARY WORK DECLARATION

Name of Candidate: Arslan Ahmed

Matric No: KHA130089

Name of Degree: The Degree of Doctor of Philosophy

Title of Project Paper/Research Report/Dissertation/Thesis ("this Work"):

EFFECT OF LASER TEXTURED DLC COATED AISI 52100 STEEL ON THE TRIBOLOGICAL BEHAVIOR FOR ENGINE APPLICATIONS.

Field of Study: Energy

I do solemnly and sincerely declare that:

(1) I am the sole author/writer of this Work;
(2) This Work is original;
(3) Any use of any work in which copyright exists was done by way of fair dealing and for permitted purposes and any excerpt or extract from, or reference to or reproduction of any copyright work has been disclosed expressly and sufficiently and the title of the Work and its authorship have been acknowledged in this Work;
(4) I do not have any actual knowledge nor do I ought reasonably to know that the making of this work constitutes an infringement of any copyright work;
(5) I hereby assign all and every rights in the copyright to this Work to the University of Malaya ("UM"), who henceforth shall be owner of the copyright in this Work and that any reproduction or use in any form or by any means whatsoever is prohibited without the written consent of UM having been first had and obtained;
(6) I am fully aware that if in the course of making this Work I have infringed any copyright whether intentionally or otherwise, I may be subject to legal action or any other action as may be determined by UM.

Candidate's Signature Date:

Subscribed and solemnly declared before,

Witness's Signature Date:

Name:

Designation:

ABSTRACT

The demand of high efficiency from automotive sector has become increasingly higher in the last few decades because of global attention towards environmental destruction, fuel economy and depletion of resources. Some of the approaches adopted to improve efficiency comprise of component's weight reduction, increase in running temperature of engine and the use of Diamond-like Carbon (DLC) coatings. The demand for higher performance from industries has pushed DLC coatings performance to their limit. Alternative methods have to be devised to further improvement their properties. Laser surface texturing can be one of the most promising techniques for improving performance of DLC coatings. The tribological performance of laser surface texturing in steel/steel contact has been found to be dependent on the texture density, diameter and depth. The first part of this thesis evaluates the possibility of improvement in amorphous hydrogenated carbon (a-C:H) coating performance through indirect laser texturing; and also, the effect of variation in texture densities, diameters and depths under the boundary lubricated conditions. Texture density, diameter and depth were varied from 10-30 %, 50-150 μm and 6-30 μm, respectively. The second, third and fourth parts of this thesis evaluate the tribological performance of laser textured amorphous hydrogenated carbon (a-C:H) and tetrahedral amorphous carbon (ta-C) coatings under various temperatures (40 to 125 ºC). To date, most of the automotive lubricants are mineral oil based, which is toxic and non-biodegradable. Because of this reason, vegetable oils are being explored as alternative base oils. In this thesis, tribological behavior of palm oil based trimethylolpropane (TMP) ester was evaluated as an alternative to the conventional base oil with textured and un-textured DLC's. Comparison was conducted between textured/un-textured coatings at various temperatures in the presence of polyalphaolefin (PAO) and TMP ester lubricants. Coating hardness and Elastic modulus were investigated using nano-indentation. Adhesion of coating was analyzed using Rockwell-C indentation

test. The tribological testing was conducted using the ball on plate reciprocating test rig. After the tribological testing, wear track topology was analyzed using a scanning electron microscope (SEM) and an atomic force microscope (AFM). The chemical composition of the worn surface was investigated using an energy dispersive spectroscopy (EDX). Structural changes of DLC coatings were investigated using a micro raman spectroscopy. The results indicated that the optimum texture density, diameter and depth of 20 %, 100 μm and 6 μm respectively could enhance the tribological performance of textured amorphous hydrogenated carbon coating. Laser textured a-C:H and ta-C coatings showed a lower wear coefficient at all temperatures tested; however, coefficient of friction is higher at 80 ºC and 125 ºC. This can be related to the lower graphitization in the case of textured coatings. Textured and un-textured ta-C coating showed lower friction and wear compared to textured and un-textured a-C:H coating. The results also indicated that micro textured DLC's show a stable coefficient of friction with TMP ester even at 125 ºC.

.

ABSTRAK

Permintaan berkecekapan tinggi dari sektor automotif menjadi semakin meningkat dalam beberapa dekad yang lalu disebabkan perhatian global ke arah kemusnahan alam sekitar, ekonomi bahan api dan pengurangan sumber. Antara pendekatan yang diguna pakai untuk meningkatkan kecekapan terdiri daripada pengurangan komponen berat badan, peningkatan dalam suhu kendalian enjin dan penggunaan penyalutan Intan seperti Karbon (DLC). Permintaan untuk prestasi yang lebih tinggi daripada industri telah mendorong prestasi salutan DLC kepada had mereka. Kaedah alternatif perlu dilakukan untuk meningkatkan lagi ciri-ciri mereka. Penteksturan permukaan dengan laser boleh menjadi salah satu teknik yang paling berpotensi untuk meningkatkan prestasi salutan DLC. Prestasi tribologi penteksturan permukaan denganlaser dalam sentuhan keluli/keluli didapati bergantung kepada ketumpatan, diameter dan kedalaman tekstur. Bahagian pertama tesis ini menilai kemungkinan peningkatan prestasi lapisan karbon terhidrogen amorfus (a-C:H) melalui penteksturan laser tidak langsung; dan juga kesan variasi kepadatan, diameter dan kedalaman tekstur dibawah keadaan-keadaan pelinciran sempadan. Ketumpatan, diameter dan kedalaman tekstur juga telah diubah masing-masing dari 10-30 %, 50-150 μm dan 6-30 μm. Bahagian yang kedua, ketiga dan keempat dari tesis ini menilai prestasi tribologi tekstur laser karbon terhidrogen amorfus (a-C:H) dan lapisan karbon tetrahedron (ta-C) dibawah pelbagai suhu (40-125 °C). Kini, kebanyakan pelincir automotif adalah minyak mineral asas yang bertoksik dan tidak mesra alam. Oleh sebab itu, minyak sayuran sedang diterokai sebagai alternatif minyak asas. Dalam tesis ini, tingkah laku tribologi trimethylolpropane berasaskan minyak sawit (TMP) ester telah dinilai sebagai alternatif kepada minyak asas konvensional dengan DLC yang bertekstur dan tidak bertekstur. Perbandingan telah dijalankan antara lapisan bertekstur dan tidak bertekstur pada pelbagai suhu dengan kehadiran pelincir polyalphaolefin (PAO) dan ester TMP. Kekerasan salutan dan modulus Young telah

dikaji dengan menggunakan lekukan nano. Lekatan salutan telah dianalisis menggunakan ujian lekukan Rockwell-C. Ujian tribologi dijalankan dengan menggunakan alat uji salingan bola di atas plat. Selepas ujian tribologi, topologi trek hausan dianalisis menggunakan mikroskop elektron pengimbas (SEM) dan mikroskop daya atom (AFM). Komposisi kimia pada permukaan yang haus disiasat menggunakan spektroskopi serakan tenaga (EDX). Perubahan struktur lapisan DLC disiasat menggunakan raman spektroskopi mikron. Keputusan menunjukkan bahawa ketumpatan optimum, diameter dan kedalaman optimum bagi tekstur ialah 20 %, 100 μm dan 6 μm dapat meningkatkan prestasi tribologi lapisan bertekstur a-C:H. Lapisan tekstur laser dan karbon terhidrogen amorfus ta-C menunjukkan pekali haus yang lebih rendah pada semua suhu yang diuji, tetapi pekali geseran adalah lebih tinggi pada suhu 80 dan 125 °C. Ini boleh dikaitkan dengan penggrafitan yang lebih rendah dalam kes lapisan bertekstur. Lapisan bertekstur dan tidak bertekstur ta-C menunjukkan geseran dan kehausan yang lebih rendah berbanding lapisan bertekstur dan tidak bertekstur a-C:H. Keputusan ini juga menunjukkan bahawa salutan bertekstur mikro DLC dengan ester TMP mempunyai pekali geseran yang lebih stabil walaupun pada suhu 125 ºC .

ACKNOWLEDGEMENTS

First, I would like to thank ALLAH Almighty for all his blessings throughout my life. Secondly, I thank Prof. Dr. Masjuki Haji Hassan, Assoc. Prof. Dr. Abul Kalam, Dr. Mahendra Varman and Prof. Dr. Riaz A. Mufti for the guidance and financial support throughout this research work. I am also thankful to my father Sarfraz Hussain, my mother Riffat Shaheen and my wife Mahrukh Liaqat for their patience, support and kindness throughout this tedious task. Lastly, I thank my friends; M. M. Quazi, K.A.H. Al Mahmud, L.S.Khuong and M. H. Mosarof for the help they provided in experimentation and result interpretation.

TABLE OF CONTENTS

LIST OF FIGURES

LIST OF TABLES

LIST OF SYMBOLS AND ABBREVIATIONS

ZDDP	:	Zincdialkyldithiophosphate
DLC	:	Diamond like carbon
a-C:H	:	Amorphous hydrogenated carbon
a-C	:	Amorphous carbon
ta-C:H	:	Tetrahedral hydrogenated carbon
ta-C	:	Tetrahedral amorphous carbon
AFM	:	Atomic force microscopy
SEM	:	Scanning electron microscopy
EHL	:	Elastrohydrodynamic lubrication
LST	:	Laser surface texturing
HAZ	:	Heat affected zone
PACVD	:	Plasma-activated chemical vapor deposition
PIII-D	:	Plasma immersion ion implantation and deposition
DLC-Untex	:	Un-textured Diamond like carbon
V	:	Wear volume
k	:	Specific wear rate coefficient
F	:	Normal load
s	:	Total distance
PAO		Polyalphaolefin
PAO-C40	:	Un-textured amorphous hydrogenated carbon coated sample tested in PAO at 40 ºC
PAO-T40	:	Textured amorphous hydrogenated carbon coated sample tested in PAO at 40 ºC
PAO-C80	:	Un-textured amorphous hydrogenated carbon coated sample tested in PAO at 80 ºC
PAO-T80	:	Textured amorphous hydrogenated carbon coated sample tested in PAO at 80 ºC

PAO-C125	:	Un-textured amorphous hydrogenated carbon coated sample tested in PAO at 125 ºC
PAO-T125	:	Textured amorphous hydrogenated carbon coated sample tested in PAO at 125 ºC
TMP-C40	:	Un-textured amorphous hydrogenated carbon coated sample tested in TMP at 40 ºC
TMP-T40	:	Textured amorphous hydrogenated carbon coated sample tested in TMP at 40 ºC
TMP-C80	:	Un-textured amorphous hydrogenated carbon coated sample tested in TMP at 80 ºC
TMP-T80	:	Textured amorphous hydrogenated carbon coated sample tested in TMP at 80 ºC
TMP-C125	:	Un-textured amorphous hydrogenated carbon coated sample tested in TMP at 125 ºC
TMP-T125	:	Textured amorphous hydrogenated carbon coated sample tested in TMP at 125 ºC
ta-C.PAO-C40	:	Un-textured tetrahedral amorphous carbon coated sample tested in PAO at 40 ºC
ta-C.PAO-T40	:	Textured tetrahedral amorphous carbon coated sample tested in PAO at 40 ºC
ta-C.PAO-C80	:	Un-textured tetrahedral amorphous carbon coated sample tested in PAO at 80 ºC
ta-C.PAO-T80	:	Textured tetrahedral amorphous carbon coated sample tested in PAO at 80 ºC
ta-C.PAO-C125	:	Un-textured tetrahedral amorphous carbon coated sample tested in PAO at 125 ºC
ta-C.PAO-T125	:	Textured tetrahedral amorphous carbon coated sample tested in PAO at 125 ºC
ta-C.TMP-C40	:	Un-textured tetrahedral amorphous carbon coated sample tested in TMP at 40 ºC
ta-C.TMP-T40	:	Textured tetrahedral amorphous carbon coated sample tested in TMP at 40 ºC
ta-C.TMP-C80	:	Un-textured tetrahedral amorphous carbon coated sample tested in TMP at 80 ºC
ta-C.TMP-T80	:	Textured tetrahedral amorphous carbon coated sample tested in TMP at 80 ºC

ta-C.TMP-C125	:	Un-textured tetrahedral amorphous carbon coated sample tested in TMP at 125 ºC
ta-C.TMP-T125	:	Textured tetrahedral amorphous carbon coated sample tested in TMP at 125 ºC
s	:	Seconds

CHAPTER 1: INTRODUCTION

1.1 Overview

The automobile industry is rapidly changing. This change is due to pressures from several fronts like higher customer expectations, fuel economy, safety, increasing international competition and stringent emission regulation. That is why automobile industry has significantly advanced in the last decade. The changes are in terms of items like electronic engine controls (Willermet et al., 1990), changes in engine design and surface modifications such as coatings and texturing.

Energy losses in automotive have been studied extensively by many independent researchers and government-funded research communities. Studies reveal that main factors, which cause losses, are thermodynamics, emission of heat by cooling process to retain required operating environment, and loss of heat by exhaust gasses. Power train mechanical losses contribute as the second largest factor, which can be equally categorized as transmission losses and engine losses. According to study of European vehicles, approximately 12% of fuel power is effectively conveyed to wheels of vehicles (Tung & McMillan, 2004). Mechanical losses which are mainly frictional losses are 15 % (Tung & McMillan, 2004). Frictional losses in a light-duty vehicle are shown in Figure 1.1. Maximum frictional loss of 25 % is from piston assembly.

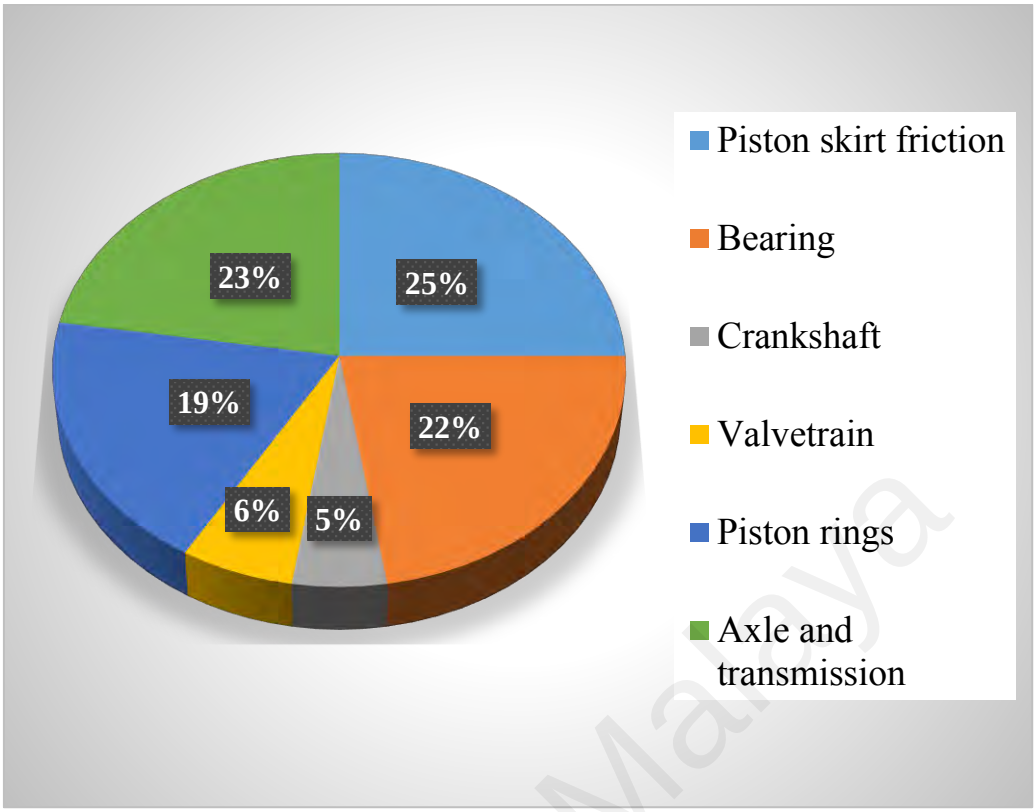

Figure 1.1: Energy losses due to friction in a light utility vehicle (Tung & McMillan, 2004)

In case of automotive engines, betterment of energy consumption is very crucial to improve efficiency and reduces an emission of CO_2. Following approaches are typically adopted to improve efficiency; component's weight reduction by using fewer massy materials and redesigning, increase in running temperature of the engine with less heat removal, and use of fewer viscous oils. These modifications challenge tougher atmosphere for engine components. For example, increase in the operational temperature or the use of less viscous oil cause reduction in film thickness and increase in wear rates. Problem of wear management is usually tackled by introducing additives for wear reduction in oils. However, a limitation has been observed, some additives such as zinc dialkyldithiophosphate (ZDDP) have the negative impact on the catalytic converter, with time effectiveness of the catalytic converter reduces and causes an increase in pollution. As strict rules for pollution controls have been introduced, an alternative approach for friction and wear reduction is highly required.

1.1.1 Laser surface texturing

Micro/Nano surfaced texturing is one such technique, which has been recognized in the past few years to reduce friction, wear, and enhance efficiency. In this technique, micro and nano surface, textures are created on one of the sliding or rolling surfaces. Figure 1.2 shows an example of micro textured steel surface. Contrary to the belief that smooth surfaces are required to reduce friction, in the process of surface texturing the roughness is increased in a particular manner to increase the tribological performance at the contact. Surface texturing has proven to reduce friction (Li et al., 2016; Qiu & Khonsari, 2011a; Shukla et al., 2016; Usman & Park, 2016; Wu et al., 2016), wear and seizer (Wang & Kato, 2003). Various applications like piston ring/cylinder liner (Tomanik, 2013), mechanical seals (Wang et al., 2014) and cutting tools (Ling et al., 2013) have been textured to improve their tribological performance.

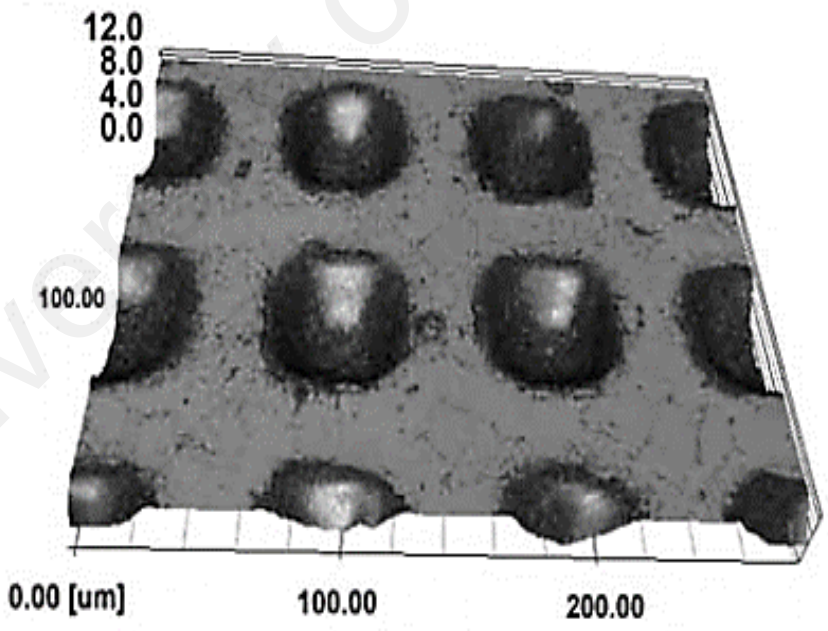

Figure 1.2: Laser micro textured surface (Nakano et al., 2007)

The major attention of tribology community came towards the surface texturing with the development of a theoretical model (Etsion, 2004). This model used Reynold's equation under Half–Sommerfeld boundary conditions for investigating performances of

mechanical seal faces. Afterwards, theoretical model was studied for Swift–Steiber cavitation boundary condition, and comparative studies with experimental analysis showed close match between the models (Etsion, 2004).

After that, many experimental and analytical studies have been conducted to achieve better tribological performances by understanding the effects of surface texturing at different operating conditions. Mechanisms by which micro/nano textures improve the tribological behavior mentioned throughout the literature are: increases the load carrying capacity through hydrodynamic effect, reduces third body abrasion by trapping wear particles, provides lubricant in a mixed lubrication regime by acting as a second lubrication source and reduces the rise in temperature at contact by keeping the lubricant at the interface (Oksanen et al., 2014).

Effect of surface texturing for improved tribological performances is determined by different parameters such as depth, density and diameter of textures. Tribological performance is also significantly influenced by the lubrication regime (boundary, mixed and hydrodynamic) and operational environment. Currently adopted surface texturing techniques are laser texturing, photo etching and CNC machining, which are able to provide dimensional precision up to few microns.

1.1.2 Diamond like carbon coating

Large number of amorphous carbon are described by term “Diamond- like carbon”, some of them contain 50% hydrogen content (a-C:H), while others have less than 1% hydrogen content (a-C). As diamond-like carbon films are comprised of sp^3 type C bonds, they possess appealing mechanical and chemical properties, which are quite similar to diamond. Generally, amorphous hydrogenated carbon (a-C:H) possesses less than 50% fraction of sp^3 bonds, while a-C films have fraction of sp^3 bonds up to 85% or more (Bewilogua & Hofmann, 2014).

Structurally amorphous hydrogenated carbon coatings are arbitrarily arranged covalent bonds in coordination of trigonal (sp^2) and hybridized tetragonal (sp^3), some of bonds having hydrogen at termination. Amorphous hydrogenated carbon can be described as a network of graphitic clusters connected into islands through sp^3 bonds (Austin, 2014). For particular deposition methods, hard carbon films are combination of graphite and diamond crystallites, whereas sputtered hard carbon films are generally like graphite. For that reason, tribological properties of DLC films are often described by tribological characteristics of diamond or graphite (Grill, 1993).

DLC coatings are increasingly being used to improve the tribological performance of engineering components like piston, piston ring, tappets, bearings, gears, seals, metal cutting and forming tools, magnetic hard disks and biomedical, due to their hardness and excellent mechanical and tribological properties (Kalin et al., 2008). However, the increasing demand from industry for higher performance has pushed DLC coating performance to its limits. In order to further enhance the coating performance, combining laser surface texturing with DLC coatings can be beneficial.

1.1.3 Environmentally friendly lubricants

Automotive engine lubricants are derived from petroleum-based and non-petroleum synthetic based chemicals. These days they are also derived from hydrocarbons, polyinternalolefins (PIO) and polyalphaolefins (PAO) (Rudnick & Shubkin, 1999; Zulkifli, 2014). Environmentally friendly lubricants based on agricultural feedstocks are gaining more and more attention in the last few decades because of the environmental concerns over the usage of mineral based lubricants (Mobarak et al., 2014). The impact of lubricant on the environment is at three stages; production, usage and disposal. Because of the environmental hazards of petroleum-based lubricants, European countries have

passed stringent regulations in order to enhance the use of environmentally acceptable lubricants (Kodali, 2002).

The interest in bio lubricants derived from vegetable resources is becoming higher. The reasons for such attention towards vegetable resource based bio lubricant is that they are biodegradable, less toxic and have good tribological properties. Several vegetable base oils often times possess better lubricating properties compared to conventional synthetic and mineral lubricants (Stachowiak & Batchelor, 2013). Ecologically friendly lubricants are being used in machinery employed in mining, agriculture and forests etc. (Kalin & Vižintin, 2006). Natural biodegradable oils show lower wear and friction; however, they possess poor thermal and oxidation stability. Various techniques are used in order to reduce the problems associated with natural biodegradable oils such as esterification, transesterification and mixing with various additives (Zulkifli et al., 2014).

Palm oil based Trimethylolpropane (TMP) ester is produced through transesterification of palm oil methyl ester. The process of transesterification improves the oxidative and thermal stability by removing the hydrogen molecule at the beta carbon position of the palm oil (Robiah et al., 2003). Researchers have been studying TMP esters as bio lubricants for use as engine lubricant and metal working fluids (Zulkifli et al., 2014).

1.2 Problem statement

In the last few years, few researchers have studied the effect of laser surface texturing on diamond-like carbon (DLC) coated surfaces. Those who have studied did not conduct thorough investigation of important texture parameters on the coating performance. Laser surface textures can be created by two methods; 1) indirect laser texturing in which DLC coating is deposited after laser texturing on the substrate, 2) direct laser texturing in which laser texturing is done on DLC deposited substrate. Mostly, researchers have used indirect

laser texturing for DLC coatings, in order to avoid coating damage. Ding et al. investigated the laser surface textured a-C carbon coating in water lubricated sliding conditions (Ding et al., 2010). The authors found that with textured a-C coating, the coefficient of friction is 15 % and wear rate is one order of magnitude lower than un-textured a-C. In another investigation, textured amorphous hydrogenated carbon coating in vacuum condition showed increased wear life compared to un-textured coating (Song et al., 2014). As it is well known that laser texture performance is dependent on texture parameters such as density, diameter and depth (Etsion, 2004). Mostly, research work has been conducted without changing the texture parameters and in oil-lubricated (Amanov et al., 2013), water lubricated (Ding et al., 2010) and vacuum (Song et al., 2014) sliding conditions. In this thesis, thorough investigation is conducted into the effect of laser texture density, diameter and depth on friction and wear characteristics of DLC coating.

The past research work on the indirect laser surface textured amorphous hydrogenated carbon coating has been conducted at room temperature (Pettersson & Jacobson, 2004; Song et al., 2014). The engine components that can be coated with DLC coating operated at higher temperatures (Al Mahmud et al., 2014), as DLC coating performance is influenced with temperature (Neville et al., 2007). Therefore, it is important to study the effect of temperature on the tribological performance of laser textured DLC coatings. Two important types of DLC coating which are also used for coating automotive components are used in this research work; namely amorphous hydrogenated carbon coating and tetrahedral amorphous carbon coating. Until now, no research work has been conducted in analyzing the temperature effect on these two textured DLC coatings.

Research work on replacing the conventional base oils such as PAO with vegetable-based bio lubricants is being gone on for several years. One such bio lubricant based on palm oil is TMP ester. Recent research work conducted by Zulkifli et al. on palm based

TMP showed that it has been potential to be used as a biodegradable base oil for automotive engine application (Zulkifli et al., 2014). The tribological research works on palm based TMP ester is conducted on steel/steel contacts. As automotive engine components are also DLC coated and in future, they will be micro textured, therefore, it is important to analyze the tribological performance of textured DLC coatings with palm based TMP ester.

1.3 Research objectives

In order to observe the behavior of various texture parameters with DLC coating and study the effect of engine operating temperature with textured coatings, the following objectives have been decided for this research work.

i. To investigate and understand the effect of indirect laser surface texture density, diameter and depth on the tribological performance of hydrogenated amorphous carbon coating.
ii. To investigate the effect of temperature on the tribological performance of indirect laser surface textured hydrogenated amorphous carbon coating in the presence of polyalphaolefin (PAO) and palm based trimethylolpropane (TMP) lubricants.
iii. To investigate the effect of temperature on the tribological performance of indirect laser surface textured tetrahedral amorphous carbon coating in the presence of polyalphaolefin (PAO) and palm based trimethylolpropane (TMP) lubricants.

1.4 Scopes of research

This thesis focusses on the effect of indirect laser micro surface texture on the tribological performance of hydrogenated and non-hydrogenated amorphous carbon films. Texture density, diameter and depth were varied from 10-30, 50-150 μm and 6-30

μm respectively; in order to investigate the tribological performance variation of amorphous hydrogenated carbon coating. These texture ranges were selected by extensive literature review. After understanding the tribological behavior variation with texture parameter's; one texture density, diameter and depth were selected for further investigations. As the variation in temperature causes the performance of DLC coatings to change, effect of change in temperature was investigated on indirect laser micro textured amorphous hydrogenated carbon and tetrahedral carbon coatings in the presence of PAO and palm based TMP lubricant. Temperature was varied from 40 to 125 ºC. This temperature range was selected in order to simulate the really automotive engine conditions. Comparisons were conducted between tribological performances of indirect laser textured and un-textured coatings, PAO lubricant and palm based TMP ester, and laser textured amorphous hydrogenated carbon and tetrahedral amorphous carbon coatings.

The tribological testing was conducted using the ball on plate reciprocating sliding test rig. The structural change of DLC coating before and after testing was evaluated using Raman's spectroscopy. Scanning electron microscope (SEM) and atomic force microscopy (AFM) was used to analyze the wear track surface morphology. Energy dispersive spectroscopy was used to analyze the elemental composition of the wear track.

1.5 Thesis organization

This thesis is divided into 5 chapters, which are as follows:

1. Chapter 1 gives an overview of the energy scenario. Lasers surface at texturing and diamond-like carbon coatings. The problems on which this research work will focus are described briefly.
2. Chapter 2 is the literature survey that includes the importance of laser surface texturing, various lubricant film regimes, mechanisms of

performance enhancement, techniques to fabricate textures, tribological behavior of textures, structure of diamond-like carbon coatings, tribological behavior of diamond-like carbon coatings and its variation with temperature, previous research work on laser textured diamond-like carbon coatings and tribological studies conducted using bio-lubricants.

3. Chapter 3 presents how the research work was conducted. It also explains the tribological and characterization techniques that have been used in present research work.
4. Chapter 4 presents the results and discussions on the variation of texture parameters and operating conditions on the tribological behavior of amorphous hydrogenated and tetrahedral carbon coating.
5. Chapter 5 presents the conclusions based upon the results obtained in the tribological investigation.

CHAPTER 2: LITERATURE REVIEW

2.1 Laser surface texturing and tribological effect of laser texture parameters

2.1.1 Surface texturing

Surface texturing is a relatively new technique but the concept of surface texturing to reduce friction at the contact is not new; it was introduced by Hamilton et al. in 1965 (Hamilton et al., 1966). Contrary to the belief that smooth surfaces are required to reduce friction, in surface texturing the roughness is increased in a specific manner to increase the tribological performance at the contact. Although surface texturing is not a new idea, however, use of lasers to create these textures is relatively new. Laser surface texturing has been proven both theoretically and experimentally to reduce friction and wear by several researchers for various applications such as; piston ring/cylinder assembly (Kligerman et al ., 2005; Ryk & Etsion, 2006), mechanical seals (Wang et al., 2014; Wang & Kato, 2003), and bearings (Marian et al., 2011; Qiu et al., 2014).

Concept of surface texturing for better tribological performances is not novel. Dimples are introduced on the surface of golf balls to achieve better aerodynamic properties. Surface textures are formed by making dimples or protrusions. However, dimple configuration is more common, particularly in boundary and elastrohydrodynamic lubrication regime. In the case of protruded surface texturing, contact area between protruded shape and surface is greater than dimple surface, which causes an increase in contact pressures and results in greater wear rates. Compared to protruded surface texturing, less clearance among bearing components can be achieved in dimple surface texturing, in boundary and elastrohydrodynamic lubrication regimes. By introducing micro dimples, multiple benefits can be achieved by surface texturing. Some key advantages include; (1) increase in lubricant retentiveness (Hsu et al., 2014), (2) reduction in further surface damage by collecting wear debris and other foreign material (Hsu et al., 2014), (3) increase in hydrodynamic pressure under full hydrodynamic lubrication

(Etsion, 2004) and (4) reduction in adhesion due to smaller contact area (Enomoto & Sugihara, 2010).

2.1.2 Surface texture parameters

The geometric texture parameters that affect the performance of textured surface are as follows: depth, diameter, density or number of dimples per unit area, aspect ratio or depth to the diameter ratio (Hsu et al., 2014). Most of the theoretical and experimental work to investigate the effects of texturing parameters have been conducted for the case of conformal mechanical contacts.

2.1.3 Lubrication

Lubrication can be defined as a technique to control friction and wear by introducing a solid, liquid or gaseous material between two interacting surfaces, which are in relative motion under some load. To meet the complexities of this topic, more simplified approaches are required to study the lubrication contacts. Three main lubrication regimes have been distinguished namely, hydrodynamic/full fluid, elastrohydrodynamic and boundary.

2.1.3.1 Fluid film lubrication

If the layer of the lubricant is so thick that the bodies cannot come into contact, such as type is called fluid film lubrication (as shown in Figure 2.1 a). This type of lubrication is considered as ideal for reducing friction and wearing of bodies in contact. The contact behavior is mainly governed by the physical properties of the lubricant like viscosity, and due to the viscous shearing of the lubricant, the characteristics of the friction arise (Taylor, 1993).

2.1.3.2 Elastrohydrodynamic lubrication

Elastrohydrodynamic lubrication (EHL) refers to the situation, when hydrodynamic pressure is insufficient to provide full support to load, and surfaces come in contact with each other (Dowson & Higginson, 1959). Contact takes place at the hills of surfaces and peaks (as shown in Figure 2.1 b). The extend of these contacts is related to many factors such as surface roughness, fluid film pressure, hardness of interacting bodies and applied normal load. Under contacting conditions, elastic deformation is produced in many asperities and therefore, both thinner fluid film lift and asperity's strength balances the normal pressure (Stachowiak & Batchelor, 2013).

2.1.3.3 Boundary lubrication

If the lubricant film thickness is so thin that the surfaces of the bodies are in contact over an area that is similar to the area formed during the dry contact, such as type of lubrication is called boundary lubrication (as shown in Figure 2.1 c). The friction characteristics are mostly determined by the in contact solid properties (Hironaka, 1984). A boundary film is often produced due to activation of chemical reactions between lubricant molecules and asperity surface, in terms of wear it can be either advantageous (anti-wear, protective) or disadvantageous (pro-wear) (Pinkus & Sternlicht, 1961). A complete and comprehensive theory of boundary lubrication has not been presented yet, involved chemical and physical mechanisms are still not understood, and however, some models are available on contact mechanism and lubrication geometry. The determination of contact lubrication type can be conducted using Dowson and Higginson formula. This is discussed in detail in section 3.6.

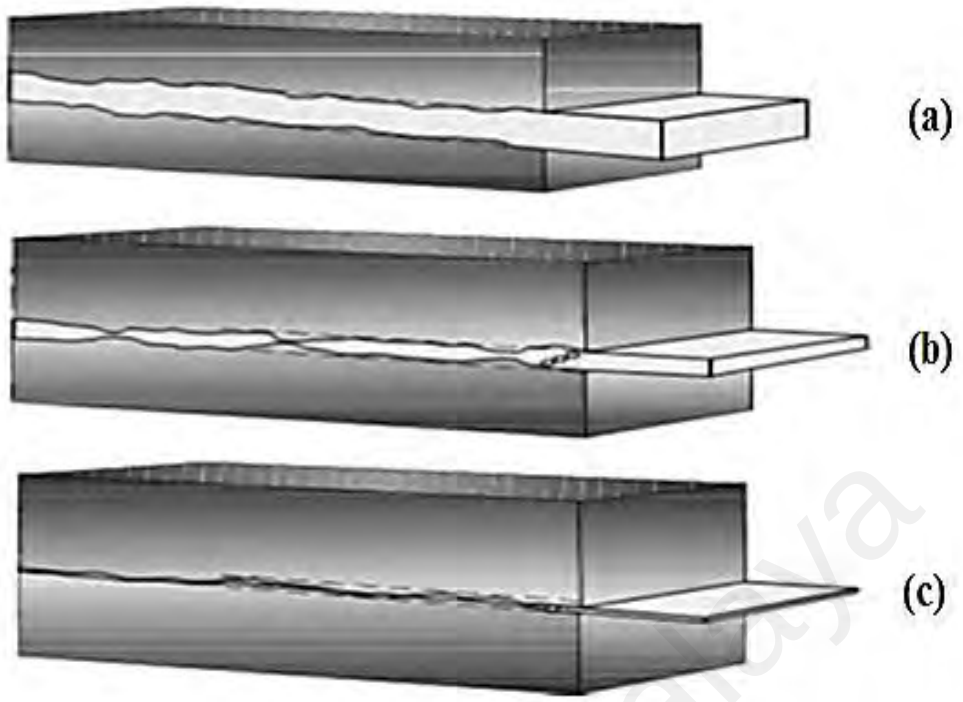

Figure 2.1: Different lubrication regime (a) Full film, (b) EHL and (c) Boundary

2.1.4 Mechanisms of tribological improvement

In the case of starved lubrication, micro textures act as micro reservoirs of lubricant (Amanov et al., 2013; Kovalchenko et al., 2011). In case of full or mixed lubrication regime, they increase load carrying capacity by serving as micro hydrodynamic bearings (Amanov et al., 2013; Ramesh et al., 2013; Tomanik, 2013). The increase in hydrodynamic pressure at different load-speed conditions is the most important benefit of micro-textures (Brizmer et al., 2003; Wang et al., 2003). Micro textures also remove debris from the contact and decrease wear (Amanov et al., 2013; Kovalchenko et al., 2011; Li et al., 2010; Vandoni et al., 2012; Zhan & Yang, 2012). Lubricant providing ability of textures is present in full, mixed and boundary lubricant. The detailed description of these mechanisms is discussed below.

2.1.4.1 Micro-hydrodynamic bearing

Micro textures act as "micro hydrodynamic bearings" in mixed and hydrodynamic lubrication regimes. As in the case of a journal bearing, due to the motion of surfaces, the lubricant is pushed into a converging wedge, and at high speed pressure is developed which provides load carrying support. This "wedge" action can be observed in the converging regions of pores. At the converging portion of each micro pore (dimple), this wedging effect takes place and thus a lifting force is present. The maximum hydrodynamic pressure can be found at this converging section. This provides hydrodynamic lift at the contact.

Micro surface texturing can also produce hydrodynamic effect between parallel sliding bodies. The mechanism can be understood by considering a one-dimensional model of single asperity in the presence of fluid film (as shown in Figure 2.2). Due to the motion of the slider with velocity (V), anti-symmetric pressure profile was generated around the micro asperity as shown in the Figure 2.2 (a). For incompressible fluids, pressure decreases in the diverging region and increases in converging regions. Since the pressure profile is anti-symmetric, therefore the load support will be zero as is evident by the area under the curve, thus there will be no separating force. This contradiction to the experimental findings can be explained by cavitation phenomena. In the cavitating negative pressure region, isobaric conditions exist. The pressure in this region cannot be lower than cavity pressure, which is the pressure at which gas bubbles are emanated by the lubricant or fluid vapor pressure. Consequently, the net area under the curve as shown in Figure 2.2 (b) is positive; and thus, creating hydrodynamic effect. The combined effect of all the micro dimples can increase the load carrying capacity of the textured surfaces (Etsion & Burstein, 1996; Hamilton et al., 1966).

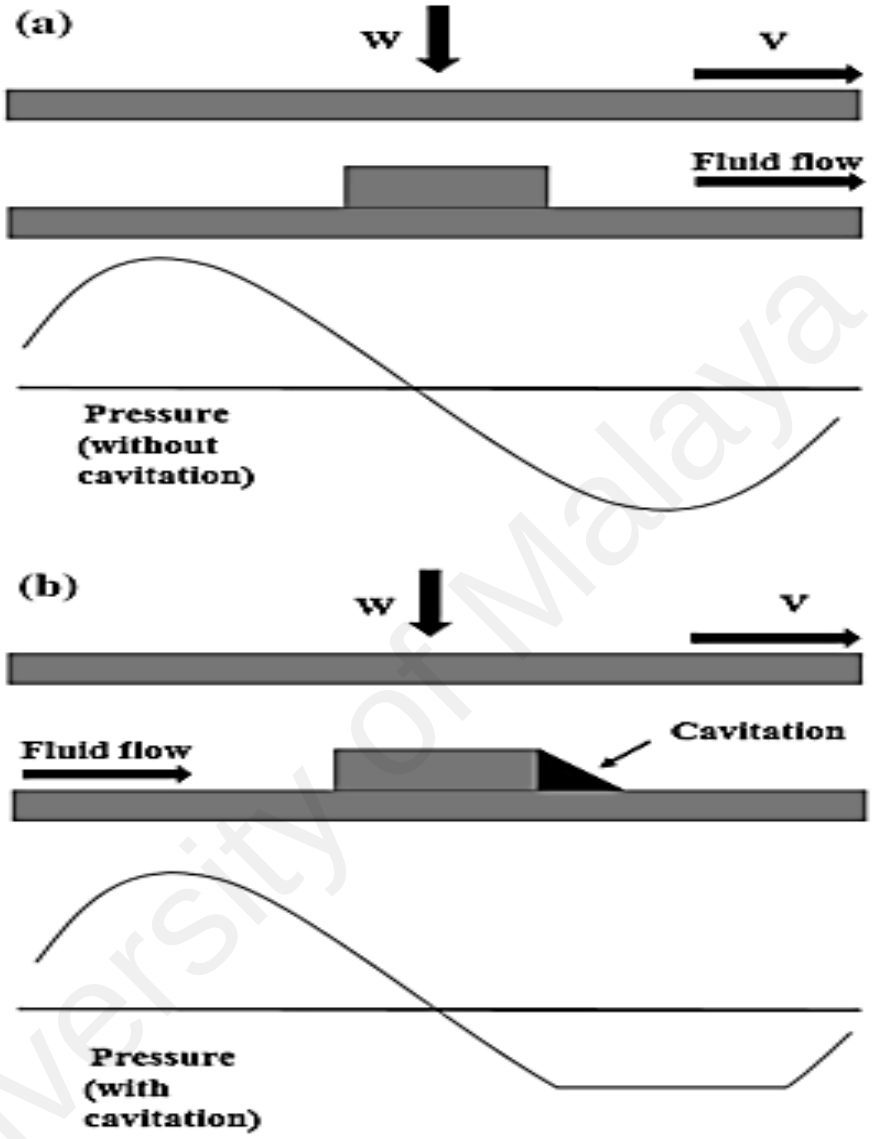

Figure 2.2: Hydrodynamic pressure profiles by a micro asperity (a) without cavitation (b) with cavitation

2.1.4.2 Lubricant reservoir

Surface textures can act as lubricant reservoirs or secondary lubricant source (Amanov et al., 2013; Kovalchenko et al., 2011; Vandoni et al., 2012; Wang & Kato, 2003). During sliding the lubricant will be drawn up to permeate the surfaces (as shown in Figure 2.3). This phenomenon can reduce friction, wear and seizer.

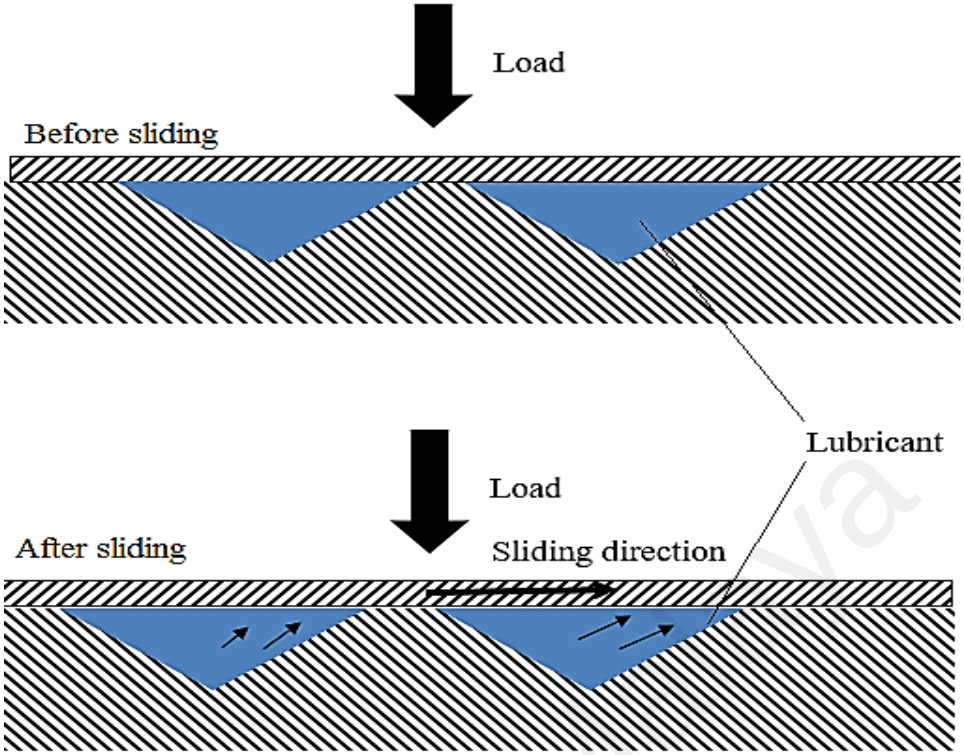

Figure 2.3: Secondary lubrication mechanism (Wang & Kato, 2003)

2.1.4.3 Wear debris storage ability

The most common wear mechanisms in the generation of wear debris are mentioned below.

I. Abrasive wear: In abrasive wear, material is removed due to hard abrasive phases. Both 2nd body and 3rd body abrasion is generated according to the morphology of abrasive phases. In the case of complex morphologies, 2nd body abrasion is realized, while 3rd body abrasion is possible for simple morphologies (Rabinowicz, 1995).

II. Adhesive wear: adhesive wear takes place when a surface slides against another surface, causing shards of one surface to stick to the other surface and eventually pull out from the original surface. Strong adhesive forces, which come into existence when atoms come into close contact with one another, mainly cause adhesive wear (Rabinowicz, 1995). At interfacial

pressure or high temperature, a strong bond can be formed between debris and sliding surfaces.

Micro surface textures can reduce wear by capturing wear debris present between the contacting surfaces as shown by an example in Figure 2.4. As shown in Figure 2.4 (a), the wear debris present between the sliding ball and un-textured stationary plate causes high contact stress, which increases friction and wear; while the textures in Figure 2.4 (b) trapped the wear particles from the tribological interface. This way textures can help in removing the unwanted wear debris from surface in dry as well as lubricated conditions (Amanov et al., 2013; Amanov et al., 2013; Ding et al., 2011; Hu & Ding, 2012; Kovalchenko et al., 2011; Li et al., 2010; Schreck & Gahr, 2005; Shum et al., 2013; Vandoni et al., 2012; Zhan & Yang, 2012). Ding et al. found that textures can help in capturing wear particles to lower the effect of fatigue wear mechanisms (Ding et al., 2011).

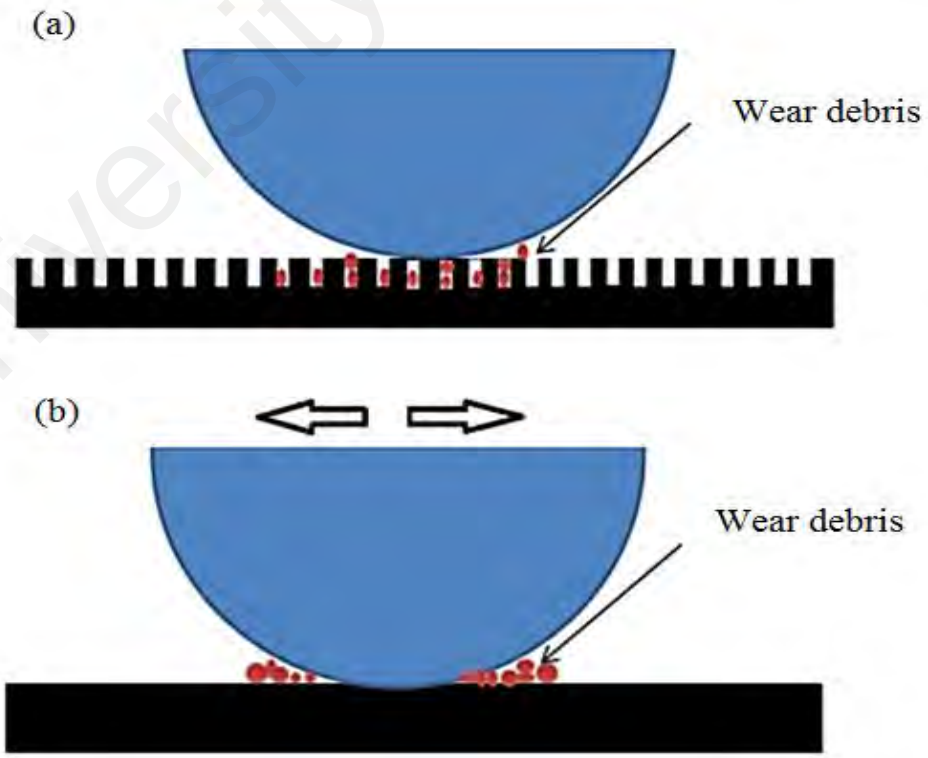

Figure 2.4: Wear particle storage ability (a) textured surface (b) un-textured surface

2.1.5 Fabrication techniques of surface textures

Surface textures can be fabricated by using different techniques, which includes photolithography and etching (Lu & Khonsari, 2007; Yan et al., 2010), shot blasting (Nakano et al., 2007), CNC micro machining and laser surface texturing (Etsion, 2005; Wakuda et al., 2003), electric discharge machining (Uhlmann & Doll, 2005), CNC ultrasonic machining (Churi, 2010), focused ion beam machining (Tseng, 2004), vibro-mechanical texturing (Greco et al., 2009), micro grinding (Masuzawa, 2000; Nguyen & Butler, 2005), micro casting (Cannon & King, 2009) and CNC drilling (Roy et al., 2014). Among these, laser surface texturing has been found to have several advantages like high spatial resolution, non-contact, processing flexibility (Gao et al., 2011; Kuršelis et al., 2012) and creation of well-defined patterns with accuracy (Kuršelis et al., 2012).

2.1.6 Laser surface texturing

LST uses high energy pulses to ablate material by rapid melting and vaporizing. Laser ablation can be defined as the removal of material by direct absorption of laser energy. The start of ablation occurs above the threshold fluence. This threshold depends on the micro-structure, morphology, absorption mechanism, material properties and defects, and laser properties, such as wavelength and pulse duration (Dong et al., 2011). Laser ablation can be divided into the following two categories depending upon the interaction of laser energy of the material: pyrolytic and photolytic processes (Meijer, 2004). In the pyrolytic process, laser energy is absorbed by the material and then transferred into heat, which causes an increase in temperature. As a result, the material melts and evaporates from the surface. In the photolytic process, the photon energy absorbed induces chemical reactions to overcome the chemical binding energy of molecules; this is also called “cold ablation” (Meijer, 2004).

The way in which the laser beam is projected to the substrate determines the texture accuracy. The methods used in this regard are as follows:

1. A fast-revolving perforated disk is used to practically chop an unfocused laser beam in order to create patterns; however, this technique is generally avoided due to its limited resolution, flexibility, and accuracy (Coblas et al., 2009).
2. A patterned mask is used to split the laser beam projected onto the sample. This technique is flexible, fast, accurate, and allows the creation of various shaped micro-features. The production cost of the mask is the main drawback to this technique.
3. A laser beam can be projected by the use of a galvanometric scanner and a computer numerical control (CNC) system, which maneuvers the beam over the sample (Vincent et al., 2008). This technique is extremely accurate due to the very short pulses (duration of pulse fs and ns). The main drawback is that this is a time-consuming process, as each texture is machined separately (Coblas et al., 2014).

Some of the important issues regarding LST are: the heat affected zone (HAZ), surface defects (burrs or bulges), and the formation of periodical surface structures. Laser beam heat can affect the substrate and cause variations in its metallurgical properties. For example, for a pore area ratio of 14–22.5%, the area ratio of the HAZ reaches 50–100%, while HAZ diameter varies from 300–450 μm around the dimples for SiC rings (Wang et al., 2001). Similarly, dimensions of the thermally affected area surrounding the hole with a diameter of 10 μm produced using Nd:YAG pulses are less than 10% of the texture diameter (Kononenko et al., 2000). Surface defects (burrs or bulges) are another main problem. Frictional behavior is affected by bulges, as they have significant height, i.e.

3.5–4.5 μm (Amanov et al., 2012). This volume of material is commonly removed from the textured surface by grinding, surface polishing, and lapping. Another issue that has been observed in ns and fs laser-textured substrate is the formation of periodical surface structures, such as, ripples that cause an increase in the roughness on the surface. This is recognized as surface acoustic waves or an interference phenomenon (Coblas et al., 2014). Researchers have used this issue of LST to their advantage to create periodical structures for controlling hydrophobicity of metals (Römer et al., 2009) and friction and wear properties of cutting tools (Sugihara & Enomoto, 2009).

The advantages of laser surface texturing systems are high precision, dimensional accuracy, and no contact force required. The disadvantages include low machining speed, high cost of equipment, and difficult maintenance and adjustment.

2.1.7 Applications of micro surface texturing

Different types of surface texturing have been used to obtain the tribological performance enhancement. These include connected textures like different patterns of grooves and disconnected independent textures like micro dimples. In the case of connected textures, the parameters that affect the tribological performance of contacting surfaces are pitch of textures, width of texture, depth of texture etc. In the case of disconnected independent textures like micro dimples. The relevant parameters are dimple depth, dimple diameter, dimple depth to diameter ratio and dimple density, etc. Several researchers have contributed to the effects of the above-mentioned parameters for the tribological performance piston ring/cylinder assembly (Abboud et al., 2007; Bolander & Sadeghi, 2006; Caciu et al., 2008; Checo et al., 2014; Etsion et al., 2006; Etsion & Sher, 2009; Gadeschi et al., 2012; Kligerman et al., 2005; Ryk & Etsion, 2006; Ryk et al., 2005; Tomanik, 2013; Wos & Michalski, 2011; Zhan & Yang, 2012), mechanical seals (Chen et al., 2012; Feldman et al., 2006; Feldman et al., 2006;

Kligerman & Shinkarenko, 2011; Qiu and Khonsari 2011a, 2011b; Wan & Xiong, 2008; Wang et al., 2014; Wang et al., 2006), bearings (Brizmer et al., 2003; Lu & Khonsari, 2007; Marian et al., 2011; Qiu et al., 2014; Qiu et al., 2012; Qiu et al. 2013; Rahmani, et al., 2010), cutting tools (Deng et al., 2013; Enomoto & Sugihara, 2010, 2011; Enomoto et al., 2012; Jianxin et al., 2012; Kawasegi et al., 2009; Koshy & Tovey, 2011; Lei et al., 2009; Ling et al., 2013; Neves et al., 2006; Obikawa et al., 2011; Sugihara & Enomoto, 2009, 2012, 2013; Wu et al., 2012; Xie et al., 2012; Xing et al., 2014; Ze et al., 2012; Zhao et al., 2010) and hydraulic motors (Pettersson & Jacobson, 2007).

2.1.7.1 Piston ring/cylinder assembly

As the piston ring/cylinder assembly accounts for 25 % of total mechanical loss in engine, several researchers are working on reducing this power loss. Different types of surface treatments for piston/cylinder assembly used to reduce the friction and wear.

Reduction of frictional losses by changing the surface roughness in the form of surface textures has been reported in case of piston rings by several researchers (Abboud et al., 2007; Bolander & Sadeghi, 2006; Caciu et al., 2008; Checo et al., 2014; Etsion et al., 2006; Etsion & Sher, 2009; Gadeschi et al., 2012; Kligerman et al., 2005; Ronen et al., 2001; Ryk & Etsion, 2006; Ryk et al., 2002; Ryk et al., 2005; Tomanik, 2013; Usman & Park, 2016; Wos & Michalski, 2011; Zhan & Yang, 2012). Mainly the textures created in case of piston rings are in the form of the array of uniform depressions or pored with similar geometrical dimensions to one another, these are usually called dimples as shown in Figure 2.5.

Lasers have been mainly used by researchers to create these dimples on piston rings. By creating dimples on the piston ring surface, researchers have found the reduction in friction at the piston ring/cylinder contact in the range of 20-50 % in comparison to un-textured piston rings (Kligerman et al., 2005; Ryk & Etsion, 2006; Ryk et al., 2005).

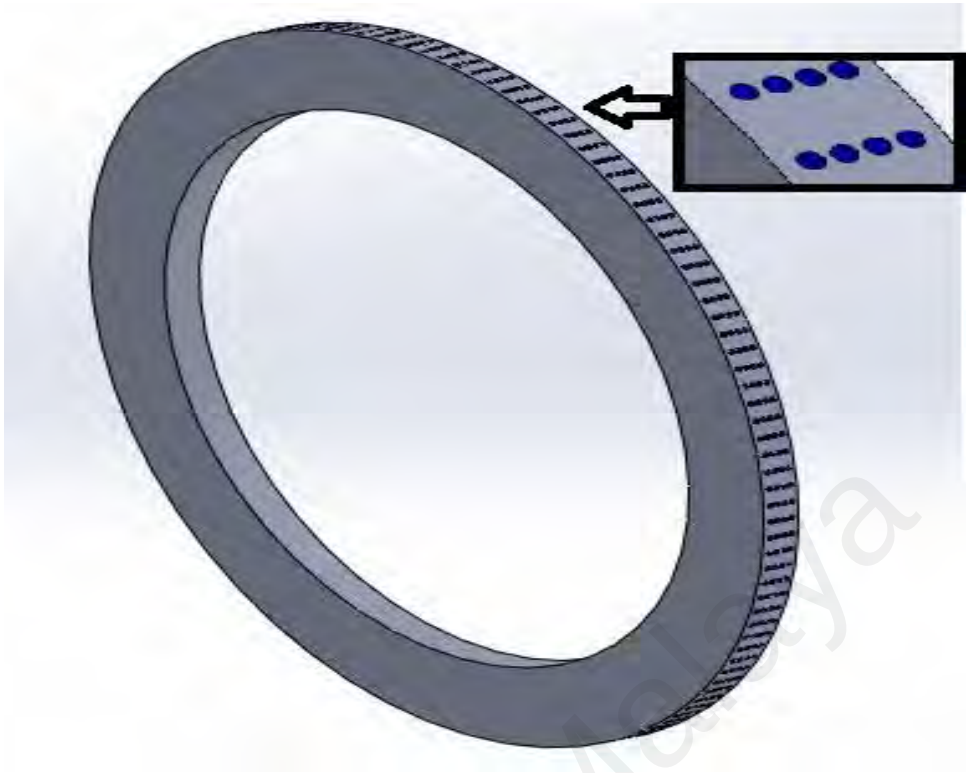

Figure 2.5: Surface textured piston ring

2.1.7.2 Cutting tools

Surface texturing to improve the cutting performance of tools is a recent endeavor. Figure 2.6 shows laser surface textured tool with rectangular textures. These textures improve the cutting performance by enhancing lubricant availability at the contact point, reducing the tool-chip contact area, and trapping wear debris (Chang et al., 2011; Silva, et al., 2013; Deng et al., 2013; Enomoto & Sugihara, 2010, 2011; Enomoto et al., 2012; Jianxin et al., 2012; Kawasegi et al., 2009; Koshy & Tovey, 2011; Lei et al., 2009; Ling et al., 2013; Obikawa et al., 2011; Sugihara & Enomoto, 2009, 2013; Wu et al., 2012; Xie et al., 2012; Xing et al., 2012; Ze et al., 2012). The benefits of surface textures have been observed in both wet and dry cutting of aluminum alloys, titanium alloys, and mild and hardened steel. To date, this technique has been successfully used in drilling, milling, and turning operations.

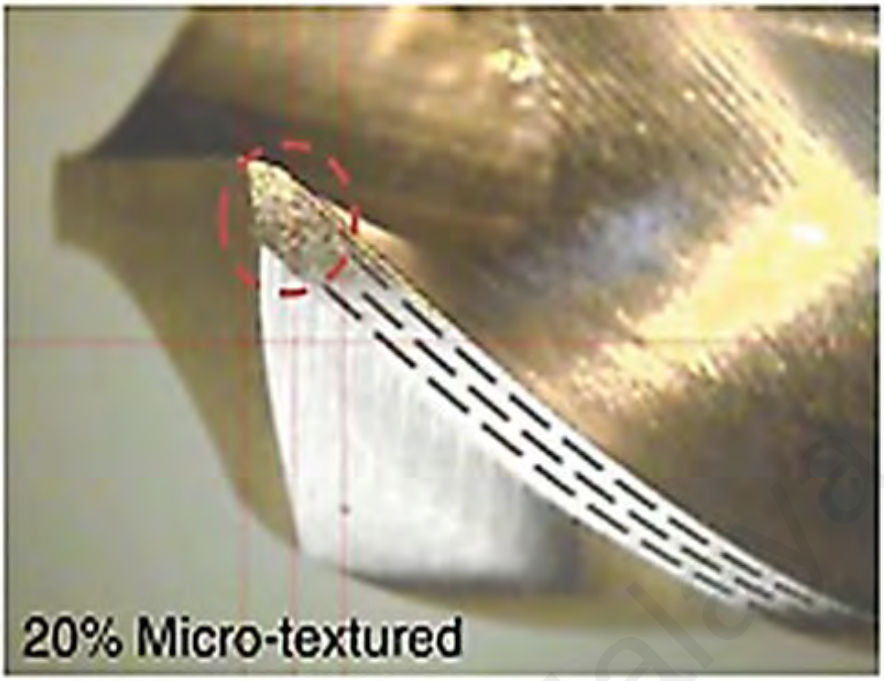

Figure 2.6: Micro-textured drill bit (Ling et al., 2013)

2.1.7.3 Mechanical seals

Surface texturing has been recognized to improve the tribological performance of mechanical seals. Through the surface texturing on mechanical seals researchers have found the reduction in friction and wear, enhanced ant seizer ability, reduction in leakage, increase in fluid film thickness and increased load carrying ability (Chen et al., 2012; Feldman et al., 2006; Feldman et al., 2006; Kligerman & Etsion, 2001; Kligerman & Shinkarenko, 2011; Qiu & Khonsari, 2011a, 2011b; So & Chen, 2005; Wan & Xiong, 2008; Wang et al., 2014; Wang et al., 2006; Wang & Hsu, 2004).

2.1.8 Effect of surface texture parameters on friction and wear characteristics

2.1.8.1 Dimple depth and diameter

Surface texture performance is dependent on its parameters. If the contact has low lubricant availability, then the deep dimples detrimental effects were observed in terms of friction and wear (Bolander & Sadeghi, 2006; Ryk et al., 2002). When there is low lubricant availability at the contact, deep dimples become micro traps of lubricant. The

lubricant starts to get concentrated around the dimples compared to un-textured contact where it is reasonable to assume that it is evenly distributed over the contact. Due to this, the hydrodynamic effect of the "micro-hydrodynamic bearing" reduces to only small area and the clearance between the surfaces reduces, thus increasing friction and wear in comparison to un-textured surfaces. This phenomenon can occur earlier if the viscosity of the lubricant is high due to low fluidity of lubricant (Ryk et al., 2002).

Wang et al. (Wang & Kato, 2003) evaluated the anti-seizer ability of a textured silicon carbide (SiC) specimens in water lubrication using critical load as the performance index. The authors found that due to an increase in dimple depth in the range (2-13.3 um), the critical load increases too (Wang & Kato, 2003). This result was in contradiction with the group's previous work (Wang et al., 2003). X. Wang et al. found that an increase in dimple depth is not beneficial for load carrying capacity. They suggested an optimum range of 2-7 μm depth (90 um diameter) in case of steel rings sliding in oil and 0.015 depth to the diameter ratio in case of SiC bearing working in water (Wang et al., 2003). Wang et al. recommended that this dissimilarity might be due to the reason that tribochemical reaction of SiC in water is the more important factor than hydrodynamic lubrication (Wang & Kato, 2003). Deep dimples can store more water for tribochemical reaction as a result they increase the anti-seizer ability. In case of oil lubrication, deep dimples do not enhance the hydrodynamic effect.

Tomanik et al. also investigated various dimple depth and diameter using an one-dimensional computer program (Tomanik, 2013). Dimple's depth has been varied from 1 to 10 μm and diameter from 10 to 100 μm. They found that higher hydrodynamic pressure can be obtained by using dimple depth of 1 μm and diameter of 10 μm in comparison to 5 μm depths and 25 μm diameters.

In the case of non-conformal contacts and under elastrohydrodynamic lubrication regime (EHL), the dimple depth is found to have effect on the local change in the lubricant film thickness (Mourier et al., 2010). Mourier et al. investigated depth effect using EHL iris Tribometer (Mourier et al., 2010). They found that if the depth of the dimple is high, the lubricant passing through the dimple has the lower pressure level, and thus, the viscosity of the lubricant will drop and this prevents the lubricant to separate the surfaces. They observed that 300 nm dimple depth increased the film thickness.

In mechanical components, i.e., gears, cams, reduction in friction due to surface texturing in line contacts has been a topic of great interest for many researchers. Hao et al. investigated the friction and wear performance under non-conformal line contacts. They observed reduction in wear marks or debris on line contact slider bearing (contact between flat disc and cylinder) which is used in cam mechanism (Hao et al., 2014).

Deciding the right dimple diameter for non-conformal contact is a bit difficult compared to conformal contacts. It was stated that surface texturing is not helpful in friction reduction when the diameter of dimple is equal to or smaller than Hertz contact width, while the coefficient of friction reduces significantly when dimple diameter is greater than Hertz contact width (Wakuda et al., 2003). Xiaolei et al observed different results in pin on disk tests, they observed that if the dimple diameter is equivalent or smaller than the contact width, the friction reduction can be observed (Xiaolei et al., 2009). Further investigation is needed in order to clarify these contradictions.

Recently, Wang et al. investigated two-phase mechanical seals with laser surface textured end faces using transparent rotating rings so that the distribution of liquid/vapour region can be observed using a camera (Wang et al., 2014). The results showed that the surface textured rings with small dimples (diameter 1000 μm and depth of 10 μm) have lower mean temperature at various speeds than flat ring and textured rings with larger

dimples (diameter 2000 μm and depth of 40 μm). The authors also found that if the dimple depth and diameter are both high, the vaporization is higher than plain end face because larger the diameter of dimples larger will be the cavitation, which will abruptly increase friction torque (Wang et al., 2014).

2.1.8.2 Dimple density

Dimple density can be defined as number of dimples per unit area. Kligerman et al. through several numerical simulations found that the area density of the dimples should be largest in order to get higher friction reduction in the case of conformal contacts. The range of dimple density chosen by researchers varies between 5-66 % (Kligerman et al., 2005).

As surface texturing increases, fluid film thickness and creates additional hydrodynamic pressure between interacting surfaces, subsequently it causes significant reduction in friction. A lot of research has been conducted with an objective to minimize the friction by surface texturing, which is equally effective in terms of wear and increases the operational life of materials. Siripuram & Stephens observed that cross-sectional area of dimples can affect friction (Siripuram & Stephens, 2004). Tonder analytically studied effects of micro dimples on pivoted bearings, and observed a significant reduction in friction under particular conditions due to increased film thickness and load capacity (Tønder, 2010). Findings of Tonder about the effects of dimple density on friction were verified experimentally and analytically in several studies (Tanu et al., 2010; Yan et al., 2010). For example, Wang et al. worked on thrust bearings with circularly textured micro dimples under water based lubrication condition, and found that friction of a coefficient reduces tremendously, and this effect becomes more significant with an increase in density and size (Wang et al., 2003).

In the case of non-conformal contact, Wakuda et al. used steel cylinders, which were sliding on the ceramic plate (Wakuda et al., 2003). They varied the texture density from 7.5 to 30 %. The lowest coefficient of friction at various sliding speeds was shown by 7.5 % density (Figure 2.7). As the density was increased to 30 % coefficient of friction also increases. Qui et al. used universal tribometer to simulate conformal contact (Qiu & Khonsari, 2011a). They varied dimple density from 15 to 58.6 %. Figure 2.8 shows that a highest dimple density of 58 % showed the lower coefficient of friction compared to less density at 4.5 N and 18 N load. The highest coefficient of friction was shown by un-textured samples. For conformal contacts, mostly authors found higher dimple density to be beneficial in reduction of coefficient of friction, whereas for non-conformal lower density has been found useful.

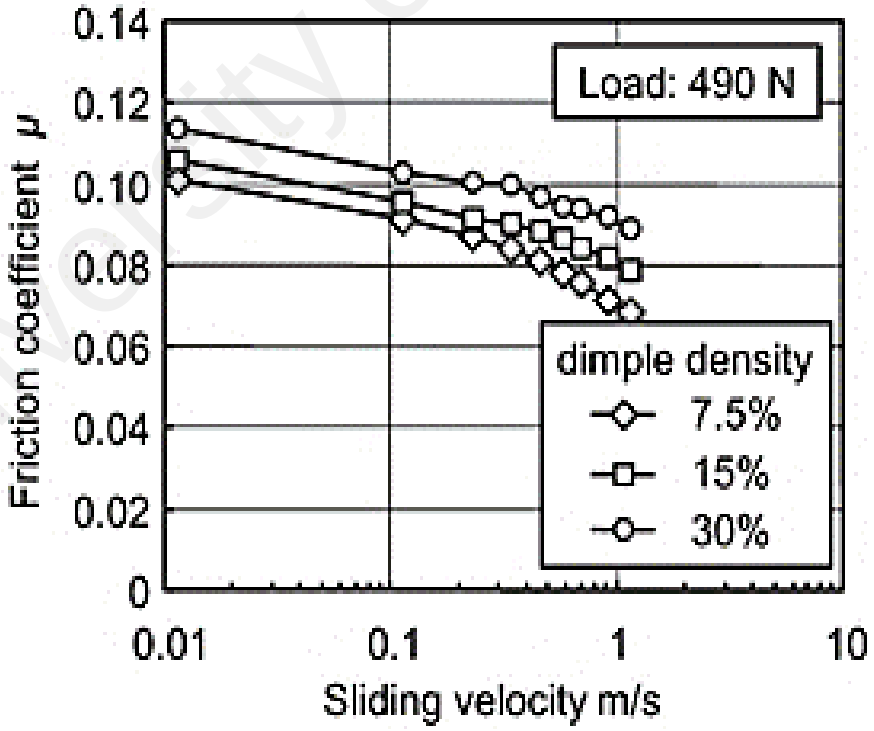

Figure 2.7: Effect of change in dimple density on coefficient of friction (Wakuda et al., 2003)

For textured 316 stainless steel, relationship between texture density and coefficient of friction were also analyzed by (Zhang et al., 2013). They reported that coefficient of friction reduces for 10 % dimple density compared to higher or lower dimple density (Figure 2.9). Wear depth was also reduced for surface textured steel than un-textured steel. It was also indicated that reduction in friction caused reduction in wear depth.

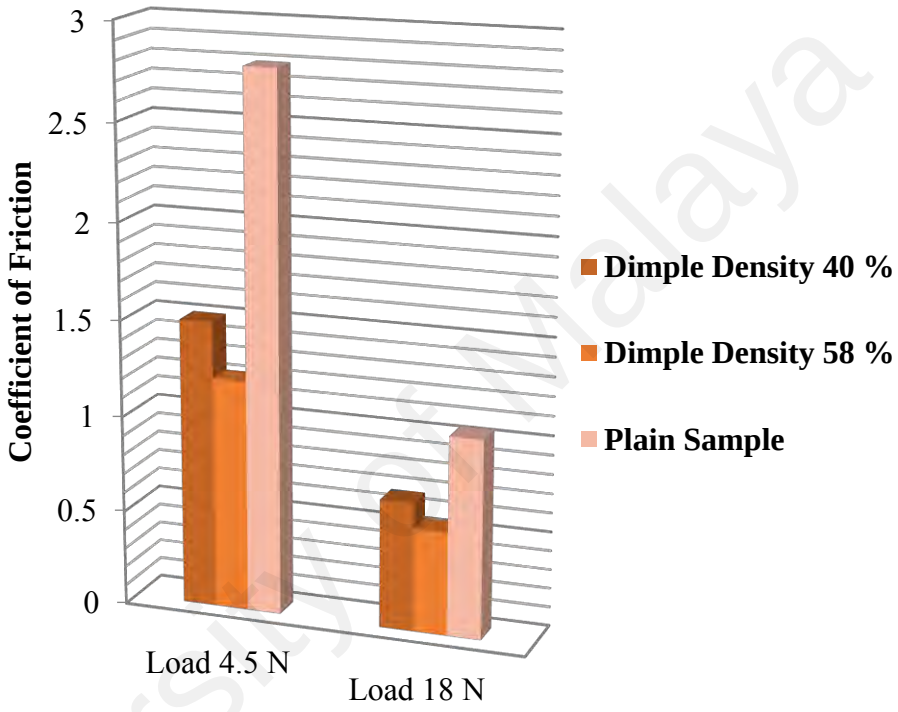

Figure 2.8: Effect of change in dimple density on coefficient of friction at various loads (Qiu& Khonsari, 2011a)

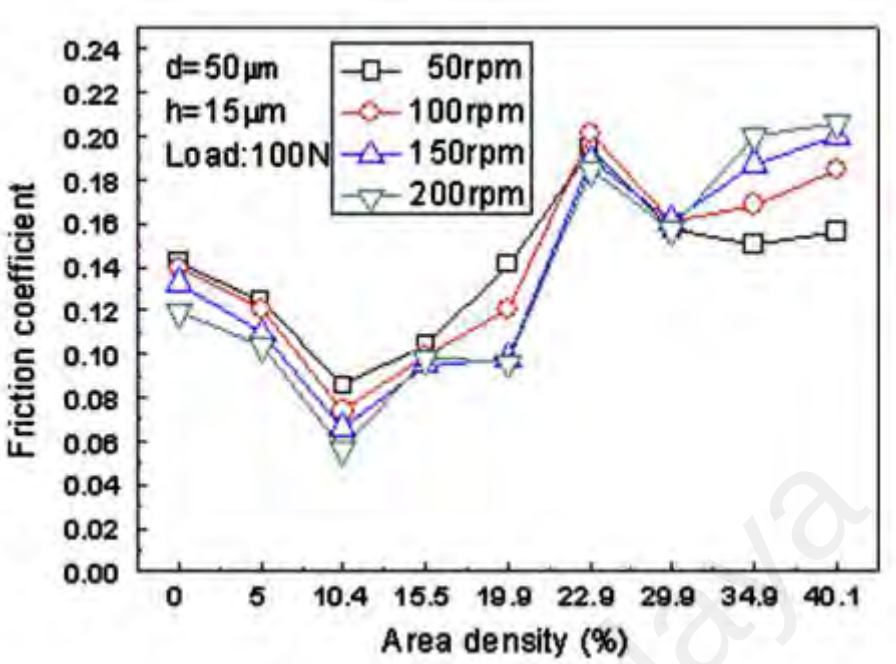

Figure 2.9: Variation in coefficient of friction with change in area density (Zhang et al., 2013)

2.2 Laser surface textured diamond like carbon coatings

2.2.1 Diamond like carbon coating

For several years, beneficial tribological properties of carbon have been acknowledged. Its performance depends upon form of carbon and its interaction with a particular operating setup. Due to remarkable lubrication properties of graphite, it has found countless applications in different fields including electrical contacts, abradable seals and metallurgical applications. In these applications, performance benefits are achieved due to sliding of basal planes over each other, which are further enhanced by adsorptive properties of water or oxygen (Hutchings, 1992). On the other hand, diamond is considered an ideal material for wear resistance due to its very high chemical inertness and hardness, which makes it beneficial in variety of applications including grinding and polishing tools, scalpels and wire drawing dies (Davis, 1991).

2.2.1.1 Types and structure of DLC coatings

Structures of sp^2 and sp^3 carbon atoms may be different in diamond like-carbon materials, while the amount of hydrogen contained by these materials can be negligibly

small or absent at all. In 1986, Robertson explained the structure of DLC as a random network in which carbon atoms are covalently bonded and have different hybridizations (Robertson, 1986). Robertson refined his model in 1997 and showed that energy of π bonds of sp^2 sites controls the structure of both ta-C and a-C:H coatings (Grill, 1999). Figure 2.10 presents the phase diagram of hydrogen, sp^2 and sp^3 contents in the different form of diamond like-carbon. Lower left-hand corner shows the graphitic carbon. The lower right-hand corner shows higher hydrogen content phases (gas or liquid molecules). Amorphous hydrogenated carbon (a-C:H) coating is present in the middle of the diagram, representing varying amounts of sp^2, sp^3 bonds and hydrogen contents. The tetrahedral amorphous carbon (ta-C) is present at the left side indicating varying amount of sp^2, sp^3 bonds.

On the basis of chemical structure, DLC coatings can be distinguished as pure (non-doped DLC coatings) and modified (doped DLC coatings). Pure or non-doped coating contained C or/and H only, whereas modified i.e., doped coatings also have some metallic (W, Mo, Ti etc.) and non-metallic (Si, F, C etc.) components. Based on practical applications of DLC coating, metal and nonmetal dopant are selected. Based on hydrogen content, DLC coatings are further classified in two major categories, namely, non-hydrogenated DLC coatings and hydrogenated DLC coatings. Non-hydrogenated DLC coatings have negligibly small hydrogen content, and they include tetrahedral (ta-C) and amorphous (a-C) DLC coatings. While hydrogenated DLC coatings contain the significant amount of hydrogen; amorphous (a-C:H) and tetrahedral (ta-C:H) DLC coatings are classified as hydrogenated DLC coatings (Velkavrh et al., 2008).

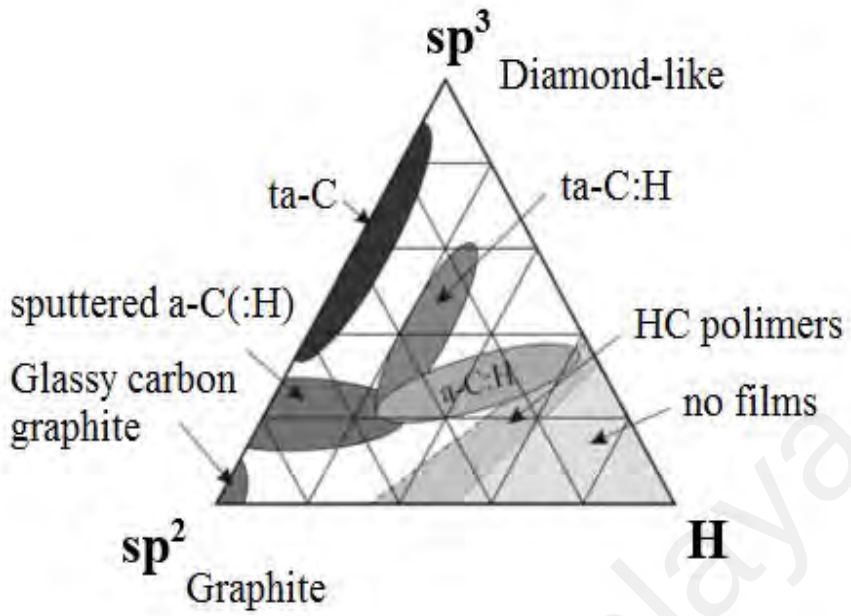

Figure 2.10: Ternary phase diagram showing sp^3, sp^2, and hydrogen contents of different DLC coatings (Robertson, 2002)

2.2.1.2 Deposition technique

Deposition technique is one of the main factors, which has significant influence on the properties of diamond-like carbon coating. Different deposition techniques have been introduced for depositing DLC films. For DLC coating there exist a wide range of deposition temperature, varying from sub-zero to 400 ºC. Depending upon the deposition technique; bias voltage, etching time and deposition gas pressure may also have a wide range of varying values. Higher flexibility of DLC coating has attracted attention from many researchers. Some common deposition techniques are magnetron sputtering, ion beam deposition, hot filament chemical vapor deposition (HFCVD), plasma-activated chemical vapor deposition (PACVD) and plasma immersion ion implantation and deposition (PIII-D) (Al Mahmud et al., 2015).

Magnetron sputtering is most commonly adopted deposition technique these days. This technique is applicable for DLC coating under both hydrogenated and non-hydrogenated conditions. Puchi-Cabrera et al. employed this technique for depositing hydrogenated DLC coating (Puchi-Cabrera et al., 2010). To improve DLC coating adhesion, they deposited an interlayer of Cr, and butane gas worked as source of hydrogen and carbon source. By following the same process Peng et al. coated non-hydrogenated DLC, but graphite source has been used in their work for deposition (Peng et al., 2001). By using a pure graphite target in Argon plasma, non-hydrogenated film with thickness up to 1 μm were made by sputtering. Working principle of magnetron sputtering is described as follows: high-energy ions created from discharge plasma are bombarded on a target plate (cathode), the bombardment process removes targeted atoms and thin film of these atoms is condensed on the substrate. Ion bombardment also caused emission of secondary electrons from the target surface. Plasma is maintained by emitted secondary electrons. Magnets are placed parallel to target in such a way that secondary electrons are trapped that increase the chance of electron collision and thus supports in sustaining plasma (Johnson & Cote, 2006; Kelly & Arnell, 2000; Tung & McMillan, 2004).

2.2.1.3 Influence of hydrogen content on DLC coating

The influence of hydrogen content on the tribological characteristics of DLC coatings can explain the sensitivity of a coefficient of friction to various environments such as humid and dry air. In the case of non-hydrogenated coatings, there exists strong adhesive forces between tribological surfaces. Therefore, value of COF in the vacuum is usually greater than 0.5. On the other hand, for hydrogenated coatings, COF is very less (COF< 0.001) (Erdemir, 2001).

For normal air exposed environment, a different behavior has been observed, coefficient of friction of non-hydrogenated decreases significantly while it increases for

hydrogenated DLC coating (Erdemir, 2001). The reason for this difference in behavior with change in environment can be explained by passivation of DLC coating surface with hydrogen. In the presence of hydrogen in DLC coatings, or when DLC coatings have hydrogenated environment, carbon and hydrogen atom's bond with each other, as a result, number of sites were contacting surfaces can form covalent bond is reduced, and thus adhesion gets lower. For non-hydrogenated DLC coatings, this mechanism does not occur due to the absence of hydrogen in the microstructure of the coating, and therefore, in inert environment or vacuum reactivity of non-hydrogenated DLC coated surfaces caused high adhesion (Sutton et al., 2013).

DLC interacting surfaces contain some unbound σ bonds. In order to minimize the coefficient of friction it is important to eliminate this type of bonds. In case of hydrogenated DLC, hydrogen can continuously passivate such bonds. Hydrogen exists within the matrix in the molecular and atomic state; and it works like a reservoir. Unwanted bonds are constantly passivated by these molecules, resulting in the decrease of surface energy. This process effectively minimizes friction (Semenov & Khrushchov, 2010).

2.2.1.4 Effect of sp^3/sp^2 ratio

Characteristics of DLC films i.e. hardness, elastic modulus, internal stresses, are directly related to the fraction of sp^3 carbon contained by films. DLC films generally have high elastic modulus, high hardness and high internal stresses. Higher the sp^3 content higher will be the hardness. Highest amount of sp^3 contents (80-88%) is found in tetrahedral carbon coating.

Al Mahmud et al. compared the tribological performance of tetrahedral amorphous and amorphous hydrogenated carbon coatings in oil lubricated conditions (Al Mahmud et al., 2014). The oil lubricated testing results indicated that due to higher sp^3 content in

tetrahedral amorphous coating the wear rate was lower than amorphous hydrogenated carbon coating. The Raman spectroscopy results showed lower transformation of sp^3 to sp^2 content which indicates that tetrahedral amorphous showed lower graphitization than amorphous hydrogenated carbon coating (Al Mahmud et al., 2014). Ronkainen et al. compared the tribological properties of amorphous hydrogenated carbon and tetrahedral amorphous carbon coatings in dry environment (Ronkainen et al., 2001). The amount of sp^3 bonds in tetrahedral amorphous and amorphous hydrogenated carbon coatings is high, however amorphous hydrogenated carbon shows more pronounced transformation to graphite structures. Some hydrogen-depleted sections are formed due to heat induced by friction. This friction induced heating can easily break down C-H bonds, so such regions become highly favorable for graphitization. As tetrahedral amorphous carbon coating has more stable sp^3 bonding than amorphous hydrogenated carbon coating, therefore for tetrahedral amorphous carbon coating graphitization rate is much lower, additionally, less pronounced transfer layer is formed for tetrahedral amorphous carbon coating compared to amorphous hydrogenated carbon coating.

2.2.1.5 Effect of temperature on friction of DLC coatings

Diamond-like carbon is a form of diamond, which is thermodynamically metastable. Graphitization or decomposition of amorphous hydrogenated carbon coating occurs once the temperature is increased. This process occurs through the release of hydrogen from the film structure. At a certain temperature normally refers to as threshold temperature, dehydrogenation of amorphous hydrogenated carbon coating to graphite crystallites occurs (Liu & Meletis, 1997). The hardness of amorphous hydrogenated carbon coating remains nearly constant up to 700 ºC, this can be due to the partial crystallization of graphite grains. The thermal stability of tetrahedral amorphous carbon coating is up to 1000 ºC temperature. This is because of lower hydrogen content in its structure (Kalish et al., 1999; Ronkainen, 2001).

Graham et al. investigated the effects of temperature on wear properties and coefficient of friction of tungsten doped DLC coating (Gharam et al., 2011). They observed that above 250 °C, the sp^3 to sp^2 bond's transformation takes place. As graphite has layered structures, it serves as a solid lubricant. Between each layer of structure, Van's der Waals bonds existed, but these bonds are not strong enough and allow the layers to slide over each other, which results in the decrease of a coefficient of friction. In lower temperature zone, coefficient of friction gradually increases by the increase in temperature as a result of evaporation of water molecules attached to the coated surface.

Wang et al. applied thermogravimetric analysis (TGA) to study the oxidation properties of DLC coating (Wang et al., 1999). They observed intense oxidation at a temperature range of 350-400 ºC. Frictional properties are also affected at this temperature range. Frictional properties are affected differently for hydrogenated and non-hydrogenated DLC coatings. Gao et al. demonstrated that hydrogen desorption occurs from the coating surface of amorphous hydrogenated carbon coating when it is heated at 147° C, which causes the increase in the coefficient of friction (Gao et al., 2005).

2.2.1.6 Effect of temperature on wear of DLC coatings

The thermal instability of DLC coating causes its wear behavior to be dependent on temperature. Some DLC coatings wear characteristics in ambient air has been observed to reduce with temperature increase from 100-300 °C (Grill, 1999). In another investigation, with the increase in temperature to 150 °C, it has been observed in the case of self-mated amorphous hydrogenated carbon coating that friction reduced and wear rate increased because of graphitization (Grill, 1999).

Highly disordered structure of DLC film steadily transforms to ordered structure at the elevated temperatures. Films form an unsteady phase during deposition, when thermal energy is introduced, structure of these films is re-oriented (Erdemir & Fenske, 1996; Wu

& Hon, 1999). At high temperature, diffusion of unbounded hydrogen atoms produced a spongy structure in the film of hydrogenated DLC. These structural and chemical changes also cause modifications in friction and wear behavior. After exposing at high temperature, final product may become highly porous and a soft graphitic thin layer may appear, which wears out rapidly. At elevated temperature, endurance limit for non-hydrogenated films is higher than hydrogenated films.

Veverkova et al. proved that at the different number of rotations (10 and 100 cycles) and loads (7 and 10 N), wear coefficients also increase with the increase in temperature in the case of tungsten doped DLC coating (Veverkova & Hainsworth, 2008). They observed that at 7 N and 10 N loads wear coefficient is higher for 10 cycles. Although, as time increases wear rate gets lower since abrasive wear occurs initially. Krumpiegl et al. investigated wear behavior and friction of amorphous carbon. Titanium doped DLC and amorphous hydrogenated carbon at 450^{o} C for both air-exposed and vacuum chamber environments. They observed that hardness is not lost after testing under vacuum chamber environment (Krumpiegl et al., 1999). However, for air exposed environment major loss of hardness is observed due to oxidation.

2.2.2 Combination of laser surface texturing and DLC coatings

Very few studies can be found related to surfacing at textured DLC coating. Tribological performance enhancement of DLC coatings using micro textures has been found by (Amanov et al., 2013; Ding et al., 2010; Dumitru et al., 2003; Enomoto & Sugihara, 2010; Komlenok et al., 2016; Koskinen et al., 2010; Oksanen et al., 2014; Pettersson & Jacobson, 2003; Pettersson & Jacobson, 2004; Song et al., 2014; Sugihara & Enomoto, 2009). Researchers have studied using mostly indirect laser texturing method, as it is difficult to control coating properties with direct laser texturing. Mostly,

researchers kept the dimensions of the textures constant. This section provides an overview of the research work conducted in this area.

2.2.2.1 Lubricant supplying and hydrodynamic effect

Ding et al. conducted tribological investigation on micro grooved amorphous carbon (a-C) coating under water lubrication, using the pin on disk linear reciprocating tests. Grooves were constructed with varying densities from 5% to 65 %. They observed that the hydrodynamic effect can be observed at 25 % groove density (as shown in Figure 2.11) (Ding et al., 2010). Coefficient of the friction increase was observed as the density increases or decreases from 25 %. This behavior can be attributed to the load carrying capacity variation. As the density was increased from 25 %, the load per unit area increased, which hindered the ability of water lubricant film to bear the load and thus the load was carried by amorphous carbon film. This causes higher wear of amorphous carbon film (Figure 2.12) and thus instability of tribological system (Ding et al., 2010).

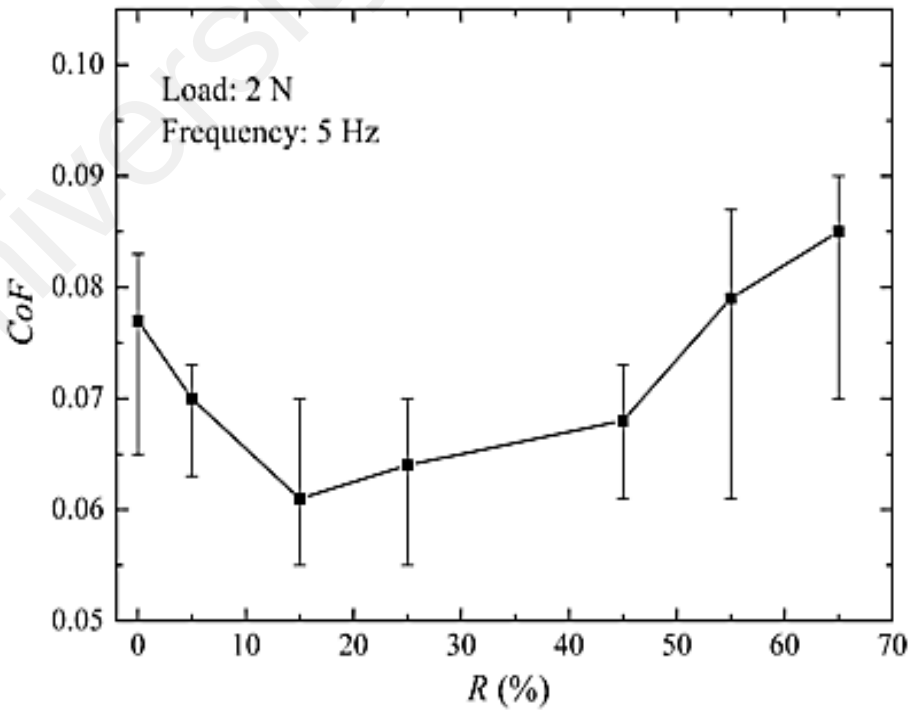

Figure 2.11: Effect of groove area density on coefficient of friction (Ding et al., 2010)

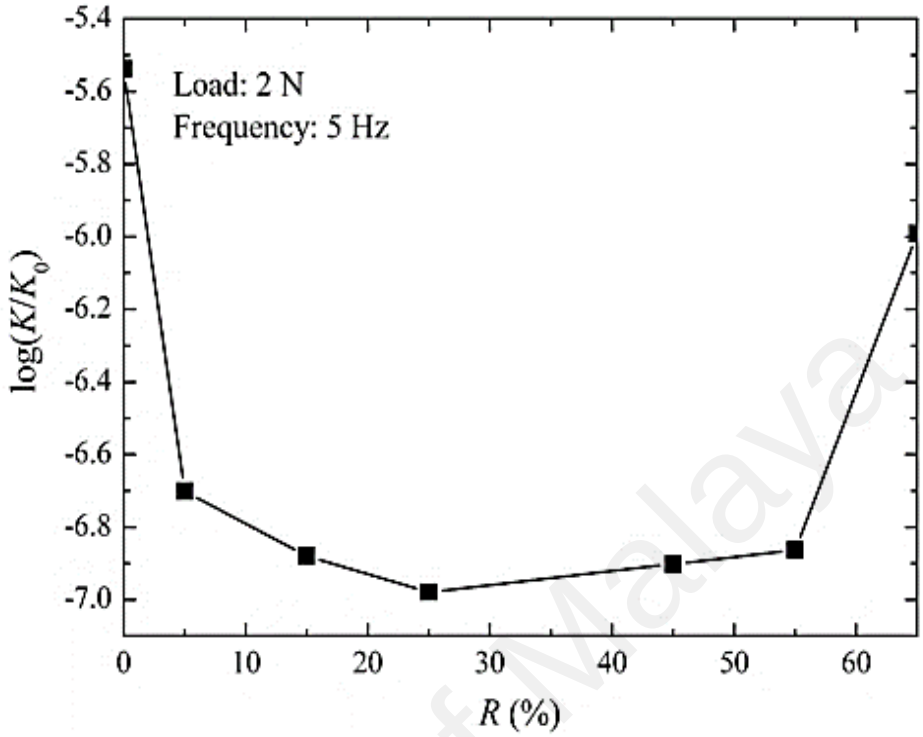

Figure 2.12: Effect of groove area density on wear rates (Ding et al., 2010)

In order to evaluate lubricating properties of textures under boundary conditions, Petterson et al. conducted ball on plate reciprocating tribological tests using poly alpha olefin as a lubricant (Pettersson & Jacobson, 2003). Textures such as grooves and squares were created with varying widths (5, 20 and 50 μm) using photolithographic technique. The results indicate that only smallest grooves and squares showed low and stable friction of 0.05. This behavior was attributed to the well working supply of lubricant from the textures at the ball/plate contact. In another study conducted by Petterson et al., similar results were found with the smallest grooves and squares (Pettersson & Jacobson, 2004).

Surface textured and un-textured DLC coatings were compared for cutting application. Various types of structures were created on the rake face of the tools to explore these effects on improving cutting tool performance, including DLC-coated sine wave-shaped

grooves (Sugihara & Enomoto, 2009); DLC-coated banded grooves in which textures were sandwiched between polished areas to ensure that lubricant leakage was prevented (Sugihara & Enomoto, 2009).

Comparison of the DLC coated sine wave grooved tool, and the DLC coated banded grooved tool in face milling experiments was conducted in dry and wet cutting conditions in order to analyze the effect of the lubricant storage and supply ability of textures (Sugihara & Enomoto, 2009). The aluminum atom concentration in EDX-Al imaging was measured in order to quantitatively analyze aluminum adhesion. In the case of wet cutting, the concentration of aluminum atoms for banded grooved tools was lowest, as compared to sine wave (parallel and perpendicular) grooves and un-textured. A reduction of the friction coefficients has also been found using the banded grooves on the tool rake face, as compared to the sine wave textured and un-textured tools. The reason for the superior performance of the DLC coated banded grooves compared to DLC coated sine wave, and un-textured DLC coated tool is that they retain and provide lubricant at the interface, keeping the lubricant leakage to a minimum (Enomoto & Sugihara, 2010). The importance of storing and providing lubricant ability has also been found in the dry cutting of aluminum. The aluminum atom concentration was found to be higher in the textured tool than the un-textured tool, which also indicates that lubricant storing/providing ability is necessary for adhesion reduction (Sugihara & Enomoto, 2009). Additionally, in the case of milling steel, sine-wave grooves did not enhance tool performance, due to a lack of lubricant storing ability.

2.2.2.2 Wear particle entrapment

Dumitru et al. (2003) evaluated the effect on an increase in load on the tribological performance of textured and un-textured amorphous hydrogenated carbon coating. The load was varied from 50 to 200 N. The textures were created using indirect laser texturing.

Dimples of 15-20 μm depth and 25 μm diameters were created. The author did not vary dimple parameters. Coefficients of friction results are shown in Figure 2.13. They observed that upon increasing the load, un-textured DLC shows the unstable coefficient of friction. The increase in load created more wear particles, which lead to abrasive wearing at the interface. Textured DLC showed the smoother coefficient of friction profile compared to un-textured DLC, which has been found to be due to the wear particle entrapment ability of textures. This ability saved the tribological system from breaking down due to abrasive wearing. Petterson et al. have also observed this ability of textures in lubricated and dry sliding conditions (Pettersson & Jacobson, 2004).

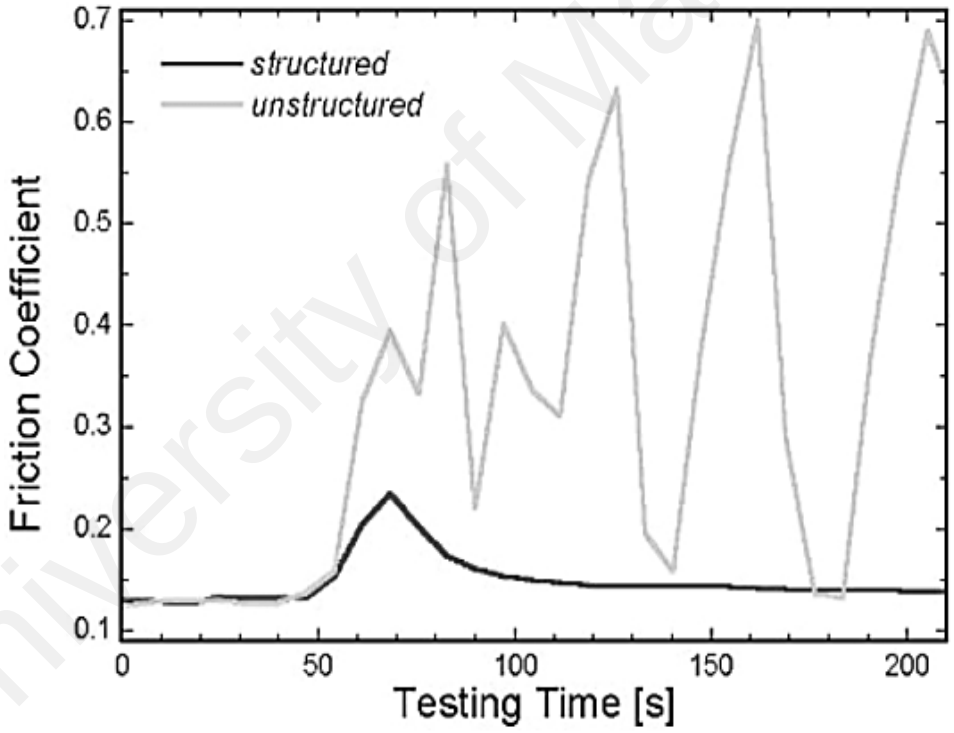

Figure 2.13: Variation of coefficient of friction with structured and unstructured DLC coating (Dumitru et al., 2003)

In case of amorphous carbon coating, Ding et al. have observed connection between particle entrapment ability of textures and coating life (Ding et al., 2010). They conducted tribological tests at room temperature. They found that at an optimum dimple density of 25 %, the service life of amorphous carbon coating is enhanced. As shown in Figure 2.14,

in the start of the test, both the coatings showed the similar coefficient of friction, however, as the test progressed towards un-textured amorphous carbon coating showed the reduced coefficient of friction compared to textured amorphous carbon. At the end of the test, the tribological system of un-textured amorphous carbon coating broke down, and textured amorphous carbon survived. The phenomenon which caused a reduction of a coefficient of friction in case of un-textured amorphous carbon coating after 20 minimums is graphitization transformation. At the end of the test, due to graphitization the un-textured amorphous carbon coating hardness decreased, and eventually film delamination occurred and coefficient of friction increased.

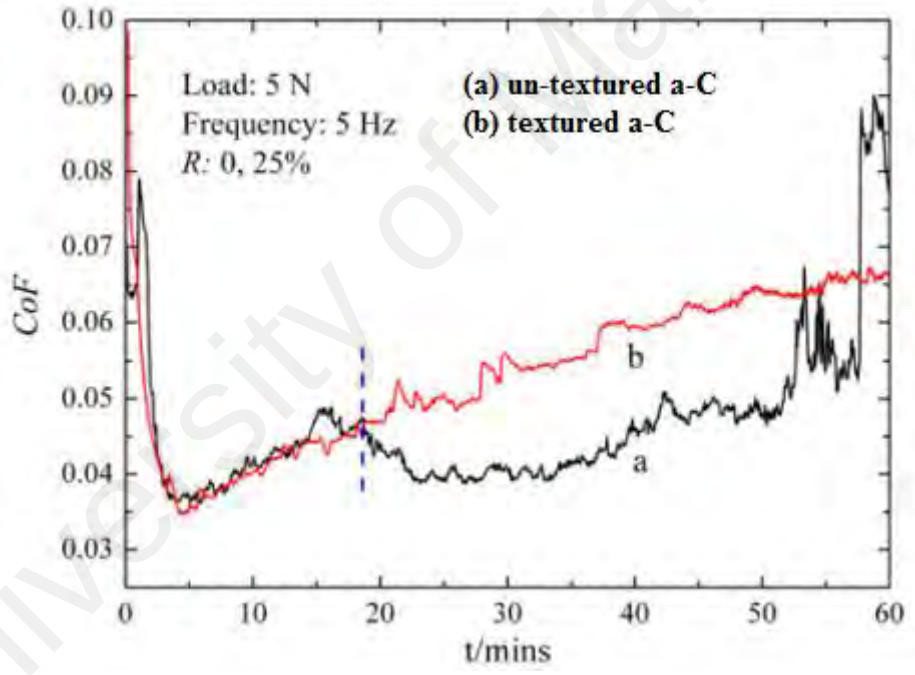

Figure 2.14: Variation of coefficient of friction with textured and un-textured a-C film (Ding et al., 2010)

The atomic structure of a-C coating consists of sp^3, sp^2 and monovalent hydrogen bonds (Neville et al., 2007). The release of hydrogen from the DLC matrix triggers the transformation from a sp^3 structure to a graphite-like sp^2 structure. Graphitization can occur because of higher contact temperature and/or high contact stress (Haque et al., 2009). Haque et al. suggested that due to the micron-sized wear particles produced during

the sliding test, the contact pressure reduces the graphitization temperature to as low as 95 ºC (Haque et al., 2009). These particles can be generated from counter ball wear (Haque et al., 2009). Ding et al. proposed that, due to fatigue wear mechanisms, a-C wear debris can be created at the contact, which can lower the graphitization temperature (Ding et al., 2010). This can explain the graphitization transformation at room temperature. The lower graphitization in the case of textured DLC at higher temperatures may be due to multiple factors, including the wear debris trapping ability and the lubricant retention ability of micro dimples. Textures can remove the wear debris from the contacting surface, which can lessen the increase in contact pressure due to the wear particles between the tribo-pairs. Amanov et al. based on their tribological investigation suggested that textures provide an easy escape to micro wear particles (Amanov et al., 2013). These particles if remain on the wear track will cause higher contact loading, which will eventually cause coating failure. Additionally, by keeping the lubricant at the interface, they can lower the rise in temperature due to friction-induced heating. In the case of textured mechanical seals, Xiao et al. (Xiao & Khonsari, 2012) observed that micro dimples could lower the interface temperature by keeping lubricant at the interface.

Tribological performance of groove textured amorphous hydrogenated carbon under the vacuum conditions for space applications, has been investigated recently by Song et al. The textures created with varying pitch distance from 0.1- 1 mm with 30 μm width and 35 μm depth. They observed that under vacuum conditions, textured amorphous hydrogenated carbon with pitch distance 0.5 mm shows prolonged wear life (Figure 2.15). The reductions in adhesive wear and abrasive wear were mainly found responsible for this enhancement (Song et al., 2014). Wear particles formed at the steel ball and amorphous hydrogenated carbon disk contacts were captured by textures, thus preventing further wear and coating delamination. The un-textured amorphous hydrogenated carbon coating delaminated at several places after the test. They also observed that by varying

texture pitch or changing the density, wear particle capturing ability changes. Higher density reduced the load carrying ability. Low density affects the wear debris entrapping ability (Song et al., 2014).

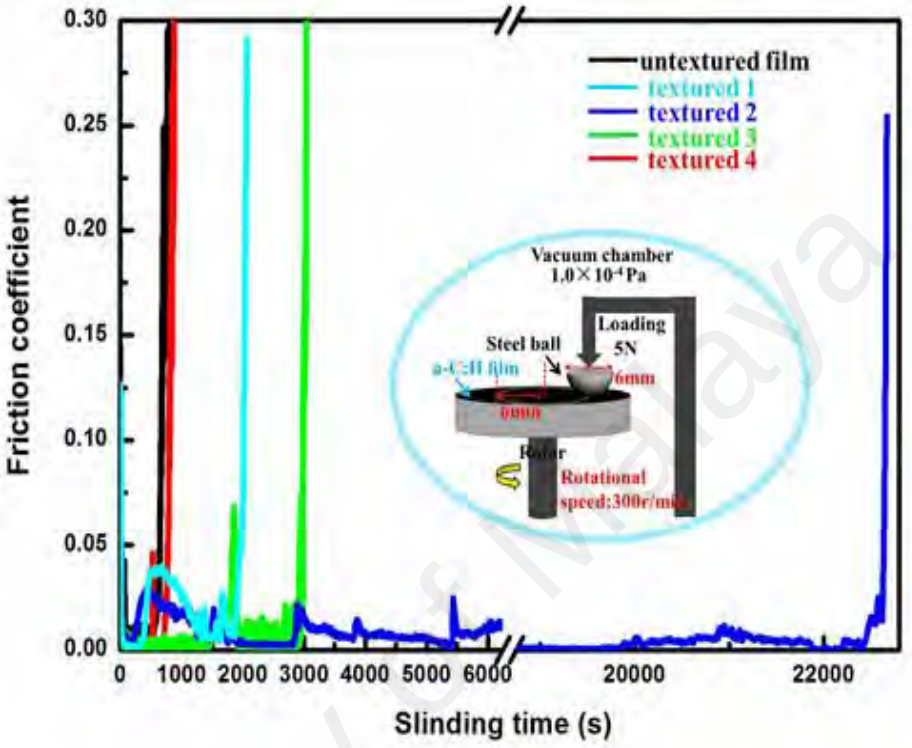

Figure 2.15: Coefficient of friction of various textured amorphous hydrogenated carbon coating samples (textured 1: 1 mm, textured 2:0.5 mm, textured 3: 0.3 mm, textured 4: 0.1 mm) in vacuum condition (Song et al., 2014)

2.3 Bio-lubricants and their tribological properties

Bio-lubricants have high biodegradability and low environmental and human toxicity. Bio-lubricants are developed from vegetable oils (soybean, palm, sunflower. Coconut, etc.), synthetic esters and petroleum oils which satisfied the already recognized toxicity and biodegradability criteria (Kumar & Sharma, 2011).

Bio-lubricant feedstock's vary from country to country and is dependent upon the geographical location. The number of oil bearing crops is higher than 350; however, worldwide attention has been given to only few; such as palm, cottonseed, peanut oil,

Jatropha oil, etc. (Singh & Singh, 2010). Palm oil is the main source of bio-lubricant and bio-diesel in Malaysia.

Vegetable oils have advantages and disadvantages. Advantages include: excellent lubricity and are biodegradable compared to mineral oil based lubricant; they have the higher viscosity index (VI), normally they have VI of 223 compared to mineral oil with VI of 90-100; they also have higher flash temperature compared to mineral oils. The disadvantages are: low oxidation stability in the natural form; unpleasant odor; limitations of low-temperature; filter clogging tendency (Mobarak et al., 2014).

In order to increase the oxidation stability and low temperature property's various techniques has been used such as esterification, transesterification of TMP and ester from vegetable feedstock, selective hydrogenation, epoxidation and addition of additives (Zulkifli et al., 2014).

2.3.1 Trimethylolpropane ester

Trimethylolpropane (TMP) ester is a synthetic lubricant. It can be produced from biodegradable or mineral resources. Biodegradable oils such as palm, jatropha and sunflower had been used to produce TMP ester (Arbain & Salimon, 2010; Zulkifli, 2014). TMP ester is produced by transesterification of methyl ester (Aziz et al., 2016). TMP ester as a bio-lubricant has been used in metal working fluid and engine oils (Zulkifli et al., 2013) etc. The main reason for using TMP ester as the bio-lubricant is that it has good thermal and oxidation stability, high viscosity index, friction and wear reducing ability.

2.3.1.1 Tribological performance of trimethylolpropane ester

Generally, researchers found that vegetable-based TMP ester has good tribological properties. Zulkifli et al. compared the anti-wear properties of palm based TMP ester with fully formulated lubricant and paraffin oil (Zulkifli et al., 2016). The authors used four

balls tribological testing equipment. At 392 N load, they observed that wear scar diameter for palm based TMP ester is lower than paraffin oil whereas it is higher than fully formulated lubricant. This was expected as fully formulated lubricant contains anti-wear additives. Based on the results the authors concluded that palm based TMP ester has comparable load carrying ability and tribological properties compared to fully formulated lubricant. Shah et al. found that TMP ester has better friction reducing properties and acceptable anti-wear properties (Shah et al., 2010).

The lower coefficient of friction shown by palm based TMP ester is because of its high polarity; because of this reason, it is easily attracted to metal surfaces. Additionally, due to longer chain lengths, they have higher lubricity. Palm oil has a carbon chain length of 18-20. That is why the formed film behaves as a crystalline solid and reduces friction (Bhushan, 2013).

In another investigation, Zulkifli et al. observed the effect of temperature on the tribological performance of palm based TMP ester (Zulkifli et al., 2014). They used four-ball tester for this tribological investigation. The authors found that palm TMP ester showed lower coefficient of friction compared to paraffin oil till 80 ºC temperature. However, as the temperature was increased from 80 to 100 ºC paraffin oil showed lower coefficient of friction compared to palm based TMP ester. The reason for this behavior at the higher temperatures is that the lubricant films formed by the fatty acid are less stable, and they break down easily.

CHAPTER 3: RESEARCH METHODOLOGY

3.1 Tribological investigation of laser texture density, diameter and depth

In order to understand the effect of dimple density, diameter and depth on the tribological performance of amorphous hydrogenated carbon coating, textured and un-textured amorphous hydrogenated carbon coated samples were created.

3.1.1 Sample preparation

3.1.1.1 Polishing

AISI 52100 steel with a hardness of approximately 60 HRC was used. Steel samples were cut into dimensions of 15×15 mm in order to use in tribological testing. Steel samples were initially polished using silicon carbide papers with a grit size range of 400 to 2500 to reduce surface roughness. Afterward, the samples were polished using diamond suspension with a particle size varying from 6 μm to 1 μm. After polishing, the average surface roughness was around 30-40 nm.

3.1.1.2 Laser surface texturing

LST uses high-energy pulses to ablate material by rapid melting and vaporizing. Laser ablation can be defined as the removal of material by direct absorption of laser energy. In present research work micro surface textures were fabricated using laser surface texturing (LST). They were fabricated in Singapore institute of manufacturing technology (SIMtech), Singapore. The specifications of laser used to create micro surface textures are given in Table 3.1.

Table 3.1: Pico second laser specifications

No	Laser Specification	Value
1	Power	10 W
2	Wavelength	1640 nm
3	Pulse frequency range	50 kHz to 8200 kHz
4	Pulse duration	10.3 pico second
5	Beam Position Speed	1000 mm/s

The samples were fabricated with various texture density, diameter and depth. After laser surface texturing, bulges were formed around the dimples. These were around 1.5-2 μm in height. Frictional behavior is affected by bulges (Amanov et al., 2012). This volume of material was removed from the textured surface by slight surface polishing with diamond suspension (particle size 0.5 μm).

Texture density was varied from 10-30 %, diameter from 50-150 μm and depth from 6-30 μm. Different texture dimensions and the sample designations are mentioned in Table 3.2. These designations will be used while discussing results in next chapters. Each sample designation indicates its texture dimensions; e.g. Dn10Di50Dp6 indicates that this sample has a texture density (Dn) of 10 %, texture diameter (Di) of 50 μm and texture depth (Dp) of 6 μm. The symbols Dn, Di, Dp indicates dimple density, diameter and depth, respectively. The texture parameter which showed better friction and wear results was used for sections 3.2, 3.3 and 3.4. The selection of laser texture parameters was conducted according to the Figure 3.1. The flow chart of experimental activities is mentioned in Figure 3.2

Table 3.2 continued: Various Indirect laser micro textured amorphous hydrogenated carbon coated samples

Sample Designation	Dimple Density	Dimple Diameter	Dimple Depth
Dn10Di50Dp6	10	50	6
Dn10Di50Dp15	10	50	15
Dn10Di50Dp30	10	50	30
Dn10Di100Dp6	10	100	6
Dn10Di100Dp15	10	100	15
Dn10Di100Dp30	10	100	30
Dn10Di150Dp6	10	150	6
Dn10Di150Dp15	10	150	15
Dn10Di150Dp30	10	150	30
Dn20Di50Dp6	20	50	6
Dn20Di50Dp15	20	50	15
Dn20Di50Dp30	20	50	30
Dn20Di100Dp6	20	100	6
Dn20Di100Dp15	20	100	15
Dn20Di100Dp30	20	100	30
Dn20Di150Dp6	20	150	6
Dn20Di150Dp15	20	150	15
Dn20Di150Dp30	20	150	30
Dn30Di50Dp6	30	50	6
Dn30Di50Dp15	30	50	15
Dn30Di50Dp30	30	50	30
Dn30Di100Dp6	30	100	6
Dn30Di100Dp15	30	100	15

Dn30Di100Dp30	30	100	30
Dn30Di150Dp6	30	150	6
Dn30Di150Dp15	30	150	15
Dn30Di150Dp30	30	150	30
a-C:H-Untex	-	-	-

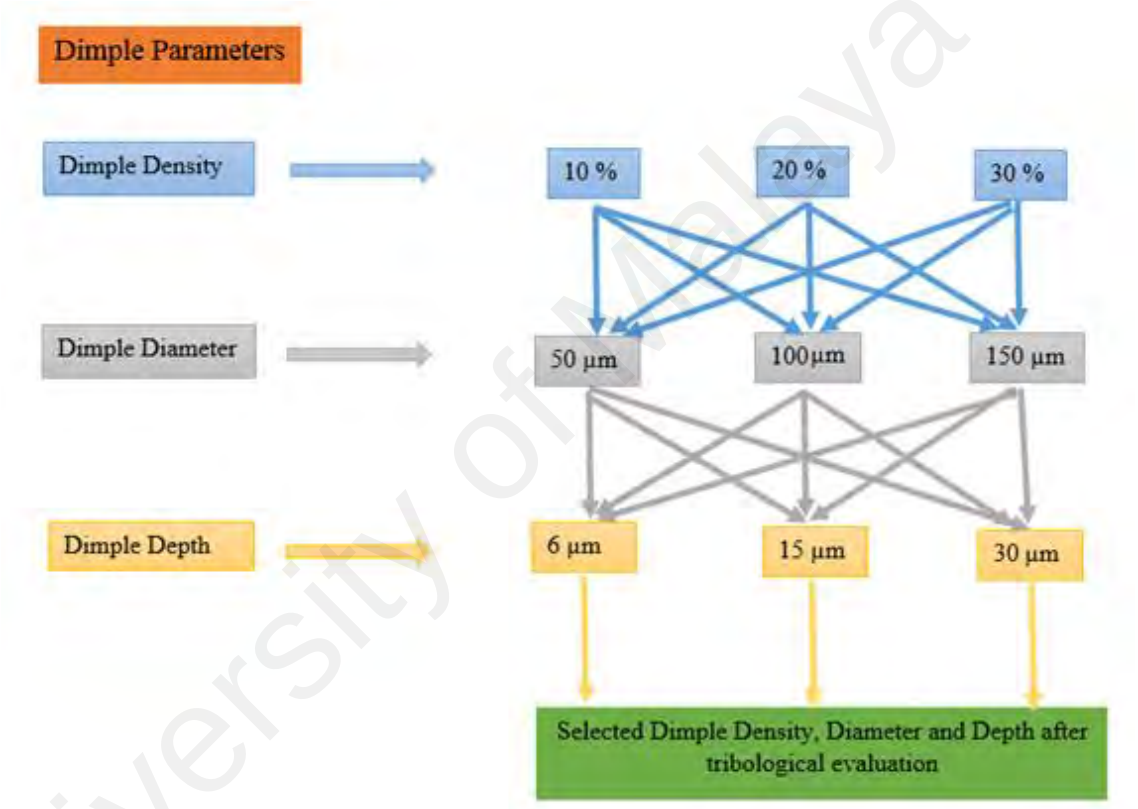

Figure 3.1: Selection of optimum laser texture parameters

3.1.1.3 Amorphous hydrogenated carbon coating deposition

Amorphous hydrogenated carbon was deposited on laser textured samples with various densities, diameters and depths. Coating company (Notion Venture Pvt. Ltd.) deposited the coating. Deposition parameters for the amorphous hydrogenated coating is in Table 3.3. Composition and important properties of materials used are listed in Table 3.4. The information regarding hydrogen content and coating thickness was provided by the coating company.

Table 3.3: Amorphous hydrogenated carbon coating deposition conditions

Stages	Time	Current (A)	Voltage (V)	Gas Pressure (mbar)
Evacuating	30 min			
Argon cleaning	30 min		75	2.5 (argon)
Chromium deposition	10 min	60	40	
DLC deposition	1 hr 30 min	20	160	0.5 (acetylene)
Cooling	30 min			

Table 3.4: Composition and important properties of the tribological pair

Physical Properties	Steel Ball	Substrate number 1	Substrate number 2
Material	AISI 52100	a-C:H	ta-C
Composition	C 0.98 %, Fe 96.5 %, Cr 1.30, Mn 0.250 %, Si 0.150 %,S ≤ 0.0250, P ≤ 0.0250	20 at. % Hydrogen	-
Roughness	~ 35 nm	~ 40 nm	~ 40 nm
Thickness		1.3-1.6 µm	1.3-1.6 µm

Hybrid magnetron sputtering (well known a physical vapor deposition) was employed for depositing amorphous hydrogenated carbon coating. The main mechanism of this technique can be explained as follows: High-energy ions created from discharge plasma are bombarded on a target plate (cathode), targeted atoms are removed by the bombardment of ions and thin film of these atoms is condensed on the substrate. Ion bombardment also causes emission of secondary electrons from the target surface; plasma is maintained by emitted secondary electrons. Magnets are placed parallel to target in such a way that secondary electrons are trapped, which increase the probability of electron collision and thus helps in sustaining plasma.

3.1.2 Mechanical properties

Hardness and elastic modulus of amorphous hydrogenated carbon coating was determined using nano indenter (TI 750 UBI, Hysitron, Inc.). Adhesion between coating

and substrate was determined using Rockwell C indentation test. The details of these tests can be seen in section 3.5.

3.1.3 Tribological investigation

In order to identify the tribological performance variation with texture density, diameter and depth, reciprocating sliding test rig (Ducom Instruments) was used. The applied load, sliding frequency, stroke length, and test duration was 100 N, 5 Hz, 2 mm, and 2 hours, respectively. This frequency and contact load was selected in order to ensure boundary lubrication regime at the interface. Two-hour duration was selected in order to have a measurable wear track. Similar duration for testing has been used by previous studies (He et al. 2015). Poly alpha olefin (PAO) was used for tribological testing. PAO was obtained from INEOS Pvt. Limited. The complete detail for the tribo-testing can be seen in section 3.6. After tribological testing, the samples were washed with n-heptane for characterization.

3.1.4 Surface characterization

Laser textured and un-textured amorphous hydrogenated carbon coated samples with various texture density, diameter and depths were characterized before and after the trio-testing using Profilometer (Veeco Dektak 150 profilometer), Scanning electron microscope (SEM) (HITACHI, Model No. TM3030), Energy dispersive x-ray spectroscopy (EDX) (HITACHI, Model No. TM3030), Atomic force microscopy (AFM) (Q-Scope^{TM} 250/400, AMBIOS technology) and Raman's spectroscopy (Gloucestershire, United Kingdom). The details of the equipment used for surface characterization can be seen in section 3.7.

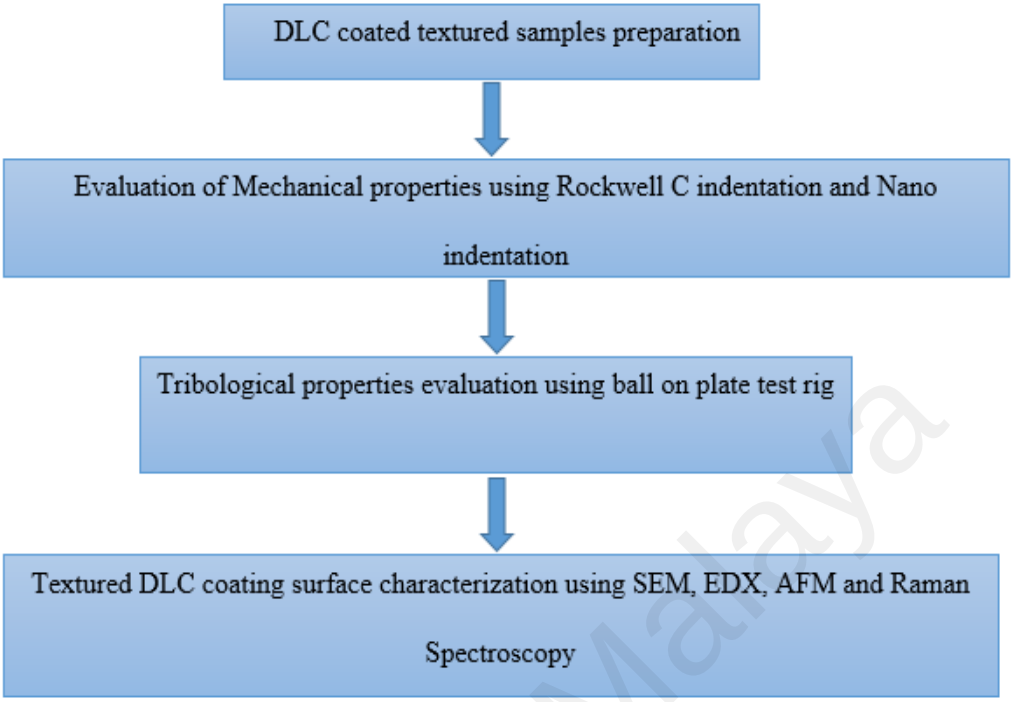

Figure 3.2: Flow chart of research activities

3.2 Tribological behavior of textured and un-textured amorphous hydrogenated carbon coating at various temperatures

The range of temperature was selected to simulate the actual engine conditions. In order to analyze and compare the behavior of textured and un-textured amorphous hydrogenated carbon coating at various temperatures, following steps were taken.

3.2.1 Sample Preparation

Two types of samples were prepared. One is un-textured coated designated as PAO-C40 (C indicates coated but non-textured sample) and another is textured coated designated as PAO-T40 (T indicates textured coated). In the designation PAO-C40, "PAO" represents the lubricant used and "40" represents the temperature at which testing was conducted. Sample TMP-C40 indicates un-textured coated samples tested at 40 ºC in palm based TMP ester. The samples used have the dimension of 15mm by 15 mm.

Table 3.5 shows the designations for various laser textured and un-textured amorphous hydrogenated carbon coated samples

Table 3.5: Various amorphous hydrogenated carbon coated samples

Sample Designation	Textured/Un-textured	Testing Temperature (C°)	Lubricant
PAO-C40	Un-textured	40	PAO
PAO-C80	Un-textured	80	PAO
PAO-C125	Un-textured	125	PAO
PAO-T40	Textured	40	PAO
PAO-T80	Textured	80	PAO
PAO-T125	Textured	125	PAO
TMP-C40	Un-textured	40	TMP
TMP-C80	Un-textured	80	TMP
TMP-C125	Un-textured	125	TMP
TMP-T40	Textured	40	TMP
TMP-T80	Textured	80	TMP
TMP-T125	Textured	125	TMP

3.2.1.1 Polishing

Samples were polished to a roughness of 30-40 nm before laser texturing. The procedure followed for polishing can be seen in section 3.1.1.1.

3.2.1.2 Laser surface texturing

Polished samples were laser textured. The texture density, diameter and depth was selected on the basis of tribological tests in section 3.1. Texture density, diameter and depth which provided lowest coefficient of friction and wear coefficient was selected.

Laser textured samples were fabricated in Singapore institute of manufacturing technology (SIMtech), Singapore. The complete details of laser texturing can be seen in section 3.1.1.2

3.2.1.3 Deposition of amorphous hydrogenated carbon coating

Amorphous hydrogenated carbon coating was deposited onto textured and un-textured samples by (Notion Venture Pvt. Ltd.). Details of coating procedure can be seen in section 3.1.1.3.

3.2.2 Mechanical Properties

Mechanical properties such as hardness, elastic modulus and adhesion of coating was determined before tribological tests. Hardness and elastic modulus were determined using nano indenter (TI 750 UBI, Hysitron, Inc.). Adhesion of amorphous hydrogenated carbon was determined using Rockwell-C indentation test. Details of these procedures can be seen in section 3.5.

3.2.3 Tribological investigation

In order to analyze the effects of temperature increase on the tribological performance of textured and un-textured amorphous hydrogenated carbon coating, reciprocating sliding test rig (Ducom Instruments) was used. The load, frequency, stroke length and temperature during the tribological testing were 100 N, 5 Hz, 2 mm and 40-125 ºC respectively. Polyalphaolefin (PAO) and palm based TMP ester were used for tribological testing. PAO was obtained from INEOS Pvt. Limited. The palm based TMP ester was obtained from University Putra Malaysia (UPM). Palm based TMP ester was produced using transesterification of palm oil methyl ester. The procedure for the production of palm based TMP ester can be found in our research group's previous article (Zulkifli et al., 2014). Further details regarding tribological testing can be seen in section 3.6. After tribological testing, the samples were washed with n-heptane for characterization.

3.2.4 Surface characterization

Surface characterization was conducted before and after the tribological investigation. Characterization techniques used can be seen in section 3.7. In order to observe structural changes in amorphous hydrogenated carbon coating due to temperature change, Raman spectroscopy (Renishaw, United Kingdom) was used. SEM (HITACHI, Model No. TM3030) and AFM (Q-Scope^{TM} 250/400, AMBIOS technology) were used to analyze the surface of wear track. Profilometer (Veeco Dektak 150 profilometer) was used to analyze the wear track. EDX (HITACHI, Model No. TM3030) was used to find the chemical composition at the wear track.

3.3 Tribological behavior of textured and un-textured tetrahedral amorphous carbon coating at various temperatures

The range of temperature was selected to simulate the actual engine conditions. Following steps were taken in order to achieve the objective of analyzing the performance of laser textured and un-textured tetrahedral amorphous carbon coating at various temperatures.

3.3.1 Sample preparation

Two types of samples were created. Textured coated sample ta-C.PAO-T40 ("ta-C" is the coating type, letters "PAO" indicates the lubricant tested, letter "T" indicates textured coated sample and number "40" represents the temperature at which tribo-testing was conducted) and un-textured coated sample ta-C. PAO-C40 (where C represents un-textured coated sample). Similarly, ta-C.TMP-C40 and ta-C.TMP-T40 indicates that TMP lubricant was used with un-textured and textured coating at 40 ºC, respectively. Textured DLC coated samples have dimension of 15 mm by 15 mm. Table 3.6 shows the designations for various laser textured and un-textured tetrahedral amorphous carbon coated samples

Table 3.6: Various laser textured and un-textured tetrahedral amorphous carbon coated samples

Sample Designation	Textured/Un-textured	Testing Temperature (C°)	Lubricant
ta-C.PAO-C40	Un-textured	40	PAO
ta-C.PAO-C80	Un-textured	80	PAO
ta-C.PAO-C125	Un-textured	125	PAO
ta-C.PAO-T40	Textured	40	PAO
ta-C.PAO-T80	Textured	80	PAO
ta-C.PAO-T125	Textured	125	PAO
ta-C.TMP-C40	Un-textured	40	TMP
ta-C.TMP-C80	Un-textured	80	TMP
ta-C.TMP-C125	Un-textured	125	TMP
ta-C.TMP-T40	Textured	40	TMP
ta-C.TMP-T80	Textured	80	TMP
ta-C.TMP-T125	Textured	125	TMP

3.3.1.1 Polishing of samples

Samples were polished to reduce surface roughness. Similar procedure was used as described in section 3.1.1.1. Final surface roughness of samples was 30-40 nm.

3.3.1.2 Laser surface texturing

Surface textured samples were created using laser ablation. Laser surface texturing was conducted in Singapore institute of manufacturing technology (SIMtech), Singapore. The texture parameters which provided lowest coefficient of friction and wear coefficient in section 3.1 were used in this section. Further details regarding laser surface texturing can be seen in section 3.1.1.2.

3.3.1.3 Deposition of tetrahedral amorphous carbon coating

Tetrahedral amorphous carbon coating was deposited by Notion Venture Pvt. Ltd. on textured and un-textured samples. Deposition parameters for the coatings were not provided by the company. Composition and important properties of materials used are listed in Table 3.3. The information regarding hydrogen content and coating thickness was provided by the coating company. Further details regarding deposition can be seen in section 3.1.1.3.

3.3.2 Mechanical properties

Mechanical properties such as hardness, elastic modulus and adhesion of tetrahedral amorphous carbon coating was determined using nano indentation (TI 750 UBI, Hysitron, Inc.) and Rockwell C indentation. The details of these procedures can be seen in section 3.5.

3.3.3 Tribological investigation

Tribological behavior variation of laser textured tetrahedral amorphous carbon coating with temperature in the presence of PAO and TMP ester was conducted using reciprocating test rig (Ducom instruments). The load, frequency, stroke length and temperature during the tribological testing were 100 N, 5 Hz, 2 mm and 40-125 ºC respectively. As mentioned in section 3.2.3, Poly alpha olefin (PAO) and palm based TMP ester was used for tribological testing. PAO lubricant was obtained from INEOS Pvt. Ltd. The palm based TMP ester was obtained from University Putra Malaysia (UPM). The details of tribological testing is mentioned in section 3.6. After tribological testing, the samples were washed with n-heptane for characterization.

3.3.4 Surface characterization

Characterization of tetrahedral amorphous carbon coating (textured and un-textured) was conducted using various technique. Profilometer (Veeco Dektak 150 profilometer)

was used to analyze wear track, SEM (HITACHI, Model No. TM3030) and AFM (Q-Scope^{TM} 250/400, AMBIOS technology) were used to observe the topography of wear track, EDX (HITACHI, Model No. TM3030) was used to observe chemical composition at the wear track and Raman spectroscopy (Renishaw, United Kingdom) was used to analyze the structural changes. Details of these techniques can be observed in section 3.7.

3.4 Comparison of tribological properties of laser textured amorphous hydrogenated carbon and tetrahedral amorphous carbon coating

A comparison was conducted in order to analyze whether laser textured amorphous hydrogenated carbon is better or worse in tribological performance compared to laser textured tetrahedral amorphous carbon coating. Coefficient of friction and wear coefficient of amorphous hydrogenated carbon and tetrahedral amorphous carbon coating were compared.

3.5 Mechanical properties of coatings

3.5.1 Adhesion of DLC coatings

Lifetime of coating highly depends upon the quality of adhesion between substrate and coating. Working life of coating is reduced by poor adhesion. Therefore, for reliability better adhesion is required. Number of methods have been introduced for evaluating the quality of adhesion (Volinsky et al., 2002). Adhesion of DLC coatings was investigated through a Rockwell C test. The classification of this test is based on the German standard VDI 3198 and had been used previously by Ronkainen et al. to evaluate amorphous hydrogenated and tetrahedral amorphous carbon coating adhesion (Ronkainen et al., 1999). In this test, a standard Rockwell C hardness tester was used to assess Rockwell C adhesion. The indentation causes layer damage adjacent to the boundary of the indentation. After indentation, optical microscope was used to evaluate the indented areas. Three indents were made on each sample, and the damage to the coating was

compared with a defined adhesion strength quality shown in Figure 3.3. The types of defects are classified as HF1 to HF6. HF1-HF4 defines sufficient adhesion whereas HF5 and HF6 indicated insufficient adhesion (Heinke et al., 1995). HF1 indicates the highest adhesion, and HF6 indicates the lowest adhesion.

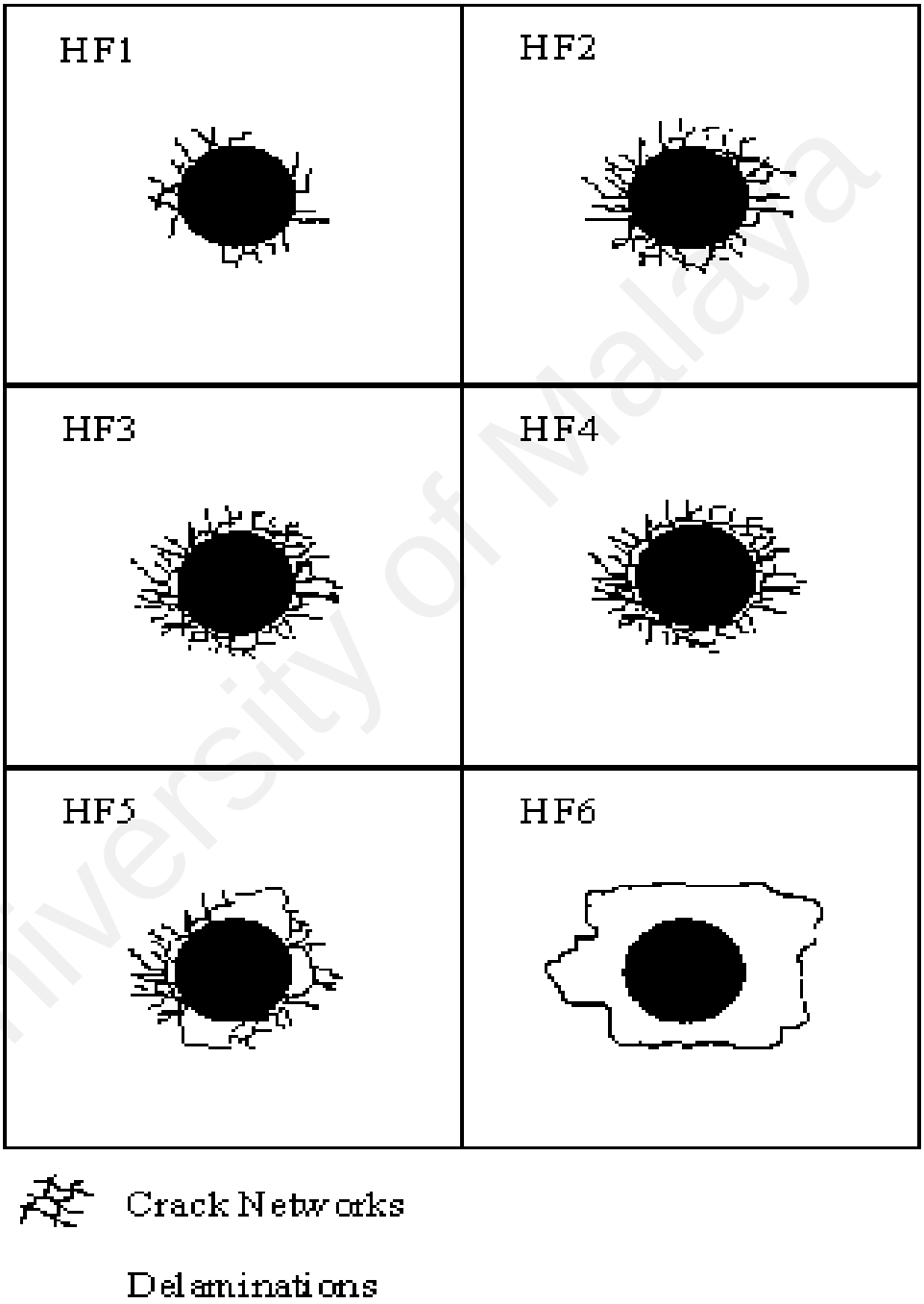

Figure 3.3: Failure modes for Rockwell C adhesion testing (Heinke et al., 1995)

3.5.2 Hardness and elastic modulus of DLC coatings

Recently, nano-indention technology has become popular for measuring hardness and elastic modulus. The working principle of nano-indentation test can be described as follow: a well-molded indenter, generally a Berkovich shaped diamond having ramped load is applied vertically on the surface of component. As the indenter moves in the surface, firstly, elastic then plastic deformations occur, and hardness of material can be evaluated by measuring depth of residual indentation. A conventional microscope is unable to show the depths of indentations having dimensions up to 10% of coating thickness. Because of this reason during indentation, depth is measured constantly instead of post assessment after indentation.

Hardness and elastic modulus of the amorphous hydrogenated carbon and tetrahedral amorphous carbon coating were determined through nano-indenter (TI 750 UBI, Hysitron, Inc.). A Berkovich indentor was used, and depth control function was used. It is recommended that the indent depth should be less than 10 % of coating thickness, this is to avoid the influence of the substrate (Austin, 2014). As coating thickness was around 1.3-1.6 μm, therefore, indent depth was kept at 80 nm. A load of 3 N for indentation. In order to obtain a statistical representation, 10 indentations were performed for each sample. Similar procedure has been used in (Austin, 2014). After indentation, elastic modulus and hardness were obtained from the computer program integrated with the nano-indentor.

3.6 Tribological testing

A reciprocating test rig (Ducom instruments) with a ball-on-plate configuration was used to examine the friction and wear behavior of textured and un-textured DLC coatings. Figure 3.4 shows the schematic diagram of reciprocating test rig. Measurement of friction force during testing is also a common practice in such experimental works. Two main

reasons of measuring friction are: (1) coefficient of friction is an important parameter in all coating applications, and; (2) coating breakdown and lubrication conditions can be identified by dramatic variations of friction. Friction and wear are described as a function of a tribo-system (Kato, 2000).

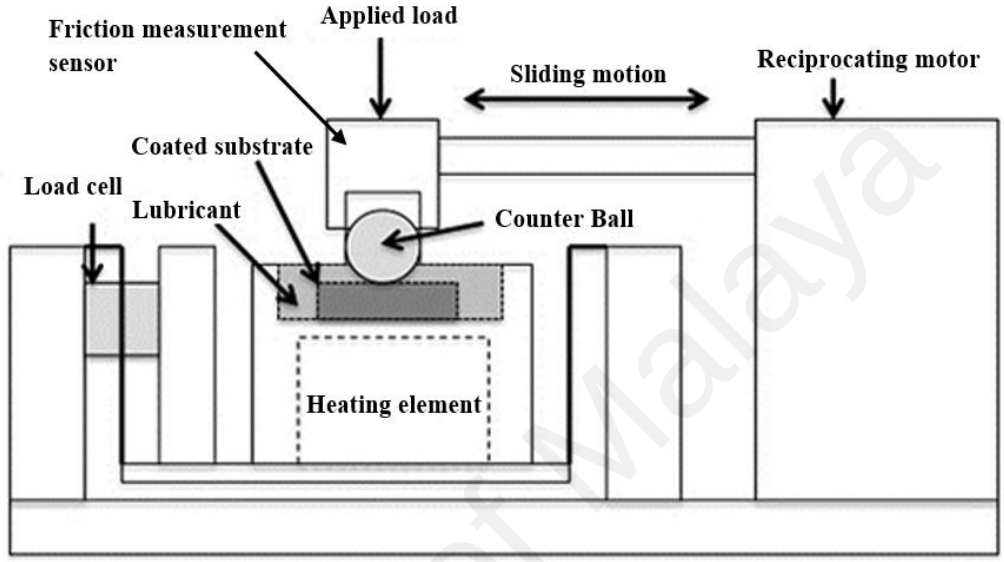

Figure 3.4: Schematic representation of reciprocating test rig (Zulkifli et al., 2013)

In order to identify the regime in which contact is operating, equation 3.1 for EHL regime by Dowson and Higginson was used (Mistry et al., 2011; Winer & Peterson, 1980).

$$\frac{h_{min}}{R'} = 1.79\left(\frac{U\eta_0}{E'R'}\right)^{0.68}(\alpha E')^{0.49}\left(\frac{w}{E'R'^2}\right)^{-0.073} \quad 3.1$$

Where h_{min} is representing minimum thickness of film (m). Symbol U shows the entraining surface velocity (m/s), given as $U = \frac{U_a + U_b}{2}$, where U_a denotes the velocities of counter ball, and U_b refers to the velocities of plate. Symbol η_0 indicates the viscosity of lubricant at atmospheric pressure (Pa.s). Symbol E' represents reduced elastic modulus (Pa) found through equation $\frac{1}{E'} = \frac{1}{2}\left(\frac{1-v_a^2}{E_a} + \frac{1-v_b^2}{E_b}\right)$, where ν is Poisson's ratio and E_a and

E_b represents the elastic modulus for corresponding ball and plate specimens. Symbol R' denotes reduced radius of curvature (m) for a ball on flat configuration, such that $\frac{1}{R'} = \left(\frac{1}{R_{ax}} + \frac{1}{R_{ay}}\right)$, where R_a is the radius of curvature for x and y direction. α is the pressure-viscosity coefficient (m^2/N) of lubricant, given as equation $\alpha = (0.6 + 0.965 \log_{10} \eta_0) \times 10^{-8}$. Symbol 'W' is representing applied normal load (N).

Lubrication regime was determined by fluid film thickness parameter 'λ' (Equation 3.2). Fluid film thickness parameter 'λ' is defined as the ratio of fluid film thickness 'h' and surface roughness 'σ'. Equation 3.3 provides composite surface roughness, where σ_1 and σ_2 are root mean square roughness of interacting surfaces. In order to identify the regime, value of 'λ' should be as follows:

1. If the value of λ is less than 1, boundary lubrication is present.
2. If the value is $1 \leq \lambda \leq 3$, mixed or elastohydrodynamic lubrication exists.
3. If the value λ is greater than 3, hydrodynamic lubrication is present.

$$\lambda = \frac{h_{min}}{\sigma} \quad 3.2$$

$$\sigma = \sigma_1^2 + \sigma_2^2 \quad 3.3$$

Before each test was performed, the ball and the DLC coated plate were cleaned with acetone in an ultrasonic bath. After the test was conducted, the samples were cleaned with *n*-heptane and stored in desiccators until surface characterization.

After the tribological testing, volume loss of steel balls was determined by mass loss method. After the removal of the tribo-layers (if any), the wear rate was calculated by V = k.F.s (Archard equation), where symbol V is the wear volume, symbol k is the specific

wear rate coefficient, symbol F is the normal load and symbol s is the total distance travelled.

3.6.1 Lubricants used for tribological testing

Polyalphaolefin (PAO) and palm based TMP ester was used for tribological testing. PAO was obtained from INEOS Pvt. Ltd. The palm based TMP ester was obtained from University Putra Malaysia (UPM). Palm based TMP ester was produced using transesterification of palm oil methyl ester. The procedure for the production of palm based TMP ester can be found in our research group's previous article (Zulkifli et al., 2014). The viscosity of obtained PAO and TMP at 40 °C was 65.1 and 40.01 cst respectively.

In boundary lubrication conditions, the micro asperities of the surfaces are in contact; that is why the rheological properties such as viscosity do not play an important role in tribological characteristics. In the boundary lubrication regime, the interaction between friction surfaces and interactions of friction surfaces and lubricant additives dominated the tribological behavior (Hironaka, 1984). As in this research work boundary lubrication was considered and lubricants without additives were used, therefore, the variation in friction and wear behavior is mostly governed by micro textures and coating type.

3.7 Characterization techniques

3.7.1 Profilometer

Surface roughness of ball and plate was measured with Veeco Dektak 150 profilometer. It is a surface profilometer, which uses contact profilometer technology to take measurements of surface topography and roughness.

3.7.2 Scanning electron microscopy (SEM)

A scanning electron microscope (SEM) (HITACHI, Model No. TM3030) operated at 10 kV, was used for wear track investigation. Scanning electron microscopy (SEM) solves many issues encountered in optical microscopy. In SEM, electron beam is bombarded on the surfaces, and images are generated by collecting emitted electromagnetic radiations. Electron gun is used to generate the electron, which is directed towards a specific point of sample surface, after passing through a number of electromagnetic lenses (Handbook for Analytical Methods for Materials, 2014). The wavelength of electron beams is shorter than reflected light, so electron microscopy has greater resolution compared to optical microscopy. Maximum theoretical resolution that can be achieved in SEM is less than 1 nm. However, spot size of the beam (area which is affected by electrons) limits the practical resolution (Handbook for Analytical Methods for Materials, 2014).

3.7.3 Energy Dispersive X-Ray spectroscopy (EDX)

Energy dispersive X-ray spectroscopy (HITACHI, Model No. TM3030) has been employed for identification of chemical composition of DLC coatings after tribological testing. EDX characterizes the x-rays emitted from the surface bombarded with electron beams. When high-energy electrons strike the targeted atom, inner shell electrons are ejected leaving a vacant space called electron hole. An outer shell electron of higher energy fills this hole, and energy is released in the form of x-ray (Handbook for Analytical Methods for Materials, 2014). As the difference of energy between shells of an atom can be quantized by the energy of emitted x-ray, therefore, these rays can be used to characterize the element from which they are emitted.

3.7.4 Raman Spectroscopy

Raman spectra was collected with an InVia Raman microscope (Gloucestershire, United Kingdom) with laser wavelength of 514 nm. A 10% laser power was used to minimize the influence of the substrate in the measurements. Three Raman measurements were taken for each sample to present a statistical representation of results so that the inaccuracies resulting from peak fitting could be minimized.

In Raman's spectroscopy, light is used to extract structural information of materials using Raman's effect. Raman spectroscopy is a standard technique for characterizing the carbon-based materials. When a light beam strikes the carbon substances, large number of photons gets elastically scattered and no energy shift is observed. However, some molecules of samples are excited by a small ratio of striking photons, and thus they are scattered inelasticity. Raman effect can be described briefly as the change in the level of energy exhibited by inelasticity scattered light. These energy shifts occur due to atomic arrangement of complex carbon structures (Ferraro, 2003). In Raman's spectrum, intensity of scattered light is plotted against the energy. In case of amorphous carbon, Raman spectra are specified by peak centered around D band (1300-1380 cm-1), and peak centered around G band (1520-1580 cm^{-1}). The D band is linked to breathing mode of sp^2 sites only for carbon chains, while stretch vibrations of any pair of sp^2 sites derive the G band. Structural information from Raman's spectra can be extracted by following general rules. The shift in the G peak and increase in the I_D/I_G ratio indicates an increase as the sp^2 fraction in the DLC film (Casiraghi et al., 2005; Ferrari & Robertson, 2000). Deconvolution of the Raman spectra into D and G peaks was conducted using licensed version of OriginPro 8.5.1 software. This software uses Gaussian function to fit peaks, which is present under multiple peak fitting tab.

3.7.5 Atomic force microscopy (AFM)

Atomic force microscopy (Q-Scope^{TM} 250/400, AMBIOS technology) was used to further analyze the wear track surface morphology. AFM test was performed to measure the changes in surface roughness of samples after tribological testing. The AFM scan was conducted for 25 μm × 25 μm area of the wear track.

In AFM, a micro scale cantilever is drawn across the surface of sample; it is usually done by using silicon and a tip radius of nanometers scale. When tip comes in close contact with the surface of samples, surface forces displace it. A laser is spotted at a particular angle on the rear surface of cantilever and motion of reflected laser spot is observed on photodiode arrays to determine the displacement. A very high atomic level resolution is achieved by controlling the position of probe with the help of piezoelectric actuators. A three-dimensional image of surface geometry can be built by quantifying the displacement of cantilever (Handbook for Analytical Methods for Materials, 2014). AFM is normally adopted for scan areas of small sizes.

CHAPTER 4: RESULTS AND DISCUSSION

4.1 Coating and lubricant properties

4.1.1 Hardness and Elastic Modulus

Hardness and elastic modulus of the amorphous hydrogenated carbon and tetrahedral amorphous carbon coating were determined through nano-indentation testing. Nano hardness and elastic modulus of DLC coatings can be seen in Table 4.1. Generally amorphous hydrogenated carbon films exhibit hardness of 15 to 50 Gpa, whereas tetrahedral amorphous carbons are harder with hardness range of 30-80 Gpa (Hauert, 2004). In this study, tetrahedral amorphous carbon coating showed higher hardness compared to be amorphous hydrogenated carbon coating. The higher hardness of tetrahedral coating can be related to higher sp^3 content (Bewilogua & Hofmann, 2014; Robertson, 1991; Ronkainen & Holmberg, 2008). Hardness/elastic modulus (H/E) ratio was calculated in order to understand the wear behavior of coatings. As H/E ratio is an indication of wear resistance of a coating (Austin, 2014). The H/E ratio was 0.12 and 0.14 for amorphous hydrogenated carbon and tetrahedral amorphous carbon coating.

Table 4.1: Hardness and elastic modulus of amorphous hydrogenated carbon and tetrahedral amorphous carbon coating

Coating	Hardness (GPa)	Elastic Modulus (GPa)	H/E Ratio
a-C:H	18.4 ± 2.2	158.5 ± 14.4	0.12
ta-C	40.5 ± 3.5	280.8 ± 18.2	0.14

4.1.2 Coating adhesion

Coating adhesion was investigated through a Rockwell C test. Ronkainen et al. used this test to evaluate amorphous hydrogenated and tetrahedral amorphous carbon coating adhesion previously (Ronkainen et al., 1999). Amorphous hydrogenated carbon coated sample showed cracks whereas tetrahedral amorphous carbon didn't show any cracks (Figures 4.1 a and 4.1 b). Hydrogenated amorphous carbon coating and tetrahedral amorphous carbon coating showed excellent adhesion according to standard VDI 3198; thus, these samples can be classified as HF1.

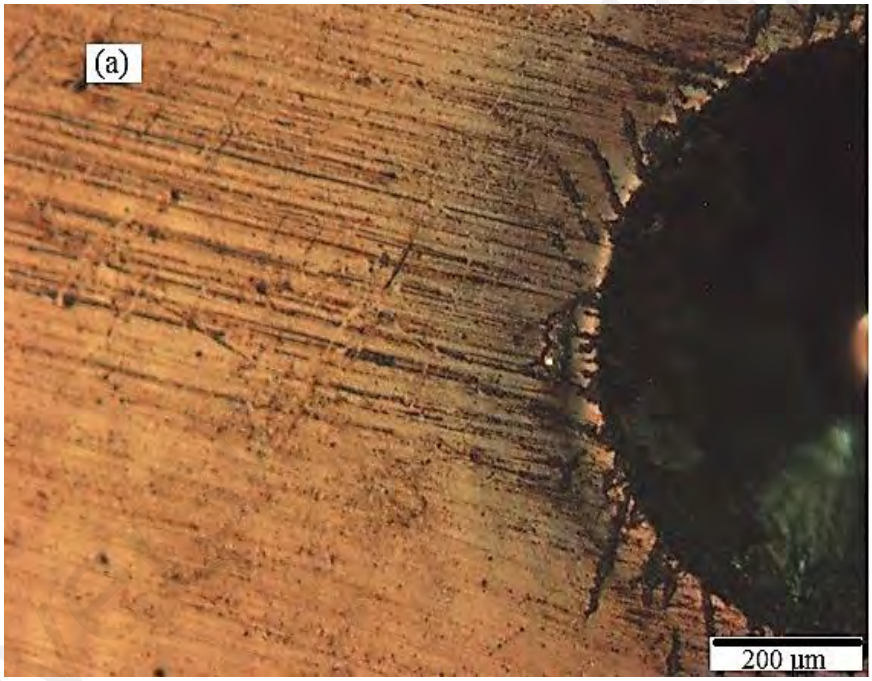

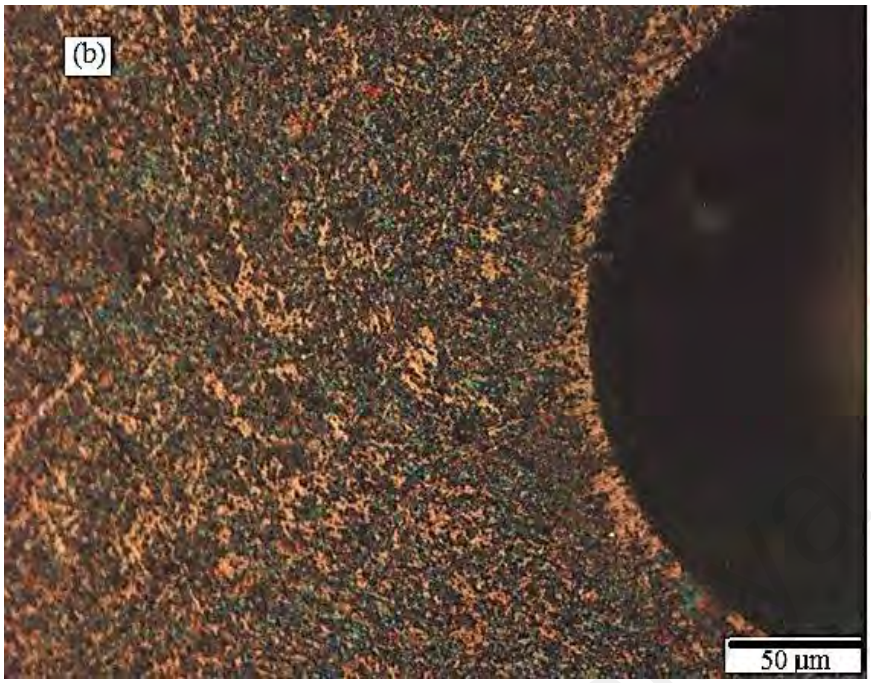

Figure 4.1 continued: The micrograph of the Rockwell C-indentation tests (a) amorphous hydrogenated carbon coating (b) tetrahedral amorphous coating

4.2 Effect of change in texture density, diameter and depth on tribological behavior of amorphous hydrogenated carbon coating

Effect of change in tribological behavior of amorphous hydrogenated carbon coating with dimple densities, diameters and depths was conducted using samples shown in Figure 4.2 and Figure 4.3. Figure 4.2 shows the SEM images of various dimple densities and diameters, whereas Figure 4.3 shows the two-dimensional profiles of various dimple depths.

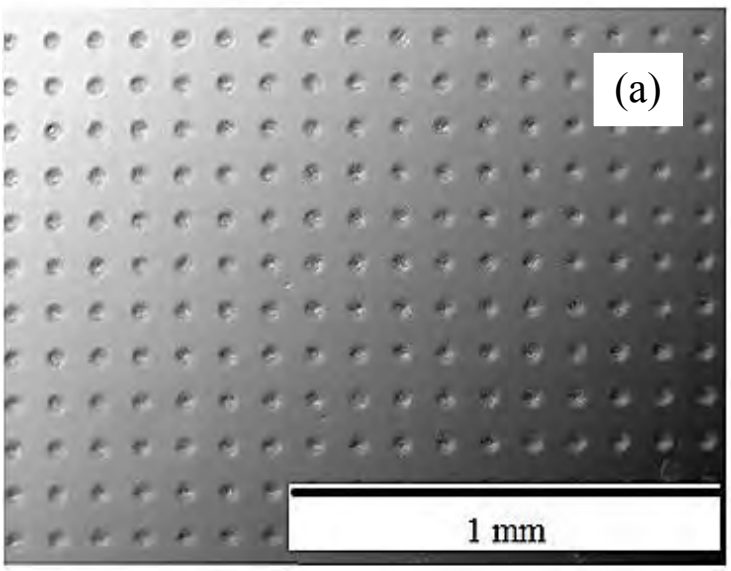

Diameter = 50 µm

Density = 30 %

Depth = 6 µm

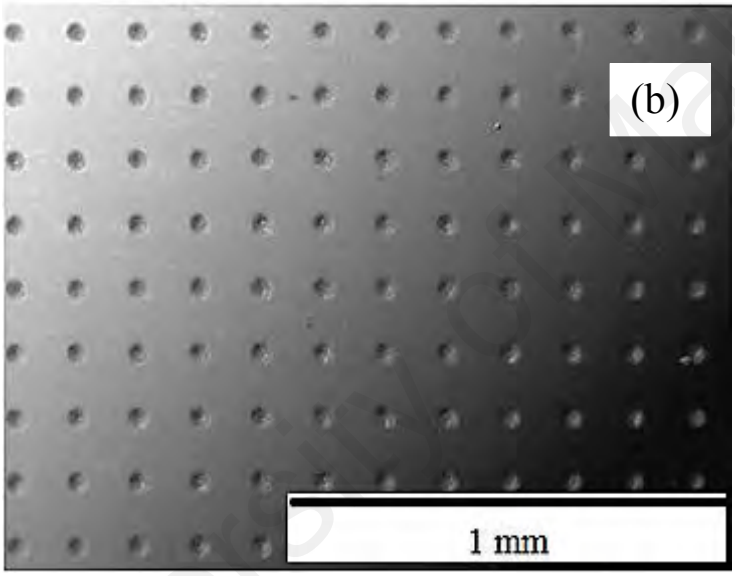

Diameter = 50 µm

Density = 20 %

Depth = 6 µm

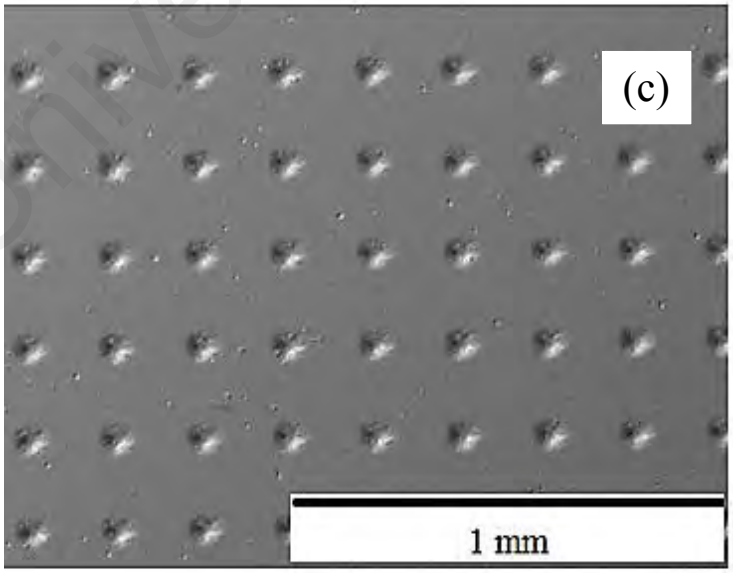

Diameter = 50 µm

Density = 10 %

Depth = 6 µm

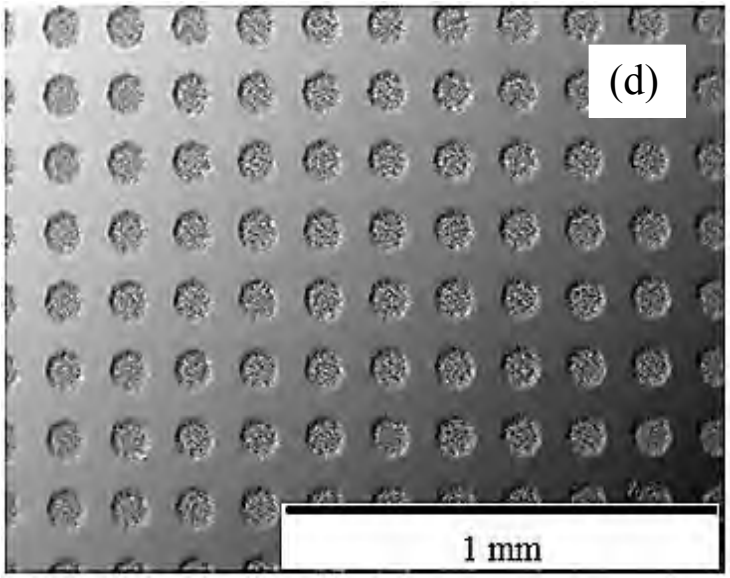

Diameter = 100 µm

Density = 30 %

Depth = 6 µm

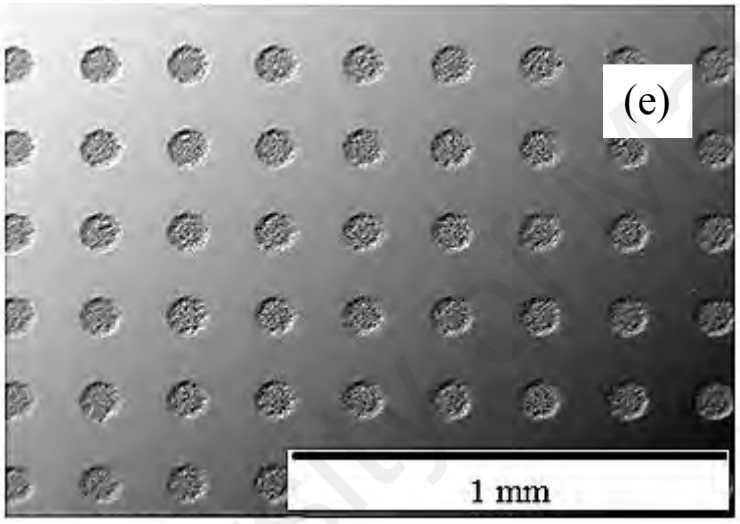

Diameter = 100 µm

Density = 20 %

Depth = 6 µm

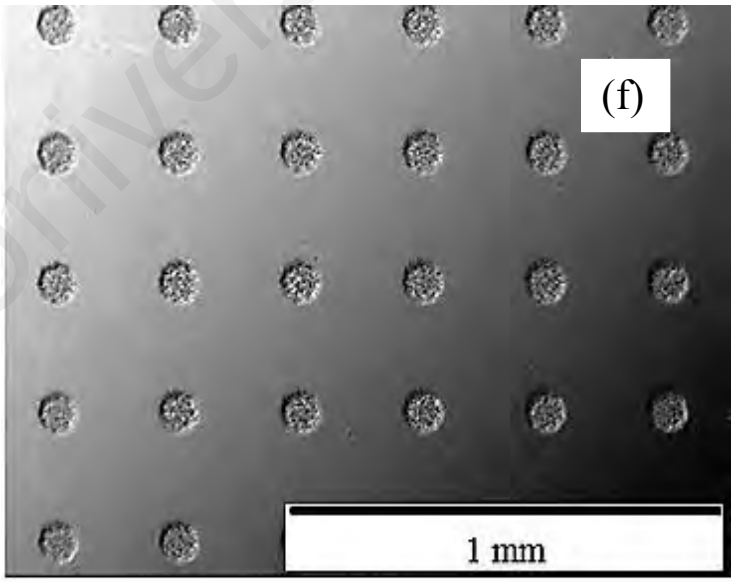

Diameter = 100 µm

Density = 10 %

Depth = 6 µm

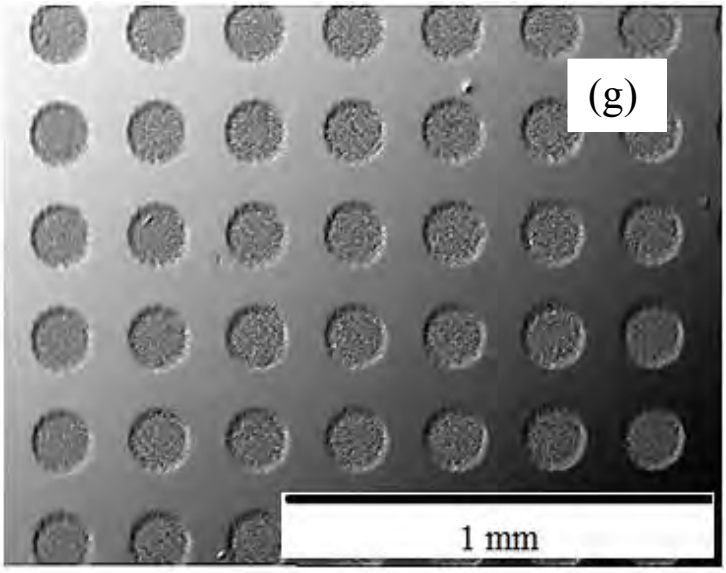

Diameter = 150 µm

Density = 30 %

Depth = 6 µm

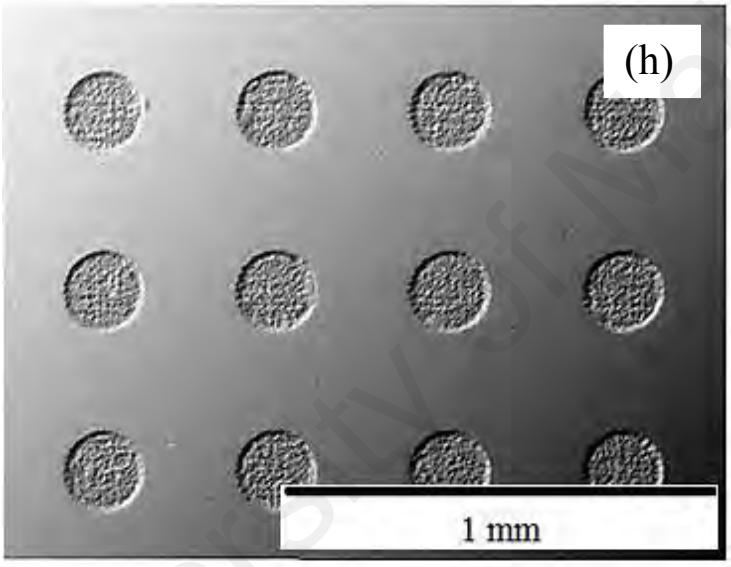

Diameter = 150 µm

Density = 20 %

Depth = 6 µm

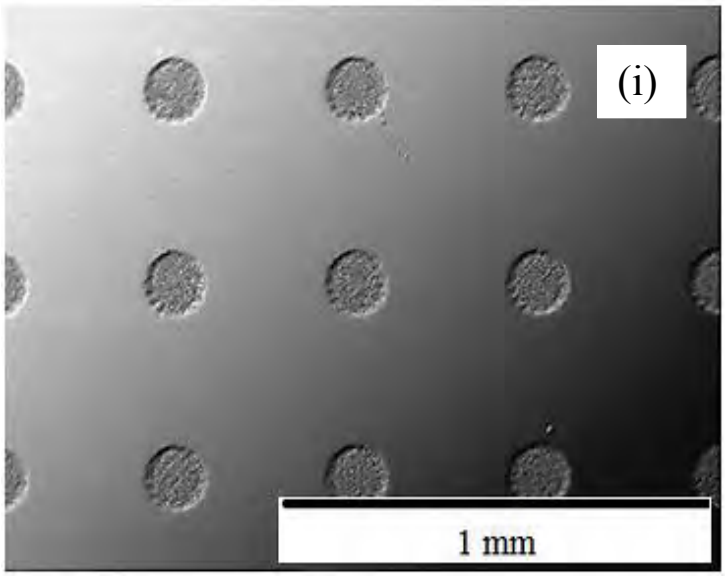

Diameter = 150 µm

Density = 10 %

Depth = 6 µm

Figure 4.2 continued: SEM topographical images of amorphous hydrogenated carbon coated textured samples (a) Dn30Di50Dp6, (b) Dn20Di50Dp6, (c) Dn10Di50Dp6, (d) Dn30Di100Dp6, (e) Dn20Di100Dp6, (f) Dn10Di100Dp6, (g) Dn30Di150Dp6, (h) Dn20Di150Dp6 and (i) Dn10Di150Dp6

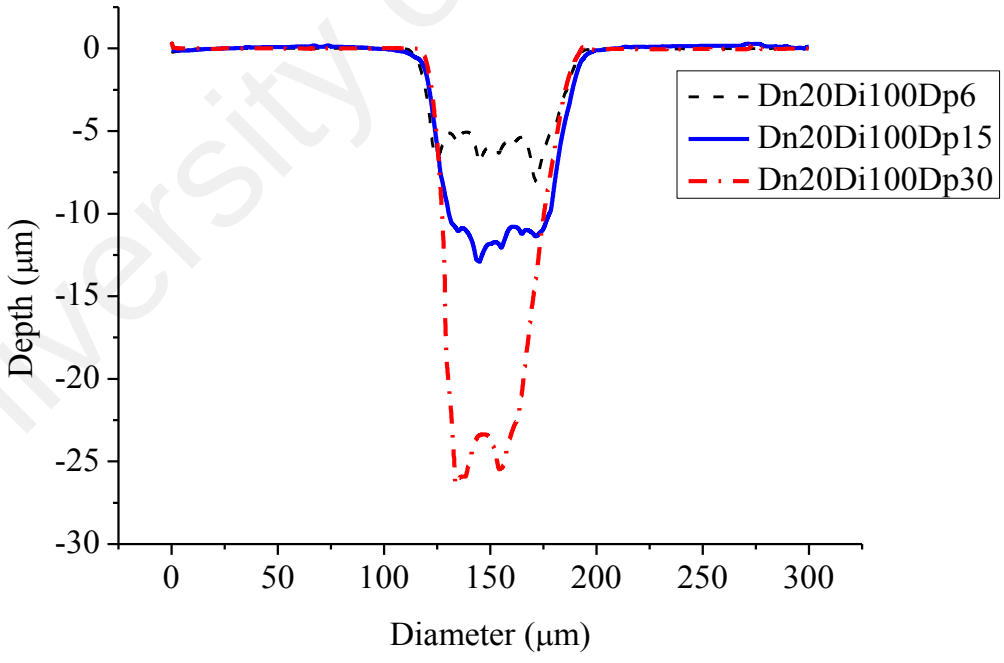

Figure 4.3: 2-dimensional profiles of amorphous hydrogenated carbon coated textured samples with different dimple depths

4.2.1 Friction and wear behavior

Figure 4.4 shows the coefficient of friction behavior of un-textured and textured amorphous hydrogenated carbon coated samples as a function of reciprocating sliding time. The average coefficient of friction values is shown in Figure 4.5. Average coefficient of friction was taken from 1600 seconds. Coefficient of friction is minimum at 30 % dimple density compared to 10 % density for all combinations of diameters and depths. In the case of 20 % dimple density, most of the dimple diameters and depth's combination showed the higher coefficient of friction than 30 % and 10 % dimple density except for the sample Dn20Di100Dp6. Sample Dn20Di100Dp6 yielded the lowest average coefficient of friction of 0.084 among all the tested samples, whereas a sample Dn20Di150Dp30 showed the highest coefficient of friction of 0.1406. Un-textured sample a-C:H-Untex showed the average coefficient of friction of 0.11. Some samples in various dimple densities showed a lower average coefficient of friction than a-C:H-Untex. Dimple's diameter of 100 μm showed the lower average coefficient of friction than 50 and 150 μm at all densities tested. With respect to dimple depth, 6 μm showed the lower average coefficient of friction regardless of dimple diameters and densities. The results indicate that the dependence of frictional behavior is on appropriate combination of dimple density, diameter and depth.

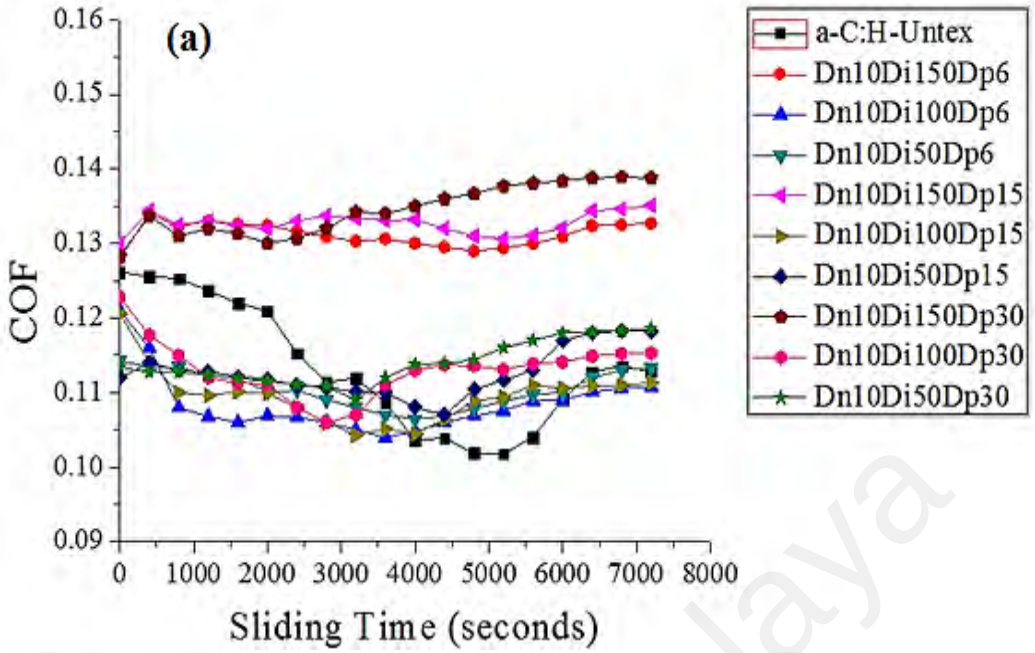

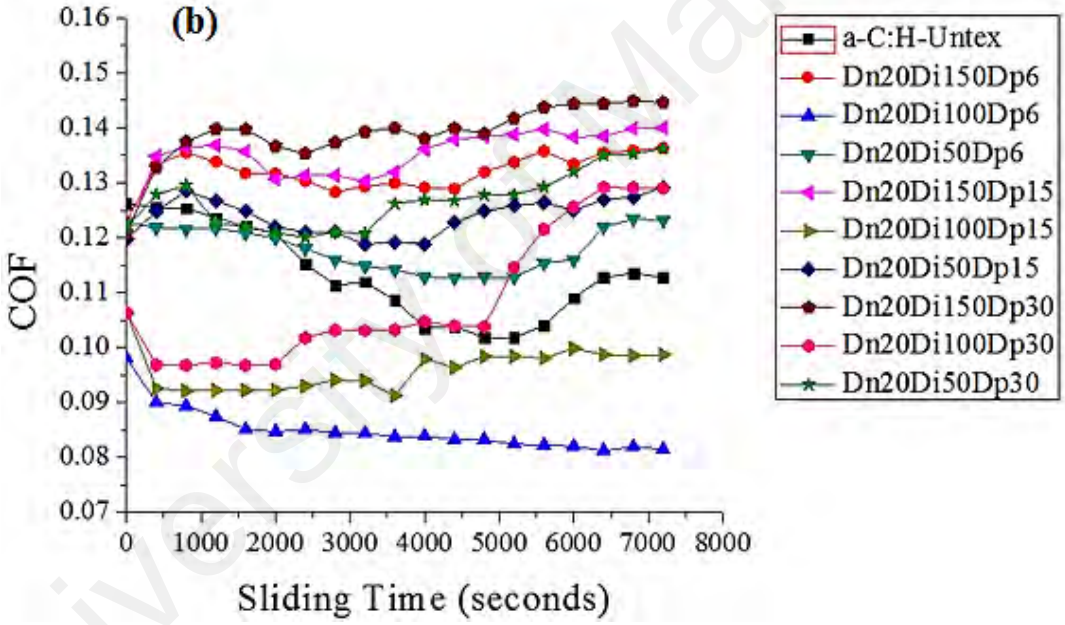

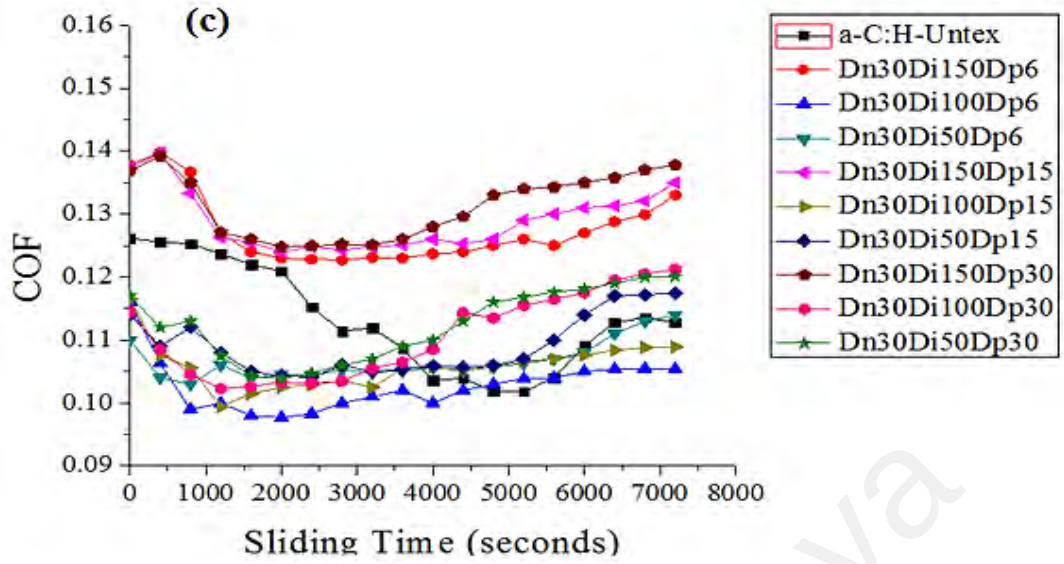

Figure 4.2 continued: Change in coefficient of friction of amorphous hydrogenated carbon coated samples with time (a) dimple density 10 %, (b) dimple density 20 % and (c) dimple density 30 %

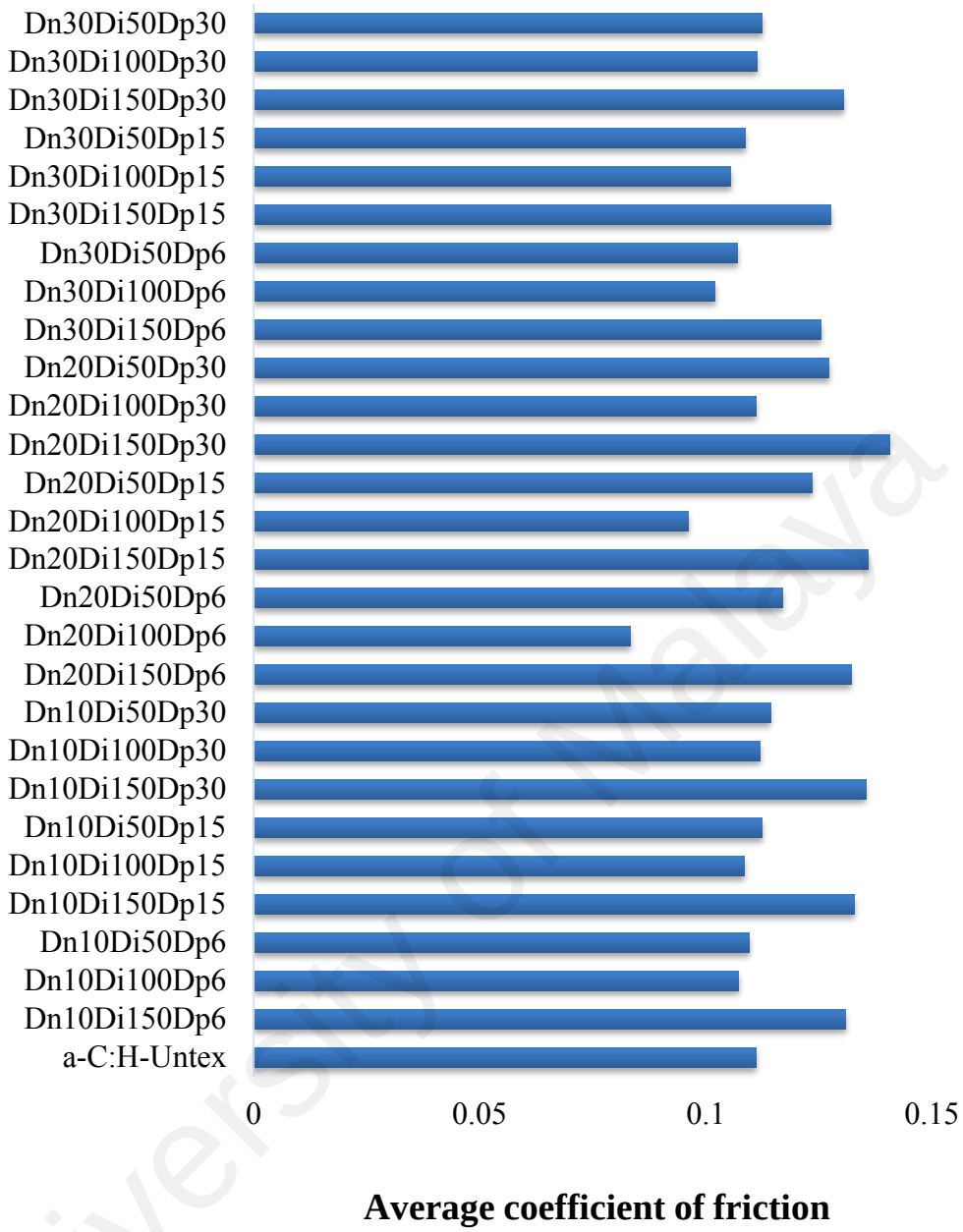

Figure 4.3: Average coefficient of friction of amorphous hydrogenated carbon coated textured/un-textured samples

Figure 4.6 shows the wear coefficient of various samples at the end of test. The wear trend was nearly opposite to the average coefficient of friction trend. Dimple's density of 30 % showed the higher wear coefficient than 20 % and 10 % density. Dimple's density of 20 % showed the lower wear coefficient than 10 % and 30 %. Sample Dn20Di100Dp6

showed the lowest and Dn30Di150Dp30 showed the highest wear coefficient. Dimple's diameter of 100 µm showed the lowest wear coefficient at all dimple densities tested. If the diameter exceeded 100 µm, wear performance degraded (as shown in Figure 4.6). The wear results also indicated that when the depth was increased from 6 - 30 µm (for various densities and diameters), the wear coefficient increases. The wear coefficient results also indicate that wear resistance of the amorphous hydrogenated carbon coating can be improved with an optimum value of dimple parameters.

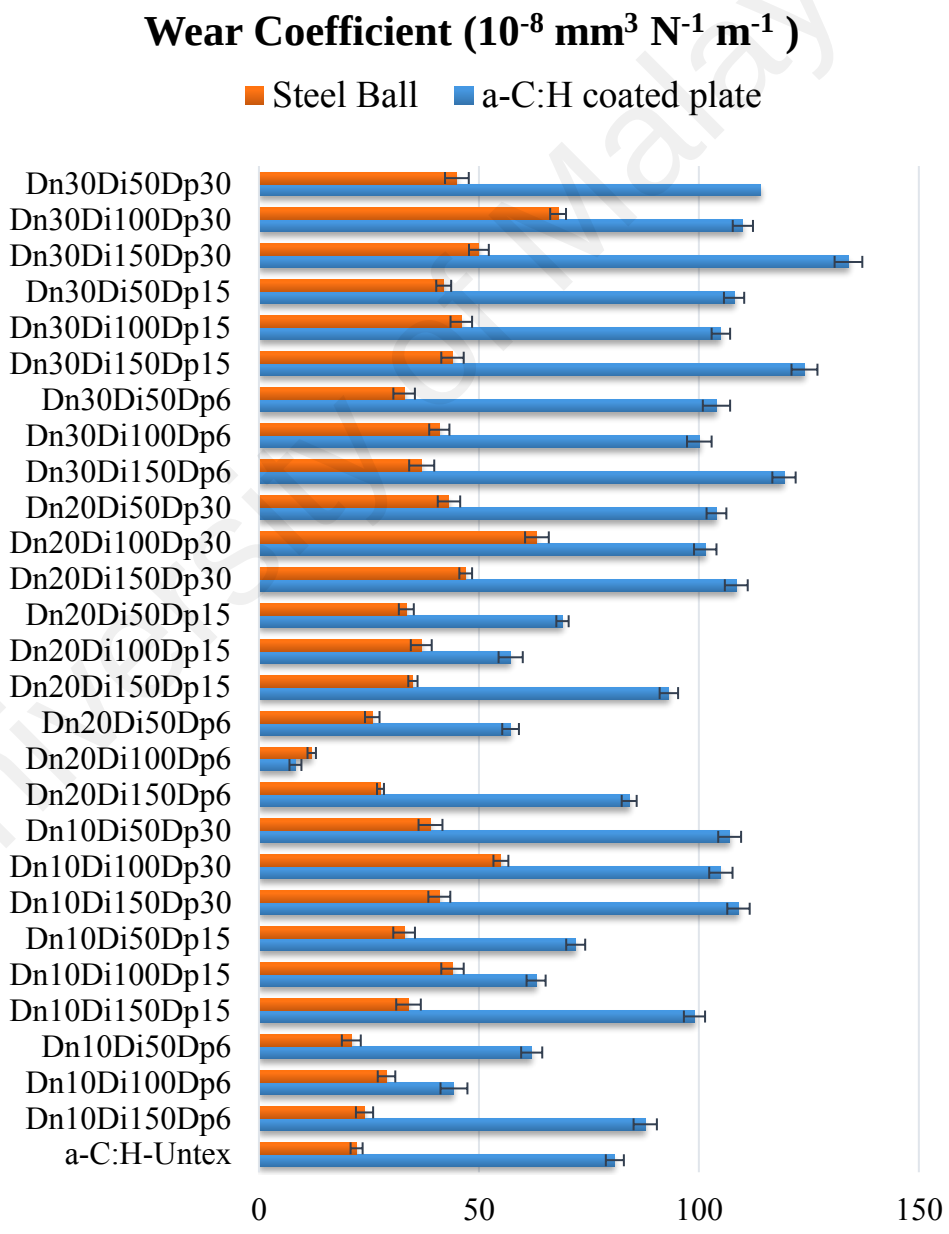

Figure 4.4: Wear coefficient of amorphous hydrogenated carbon coated textured/un-textured samples after tribological testing

The fluid film thickness ratio between the ball on flat contact calculated by using the Dowson and Higginson equation for elastrohydrodynamic lubrication (Mistry et al., 2011; Winer & Peterson, 1980) was found to be less than 1. The film thickness ratio is the ratio of minimum film thickness and composite surface roughness (Mistry et al., 2011; Winer & Peterson, 1980). When the film thickness ratio is lower than 1, the contact operates in boundary lubrication. Under the boundary conditions considered in the present study, the friction and wear variation has been thought to be only due to dimple density, diameter and depth variation. Due to the relative movement, the lubricant stored in the dimples can be drawn up, which facilitates enhancement in tribological performance (Amanov, et al., 2013). However, it was observed in the present study that this enhancement depends upon the selection of appropriate dimple diameter relative to the contact width, density and depth. The lower coefficient of friction of Dn20Di100Dp6 in the boundary regime can be attributed to the lubricant supplying and wear debris trapping ability of optimum dimple parameters. Reduction in coefficient of friction at particular dimple parameters due to lubricant reinforcement ability of textures has been noticed previously (Ding et al., 2010).

In the case of textured ceramic and steel materials (uncoated), Wakuda et al. found that with the increase in texture density from 7.5 % to 30 %, coefficient of friction increases (Wakuda et al., 2003). Whereas in our investigation it was observed that 30% density showed lower coefficient of friction than 10 % density. This difference can be due to graphitization phenomenon of DLC coated substrate. The effect of increase in graphitization with density and diameter is discussed in section 4.2.2.2.

At 20 % dimple density, when dimple diameter is changed and depth is kept at 6 μm, Dn20Di100Dp6 yielded the lowest coefficient of friction of 0.083, whereas sample

Dn20Di150Dp6 showed the highest average coefficient of friction of 0.132. Textured samples (Dn20Di150Dp6 and Dn20Di50Dp6) exhibited higher average coefficient of friction of 0.132, 0.117, respectively, compared with un-textured sample (a-C:H-Untex) with coefficient of friction of 0.111 (as shown in Figure 4.6). The samples where depth was kept at 15 μm and diameter was varied from 50-150 μm, sample Dn20Di100Dp15 showed lowest average coefficient of friction of 0.096. The samples Dn20Di150Dp15 and Dn20Di50Dp15 showed higher coefficient of friction of 0.136 and 0.124 compared to a-C:H-Untex. As the depth was further increased to 30 μm and diameter was varied from 50-150 μm, Dn20Di100Dp30 showed lower coefficient of friction of 0.111 compared to Dn20Di150Dp30 and Dn20Di50Dp30. Among all the samples tested at 20 % density, Dn20Di100Dp6 showed the lowest average coefficient of friction. The average coefficient of friction behavior shows that at an appropriate dimple diameter regardless of dimple depth value, reduction in coefficient of friction can be achieved. The results also show that increasing or decreasing dimple diameter from optimum value can have negative affect on coefficient of friction. At 10 and 30 % density, similar to 20 % density when dimple diameter is varied from 100 μm, coefficient of friction and wear coefficient increases.

The optimum dimple diameter depends on contact width-to-dimple diameter ratio (Vilhena et al., 2009). At a contact load of 100 N, Hertz contact width is approximately 270 μm. At an optimum dimple depth of 6 μm and density of 20 %, if the dimple diameter is much smaller (50 μm in the sample Dn20Di50Dp6) compared to contact width, the coefficient of friction behavior of textured sample is almost similar to sample a-C:H-Untex. An optimum dimple diameter relative to contact width for point contacts has been noted by Vilhena et al. (2006) in uncoated steel material investigation. Vilhena et al. (2006) suggested that contact load per unit area, coefficient of friction, and wear rate increase if dimple diameter and contact width are nearly similar, as in the case of sample

Dn20Di150Dp6; this may explain the increase in the coefficient of friction and wear rate as dimple diameter exceeds 100 μm.

In the case of samples, where dimple depth is changed by keeping density and diameter constant, the depth of 6 μm showed the lowest average coefficient of friction (Figure 4.5). The average coefficient of friction increases as dimple depth increases. Wear trend is similar to the average coefficient of friction trend. This increase in the coefficient of friction and wear is due to the change in dimple depth when diameter and density are held constant. At dimple density of 20 % and diameter of 100 μm (Figure. 4.4 b), at the start of the test, the three samples (Dn20Di100Dp6, Dn20Di100Dp15 and Dn20Di100Dp30) exhibited similar coefficient of frictions; as the test progressed, samples (Dn20Di100Dp15 and Dn20Di100Dp30) showed an increase in the coefficient of friction. In the case of sample Dn20Di100Dp30, a sudden increase in the coefficient of friction was observed at 2400 s (Figure. 4.4 b). In the case of sample Dn20Di100Dp15, this condition occurred after 3600 s. After 5000 s, the coefficient of friction of sample Dn20Di100Dp30 became unstable (Figure. 4.4 b). This instability can be due to metal-to-metal contact as amorphous hydrogenated carbon coating delaminated, this wear behavior will be discussed in section 4.2.2.1. Thus, a possible situation is that as the dimple depth increases, the deep dimples serve as micro traps of lubricant and remove the remaining oil from their vicinity, thus changing the lubrication regime from the boundary to be starved (Ryk et al., 2002). This abrupt increase in the coefficient of friction due to oil starvation is consistent with previous literature (Demas et al., 2005; Mishra & Polycarpou, 2011).

Tribological performance is decreased as dimple depth increases in non-conformal contacts in an elastrohydrodynamic regime (EHL) regime (Mourier et al., 2006). Mourier et al. found that an increase in dimple depth reduces local film thickness in an EHL regime

under rolling-sliding conditions. Moreover, lubricant film thickness may even collapse if dimples are very deep. By contrast, lubricant film thickness can be significantly enhanced if dimples are shallow; thus, reducing friction and wear (Mourier et al., 2006). In this study, it was found that in the case of the boundary lubrication regime, an increase in dimple depth reduces the lubricant presence to such extent that contact becomes starved. Increasing in the coefficient of friction due to oil starvation has been noticed previously (Ryk et al., 2002). If the contact is starved, deep dimples become oil traps, which make the contact more starved; thus, increasing coefficient of friction (Ryk et al., 2002).

4.2.2 Various textured amorphous hydrogenated carbon coating characterization

4.2.2.1 SEM/EDX and AFM analysis

Figure 4.7 shows the SEM micrographs of the amorphous hydrogenated carbon coated samples. Sample Dn10Di100Dp6 and Dn30Di100Dp6 showed irregular delamination at the wear track whereas Dn20Di100Dp6 shows only polishing wear. Sample a-C:H-Untex also showed delamination at the wear track. EDX results can be seen in Table 4.2. Higher increase in atomic percentage of Fe and Cr can be observed in case of Dn10Di100Dp6, Dn30Di100Dp6 and a-C:H-Untex (Figures 4.7a, 4.7c and 4.7h). This indicates that delamination occurred due to which interlayer was exposed. Increase in atomic percentage of Cr has been observed in case of Dn20Di100Dp6 whereas small change in Fe was observed. The EDX elemental analysis also confirms that at 10 % and 30 % densities, delamination occurs whereas polishing wear occurs at 20 % density. The instability in the coefficient of friction trend with time for samples Dn10Di100Dp6 and Dn30Di100Dp6 (Figures 4.4 a and 4.4 c) can be due to delamination at the wear track, whereas a sample Dn20Di100Dp6 (Figure 4.4 b) showed the smooth and stable coefficient of friction trend due to only polishing wear.

Samples where dimple density and depth were kept at 20 % and 6 µm and diameter were changed from 50 - 150 µm; Dn20Di50Dp6 and Dn20Di150Dp6 showed irregular delamination at the wear track (Figures 4.7 d and 4.7 e). Additionally, abrasive wear marks can be observed at the wear track of Dn20Di50Dp6 and Dn20Di150Dp6 (Figures 4.7 d and 4.7 e). This behavior shows that if dimple density is optimum and dimple diameter is not optimum, wear particle capturing ability of textures is less. EDX elemental analysis of Dn20Di50Dp6 and Dn20Di150Dp6 show the higher increase in Fe and Cr compared to Dn20Di100Dp6. The instability in the coefficient of friction trend of Dn20Di50Dp6 and Dn20Di150Dp6 can be due to abrasive wear and coating delamination (Figures 4.4 a and 4.4 c).

Figures 4.7 b, 4.7 f, and 4.7 g show the SEM images of the amorphous hydrogenated carbon coated samples from various dimple depths at dimple density of 20 % and dimple diameter of 100 µm after friction testing. Sample Dn20Di100Dp15 (Figure 4.7 f) exhibited irregular coating delamination, whereas a sample Dn20Di100Dp30 (Figure 4.7 g) showed nearly complete coating delamination. Spallation and delamination are shown in the case of Dn20Di100Dp15. When the coating is present, but it is loosely bounded to the surface, the phenomenon is called spallation, where as in delamination the coating is removed from the surface. Spallation phenomenon comes before delamination. Once the adhesion of coating is gone, coating spalls. The EDX of the samples is listed in Table 4.2; Fe and Cr increased in the case of samples Dn20Di100Dp15 and Dn20Di100Dp30 compared to Dn20Di100Dp6. The abrupt increase in the coefficient of friction trend Dn20Di100Dp30 at 5000 s can be due to excessive coating delamination (Figure 4.4 b). SEM and EDX results indicate that depth of the dimples also has the profound effect on the wear behavior of amorphous hydrogenated carbon coating.

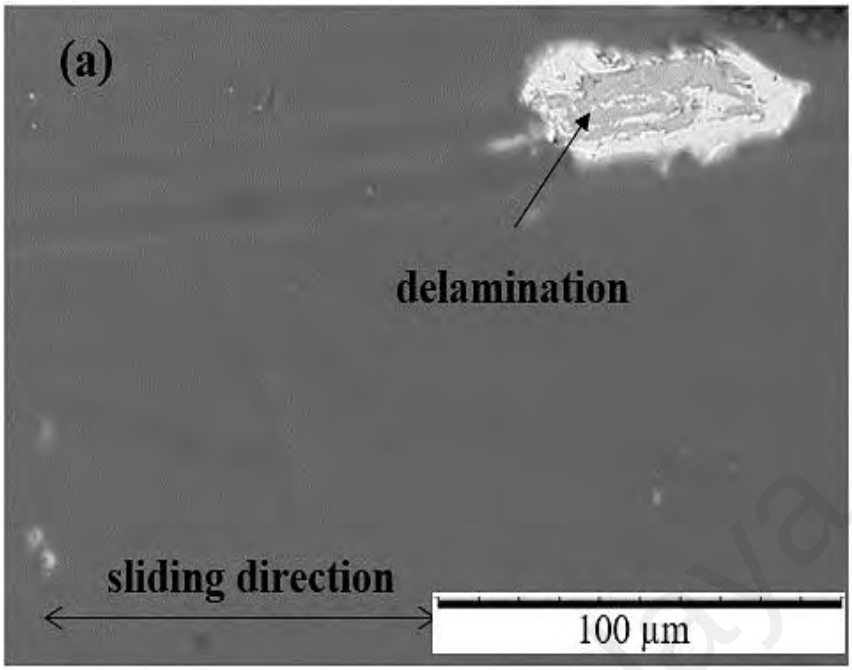

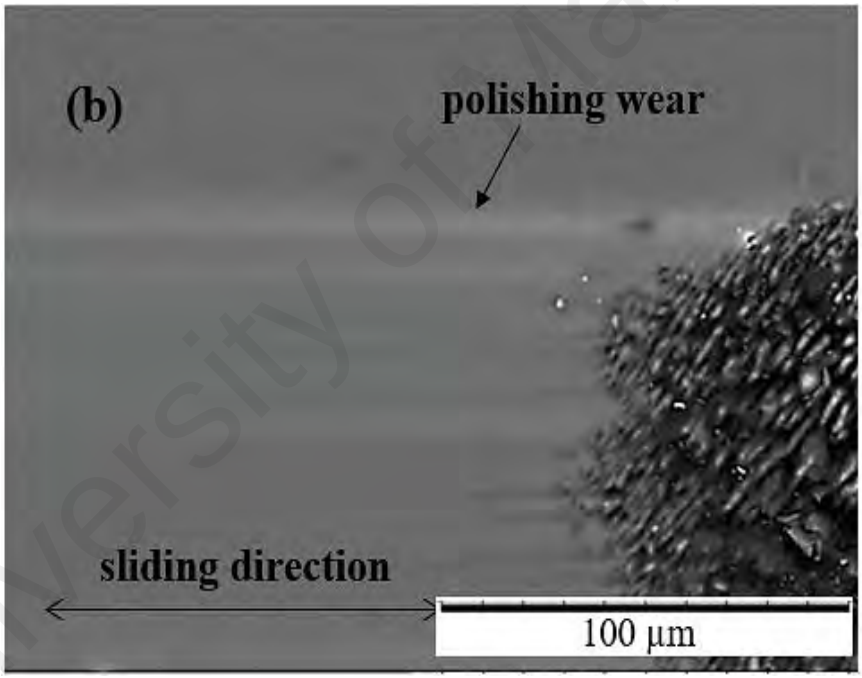

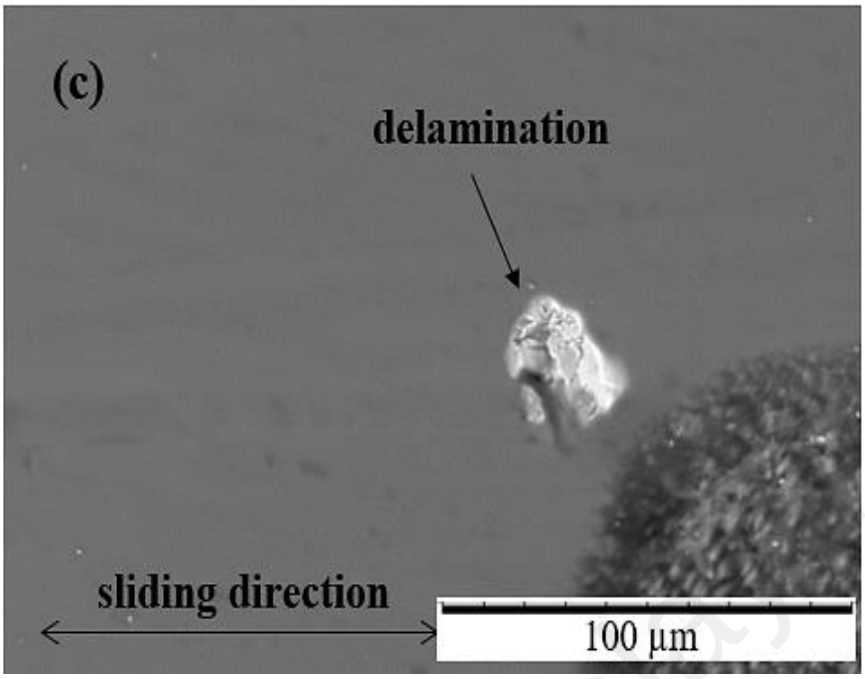
(c)
delamination
sliding direction
100 µm

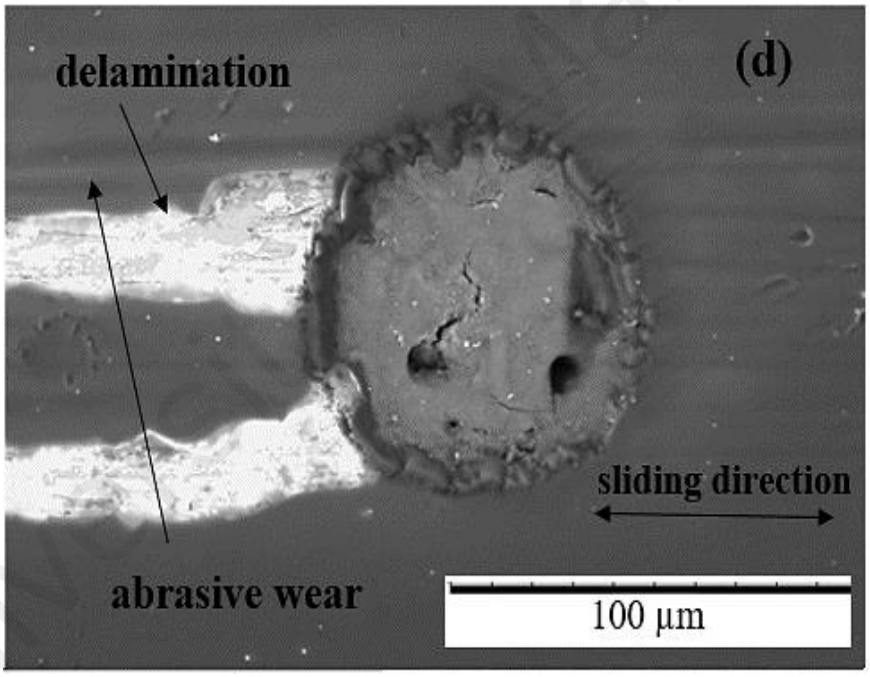
delamination
(d)
sliding direction
abrasive wear
100 µm

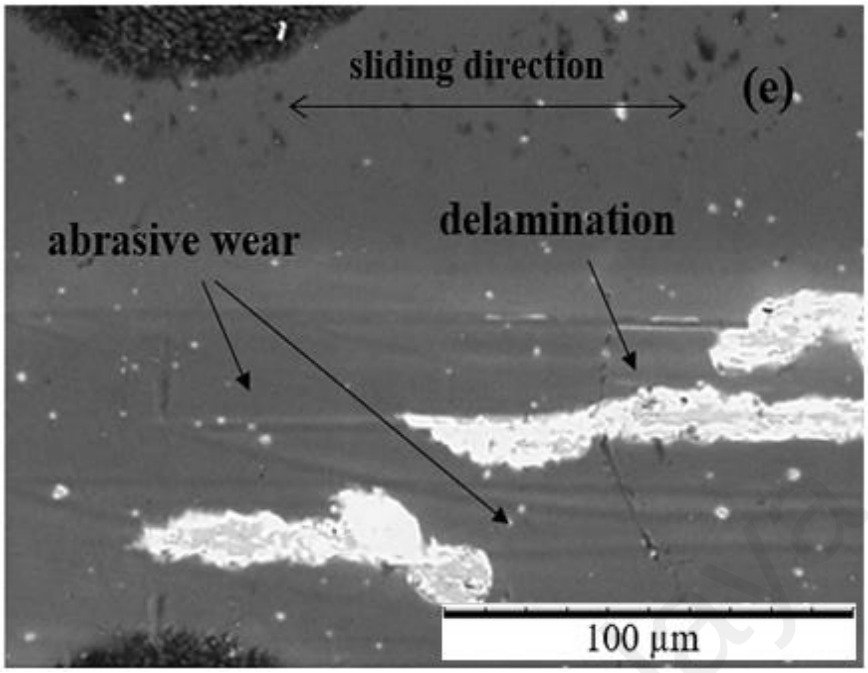
sliding direction
(e)
abrasive wear
delamination
100 µm

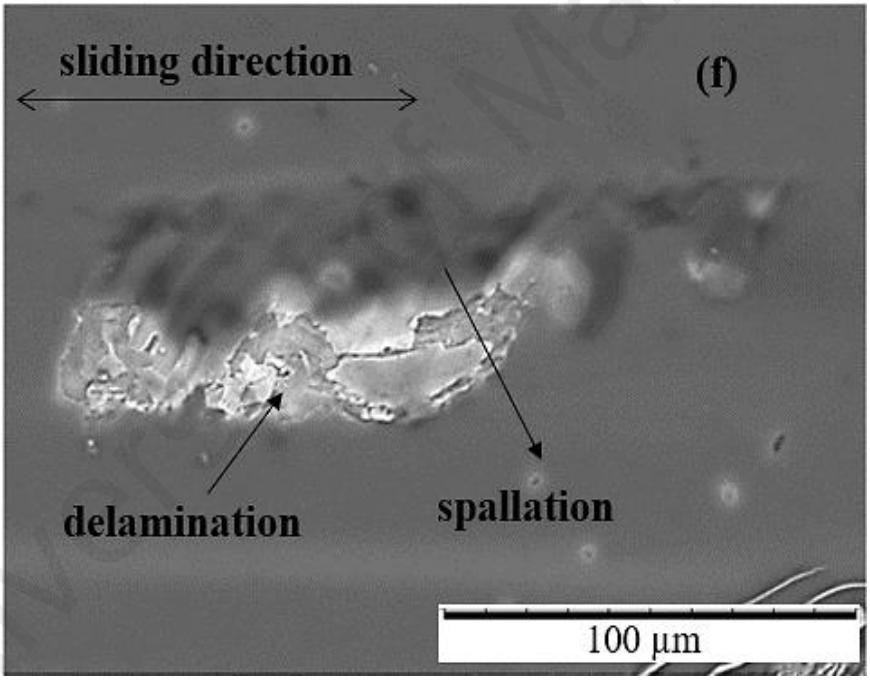
sliding direction
(f)
delamination
spallation
100 µm

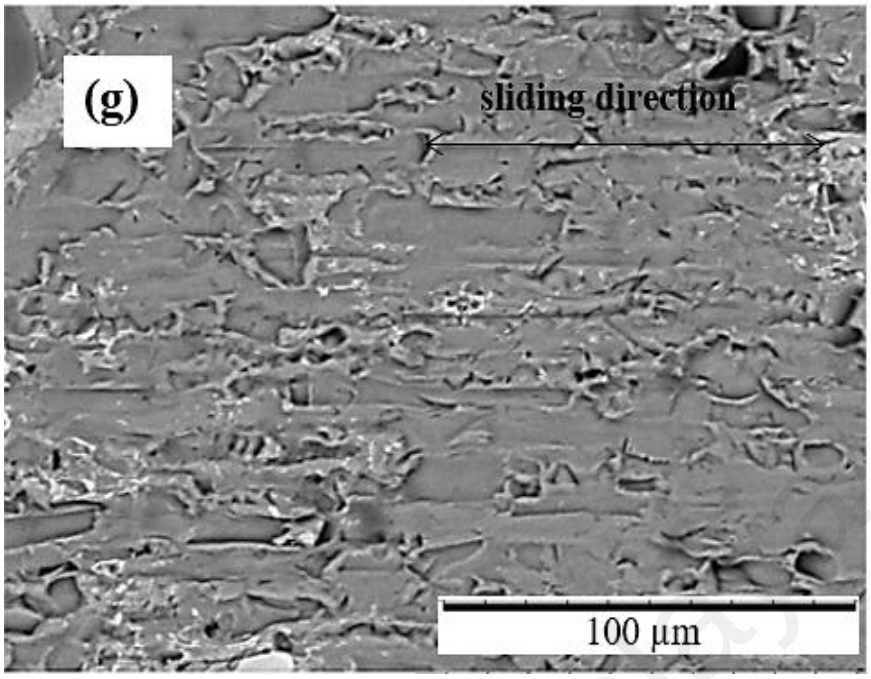

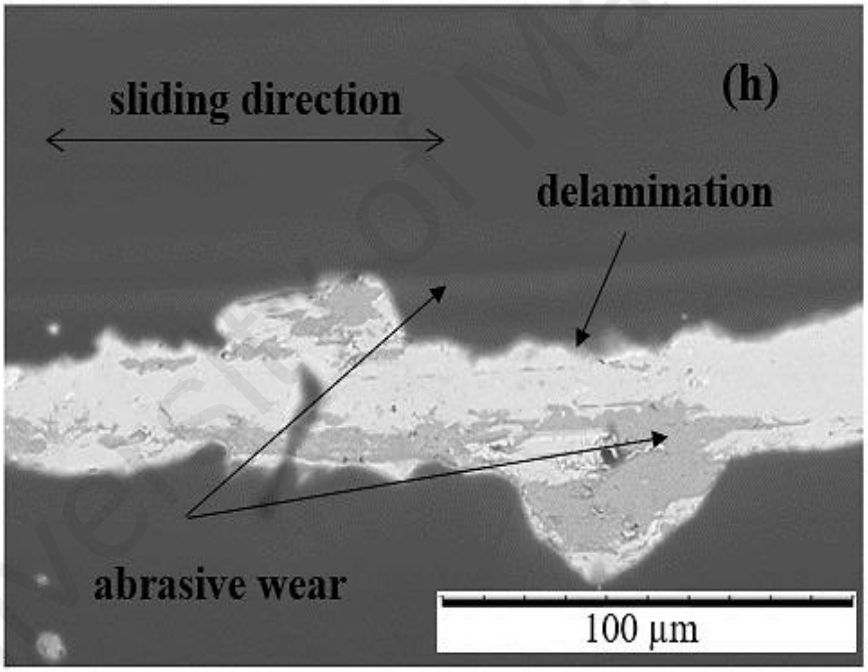

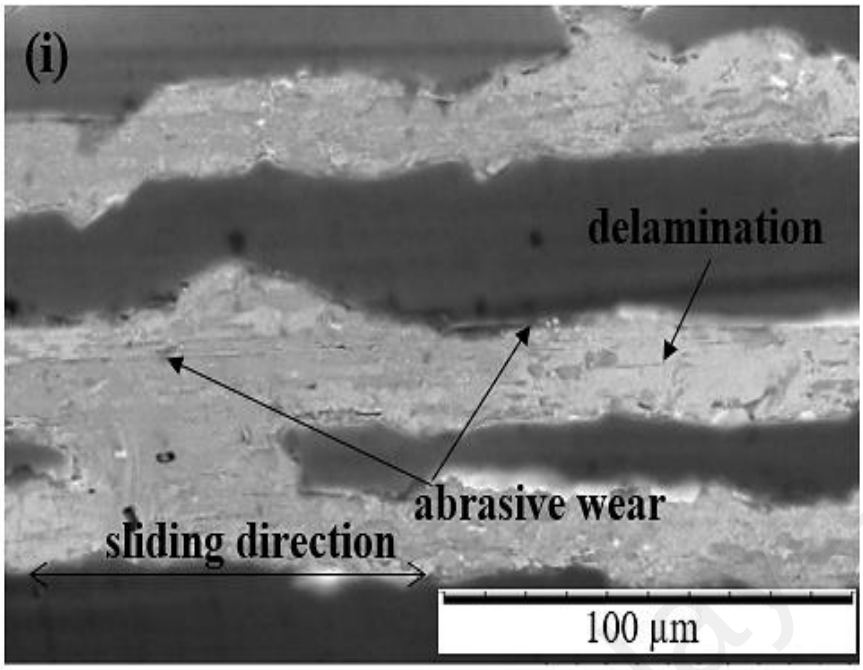

Figure 4.5 continued: SEM images of wear track after friction testing (a) Dn10Di100Dp6, (b) Dn20Di100Dp6, (c) Dn30Di100Dp6, (d) Dn20Di50Dp6, (e) Dn20Di150Dp6, (f) Dn20Di100Dp15, (g) Dn20Di100Dp30, (h) a-C:H-Untex and (i) Dn30Di150Dp6

Wear track surface profile was investigated through AFM imaging (Figure 4.8). Figure 4.9 shows the average surface roughness of un-textured sample and textured samples with varying dimple density, diameter and depth. The surface roughness of the polished sample was approximately 30-40 nm. Lowest average roughness was shown by 20 % dimple density compared to 10 % and 30 % density at 6 µm dimple depth and 100 µm diameter. However, sample with 30 % dimple density showed lower roughness than 10 % dimple density. The lower average roughness of 20 % density is due to polishing wear. This also represents that wear particle capturing ability was higher in this case. The morphological characteristics of wear track of sample Dn20Di100Dp6 (Figure 4.8 b) indicated that asperities were polished; thus, surface roughness was further reduced, and a smooth surface was obtained. The microgrooves in the case of sample Dn10Di100Dp6 (Figure 4.8 a) was more evident than Dn30Di100Dp6 (Figure 4.8 c). This phenomenon may be caused by the trapped wear particles that scratched the surface during sliding; this

has been observed previously (Amanov et al., 2013). The reason for this behavior shown by 10 % dimple density can be due to the higher distance between the dimples, which reduces the chance for capturing wear particles by the textures compared to 20 % and 30 % dimple density at 100 μm dimple diameter.

Figures 4.8 b, 4.8 d and 4.8 e shows the samples with various dimple diameters at 20 % dimple density. Lowest average roughness was shown by Dn20Di100Dp6 compared to Dn20Di50Dp6 and Dn20Di150Dp6 (Figure 4.9). The lower surface roughness indicates that polishing of surface roughness occurred. Indeed, the dimples of sample Dn20Di100Dp6 can remove wear particles from the wear track to prevent further wear; by contrast, other samples with various dimple diameters failed to efficiently remove wear particles.

Figures 4.8 b, 4.8 f, and 4.8 g showed AFM images samples from different dimple depths. Sample Dn20Di100Dp6 shows the lower average surface roughness than samples Dn20Di100Dp15 and Dn20Di100Dp30 (Figure 4.9). The surface morphological characteristics of samples Dn20Di100Dp15 and Dn20Di100Dp30 (Figures 4.8 f and 4.8 g) show lower abrasive wear marks than those of sample a-C:H-Untex (Figure 4.8 h). This result indicated that the wear particle capturing ability of dimples sustained by maintaining an optimum dimple density and diameter, even by increasing dimple depth. Thus, the mode of wear in the case of samples Dn20Di100Dp6, Dn20Di100Dp15 and Dn20Di100Dp30 is mainly adhesive wear.

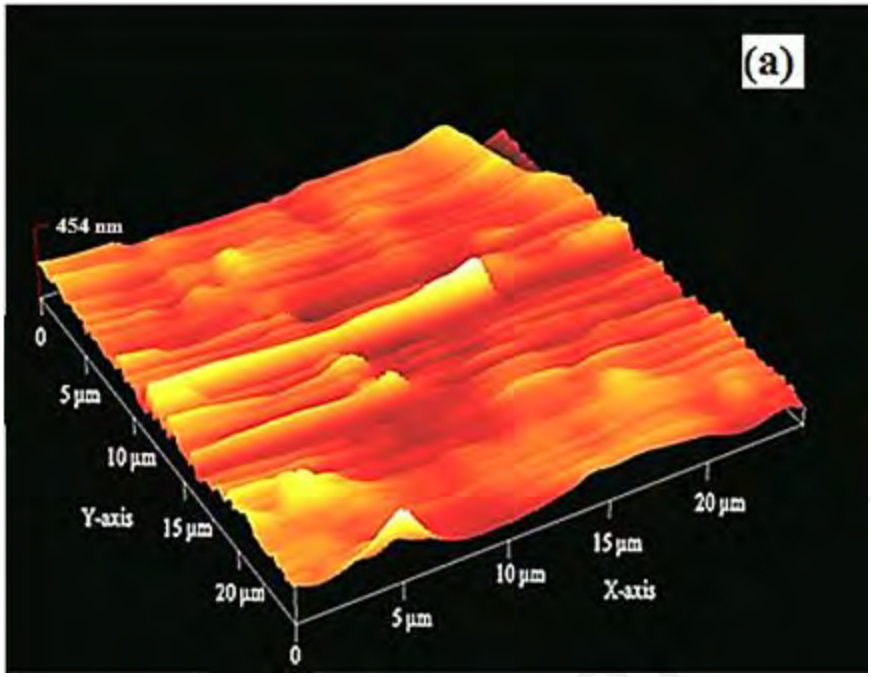

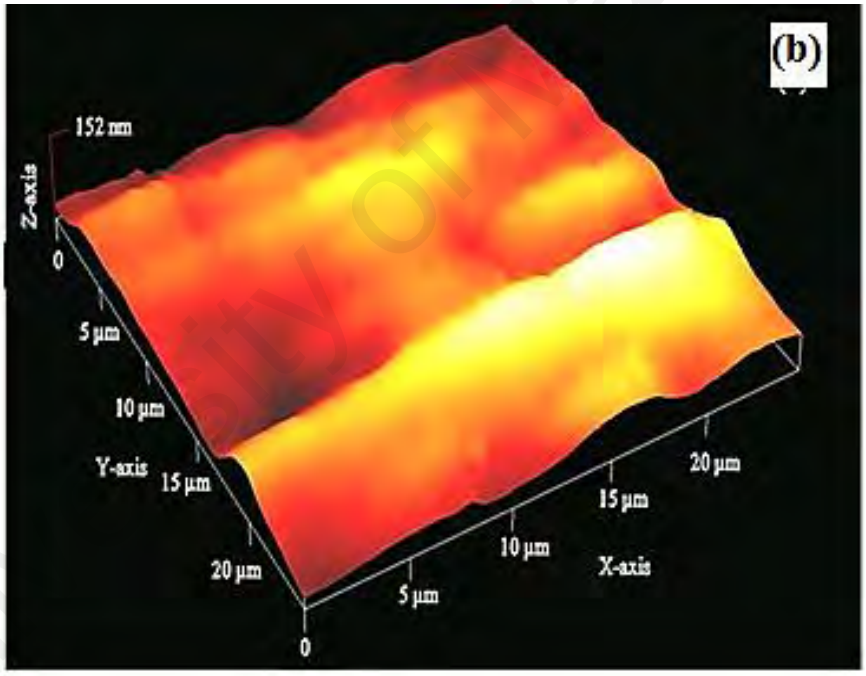

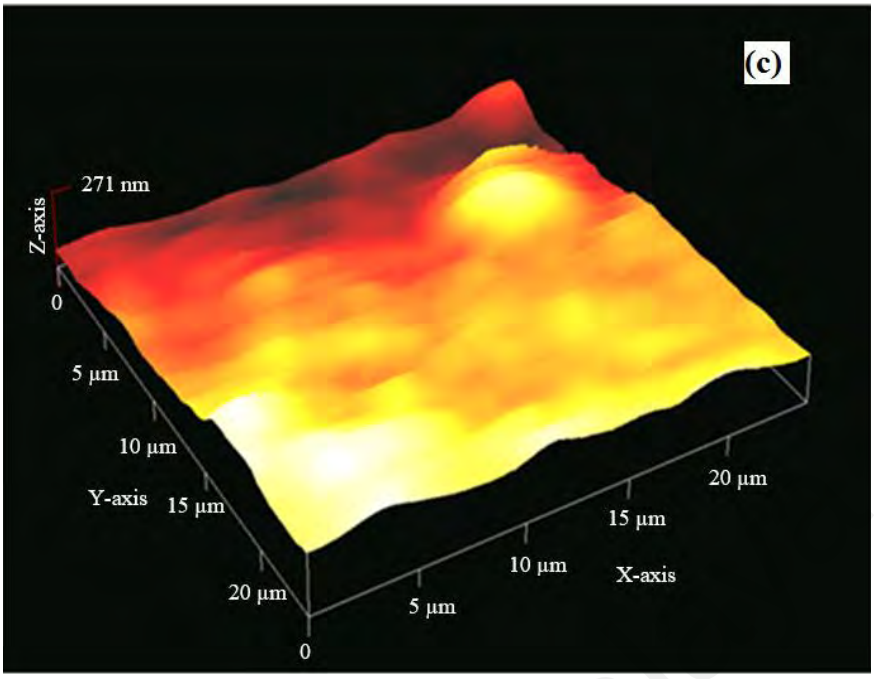
(c)
271 nm
Z-axis
0
5 µm
10 µm
Y-axis
15 µm
20 µm
0
5 µm
10 µm
15 µm
20 µm
X-axis

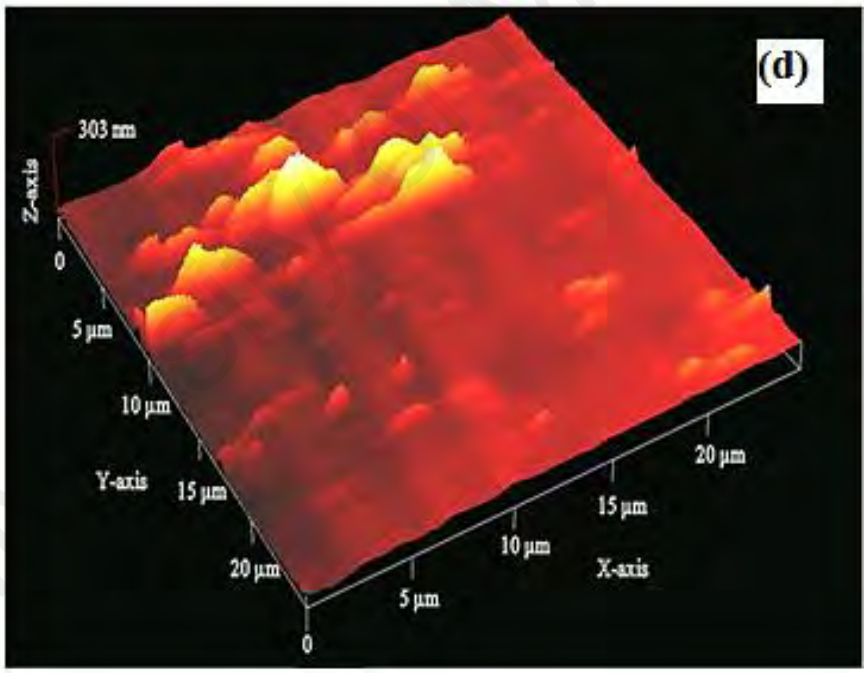
(d)
303 nm
Z-axis
0
5 µm
10 µm
Y-axis
15 µm
20 µm
0
5 µm
10 µm
15 µm
20 µm
X-axis

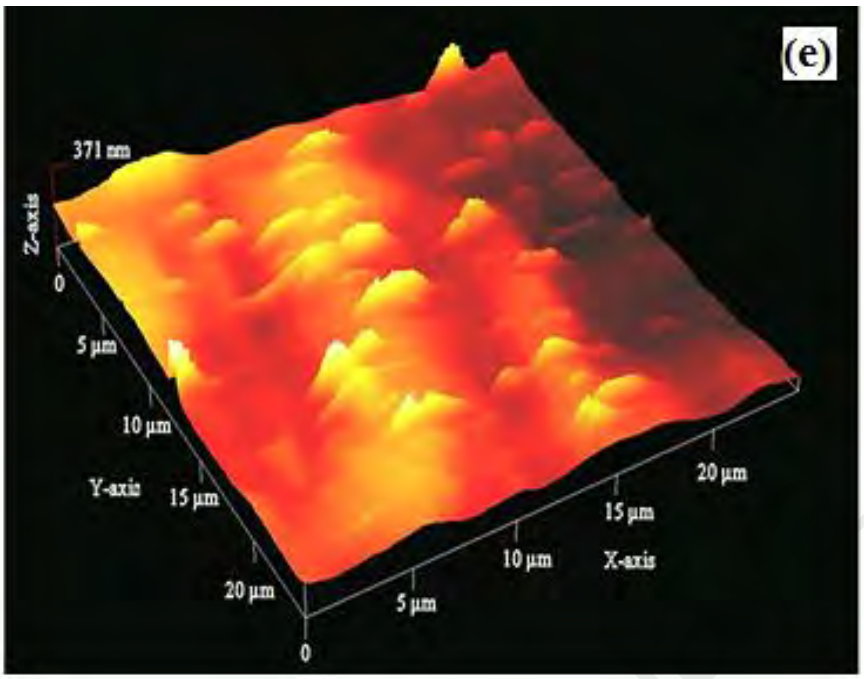
(e)
371 nm
Z-axis
0
5 µm
10 µm
Y-axis
15 µm
20 µm
5 µm
10 µm
X-axis
15 µm
20 µm
0

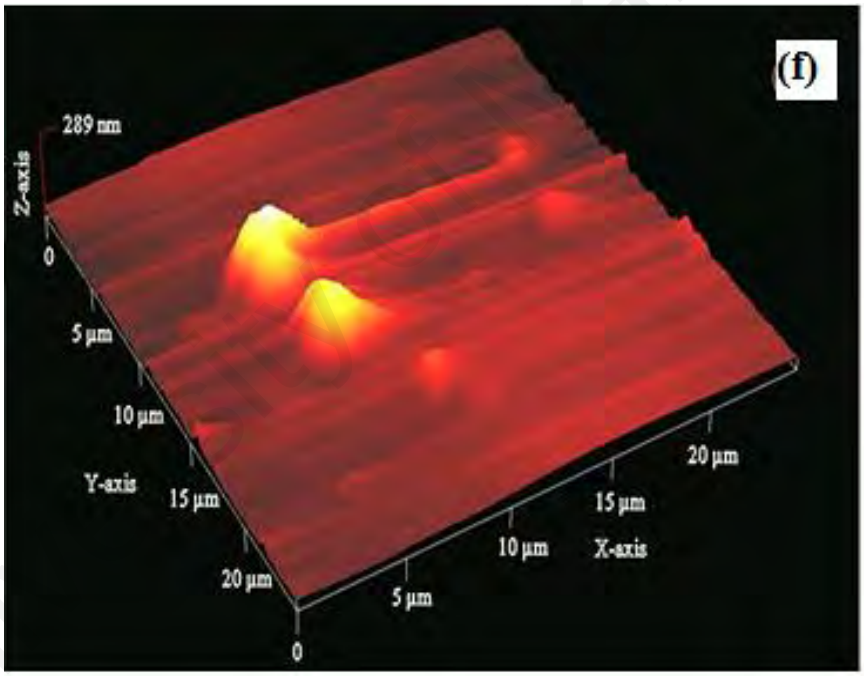
(f)
289 nm
Z-axis
0
5 µm
10 µm
Y-axis
15 µm
20 µm
5 µm
10 µm
X-axis
15 µm
20 µm
0

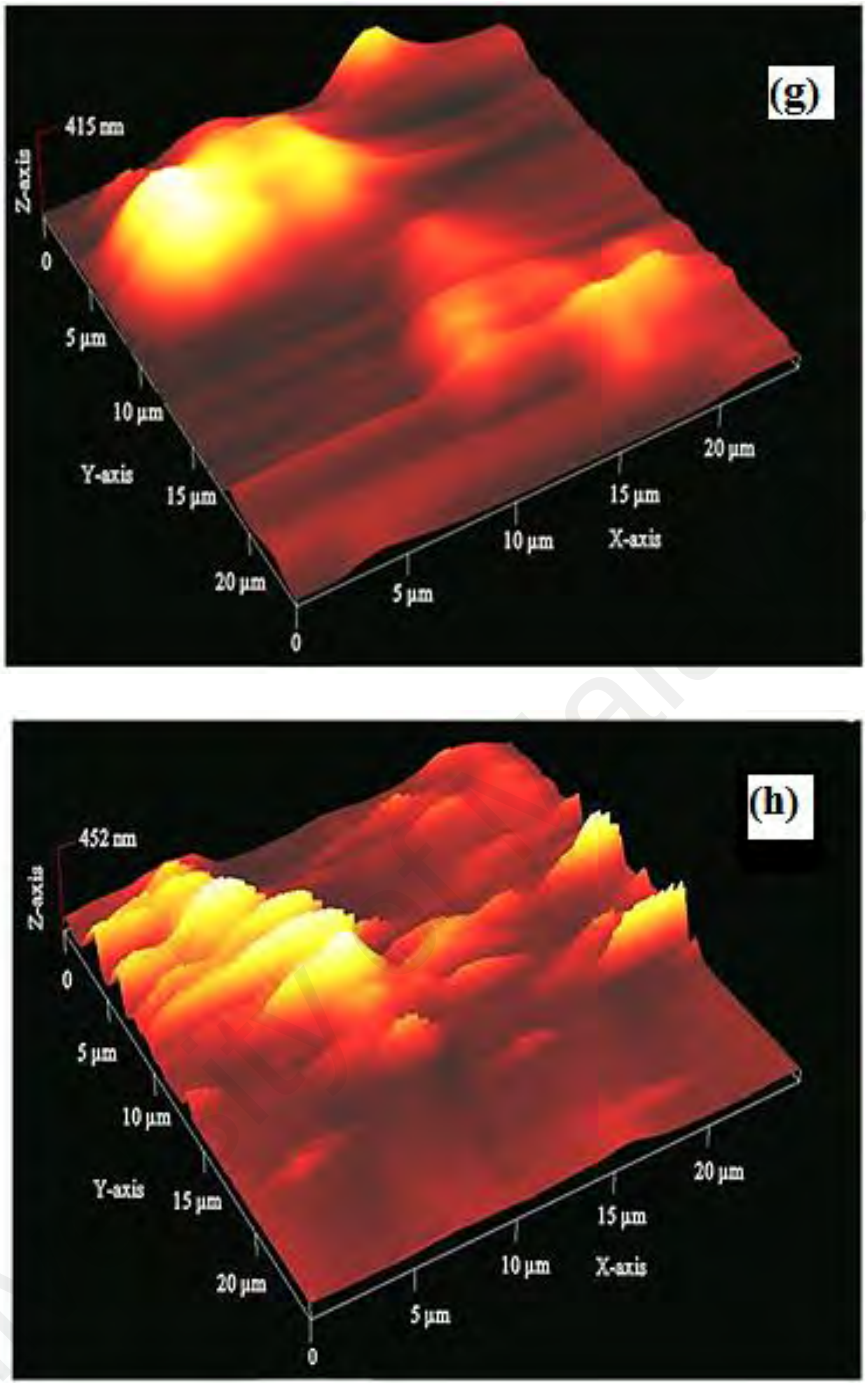

Figure 4.6 continued: AFM images of textured amorphous hydrogenated carbon coated samples (a) Dn10Di100Dp6, (b) Dn20Di100Dp6, (c) Dn30Di100Dp6, (d) Dn20Di50Dp6, (e) Dn20Di150Dp6, (f) Dn20Di100Dp15, (g) Dn20Di100Dp30 and (h) a-C:H-Untex

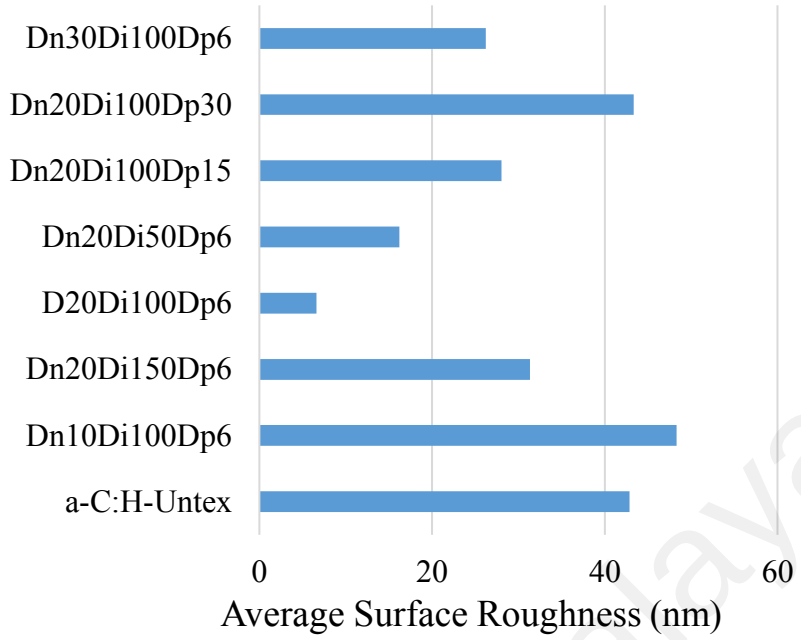

Figure 4.7: Average surface roughness values for un-textured/textured amorphous hydrogenated carbon coated samples

Scratch marks indicating abrasive wearing were observed on counter surface ball that rubbed against sample a-C:H-Untex (Figure 4.10 a) compared with counter surface ball that rubbed against Dn20Di100Dp6 (Figure 4.10 b). This confirms that wear particles were captured by the textures. Figure 4.6 shows the wear coefficient of the steel ball that rubbed against various samples. The lower wear coefficient is found in the case of sample Dn20Di100Dp6 counter ball compared to a-C:H-Untex. Raman spectroscopy revealed that graphitization rate in the case of sample Dn20Di100Dp6 was lower than that in other samples (Figure 4.11). Therefore, the reduction in wear of sample Dn20Di100Dp6 counter ball was mainly caused by texture mechanisms.

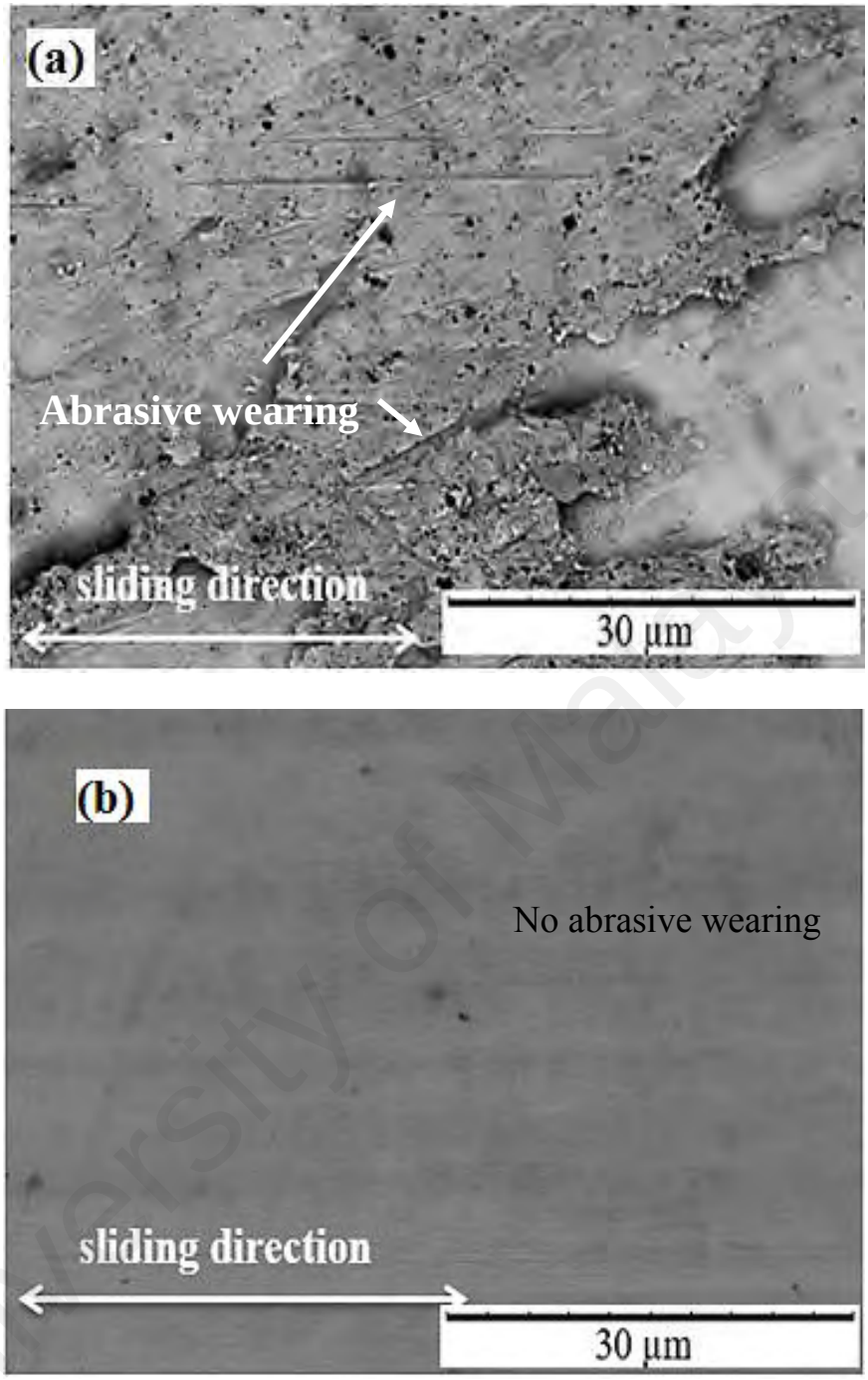

Figure 4.8: SEM images of steel balls which rub against (a) a-C:H-Untex (b) Dn20Di100Dp6

Table 4.2: EDX analysis of un-textured/textured coated samples

Specimen	Elements (Atomic %)					
	C	O	Cr	Fe	Si	Mn

a-C:H-as deposited	96.27	0.56	2.83	0.34	-	-
a-C:H-Untex	80.81	1.10	10.19	7.90	-	-
Dn20Di50Dp6	82.32	1.67	11.09	4.92	-	-
Dn20Di100Dp6	95.41	0.43	3.65	0.51	-	-
Dn20Di150Dp6	78.81	1.31	13.19	6.69	-	-
Dn20Di100Dp15	87.01	1.35	8.98	2.66	-	-
Dn20Di100Dp30	39.04	2.10	13.34	44.87	0.42	0.23
Dn10Di100Dp6	84.23	1.99	8.45	5.33	-	-
Dn30Di100Dp6	89.71	0.89	6.81	2.59	-	-

4.2.2.2 Raman analysis

The lowest average coefficient of friction of sample Dn20Di100Dp6 can be attributed to graphitization, surface texturing, or both. A thin graphitic transfer film forms on a counter surface because of coated plate graphitization (Liu et al., 1996); as a result, coefficient of friction is decreased because the low shear strength of basal planes provides easy slip between tribo-pairs (Sánchez-López et al., 2003). Raman spectroscopy was performed to investigate whether or not graphitization is the main reason for the improved performance of sample Dn20Di100Dp6. As 100 μm diameter and 6 μm depth has shown better coefficient of friction and wear coefficient results than other dimple dimeters and depths that is why for comparison purposes Raman spectra of Dn10Di100Dp6, Dn20Di100Dp6 and Dn30Di100Dp6 were collected.

Figure 4.11 illustrates amorphous hydrogenated carbon coating spectrums for various textured/un-textured samples before and after friction test. For quantitative analysis, the Raman spectra was fitted into D and G peaks. The G peak indicates the stretching vibration of sp^2 carbon in C=C chains and aromatic ring, whereas the D peak indicates

the breathing mode of sp^2 carbon in the aromatic rings (Casiraghi et al., 2005). The I_D/I_G ratio and the G peak position can be generally used to characterize sp^3/sp^2 bonding ratio (Casiraghi et al., 2005). The shift in G peak and increase in I_D/I_G ratio indicate an increase in sp^2 fraction (graphite) in the DLC film (Ferrari & Robertson, 2000).

The samples Dn30Di100Dp6, Dn20Di100Dp6 and Dn10Di100Dp6 showed G peak shift from 1554 to 1564, 1557 and 1560, respectively. The samples Dn30Di100Dp6, Dn20Di100Dp6 and Dn10Di100Dp6 showed I_D/I_G ratio increase from 1.32 to 1.50, 1.33 and 1.45, respectively. Higher I_D/I_G ratio and G peak shift has been observed in the case of Dn30Di100Dp6 after testing compared to Dn20Di100Dp6 and Dn10Di100Dp6. These results indicate that with the change in dimple density, the graphitization behavior changes. Lower average coefficient of friction in the case of Dn30Di100Dp6 than Dn10Di100Dp6 can be due to higher graphitization. However, Dn20Di100Dp6 showed lower average coefficient of friction than Dn30Di100Dp6. This result indicates that the lower average coefficient of friction of Dn20Di100Dp6 is related to mechanism of textures rather than graphitization. Due to graphitization, the coating becomes soft, which can increase coating wear (Haque et al., 2009). The sample Dn30Di100Dp6 showed higher wear coefficient than Dn10Di100Dp6 and Dn20Di100Dp6. Higher graphitization of Dn30Di100Dp6 compared to Dn10Di100Dp6 can be due to higher contact loading, as higher number of dimples in the case of Dn30Di100Dp6 causes reduction in contact area.

The higher graphitization transformation in the case of sample Dn10Di100Dp6 and Dn30Di100Dp6 can be attributed to high contact pressure generated by wear debris. Wear particle-induced graphitization has been confirmed by Ding et al. (2010) in the case of a-C coating. Lower graphitization in the case of sample Dn20Di100Dp6 can be due to capture of wear debris from the interface, which prevented coating graphitization. Graphitization rates of samples Dn10Di100Dp6 and Dn30Di100Dp6 were different from

each other; this result indicated that the wear debris capturing ability varies with dimple density.

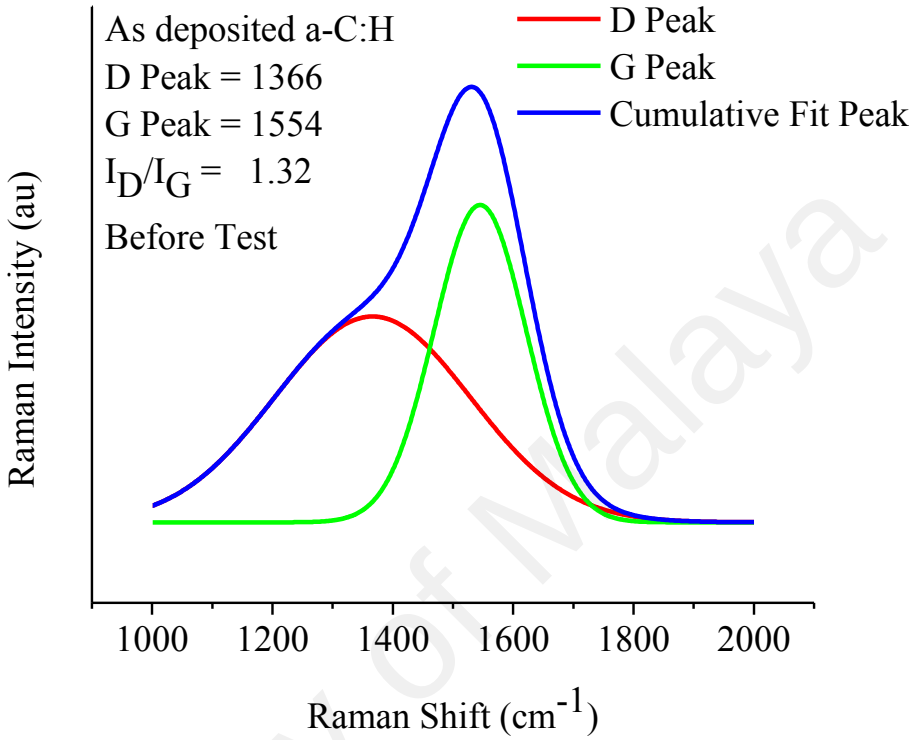

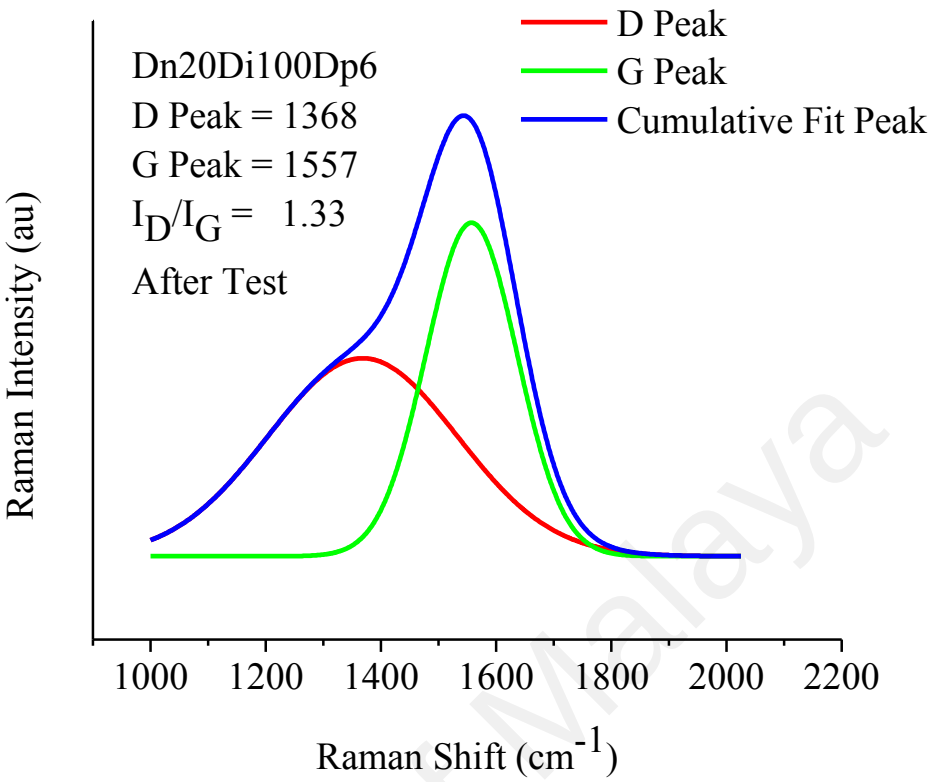

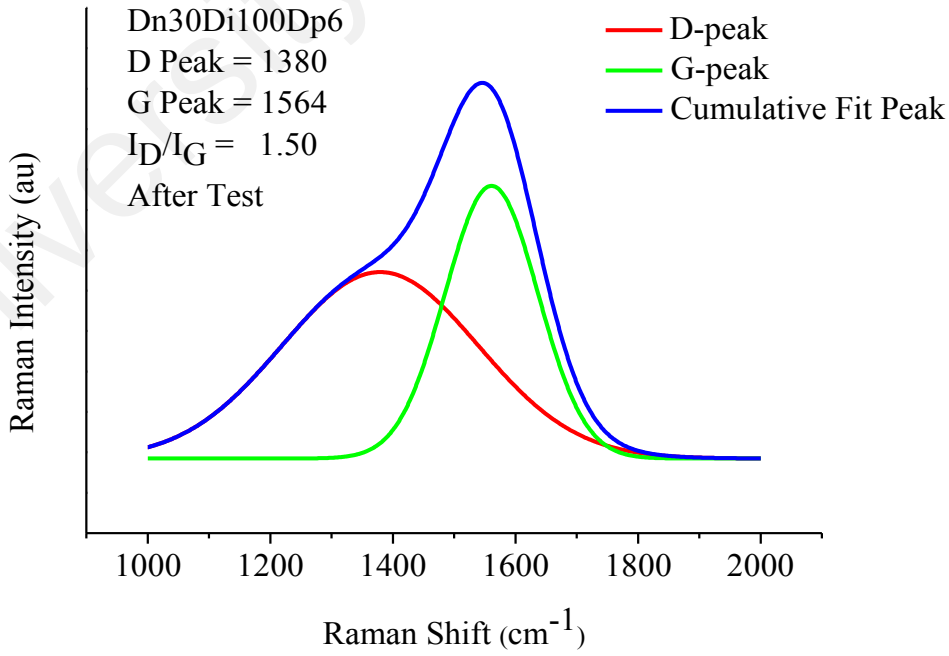

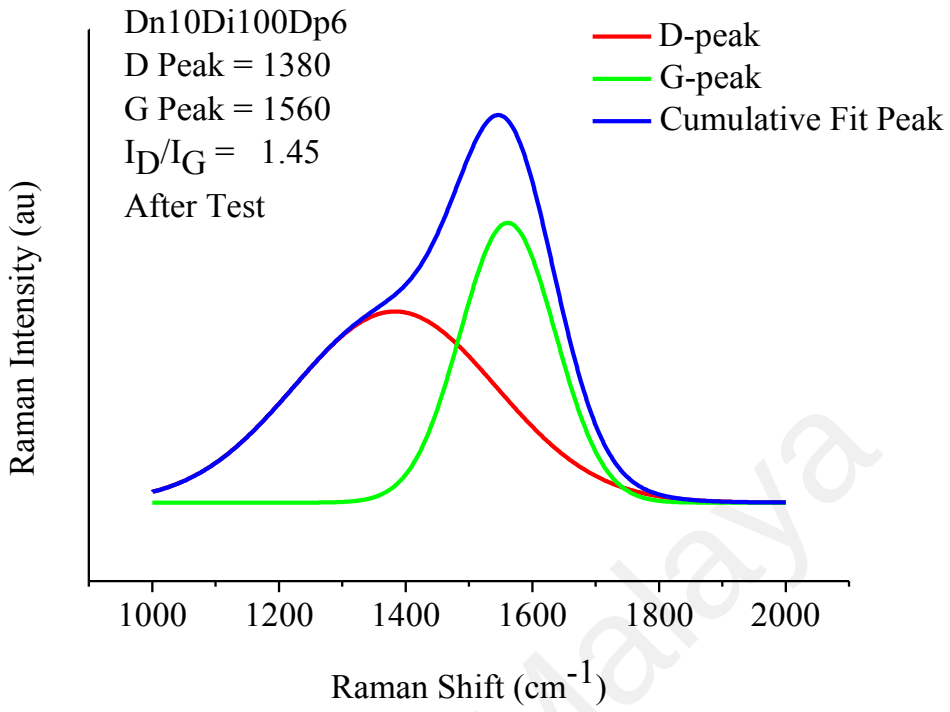

Figure 4.9 continued: Raman spectra of various amorphous hydrogenated carbon coated samples after friction testing

4.3 Effect of surface texture on tribological performance of amorphous hydrogenated carbon coating at various temperatures

4.3.1 Friction and wear behavior

Figures 4.12 a, 4.12 b, 4.12 c shows the coefficient of friction variation with time for textured coated and un-textured coated samples under PAO and palm based TMP lubrication. Figure 4.13 shows the wear coefficient for various samples under PAO and palm based TMP lubrication. Textured coated samples showed relatively stable coefficient of friction with time compared to un-textured coated samples. As the temperature increases, the coefficient of friction for un-textured amorphous hydrogenated carbon decreases, whereas it increases for textured amorphous hydrogenated carbon coating.

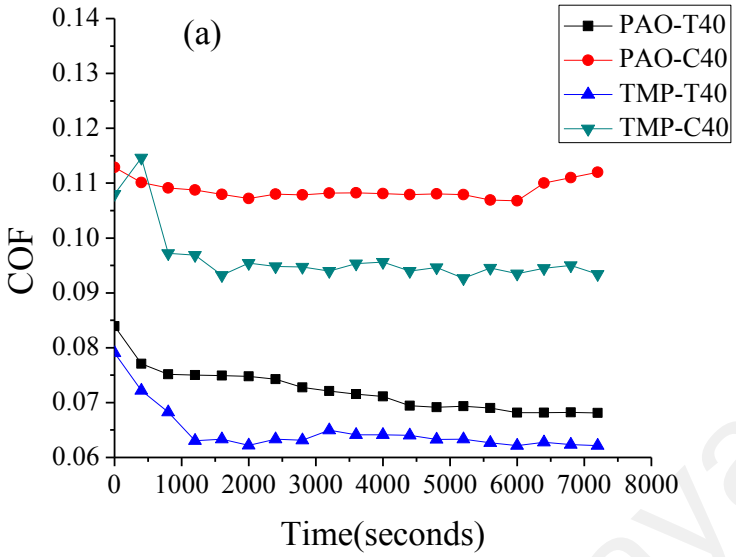

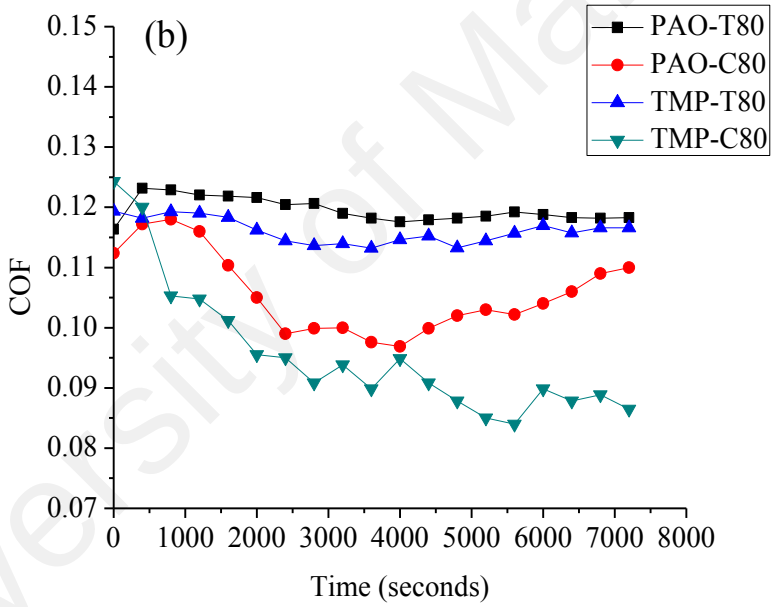

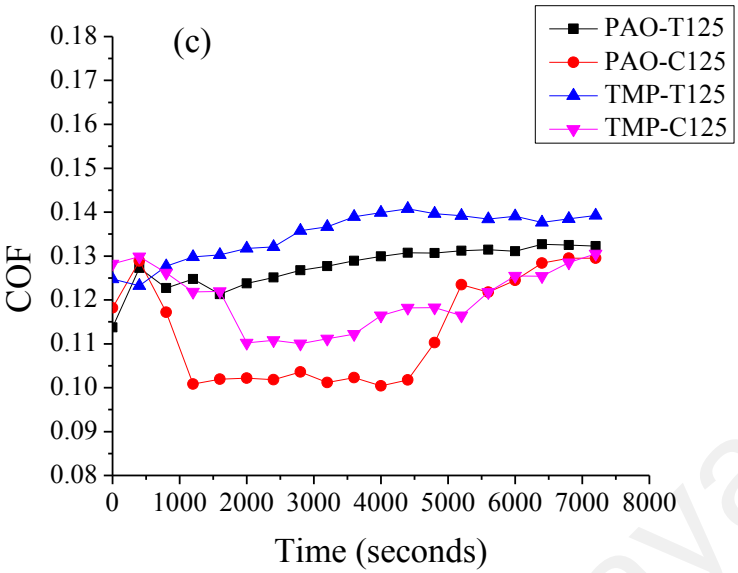

Figure 4.10 continued: Change in coefficient of friction of amorphous hydrogenated carbon coated samples with time (a) temperature 40º C, (b) temperature 80º C and (c) temperature 125º C

Samples PAO-T40 and TMP-T40 showed lower coefficient of friction compared to samples PAO-C40 and TMP-C40 throughout the friction test (Figure 4.12 a). Textures helped in lowering the coefficient of friction for lubricants tested by acting as lubricant reservoirs and wear particle traps. In textured and un-textured cases, palm based TMP showed lower coefficient of friction throughout the test compared to PAO lubricant. Samples PAO-T40 and TMP-T40 showed lower wear coefficient compared to un-textured samples. Sample PAO-C40 showed higher wear coefficient compared to sample TMP-C40. Better lubricity of palm based TMP lubricant has been observed previously by Zulkifli et al. (Zulkifli et al., 2014) in steel-steel contact.

Figure 4.12 b shows that coefficient of friction curve of sample PAO-T80 was lower than PAO-C80 at the start of the test. After 1,000 seconds, the coefficient of friction reduced for sample PAO-C80, whereas sample PAO-T80 remained stable till the end of the test; however, sample PAO-C80 showed an increase in coefficient of friction after 4,600 s. Sample TMP-C80 showed similar unstable behavior as sample PAO-C80.

Sample TMP-T80 showed lower coefficient of friction nearly throughout the test compared to sample PAO-T80. Similar to sample PAO-T80, sample TMP-T80 also showed stable coefficient of friction throughout the test. Textured samples (PAO-T80 and TMP-T80) showed lower wear coefficient compared to un-textured samples (PAO-C80 and TMP-C80). Samples TMP-C80 and TMP-T80 showed lower wear coefficient than samples PAO-C80 and PAO-T80, respectively (Figure 4.13).

Coefficient of friction in the case of samples PAO-C125 and PAO-T125, showed a sudden increase in the start. As the test progressed, coefficient of friction reduced for sample PAO-C125 until 5,400 s; afterwards, it increased and did not stabilize till the end of the friction test (Figure 4.12 c). Sample TMP-C125 showed sudden decrease in coefficient of friction at 2000 s and then showed sudden increase at 5000 s. After the initial instability, coefficient of friction in the case of sample PAO-T125, steadily increased to 0.132 at the end of the test (Figure 4.12 c). Sample TMP-T125 showed higher coefficient of friction compared to sample PAO-T125, the coefficient of friction curve of the sample TMP-T125 was nearly stable throughout the test. Wear coefficient behavior at 125 °C with respect to textured and un-textured samples was nearly similar to 40 and 80 °C (Figure 4.13). Textured samples showed lower wear coefficient compared to un-textured samples. Wear coefficient of samples tested in palm based TMP lubricant was higher compared to PAO lubricant. This behavior was different to tests conducted at temperature 40 °C and 80 °C, where palm based TMP showed lower wear coefficient irrespective of whether they are textured or un-textured.

Palm based TMP ester performance reduces at temperature higher than 80 °C. At higher temperature the COF and wear increases. This is related to the lower stability of tribo-film formed by fatty acids at higher temperature (Zulkifli et al. 2013).

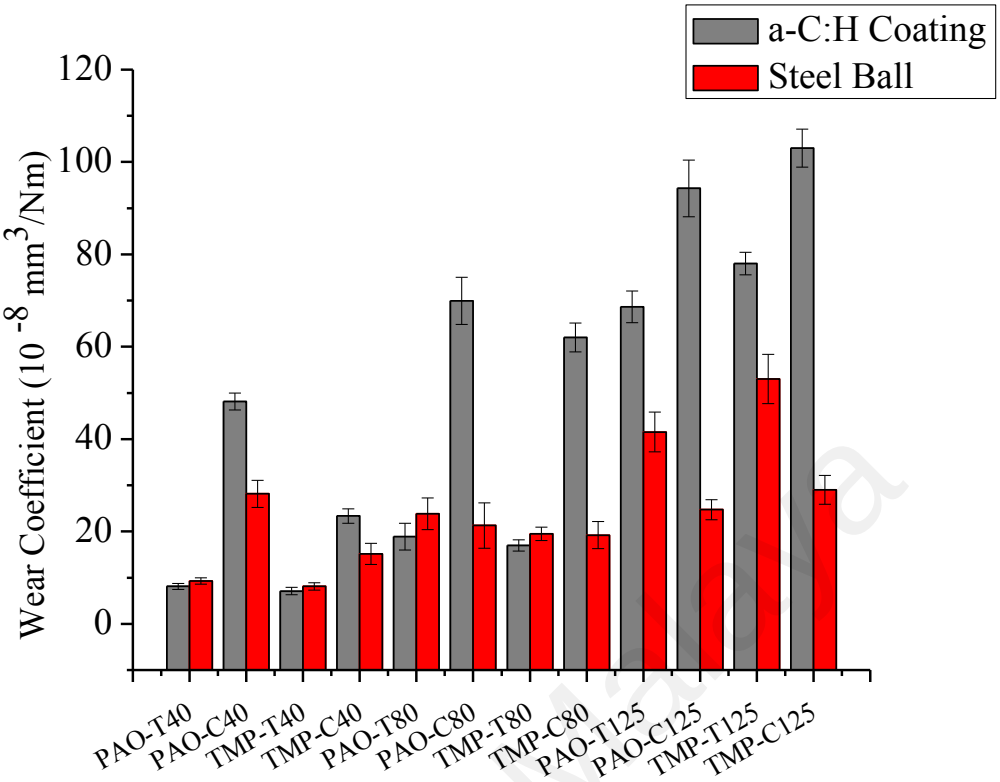

Figure 4.11: Wear coefficient of amorphous hydrogenated carbon coated textured/un-textured samples after tribological testing at various temperatures

The lower coefficient of friction in the case of palm based TMP lubricant at 40 ºC and 80 ºC in textured and un-textured case can be due to its high polarity (Gellman & Spencer, 2002). Lubricity is a surface energy phenomenon, as palm based TMP has higher polarity it is easily attracted towards the metal surface (Zulkifli et al., 2013). The higher polarity forms a higher affinity for metal from one end of the molecule and allows a non-polar hydrocarbon to extend out and provide a barrier between the tribo-pair (Canter, 2009; Zulkifli et al., 2014). In addition, palm oil has longer carbon chain length (18-20), due to which the formed film behaves as a crystalline solid and reduces the coefficient of friction (Bhushan, 2013). The higher coefficient of friction and wear in case of palm based TMP lubricant compared to PAO lubricant at 125º C can be due to the unstable film formation of palm based TMP lubricant at higher temperatures. This has been observed previously.

At higher temperature's film formed by fatty acid chains are unstable, thus increasing friction and wear (Rafiq et al., 2012) (Zulkifli et al., 2014).

The reason for the decrease in coefficient of friction of un-textured amorphous hydrogenated carbon coating at 40, 80 and 125 °C can be due to graphitization transformation. The reduction in coefficient of friction due to graphitization has been noticed previously (López et al., 2003). Highly disordered structure of DLC film steadily transforms to ordered structure at the elevated temperatures. Films form an unsteady phase during deposition, when thermal energy is introduced, structure of these films is re-oriented (Erdemir & Fenske, 1996; Wu & Hon, 1999). At high temperature, diffusion of unbounded hydrogen atoms produces a spongy structure for the film of hydrogenated DLC. These structural and chemical changes also cause modifications in friction and wear behavior. After exposing at high temperature, final product may become highly porous and a soft graphitic thin layer may appear, which wears out rapidly. At elevated temperature, endurance limit for non-hydrogenated films is higher than hydrogenated films.

Due to graphitization, the coating layer becomes soft and the load-bearing capacity reduces and wear increases (Kalin et al., 2010). This could be the reason for the higher wear rate in the case of un-textured amorphous hydrogenated carbon at 40 °C, 80 °C and 125 °C, as can be seen in Figure 4.13. Wear coefficient results nearly followed the coefficient of friction trend in the textured amorphous hydrogenated carbon case, whereas, in the case of un-textured a-C:H, It was opposite to the coefficient of friction trend. This opposite trend of un-textured amorphous hydrogenated carbon can be explained by the fact that graphitization helps in reduction of a coefficient of friction; However, the adverse effect of graphitization transformation is increased wear rate. This will be further discussed in section 4.3.2. The increase in the coefficient of friction for

un-textured amorphous hydrogenated carbon in palm based TMP and PAO lubricant at the later part of friction testing may be due to coating delamination. This will be further discussed in section 4.3.3. The friction and wear performance of amorphous hydrogenated carbon coating deteriorates with the increase in temperature (Bremond et al., 2003). It was observed in a previous study that the tribological performance of amorphous hydrogenated carbon coating starts to change around 100 ºC (Vanhulsel et al., 1998). However, the textured amorphous hydrogenated carbon showed higher wear resistance compared to the un-textured amorphous hydrogenated carbon even at temperature above 100 °C.

4.3.2 Wear track characterization of amorphous hydrogenated carbon coating

4.3.2.1 Raman analysis

Raman spectroscopy was used to investigate the graphitization behavior of amorphous hydrogenated carbon coating. Three Raman measurements were taken to present a statistical representation of results so that the inaccuracies resulting from peak fitting could be minimized.

The atomic structure of amorphous hydrogenated carbon coating consists of sp^3, sp^2 and monovalent hydrogen bonds (Neville et al., 2007). The release of hydrogen from the amorphous hydrogenated carbon coating matrix triggers the transformation from a sp^3 structure to a graphite-like sp^2 structure. Graphitization can occur because of higher contact temperature and/or high contact stress (Haque et al., 2009). Haque et al. (Haque et al., 2009) suggested that due to the micron-sized wear particles produced during the sliding test, the contact pressure reduces the graphitization temperature to as low as 95 ºC. These particles can be generated from counter ball wear (Haque et al., 2009). Ding et al. (Ding et al., 2010) proposed that, due to fatigue wear mechanisms, DLC wear debris

can be created at the contact, which can lower the graphitization temperature. This can explain the graphitization transformation at 40 ºC in our study.

Figure 4.14 and Figure 4.15 shows the Raman spectra's for various textured and un-textured samples tested under PAO and palm based TMP lubrication. Raman spectra were fitted into D and G peaks for quantitative analysis. The G peak indicates the stretching vibration of sp^2 carbon in C = C chains and aromatic rings, whereas the D peak indicates the breathing mode of sp^2 carbon in the aromatic rings (Casiraghi et al., 2005). The shift in the G peak and increase in the I_D/I_G ratio indicate an increase in the sp^2 fraction (graphite) in the DLC film (Casiraghi et al., 2005; Ferrari & Robertson, 2000). The G peak and I_D/I_G ratio of as deposited amorphous hydrogenated carbon coating was 1533.77 cm^{-1} and 1.17 respectively. The G peak, in the case of the samples PAO-T40 and TMP-T40 (Figures 4.14 and 4.15) shifted slightly from the as deposited coating. Whereas PAO-C40 and TMP-C40 (Figures 4.14 and 4.15) showed the higher increase in the G peak shifts from the as deposited value. The I_D/I_G ratio increase was also low for samples PAO-T40 and TMP-T40 (Figures 4.14 and 4.15) than PAO-C40 and TMP-C40 (Figures 4.14 and 4.15). This indicates that, at lower temperatures, textured amorphous hydrogenated carbon showed slight graphitization transformation in the presence of PAO and palm based TMP lubricants compared to un-textured amorphous hydrogenated carbon. This result confirms that the lower coefficient of friction of PAO-T40 and TMP-T40, was not because of graphitization, rather, the mechanism of textures (fluid/ debris reservoir) was responsible for this. In the case of PAO-C40 (Figure 4.14), G peak shifted from 1533.77 cm^{-1} to 1555.27 cm^{-1} and I_D/I_G ratio increased from 1.17 to 1.51. This shows that at 40 ºC higher graphitization transformation occurred for un-textured amorphous hydrogenated carbon. In the case of TMP-C40 change in the G peak position from 1533.77 cm^{-1} to 1548.39 cm^{-1} and I_D/I_G ratio changed from 1.17 to 1.31 has been observed. Due to graphitization, the coating becomes soft and thus wears coefficient increases. The lower

wear coefficient for the case of PAO-T40 and TMP-T40 can be related to reduction in graphitization. In addition, TMP-C40 showed reduced wear coefficient compared to PAO-C40. This can also be related to the better lubricity of palm based TMP at the low temperatures. The dependence of graphitization is on sliding distance, load, and contact type. PAO and palm based TMP both showed graphitization. No relationship was found, which indicate that palm based TMP affects the graphitization behavior.

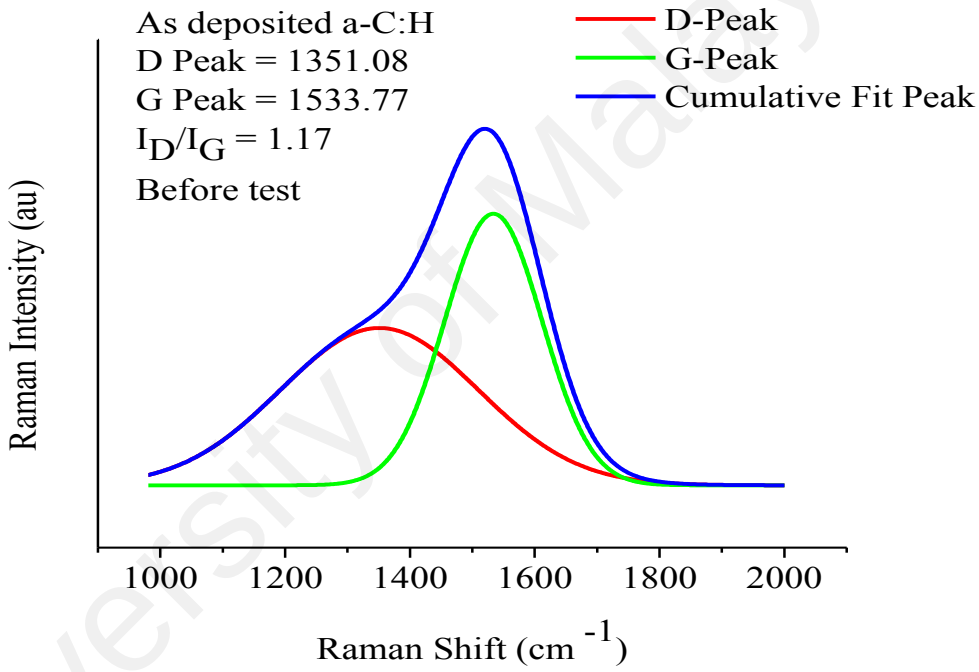

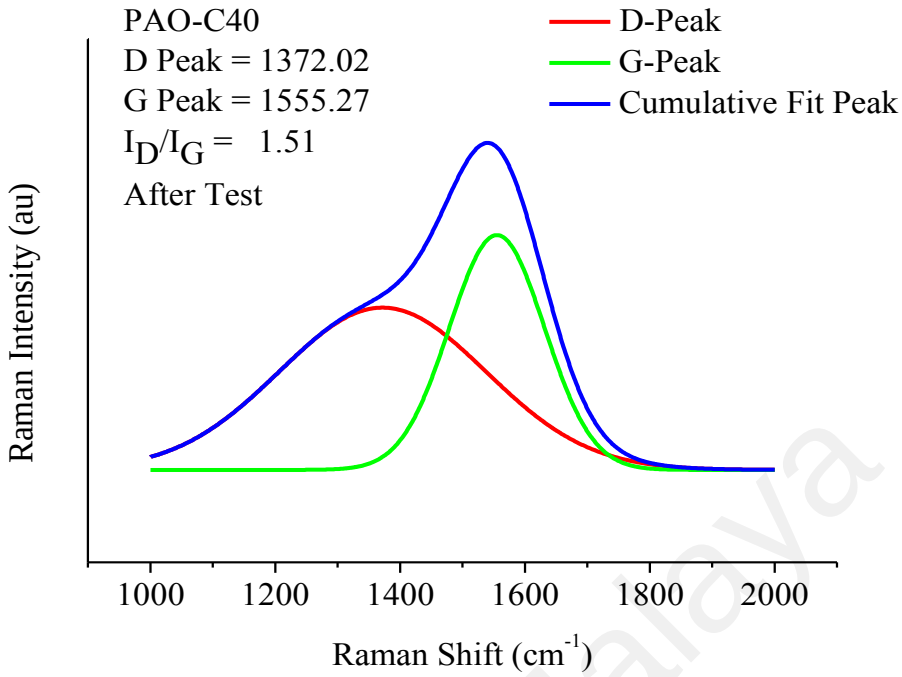

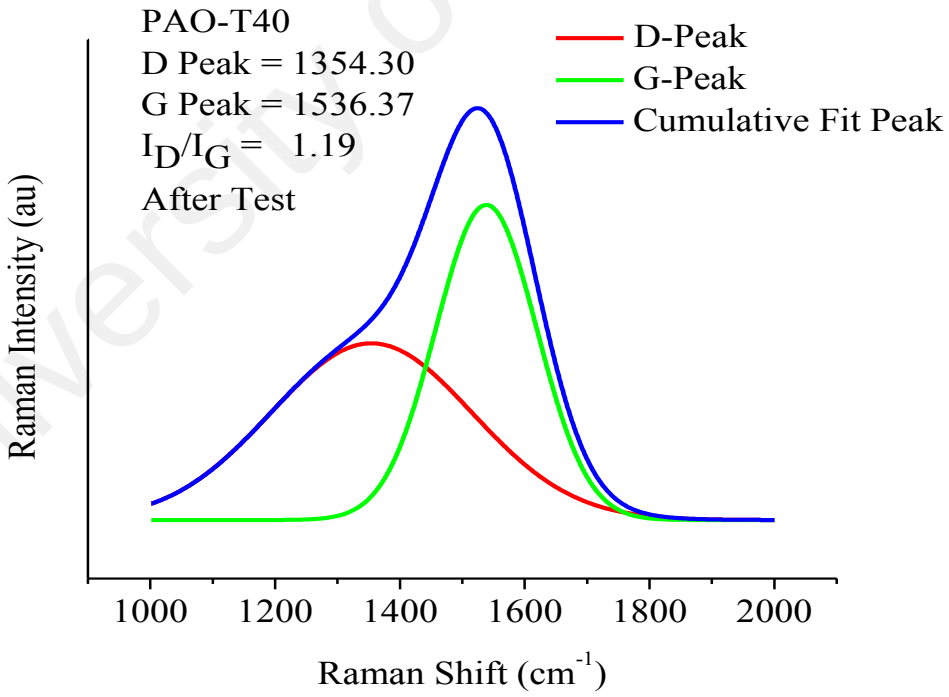

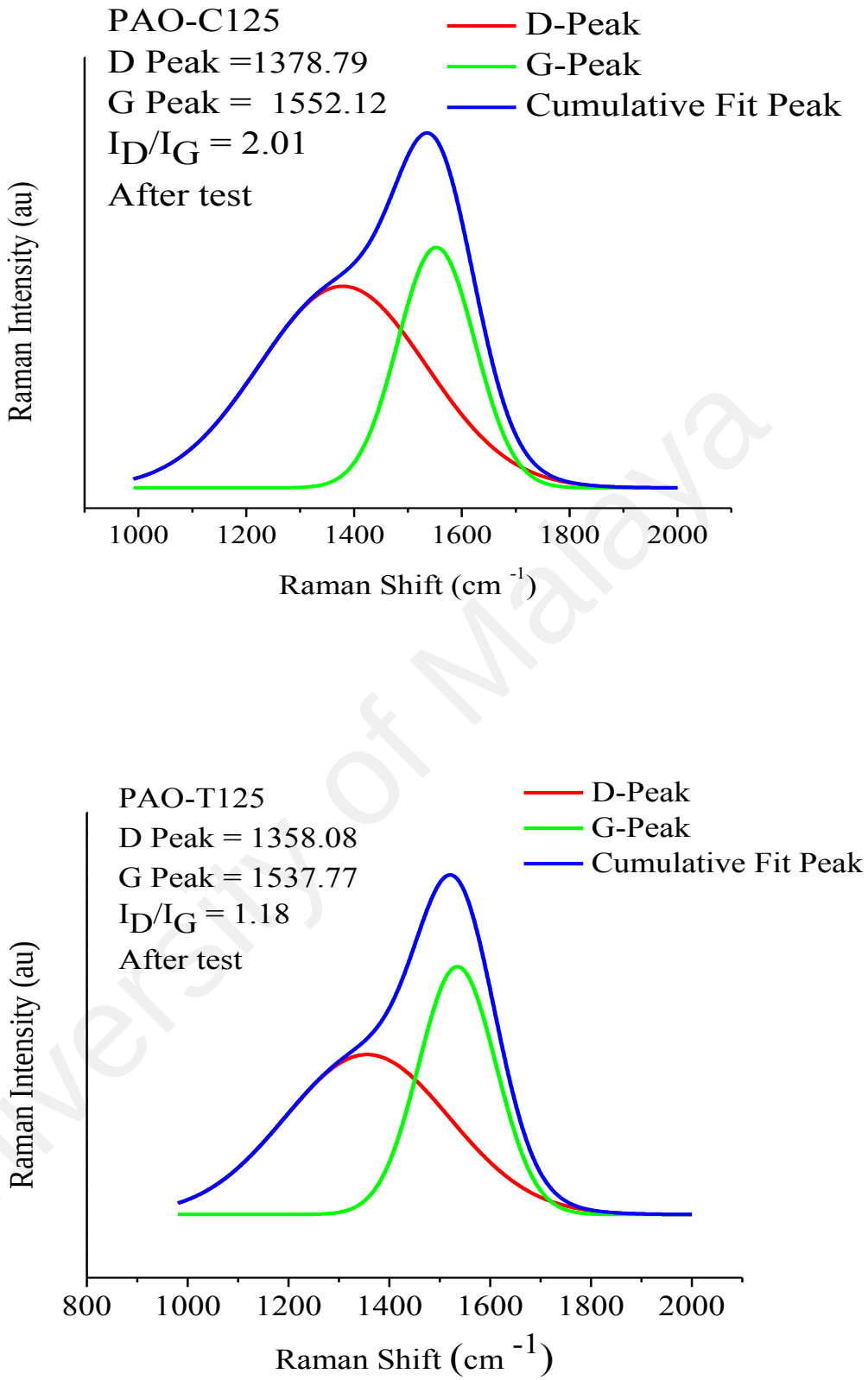

Figure 4.12 continued: Raman spectra of various textured/un-textured amorphous hydrogenated carbon coating at various temperatures in the presence of PAO lubricant

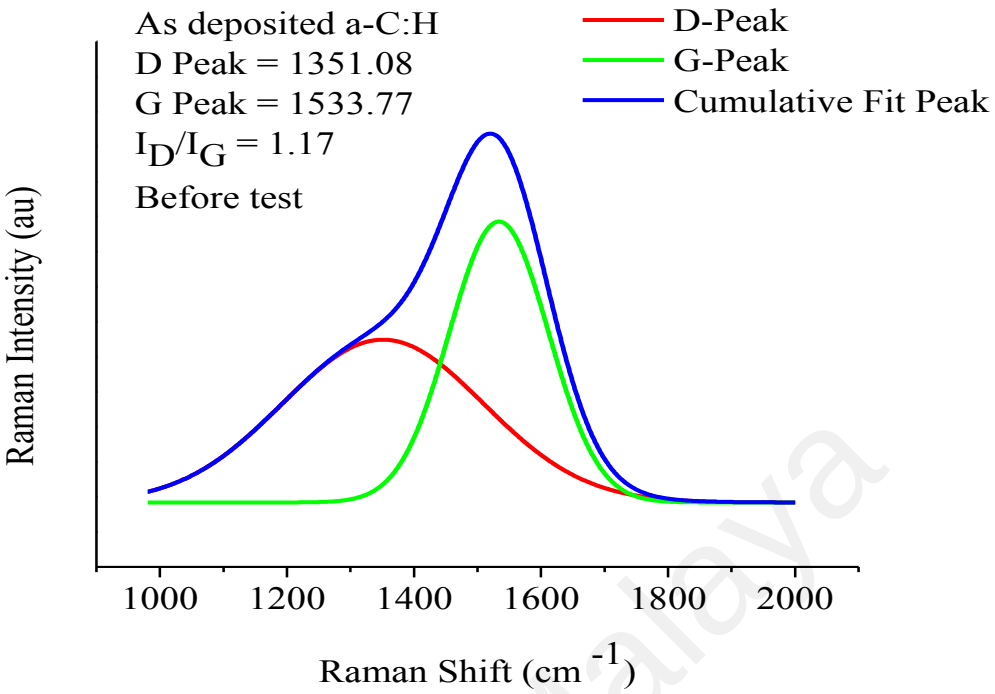

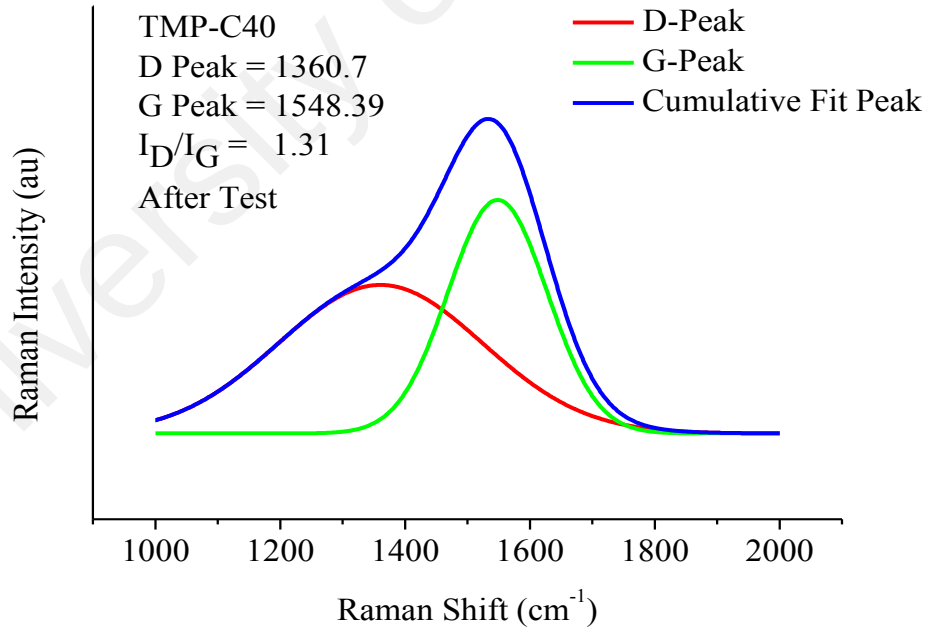

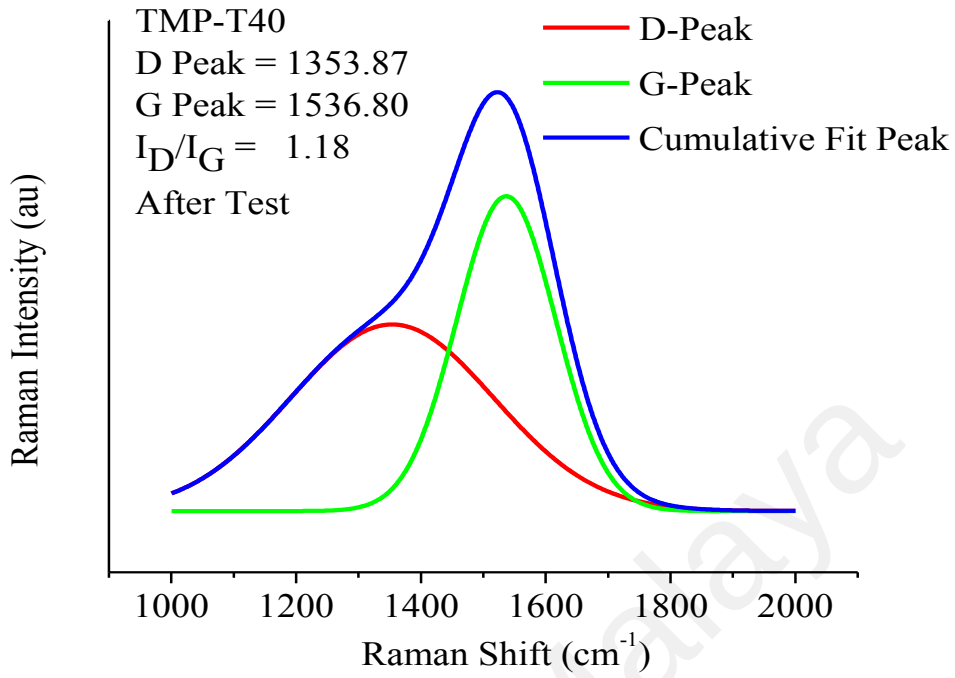

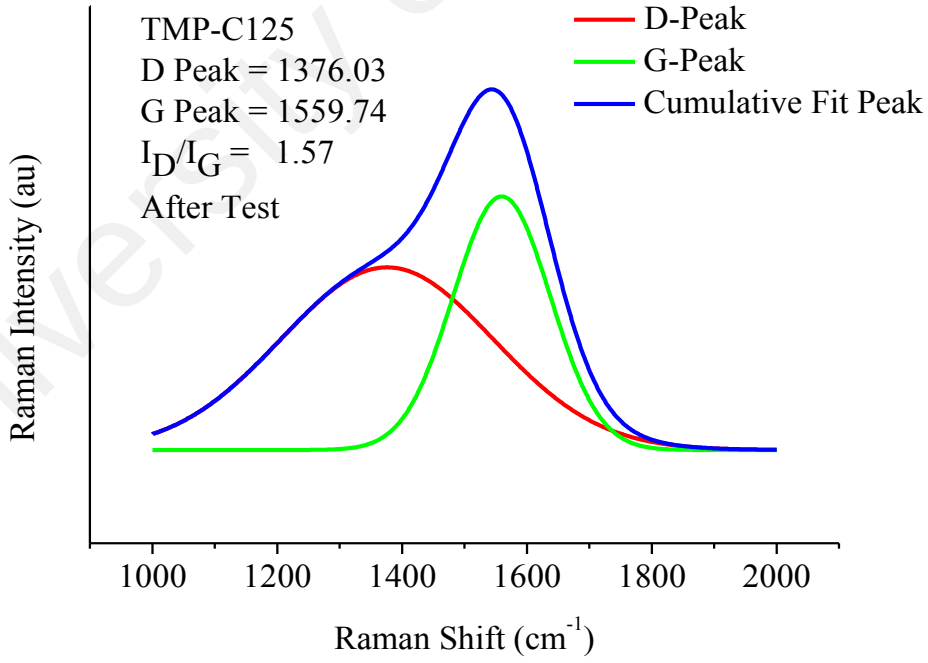

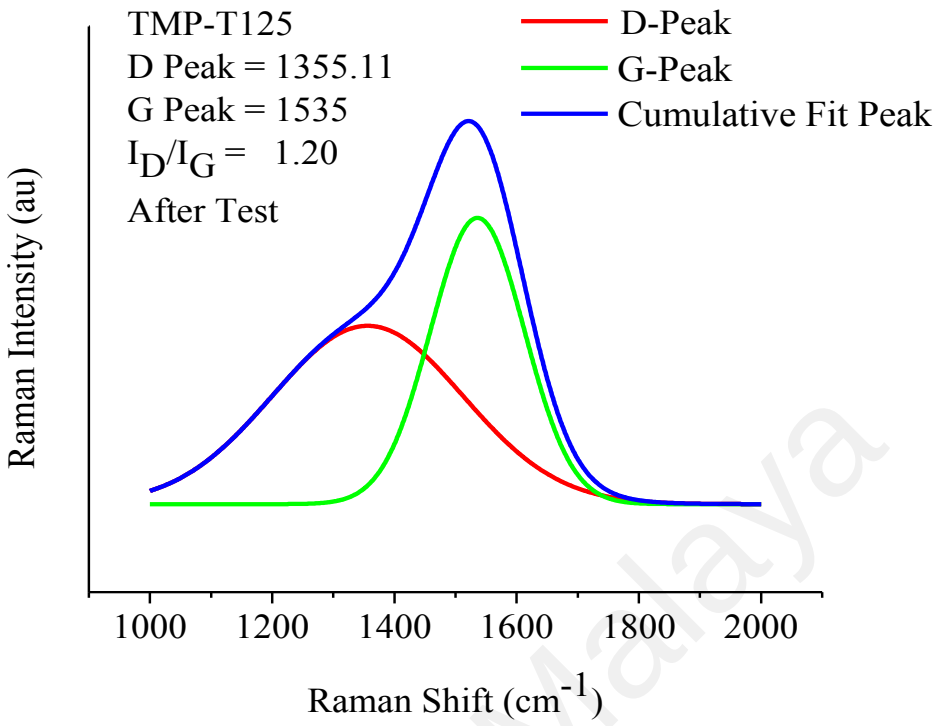

Figure 4.13 continued: Raman spectra of various textured/un-textured amorphous hydrogenated carbon coating at various temperatures in the presence of palm based TMP lubricant

In the case of samples PAO-C125 and TMP-C125, the G peaks shifted from 1533.77 cm^{-1} to 1552.12 cm^{-1} and 1559.74 cm^{-1}, respectively. In addition, the I_D/I_G ratio for samples PAO-C125 and TMP-C125 increased from 1.17 to 2.01 and 1.57, respectively (Figures 4.14 and 4.15). This shows that, as the temperature increased to 125 ºC graphitization transformation increased. In the case of PAO-T125 and TMP-T125, the G peaks shifted from 1533.77 cm^{-1} to 1537.77 cm^{-1} and 1535 cm^{-1}, respectively. Whereas, the I_D/I_G ratio samples PAO-T125 and TMP-T125 increased from 1.17 to 1.18 and 1.20, respectively. These results indicate that even at higher temperatures a lower graphitization transformation can be observed from the case of textured coating irrespective of lubricant used. The Raman analysis shows that graphitization

transformation of textured amorphous hydrogenated carbon was too low compared to un-textured amorphous hydrogenated carbon.

The lower graphitization in the case of textured amorphous hydrogenated carbon at higher temperatures may be due to multiple factors, including the wear debris trapping ability and the lubricant retention and providing the ability of micro dimples. Textures can remove the wear debris from the contacting surface, which can reduce the increase in contact pressure due to the wear particles between the tribo-pairs. Additionally, by keeping the lubricant at the interface, they can lower the rise in temperature due to friction-induced heating. In the case of textured mechanical seals, Xiao et al. (Xiao & Khonsari, 2012) observed that micro dimples could lower the interface temperature by keeping lubricant at the interface.

4.3.2.2 SEM/EDX and AFM analysis

Figure 4.16 shows the SEM images of wear tracks; the white arrow indicates the sliding direction. EDX quantitative analyses of the SEM images, are shown in Table 4.3. Polishing wear was observed from the case of samples PAO-T40 and TMP-T40 (Figures 4.16 a and 4.16 c). The polishing wear process is the one in which micro grooves are not seen before the complete removal or delamination of coating. The brighter areas present on the wear tracks are due to the thinning of coating and exposure of silver-colored CrN. Samples PAO-C40 and TMP-C40 showed coating spallation and partial delamination on the wear track (Figures 4.16 b and 4.16 d). Sample PAO-T125 showed coating spallation on the wear track (Figure 4.16 e), whereas a sample TMP-T125 (Figure 4.16 g) showed spallation and delamination at few spots. Samples PAO-C125 and TMP-C125 (Figures 4.16 f and 4.16 h) exhibited scratch marks and extensive coating delamination. Samples PAO-C125 and TMP-C125 showed a higher increase of Fe and decrease of C compared to as-deposited amorphous hydrogenated carbon coating (Table 4.3), which indicates that

coating peeled off during the sliding test. Sample PAO-T125 showed fewer increases in Fe and decrease in C compared to sample PAO-C125 (Table 4.3). The scratches present on samples PAO-C125 indicated the abrasive wearing of coating by the wear particles present at the interface (Figures 4.16 f). The absence of the abrasive wear marks on samples PAO-T40, TMP-T40, PAO-T125 and TMP-T125 are due to the textures (Figures 4.16 a, 4.16 c, 4.16 e and 4.16 g), which trap these wear particles and causes lower abrasive wearing.

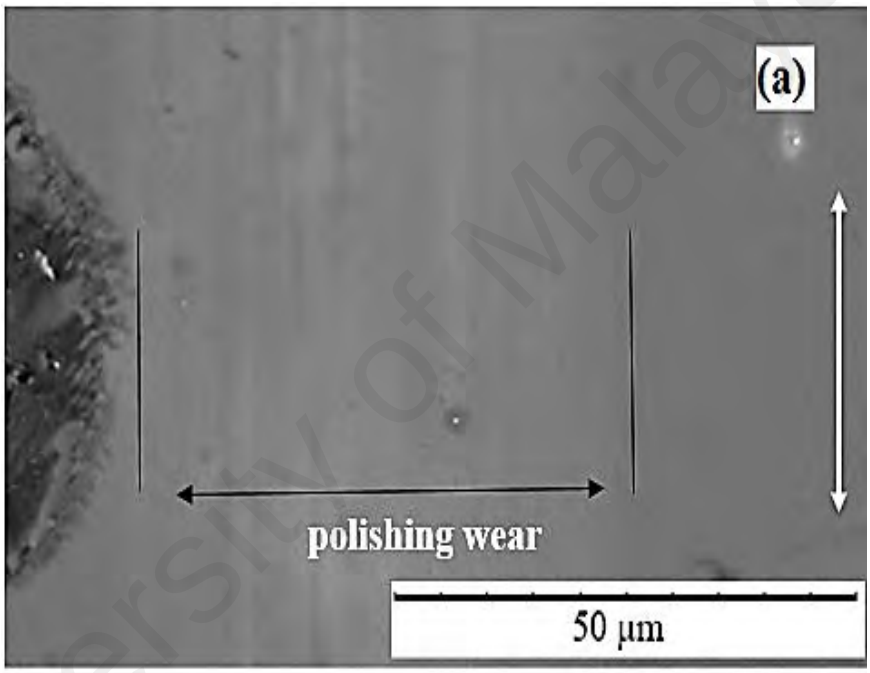

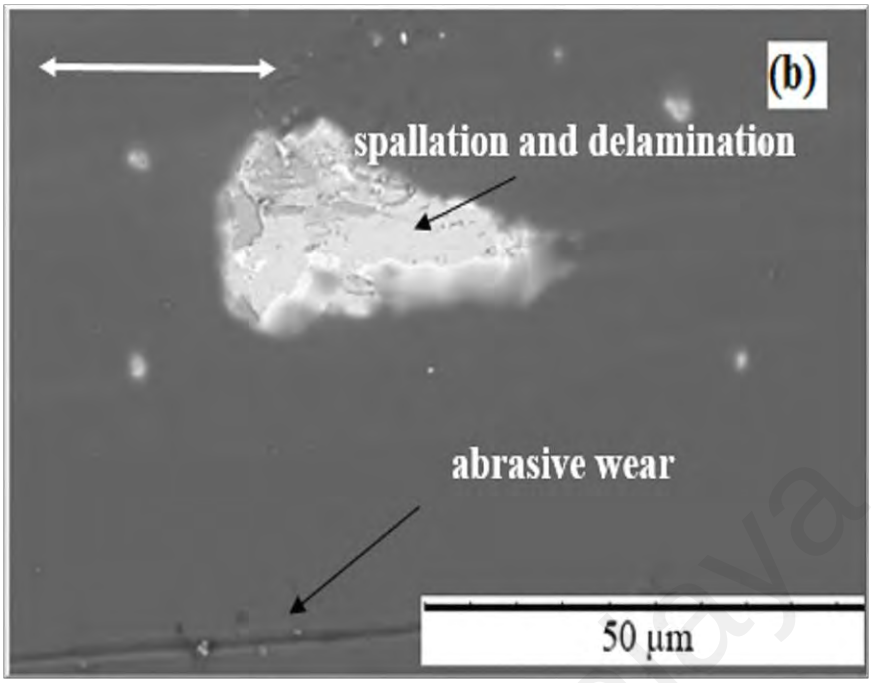

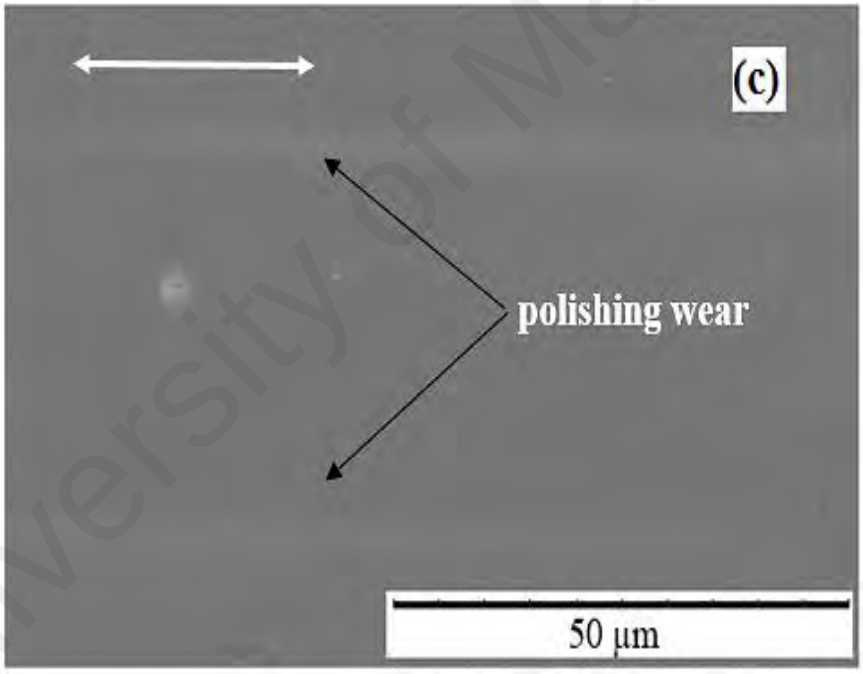

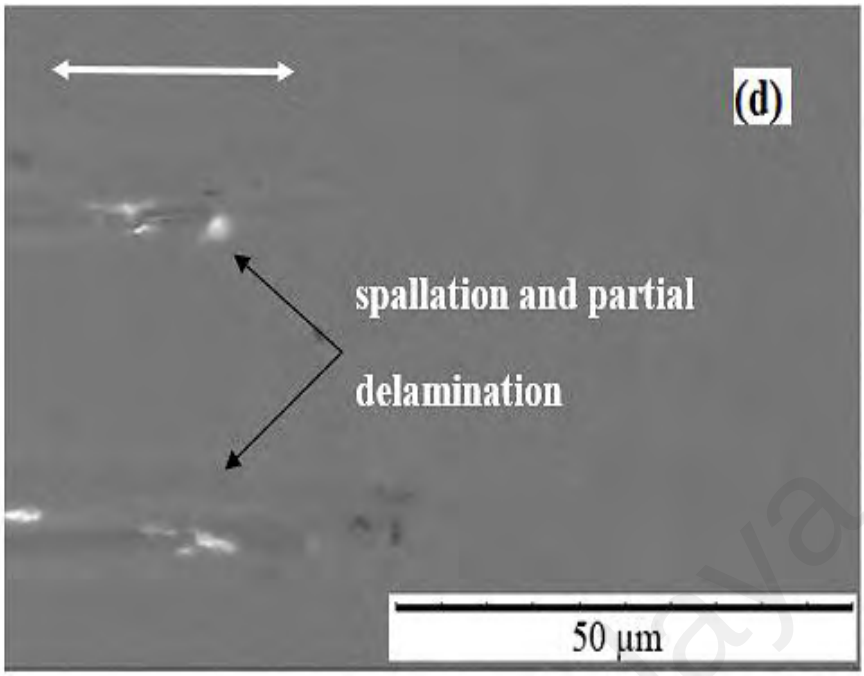

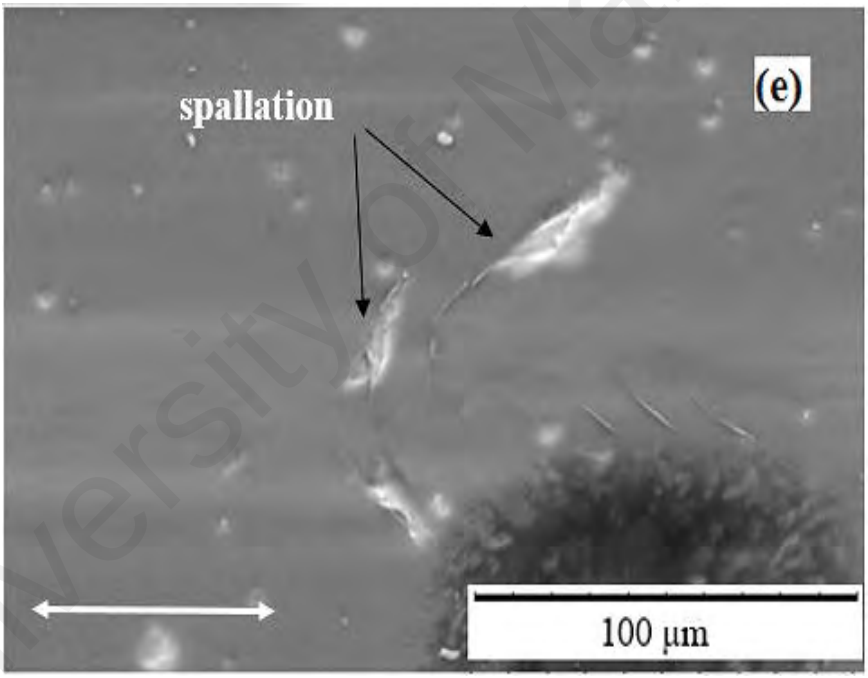

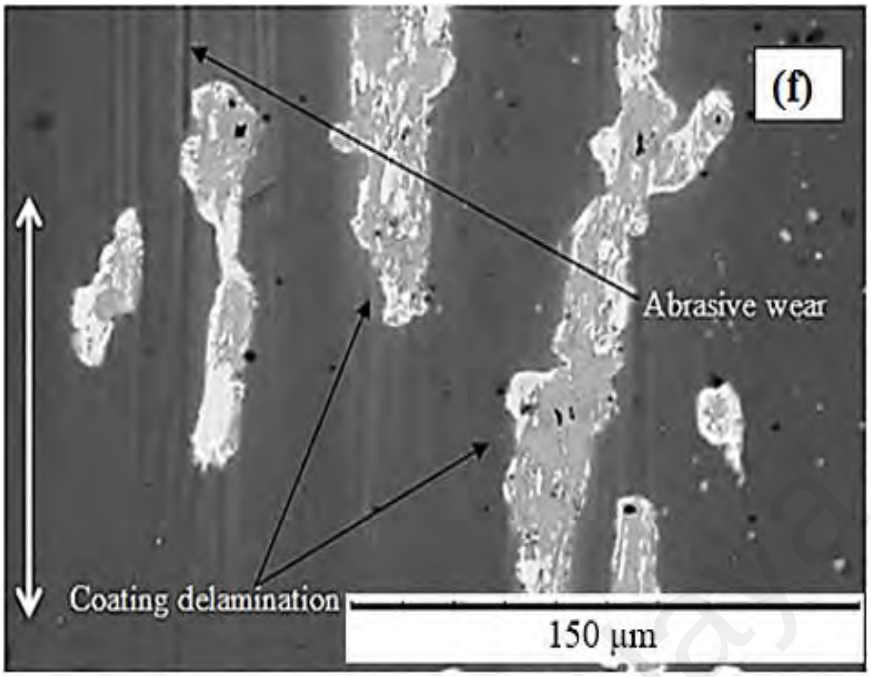

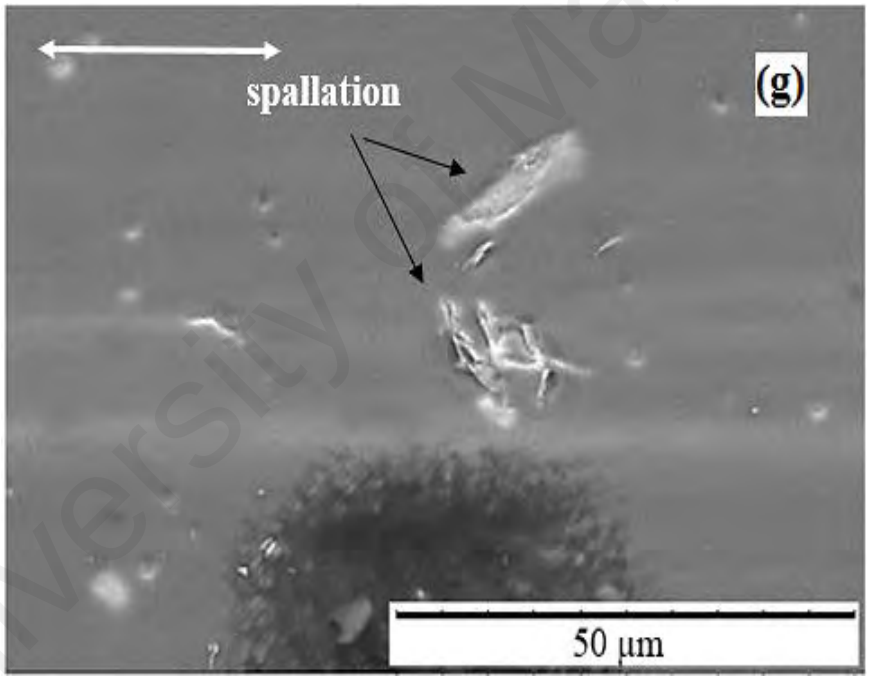

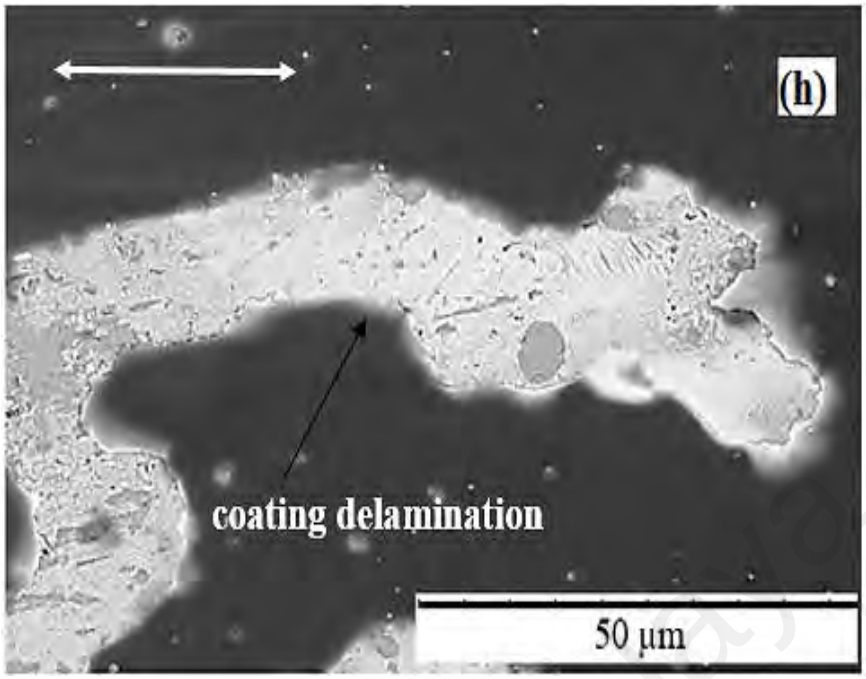

Figure 4.14 continued: SEM images of wear track after friction testing (a) PAO-T40, (b) PAO-C40, (c) TMP-T40, (d) TMP-C40, (e) PAO-T125, (f) PAO-C125, (g) TMP-T125 and (h) TMP-C125

Table 4.3: EDX analysis of un-textured/textured amorphous hydrogenated carbon coated samples at various temperatures

Specimen	Elements (Atomic %)					
	C	O	Cr	Fe	Si	Mn
a-C:H-as deposited	97.01	0.45	2.20	0.34	-	-
PAO-T40	93.48	0.75	4.92	0.85	-	-
PAO-C40	84.38	1.12	8.92	5.58	-	-
TMP-T40	94.12	2.45	2.91	0.52	-	-
TMP-C40	89.99	2.77	5.67	1.57	-	-
PAO-T125	85.18	0.84	8.44	5.54	-	-
PAO-C125	36.84	1.40	18.32	42.89	0.55	-
TMP-T125	83.01	2.45	9.22	5.32	-	-
TMP-C125	34.23	3.45	21.22	41.10	-	-

To further analyze the wear track, AFM was used. Figure 4.17 shows the AFM images of samples at various temperatures. Un-textured coated samples PAO-C40, PAO-C125, TMP-C40 and TMP-C125 showed sharp grooves that were created by the wear particles present in the interface (Figure 4.17 b, 4.17 d, 4.17 f and 4.17 h). These particles scratch the surface during sliding. Textured coated samples PAO-T40, PAO-T125, TMP-T40 and TMP-T125 did not show sharp grooves on the wear tracks (Figure 4.17). As it has been discussed in the previous paragraph, the wear particle capturing ability of textures helps in reducing the formation of sharp grooves on the track. Figure 4.18 shows the average roughness (Ra) of the samples. Sample TMP-T40 showed the lowest and TMP-C125 showed the highest average roughness. The general trend followed by all the samples is that average surface roughness increases with the increase in temperature. However, this increase is lower in the case of textured samples. Wear particle capturing and lubricant providing ability helps in lowering the surface roughness.

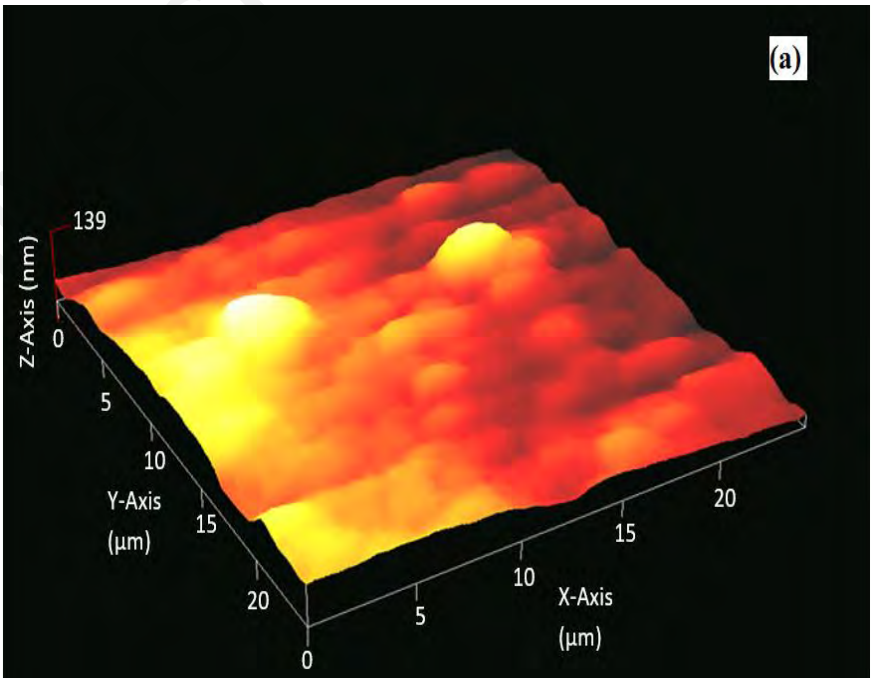

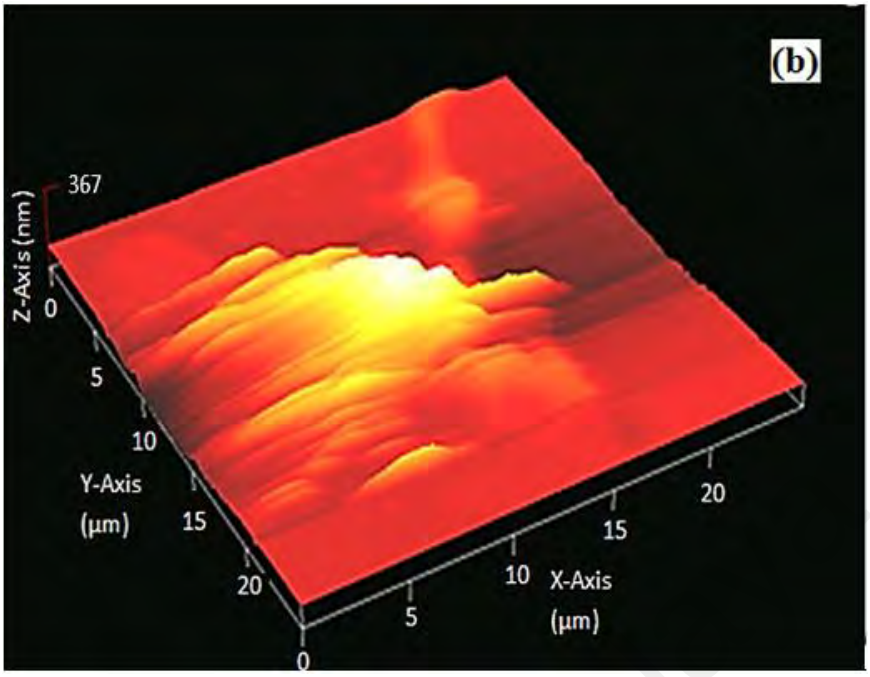
(b)
367
Z-Axis (nm)
0
5
10
Y-Axis
(µm)
15
20
0
5
10
15
20
X-Axis
(µm)

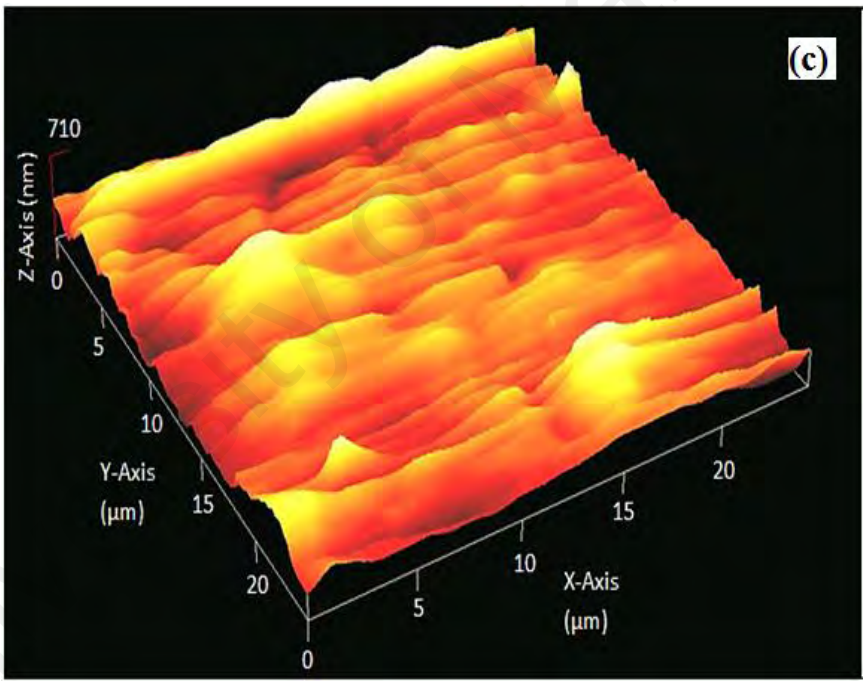
(c)
710
Z-Axis (nm)
0
5
10
Y-Axis
(µm)
15
20
0
5
10
15
20
X-Axis
(µm)

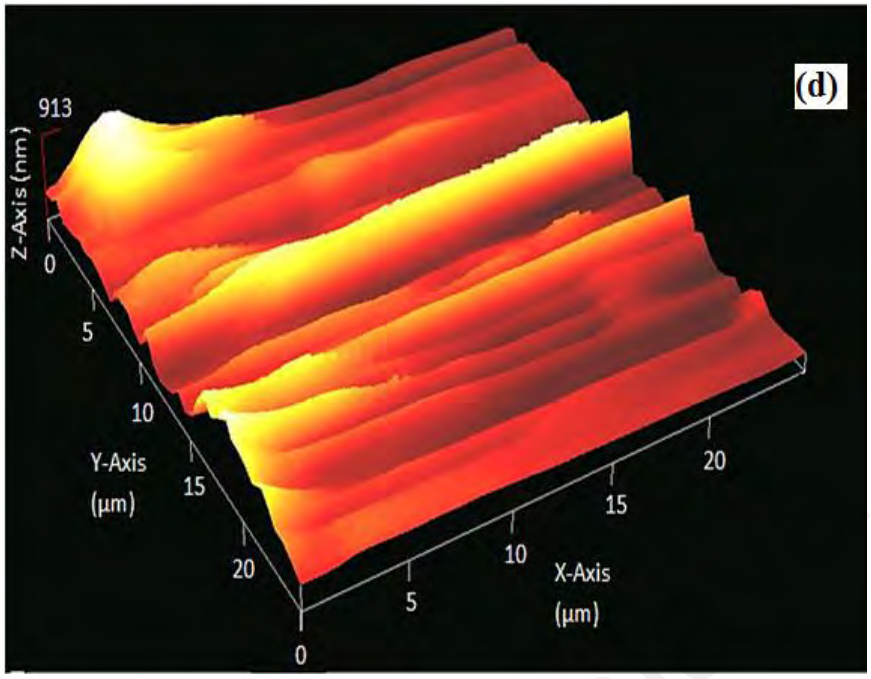

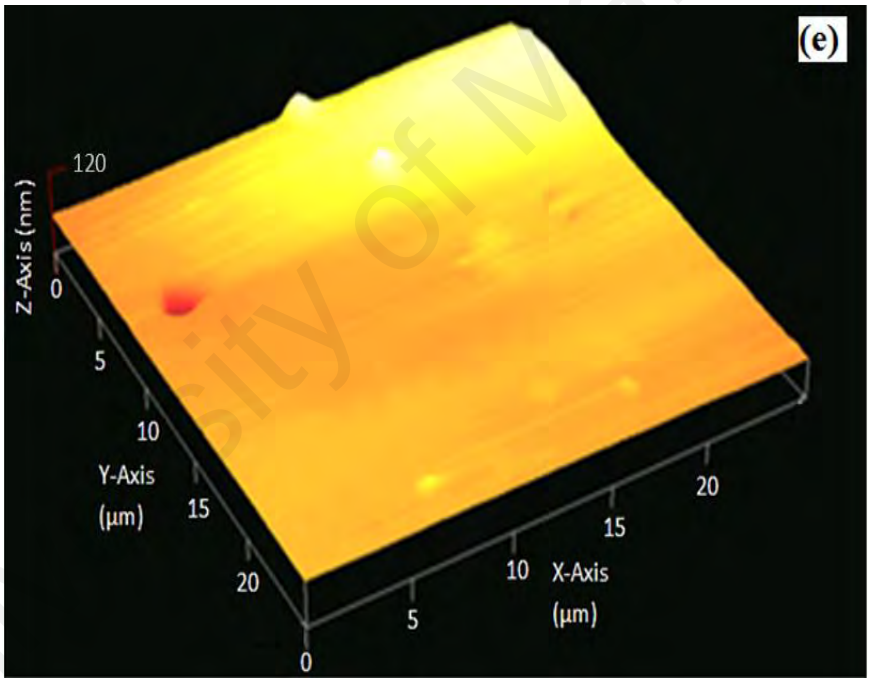

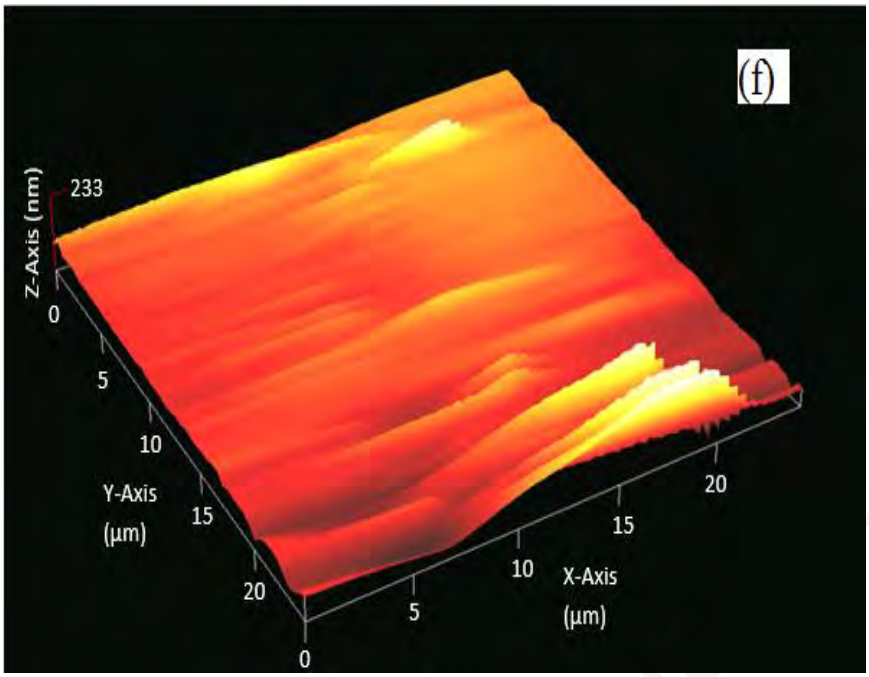
(f)
Z-Axis (nm)
233
0
5
10
15
20
Y-Axis
(µm)
0
5
10
15
20
X-Axis
(µm)

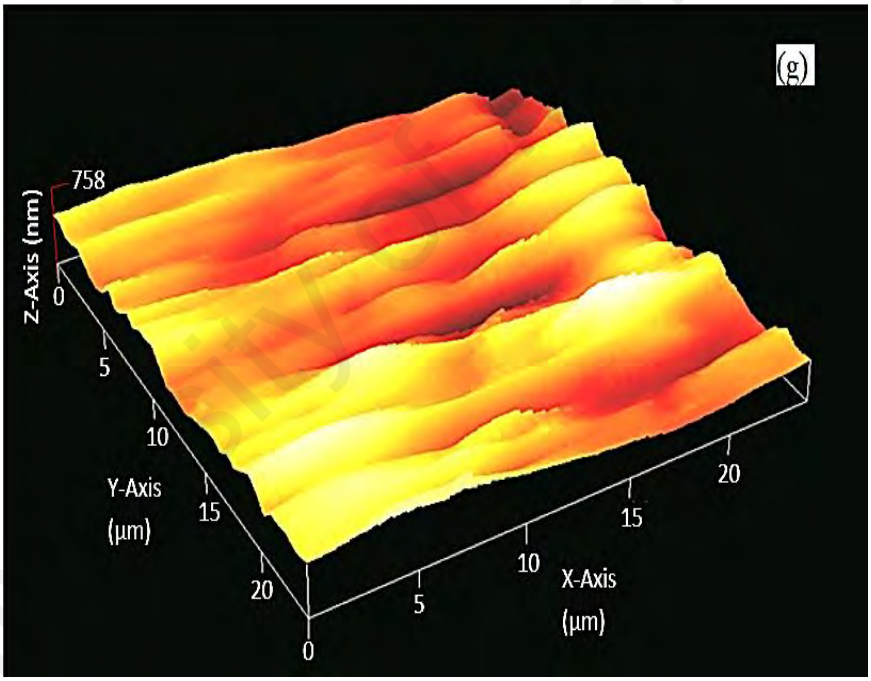
(g)
Z-Axis (nm)
758
0
5
10
15
20
Y-Axis
(µm)
0
5
10
15
20
X-Axis
(µm)

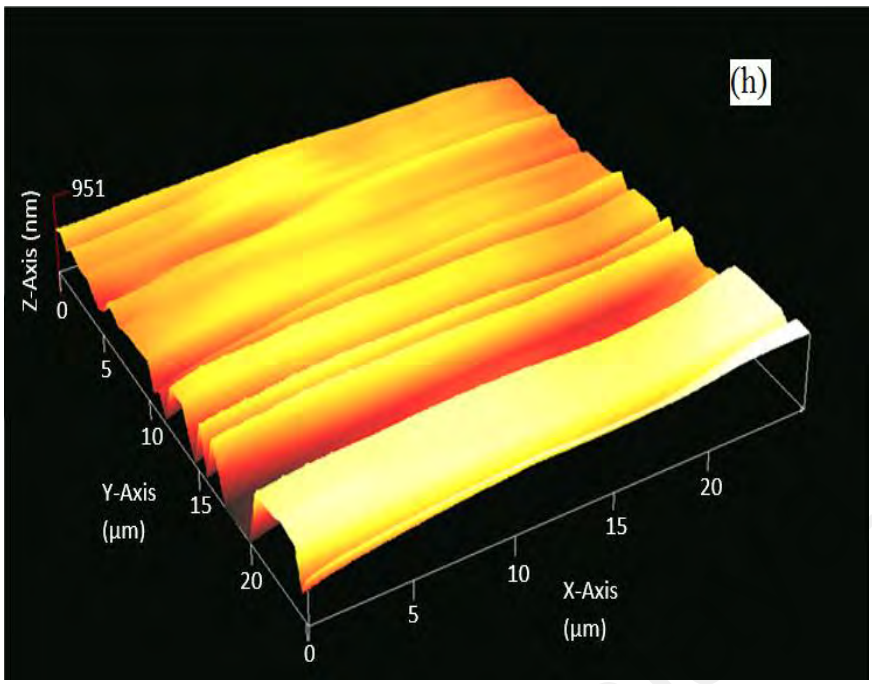

Figure 4.15 continued: AFM images of wear track after friction testing (a) PAO-T40, (b) PAO-C40, (c) PAO-T125, (d) PAO-C125 (e) TMP-T40, (f) TMP-C40, (g) TMP-T125 and (h) TMP-C125

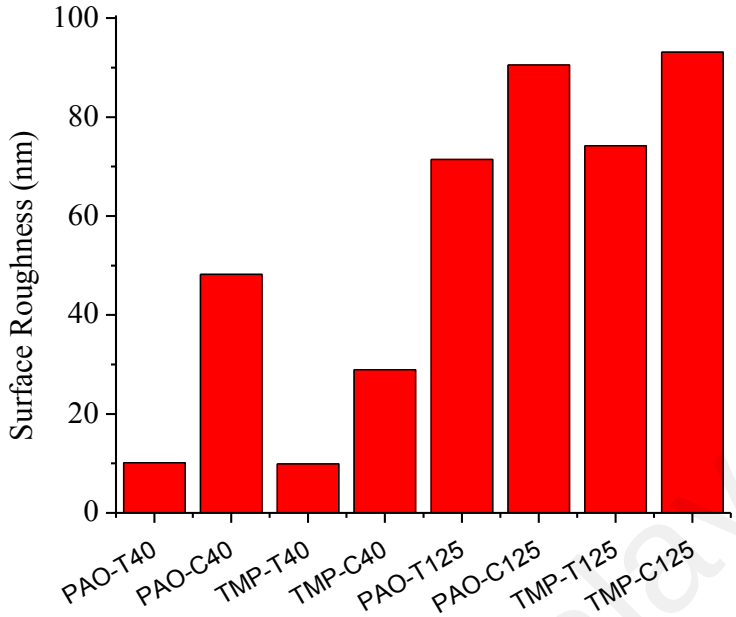

Figure 4.16: Average surface roughness at the wear track after friction testing

Figure 4.19 shows the wear rate of the counter ball, in the case of textured and un-textured amorphous hydrogenated carbon samples. The steel ball, which rubbed against sample PAO-T125 (Figure 4.19 a), showed smoother surface, whereas the ball which rubbed against PAO-C125 showed slight grooves (Figure 4.19 b). The ball that rubbed against sample TMP-T125 (Figure 4.19 c) and TMP-C125 (Figure 4.19 d) showed similar behavior to PAO-T125 and PAO-C125. The reduction in wear of the PAO-T125 and TMP-T125 counter ball can be caused by the mechanism of dimples. In the case of textured amorphous hydrogenated carbon, the counter ball wear rate increases with the increase in temperature (Figure 4.13). At 125 ºC, the un-textured amorphous hydrogenated carbon showed lower wear rate than textured amorphous hydrogenated carbon. The reduction in wear rate in the case of un-textured amorphous hydrogenated carbon can be attributed to the fact that, due to graphitization, a graphitic transfer film forms on the counter surface, which provides an easy slip between the contacting surfaces (C. Donnet, 1998). In the case of textured a-C:H, the increase in wear rate of the counter ball with regard to temperature can be due to the lower graphitization with temperature,

which reduces the formation of graphitic transfer film. This has been confirmed with raman spectroscopy in section 4.3.2.1.

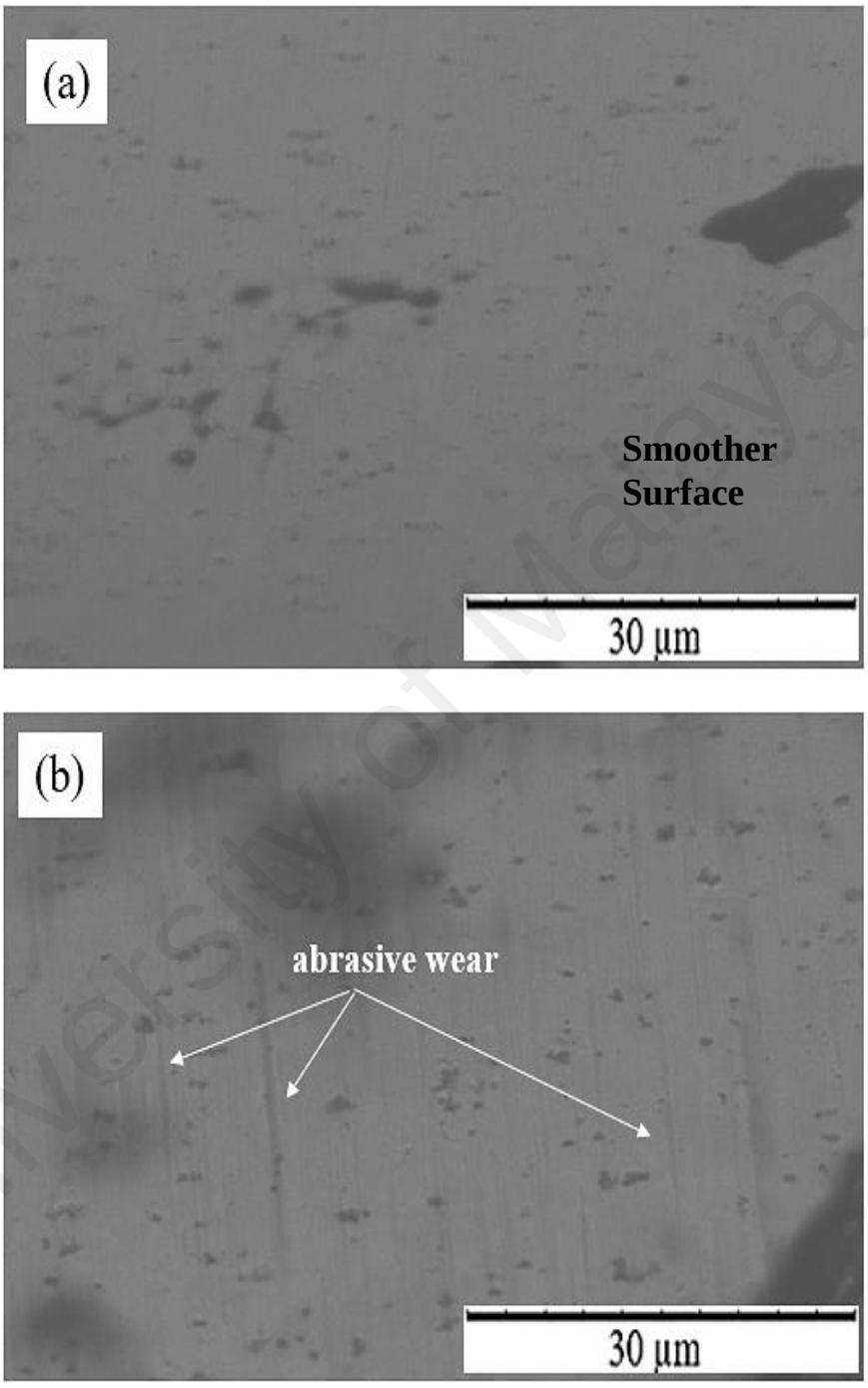

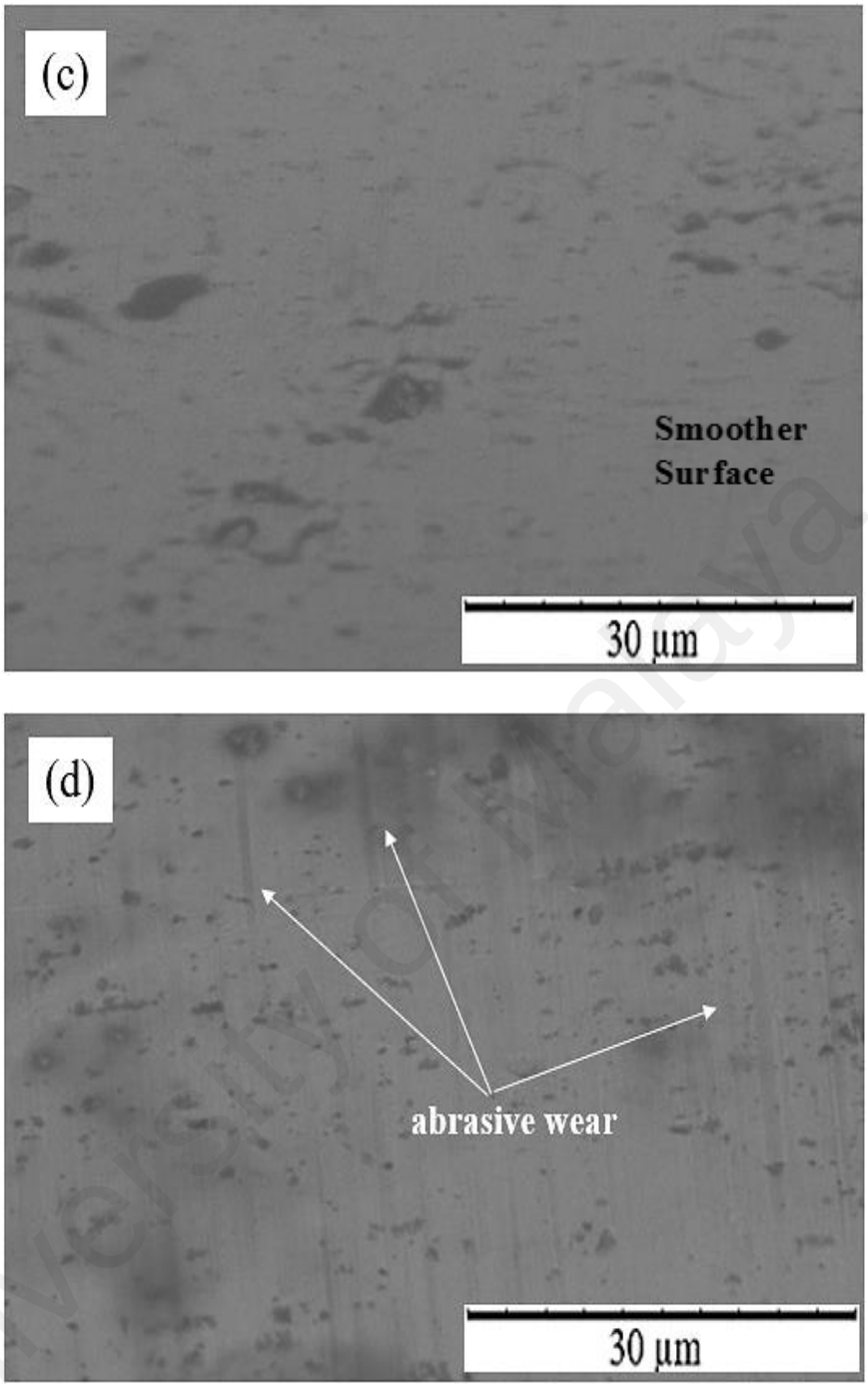

Figure 4.17 continued: SEM images of steel balls which rub against (a) PAO-T125, (b) PAO-C125, (c) TMP-T125 and (d) TMP-C125

4.4 Effect of surface texture on tribological performance of tetrahedral amorphous carbon coating at various temperatures

4.4.1 Friction and wear behavior

Figure 4.20 shows the coefficient of friction variation with time for textured tetrahedral amorphous carbon coated and un-textured tetrahedral amorphous carbon coated samples under PAO and palm based TMP lubrication.

Samples ta-C.PAO-T40 and ta-C.TMP-T40 showed stable and lower coefficient of friction compared to samples ta-C.PAO-C40 and ta-C.TMP-C40 throughout the friction test (Figure 4.20 a). Lower coefficient of friction of textured tetrahedral amorphous carbon coating can be related to the ability of micro textures to provide lubricant at the interface and capture wear particles. Dumitru et al. observed stable coefficient of friction with textured DLC compared to un-textured DLC (Dumitru et al., 2003). They concluded that textures trap hard wear debris which causes abrasive wear and as a result make friction unstable (Dumitru et al., 2003). In textured and un-textured cases, palm based TMP showed lower coefficient of friction throughout the test compared to PAO at 40 ºC. As previously mentioned, in case of amorphous hydrogenated carbon coating that the lower coefficient of friction in TMP lubricant at 40 ºC in textured and un-textured case can be due to its high polarity (Gellman & Spencer, 2002). Due to this, it is easily attracted to steel surface. The higher polarity forms a higher affinity for metal at one end of the molecule and allows a non-polar hydrocarbon to extend out and provide a barrier between the tribo-pair (Canter, 2009; Zulkifli et al., 2014). In addition, palm oil has longer carbon chain length (18-20), due to which the formed film behaves as a crystalline solid and reduces coefficient of friction (Bhushan, 2013). After 800 s, ta-C.PAO-C40 showed stable coefficient of friction until 2800 s, ta-C.TMP-C40 showed nearly stable coefficient of friction until 4800 s. Both the samples nearly stabilized around 5600 s and remained stable until the end of test. Figure 4.21 shows the wear coefficient for various samples

tested with PAO and palm based TMP ester. Sample ta-C.TMP-C40 showed lower wear coefficient than sample ta-C.PAO-C40 (Figure 4.21). Textured sample ta-C.TMP-T40 showed lower wear coefficient than un-textured sample ta-C.PAO-T40 (Figure 4.21). In textured and un-textured cases, palm based TMP lubricant showed lower wear coefficient compared to PAO lubricant at 40 ºC. Better lubricity of palm based TMP lubricant was also observed in the case of amorphous hydrogenated carbon coating in section 4.3.1.

At 80 ºC temperature, textured samples ta-C.PAO-T80 and ta-C.TMP-T80 exhibited stable coefficient of friction. PAO lubricated sample ta-C.PAO-T80 showed higher coefficient of friction compared to palm based TMP lubricated sample ta-C.TMP-T80. Coefficient of friction of un-textured samples (ta-C.TMP-C80 and ta-C.PAO-C80) exhibited unstable behavior. The lower coefficient of friction of un-textured tetrahedral amorphous carbon coating at 80 ºC can be due to graphitization phenomenon. The graphitization phenomenon will be discussed in detail in section 4.4.2.1. Figure 4.21 shows that textured samples (ta-C.PAO-T80 and ta-C.TMP-T80) showed lower wear coefficient compared to un-textured samples (ta-C.PAO-C80 and ta-C.TMP-C80). Amorphous hydrogenated carbon coating also showed similar behavior at 80 ºC in section 4.3.1.

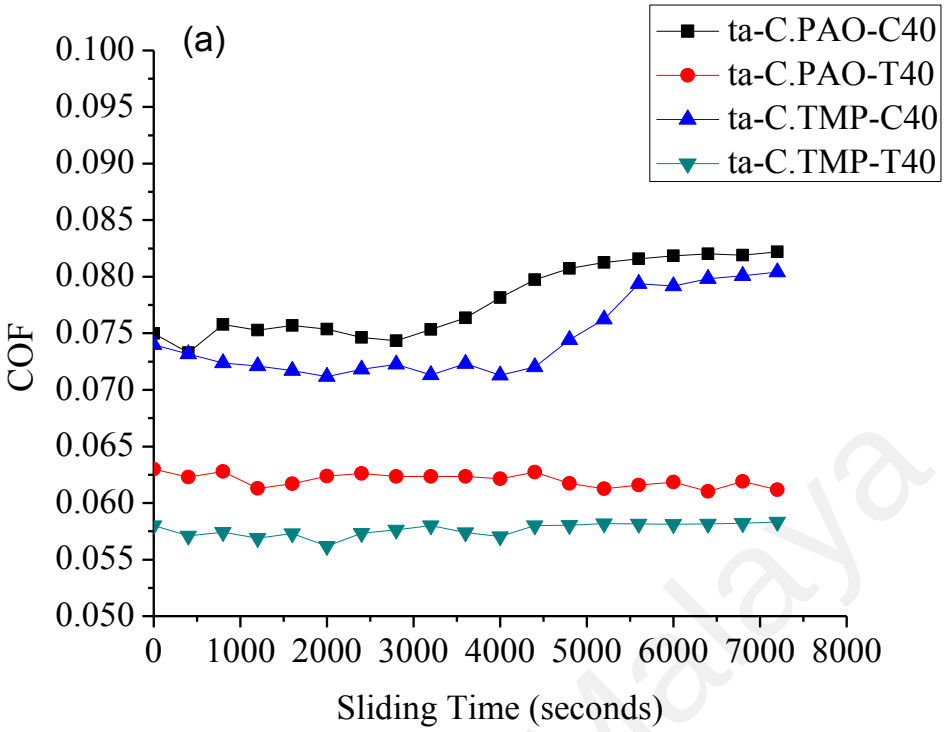

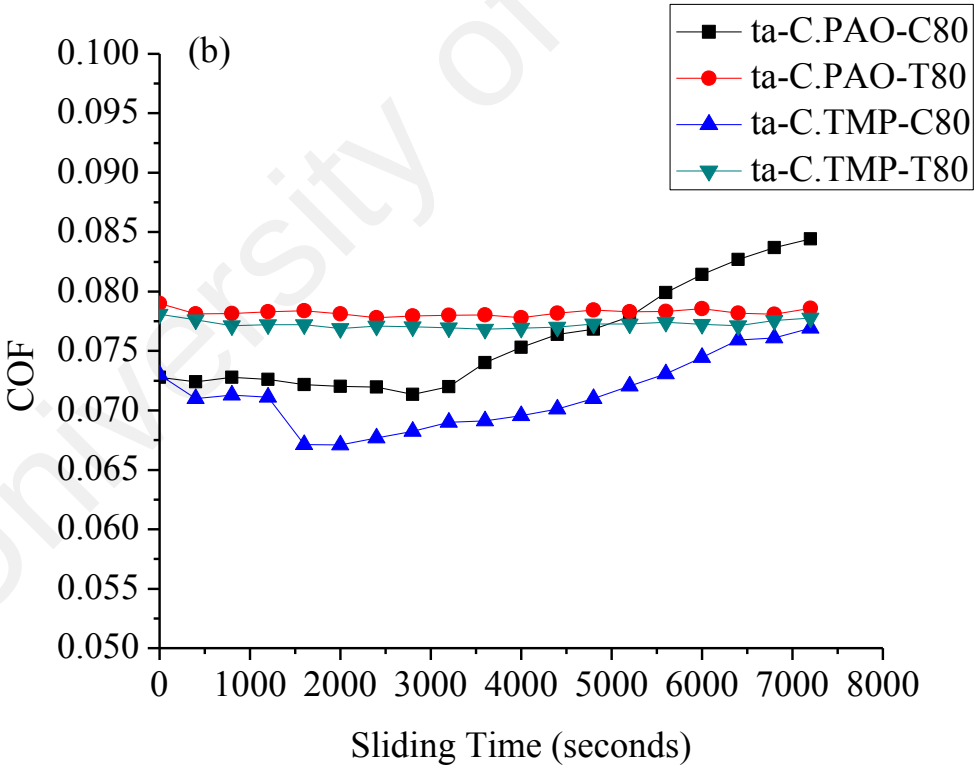

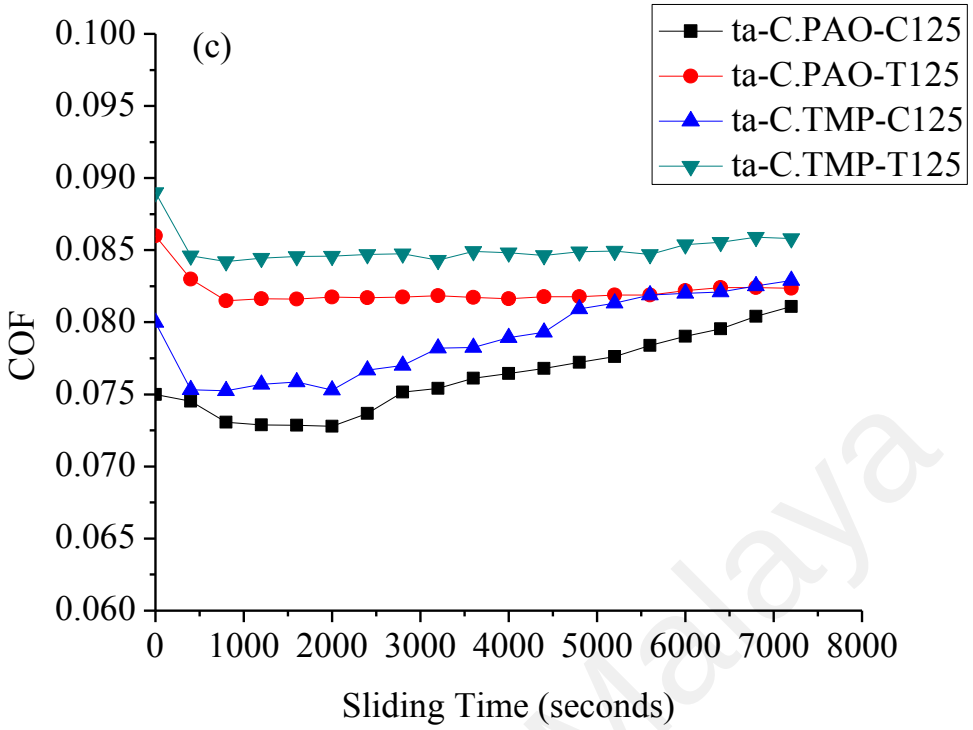

Figure 4.18 continued: Change in coefficient of friction of tetrahedral amorphous carbon coated samples with time (a) temperature 40 ºC, (b) temperature 80 ºC and (c) temperature 125 ºC

Figure 4.20 c shows coefficient of friction of textured and un-textured tetrahedral amorphous carbon film at 125 °C. After initial instability, sample ta-C.PAO-T125 showed a steady coefficient of friction till the end of the test. Sample ta-C.TMP-T125 also showed stable coefficient of friction throughout the test. Coefficient of friction in the case of ta-C.PAO-C125 and ta-C.TMP-C125 increased after 2000 s. Coefficient of friction of these samples kept on increasing until the end of the test. Unlike tests conducted at 80 °C, PAO showed lower coefficient of friction compared to palm based TMP lubricant at 125 °C, additionally un-textured tetrahedral amorphous carbon coating showed lower coefficient of friction compared to textured tetrahedral amorphous carbon coating. Similar behavior was observed in the case of amorphous hydrogenated carbon coating in section 4.3.1. This behavior can be explained by suppression of graphitization by the textures. As it has been observed that graphitization reduces coefficient of friction,

therefore un-textured tetrahedral amorphous carbon coating showed lower coefficient of friction at 125 °C. The reduction in graphitization transformation can explain the lower increase in the wear rate of textured tetrahedral amorphous carbon coating compared to un-textured tetrahedral amorphous carbon coating at various temperatures tested in both lubricants. Wear coefficient results at 125 °C with respect to textured and un-textured samples was similar to 40 and 80 °C (Figure 4.21). Samples ta-C.PAO-T125 and ta-C.TMP-T125 showed lower wear coefficient than samples ta-C.PAO-C125 and ta-C.TMP-C125. Wear coefficient of samples tested in palm based TMP lubricant was higher compared to PAO lubricant at 125 °C. This behavior was dissimilar to tests conducted at temperature 40 and 80 °C where palm based TMP showed lower wear irrespective of whether they are textured or un-textured. The higher coefficient of friction and wear in case of PAO compared to palm based TMP at 125 ºC can be due to the unstable film formation of palm based TMP at higher temperatures. At higher temperatures film formed by fatty acid chains are unstable, thus increasing friction and wear (Chiong et al., 2012)

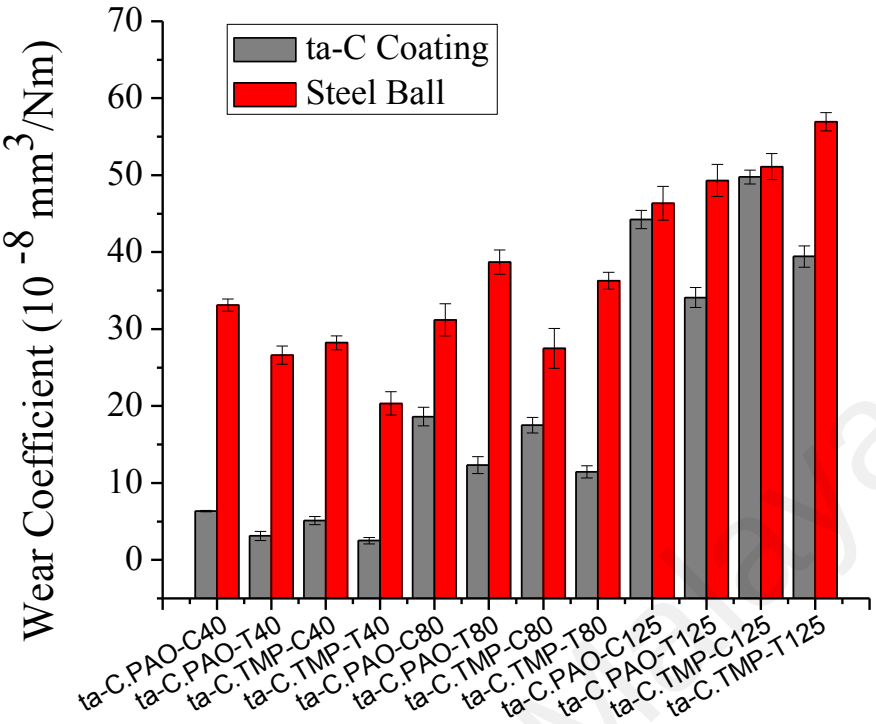

Figure 4.19: Wear coefficient of tetrahedral amorphous carbon coated textured/un-textured samples after tribological testing at various temperatures

Due to graphitization, the coating layer becomes soft and the load bearing capacity reduces and wear increases (Kalin et al., 2010). This could be the reason for the higher wear rate in the case of un-textured tetrahedral amorphous carbon coating at 40 °C, 80 °C and 125 °C, as can be seen in Figure 4.21. With the increase in temperature, graphitization increases and thus wear coefficient increases for tetrahedral amorphous carbon coating (Al Mahmud et al., 2014).

4.4.2 Wear track characterization of tetrahedral amorphous carbon coating

4.4.2.1 Raman analysis

In order to investigate the behavior of graphitization for tetrahedral amorphous carbon coating Raman spectroscopy was used. Tetrahedral amorphous carbon coating is a metastable form of amorphous carbon and friction induced graphitization can occur

(Donnet & Erdemir, 2007). In order to avoid inaccuracies, three Raman spectra was collected for each sample to avoid inaccuracies from peak fitting.

Figures 4.22 and 4.23 shows the spectra's for samples tested in PAO and palm based TMP lubricants respectively. After coating deposition, the G peak position was at 1558.18 cm^{-1} and the I_D/I_G ratio was 1.12. After tribological testing, tetrahedral amorphous carbon coated samples ta-C.PAO-C40 and ta-C.TMP-C40 showed G peak at 1566.39 cm^{-1} and 1566.32 cm^{-1} respectively. The I_D/I_G ratio of 1.42 and 1.5 was shown by tetrahedral amorphous carbon coated samples ta-C.PAO-C40 and ta-C.TMP-C40 respectively. Textured tetrahedral amorphous carbon coated samples ta-C.PAO-T40 and ta-C.TMP-T40 showed G peak at 1560 cm^{-1} and 1559.55 cm^{-1} respectively. The I_D/I_G ratio for textured tetrahedral amorphous carbon coated samples ta-C.PAO-T40 and ta-C.TMP-T40 was 1.14 and 1.15, respectively (Figures 4.22 and 4.23). The shift in the G peak and increase in the I_D/I_G ratio indicate an increase in the sp^2 fraction (graphite) in the DLC film (Casiraghi et al., 2005; Ferrari & Robertson, 2000). The higher increase in G peak and I_D/I_G ratio of un-textured coated samples compared to textured samples indicates that at 40 ºC, un-textured tetrahedral amorphous carbon coated samples ta-C.PAO-C40 and ta-C.TMP-C40 showed higher graphitic transformation. As was discussed in section 4.3.2.1, graphitic transformation reduces coefficient of friction, whereas it increases wear coefficient. However, textured tetrahedral amorphous carbon coated samples ta-C.PAO-T40 and ta-C.TMP-T40 showed less coefficient of friction and wear coefficient than un-textured samples even though textured tetrahedral amorphous carbon coated samples showed lower graphitic transformation at 40 ºC. This indicates that lower coefficient of friction and wear coefficient of textured tetrahedral amorphous carbon coated samples can be because of textures behaving as lubricant/wear particle reservoirs. Similar results were observed in the case of amorphous hydrogenated carbon coated samples at 40 ºC in section 4.3.2.1.

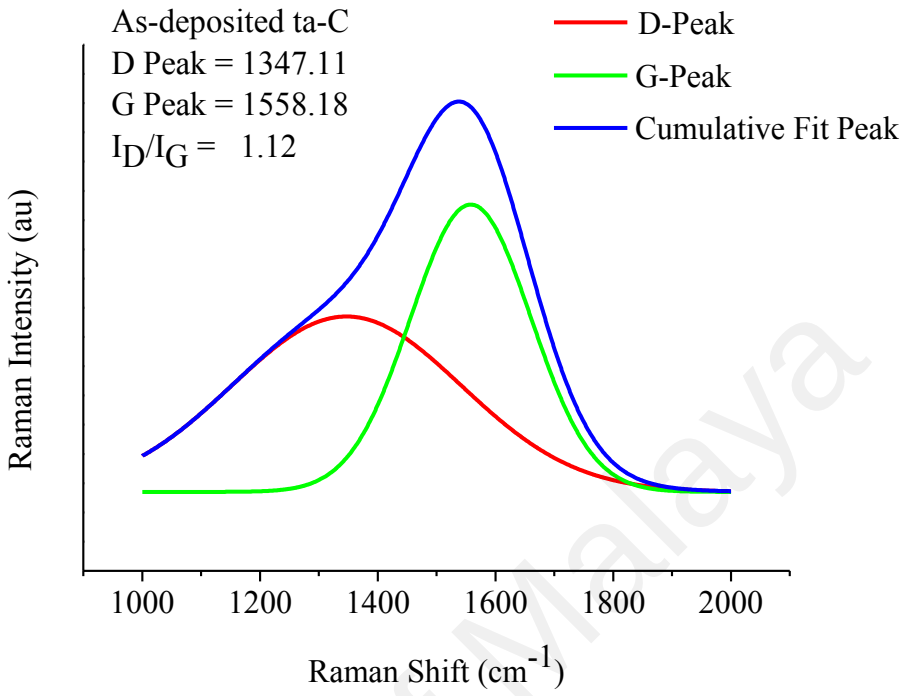

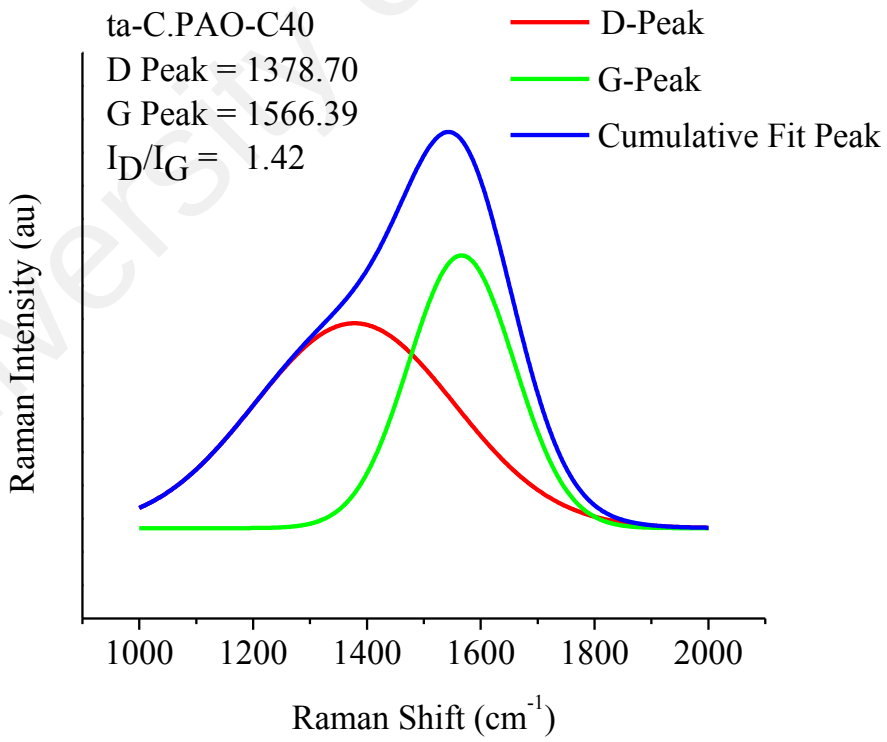

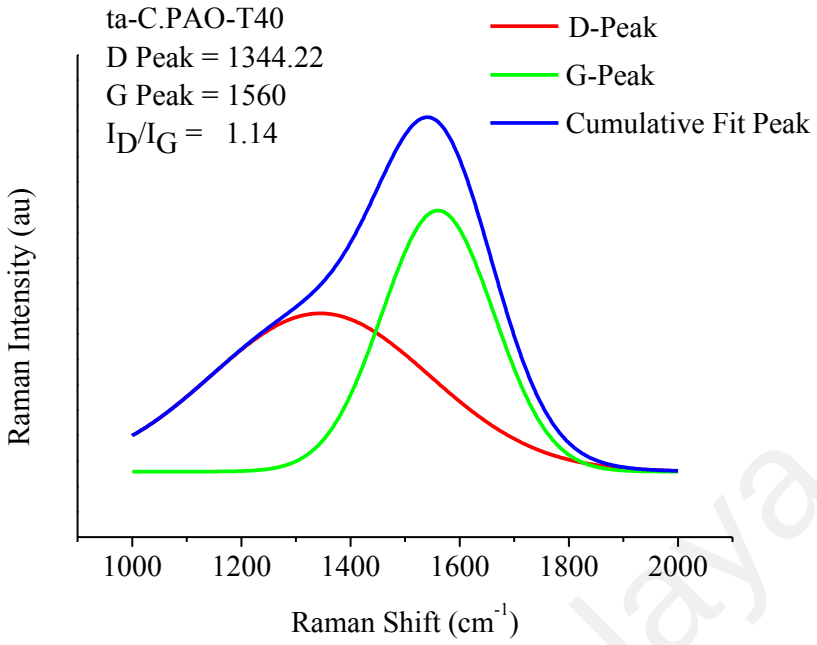

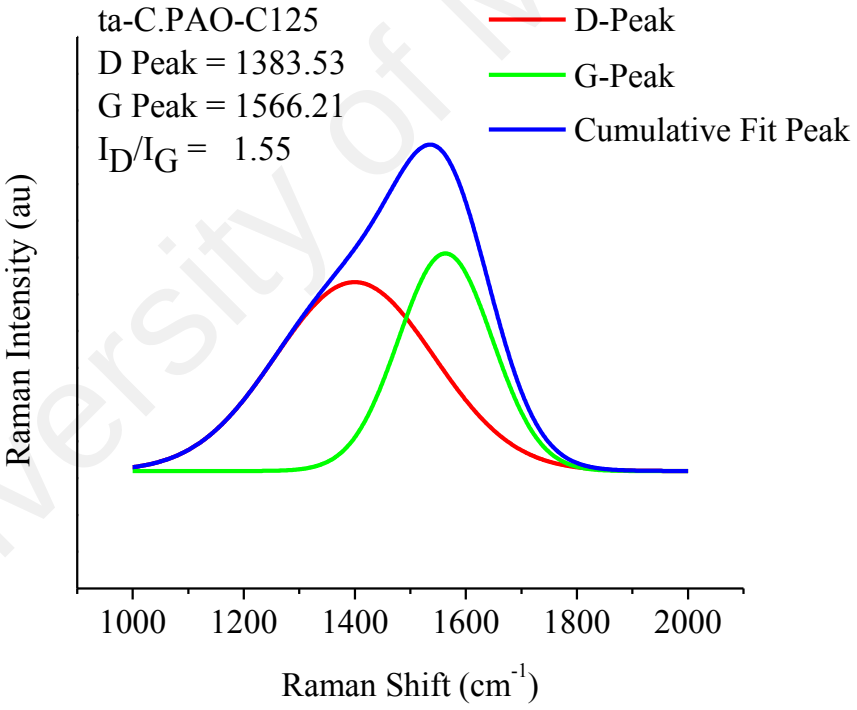

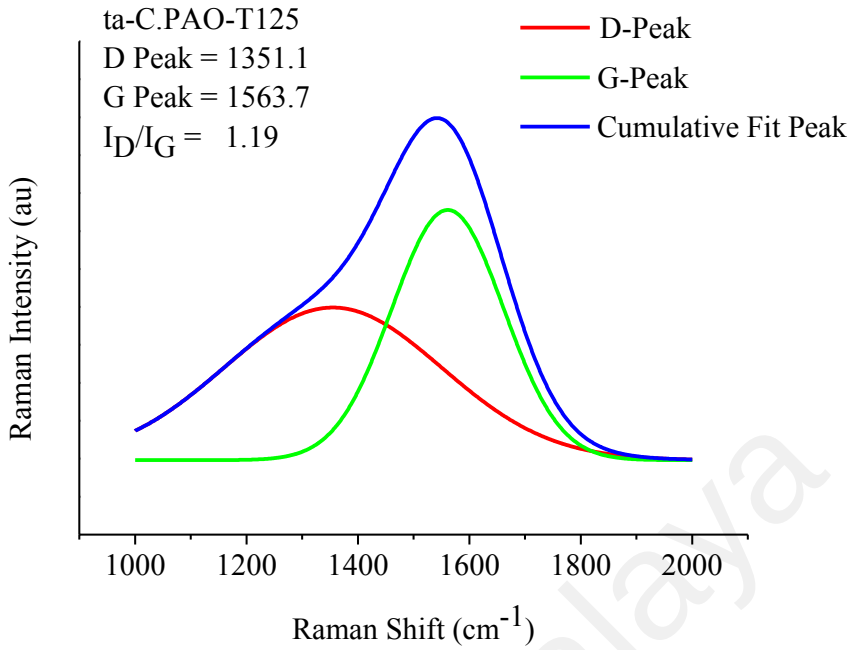

Figure 4.20 continued: Raman spectra of various textured/un-textured tetrahedral amorphous carbon coating at various temperatures in the presence of PAO lubricant

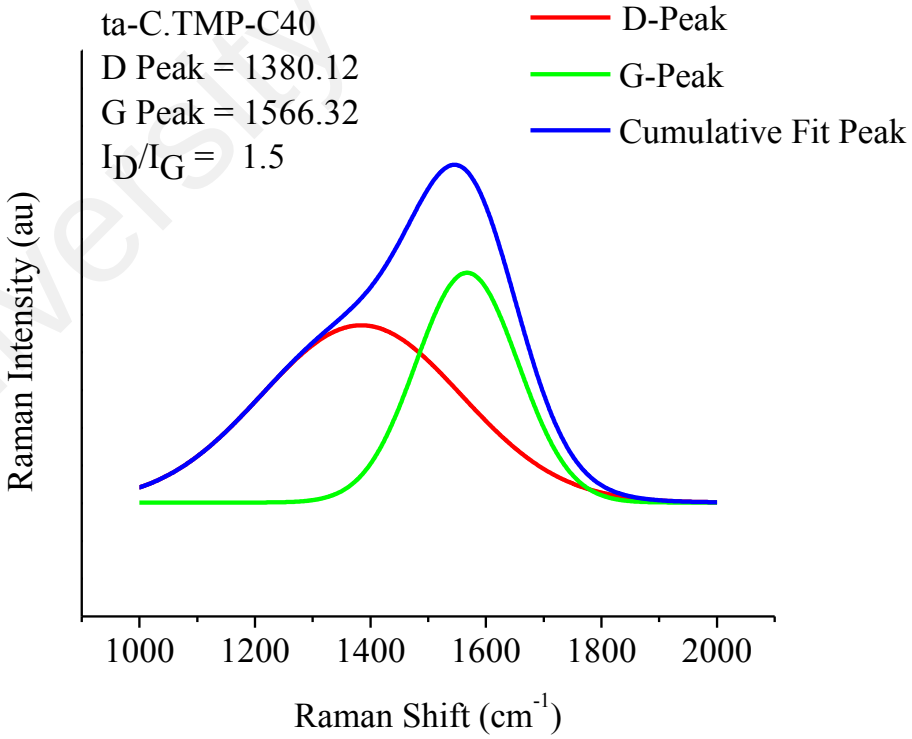

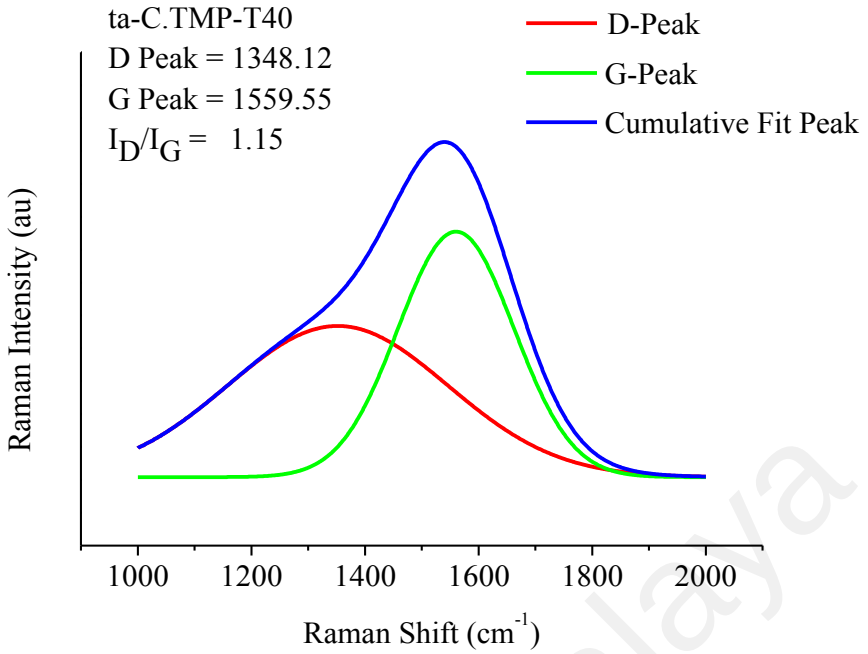

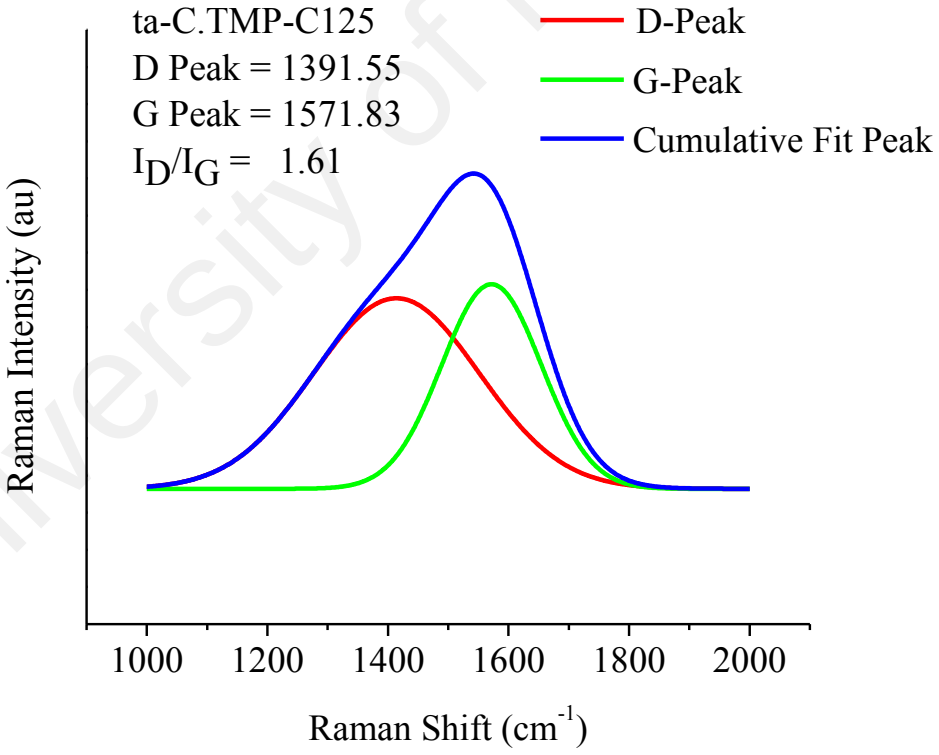

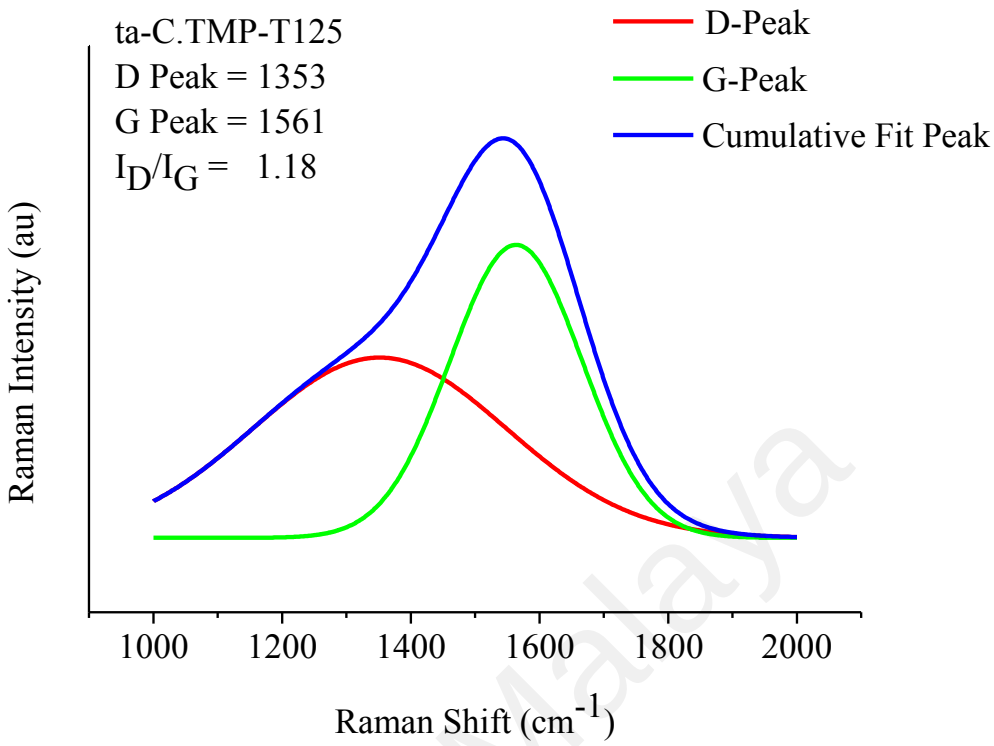

Figure 4.21 continued: Raman spectra of various textured/un-textured tetrahedral amorphous carbon coating at various temperatures in the presence of palm based TMP lubricant

At a temperature of 125 ºC, textured tetrahedral amorphous carbon coated samples ta-C.PAO-T125 and ta-C.TMP-T125 showed G peak at 1563.7 cm^{-1} and 1561 cm^{-1} and I_D/I_G ratio of 1.19 and 1.18, respectively. Un-textured tetrahedral amorphous carbon coated samples ta-C.PAO-C125 and ta-C.TMP-C125 showed G peak at 1566.21 cm^{-1} and 1571.83 cm^{-1} whereas I_D/I_G ratio of 1.55 and 1.61 respectively. The higher increase in G peak position and I_D/I_G ratio value for un-textured tetrahedral amorphous carbon coated samples at 125 ºC compared to as deposited tetrahedral amorphous carbon coating can be due to the absence of textures. As textured tetrahedral amorphous carbon coated samples showed less increase in G peak shift and I_D/I_G ratio value. Similar to friction and wear results found in amorphous hydrogenated carbon coating at 125 ºC, textured tetrahedral amorphous carbon coated samples showed higher coefficient of friction (Figures 4.20 c) and lower wear coefficient (Figures 4.21) than un-textured tetrahedral amorphous carbon

coated samples. These results can be explained by taking into account the mechanism of textures to capture wear particles and prevent graphitic transformation, thus preventing higher wear rate. As higher graphitization occurred in the case of un-textured tetrahedral amorphous carbon coated samples at 125 ºC, lower coefficient of friction is expected compared to textured samples.

4.4.2.2 SEM/EDX and AFM analysis

SEM images of wear tracks after friction testing are shown in Figure 4.24. Polishing wear was observed in the case of samples ta-C.PAO-T40 and ta-C.TMP-T40 (Figure 4.24 a and 4.24 c). Samples ta-C.PAO-C40 and ta-C.TMP-C40 showed slight coating spallation on the wear track (Figure 4.24 b and 4.24 d). Samples ta-C.PAO-T125 and ta-C.TMP-T125 (Figures 4.24 e and 4.24 g) did not show spallation at the wear track whereas samples ta-C.PAO-C125 and ta-C.TMP-C125 exhibited excessive coating spallation (Figures 4.24 f and 4.24 h).

The wear behavior was confirmed by EDX analysis (Table 4.4). Samples ta-C.PAO-C125 and ta-C.TMP-C125 showed a higher increase of Fe and decrease of C compared to as-deposited tetrahedral amorphous carbon coating (Table 4.4), which indicates that coating spallation occurred during the sliding test. Sample ta-C.PAO-T125 showed slight increase in Fe and decrease in C compared to ta-C.PAO-C125 (Table 4.4).

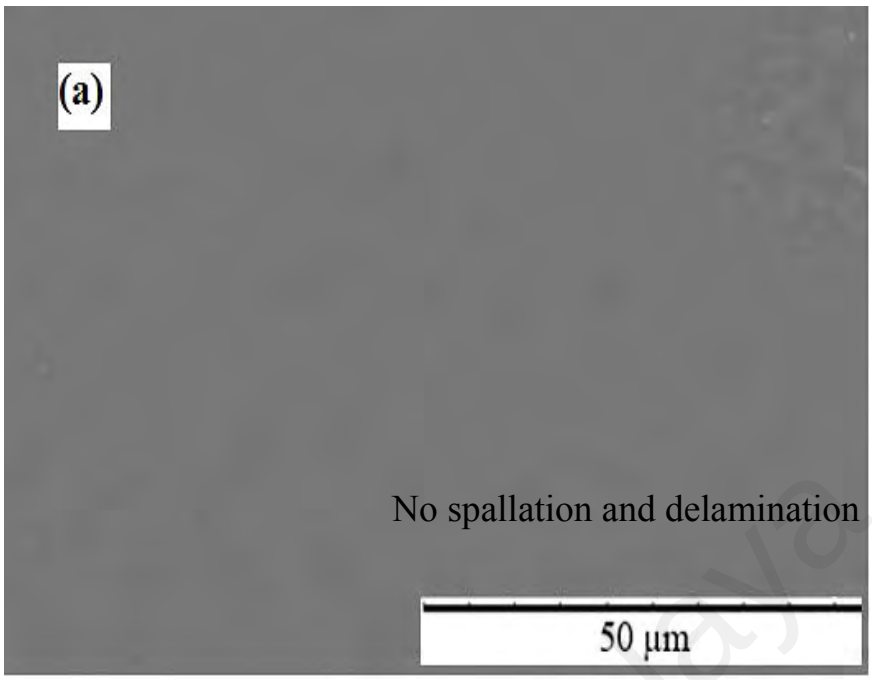

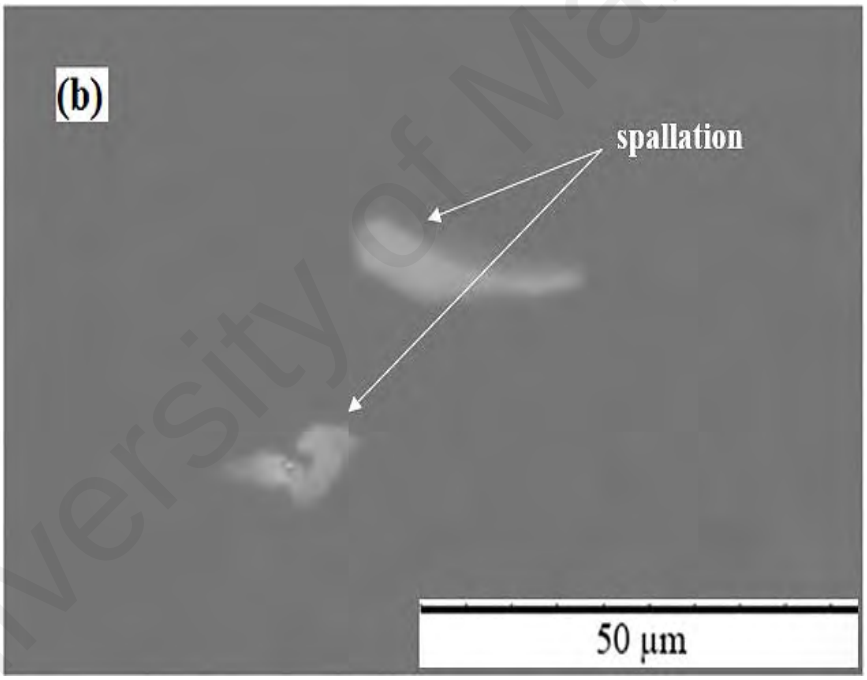

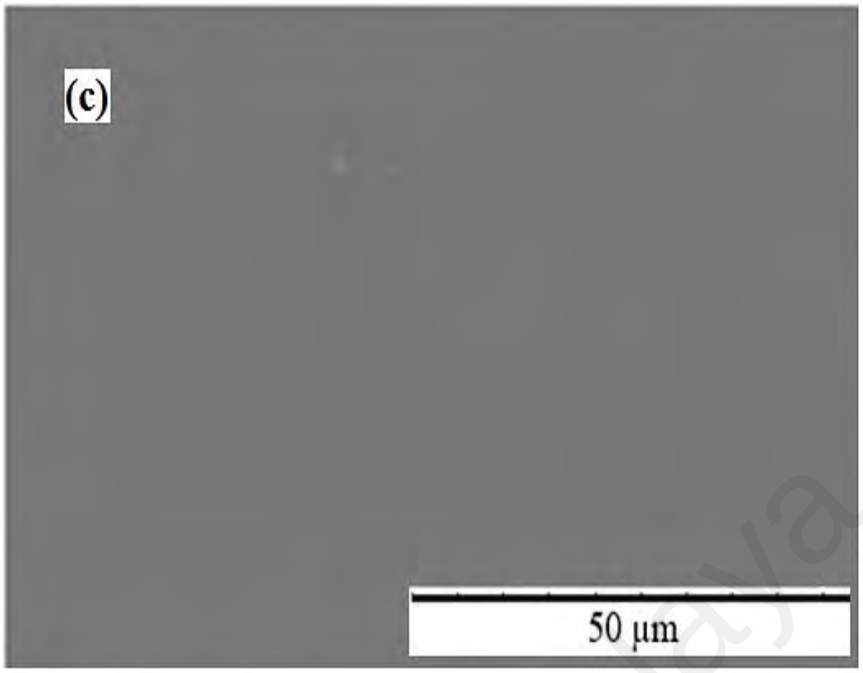

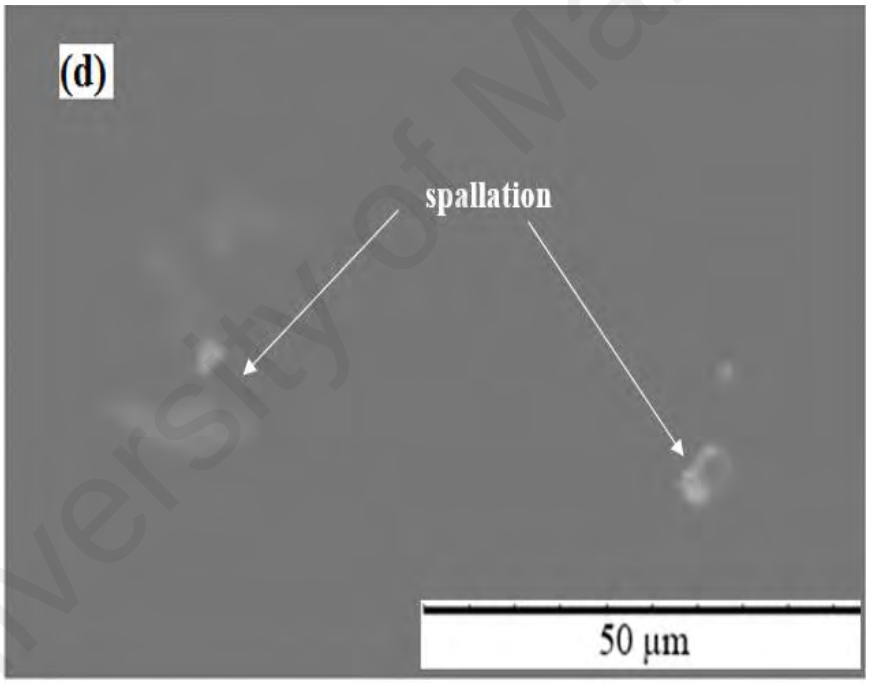

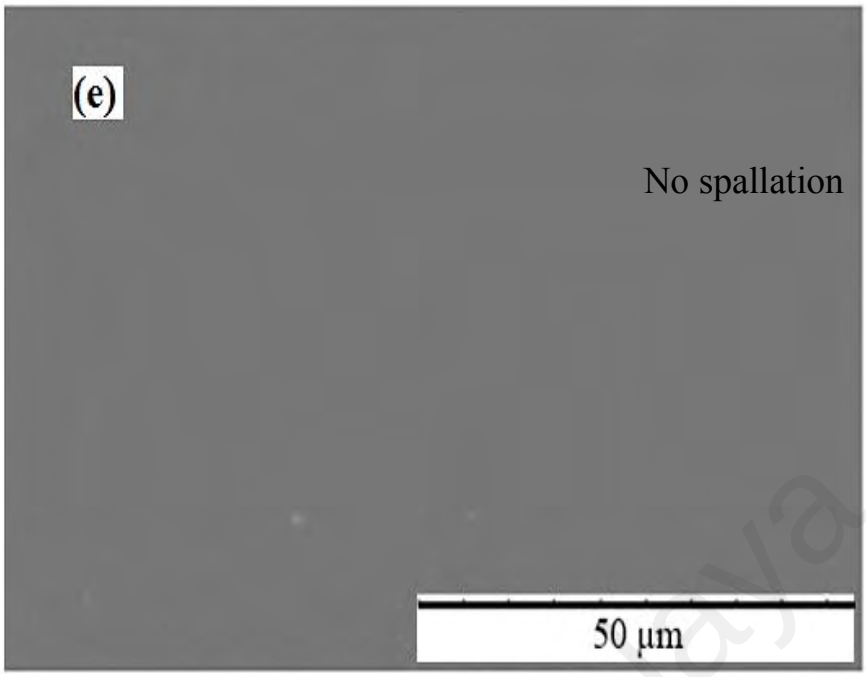

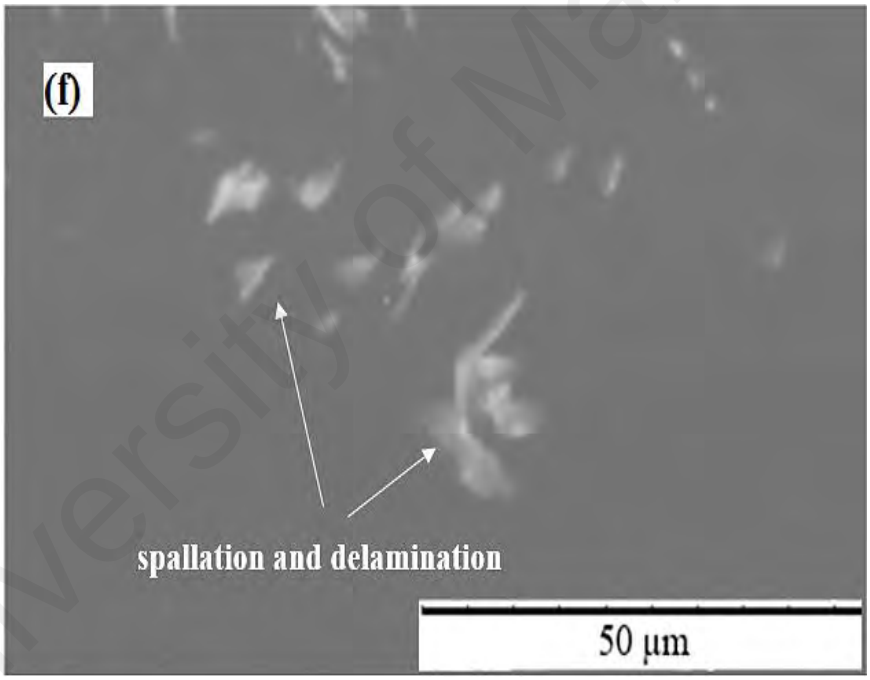

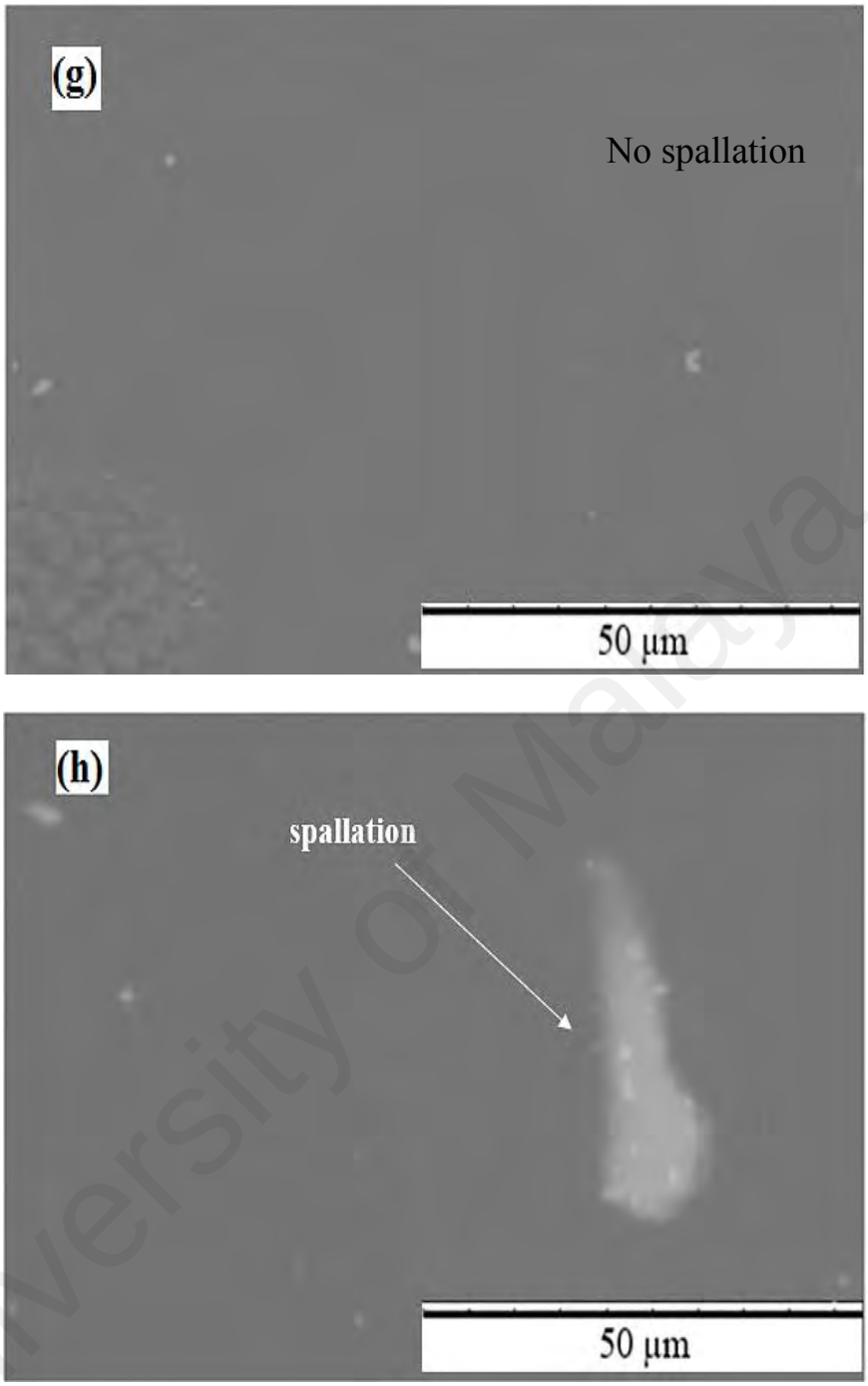

Figure 4.22 continued: SEM images of wear track after friction testing (a) ta-C.PAO-T40, (b) ta-C.PAO-C40, (c) ta-C.TMP-T40, (d) ta-C.TMP-C40, (e) ta-C.PAO-T125, (f) ta-C.PAO-C125, (g) ta-C.TMP-T125 and (h) ta-C.TMP-C125

To analyze the topography of the wear scar, AFM was used. Figure 4.25 shows the AFM images of tetrahedral amorphous carbon coated samples at various temperatures. Un-textured coated samples (ta-C.PAO-C40, ta-C.TMP-C40, ta-C.PAO-C125 and ta-C.TMP-C125) showed sharp grooves that can be created by the wear particles present at

the interface (Figures 4.25 b, 4.25 d, 4.25 f and 4.25 h). During sliding micro wear particles are formed at the interface; these particles can be from steel ball and/or hard coating. The coating wear debris are hard enough to scratch the wear track. Textured coated samples (ta-C.PAO-T40, ta-C.TMP-T40, ta-C.PAO-T125 and ta-C.TMP-T125) showed smoother wear tracks compared to un-textured samples (Figures 4.25 a, 4.25 c, 4.25 e and 4.25 g). Wear particles formed at the interface are captured by the textures in order to prevent excessive wearing (Oksanen et al., 2014). Similar behavior has been observed in the case of amorphous hydrogenated carbon coating in section 4.3.2.2.

Average surface roughness (Ra) of the tetrahedral carbon coated samples is shown in Figure 4.26. Sample ta-C.TMP-T40 showed the lowest Ra value of 8.12 nm and ta-C.TMP-C125 showed the highest average roughness of 68.09 nm. Tetrahedral amorphous carbon coated samples tested in palm based TMP showed lower roughness at 40 ºC compared to PAO lubricant, however at 125 ºC palm based TMP lubricated samples showed higher average roughness. With the increase in temperature average surface roughness increases for textured and un-textured tetrahedral coated samples. In the case of textured coated samples, the increase in average surface roughness with temperature is small compared to un-textured coated samples. Due to lower average surface roughness, coefficient of friction is stable in case of laser textured tetrahedral amorphous coating compared to un-textured coating (Figure 4.20).

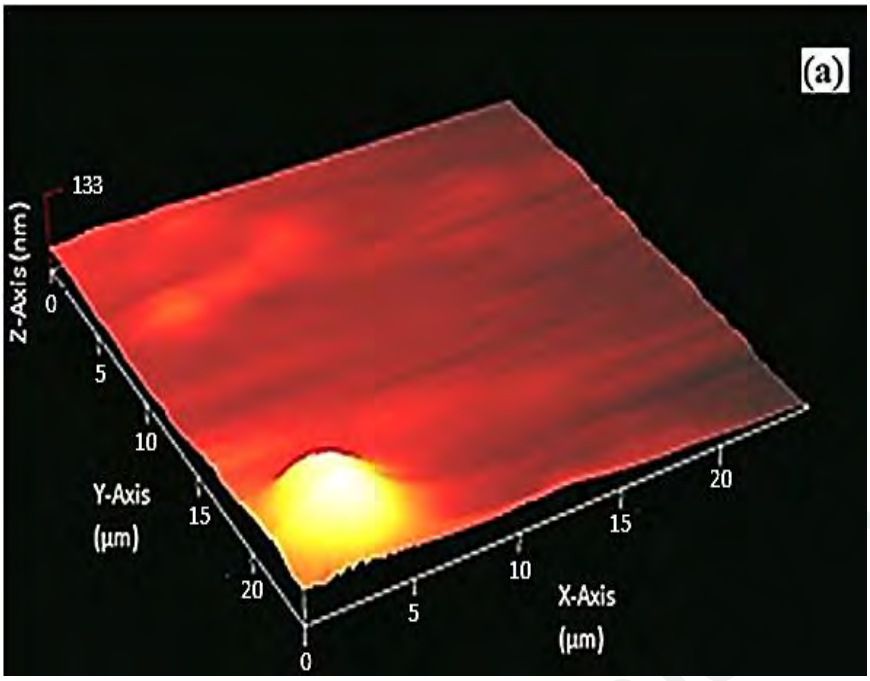

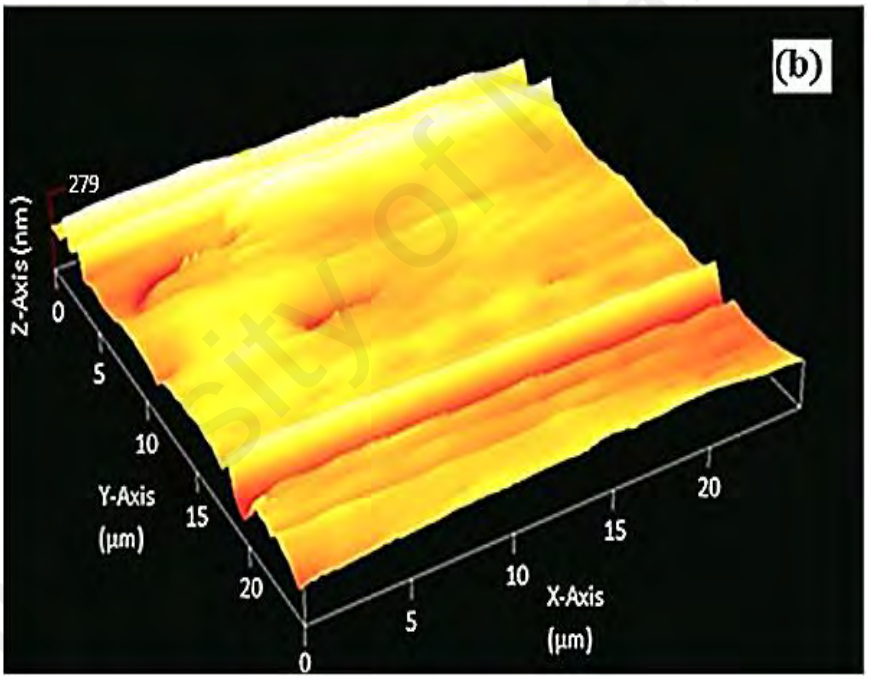

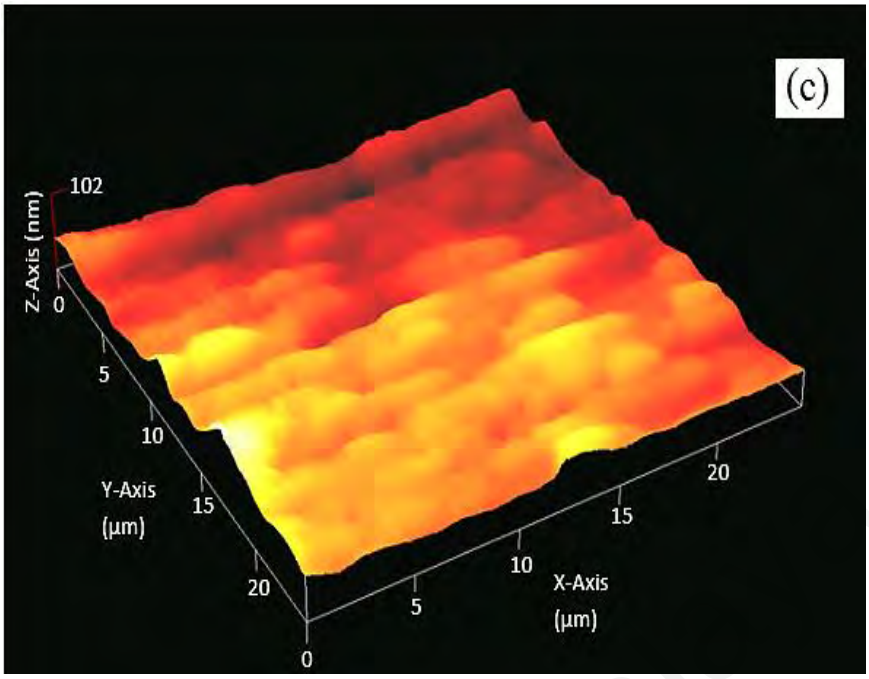
(c)
102
Z-Axis (nm)
0
5
10
15
20
Y-Axis
(µm)
0
5
10
15
20
X-Axis
(µm)

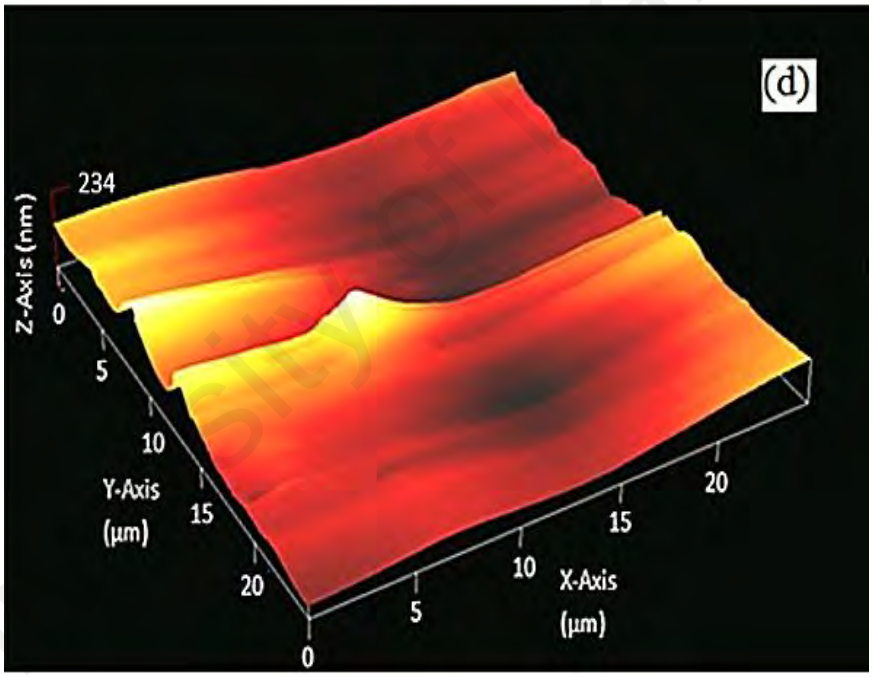
(d)
234
Z-Axis (nm)
0
5
10
15
20
Y-Axis
(µm)
0
5
10
15
20
X-Axis
(µm)

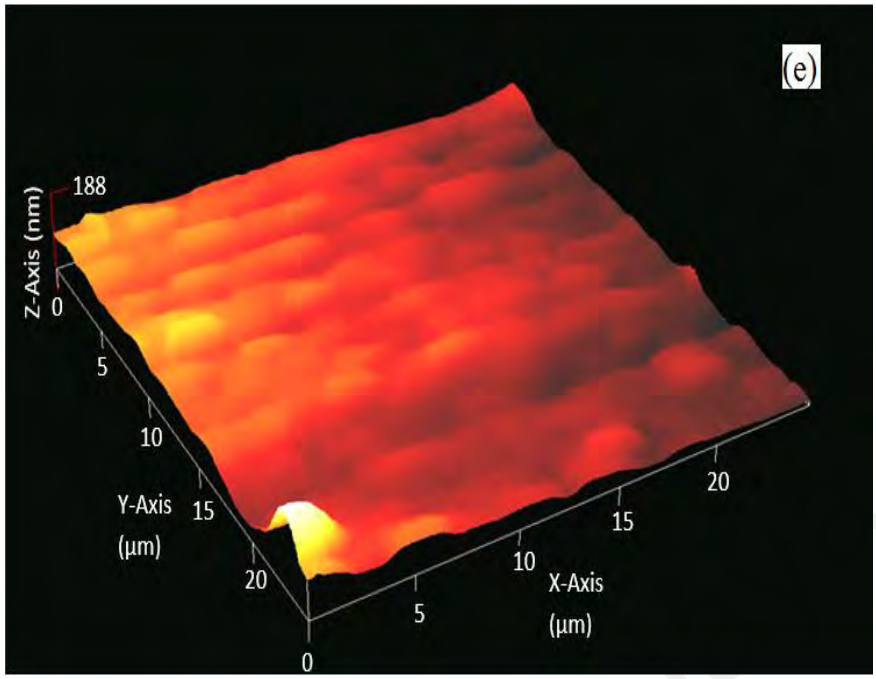
(e)
188
Z-Axis (nm)
0
5
10
Y-Axis
(µm)
15
20
0
5
10
X-Axis
(µm)
15
20

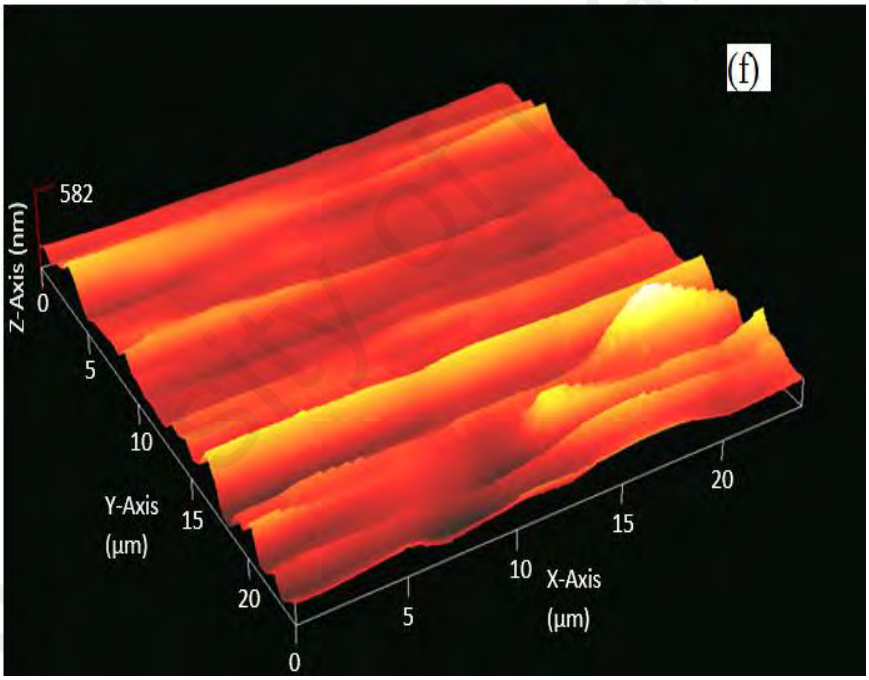
(f)
582
Z-Axis (nm)
0
5
10
Y-Axis
(µm)
15
20
0
5
10
X-Axis
(µm)
15
20

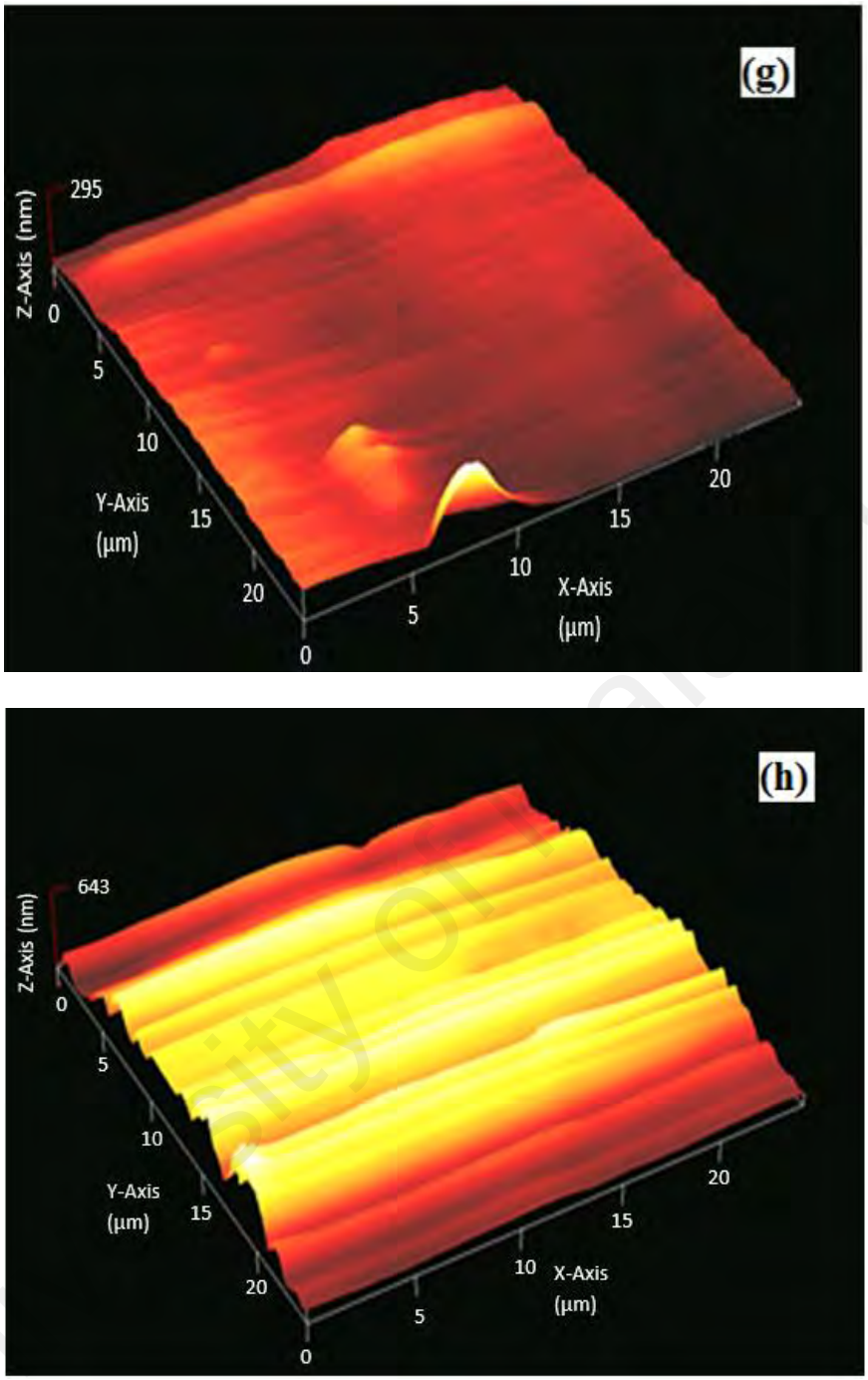

Figure 4.23 continued: AFM images of wear track after friction testing (a) ta-C.PAO-T40, (b) ta-C.PAO-C40, (c) ta-C.TMP-T40, (d) ta-C.TMP-C40, (e) ta-C.PAO-T125, (f) ta-C.PAO-C125, (g) ta-C.TMP-T125 and (h) ta-C.TMP-C125

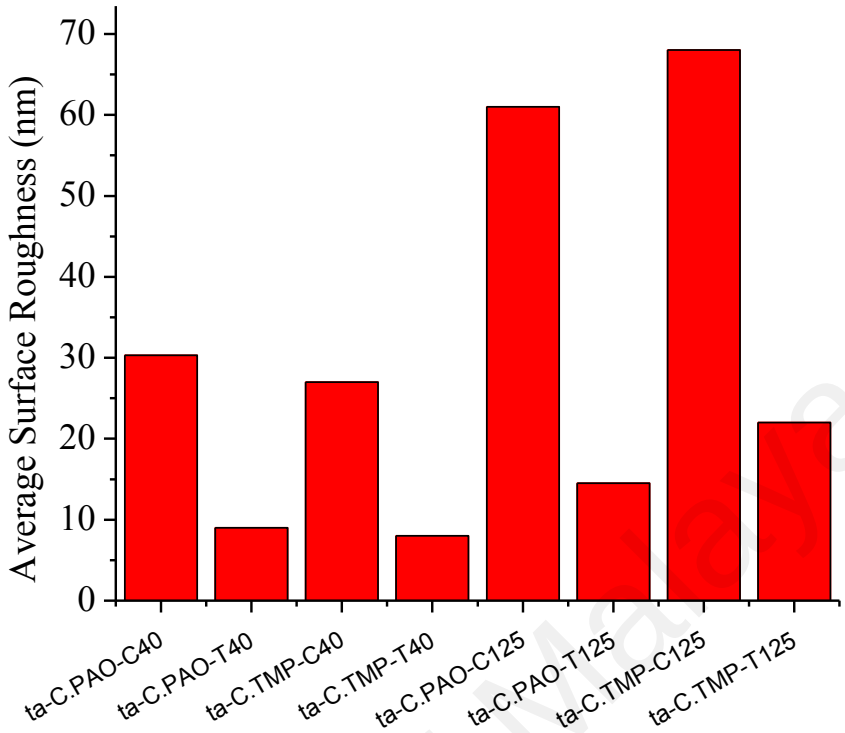

Figure 4.24: Average surface roughness at the wear track after friction testing

The friction and wear behavior of a tribo system is also dependent on the counter surface body (Stachowiak & Batchelor, 2013). In our case, the counter body is a steel ball. Counter ball wear for textured and un-textured tetrahedral amorphous carbon coated samples can be seen in Figure 4.27. Severe scratches indicating abrasive wearing can be observed in the case of samples ta-C.PAO-C125 and ta-C.TMP-C125 (Figure 4.27 b and 4.27 d). Counter balls which rubbed against textured samples ta-C.PAO-T125 and ta-C.TMP-T125 showed slight grooves (Figure 4.27 a and 4.27 c). These results can be due to micro textures which can provide lubricant and capture the wear particles from the contact, thus lowering counter surface excessive abrasive wearing. At higher temperatures, textured coated samples showed higher ball wear coefficient compared to un-textured coating (Figure 4.21). This behavior was also observed in the case of amorphous hydrogenated carbon coating (section 4.3.2.2). Formation of graphitic transfer film can be responsible for lowering wear rate of counter body (Mobarak et al., 2014).

The increase in counter ball wear rate for textured coated samples can be related to reduced graphitization transformation caused by the textures. As discussed in Raman spectroscopy section (Section 4.4.2.1), textured samples show lower graphitization transformation, whereas higher graphitization transformation was observed in case of un-textured tetrahedral amorphous carbon coated samples.

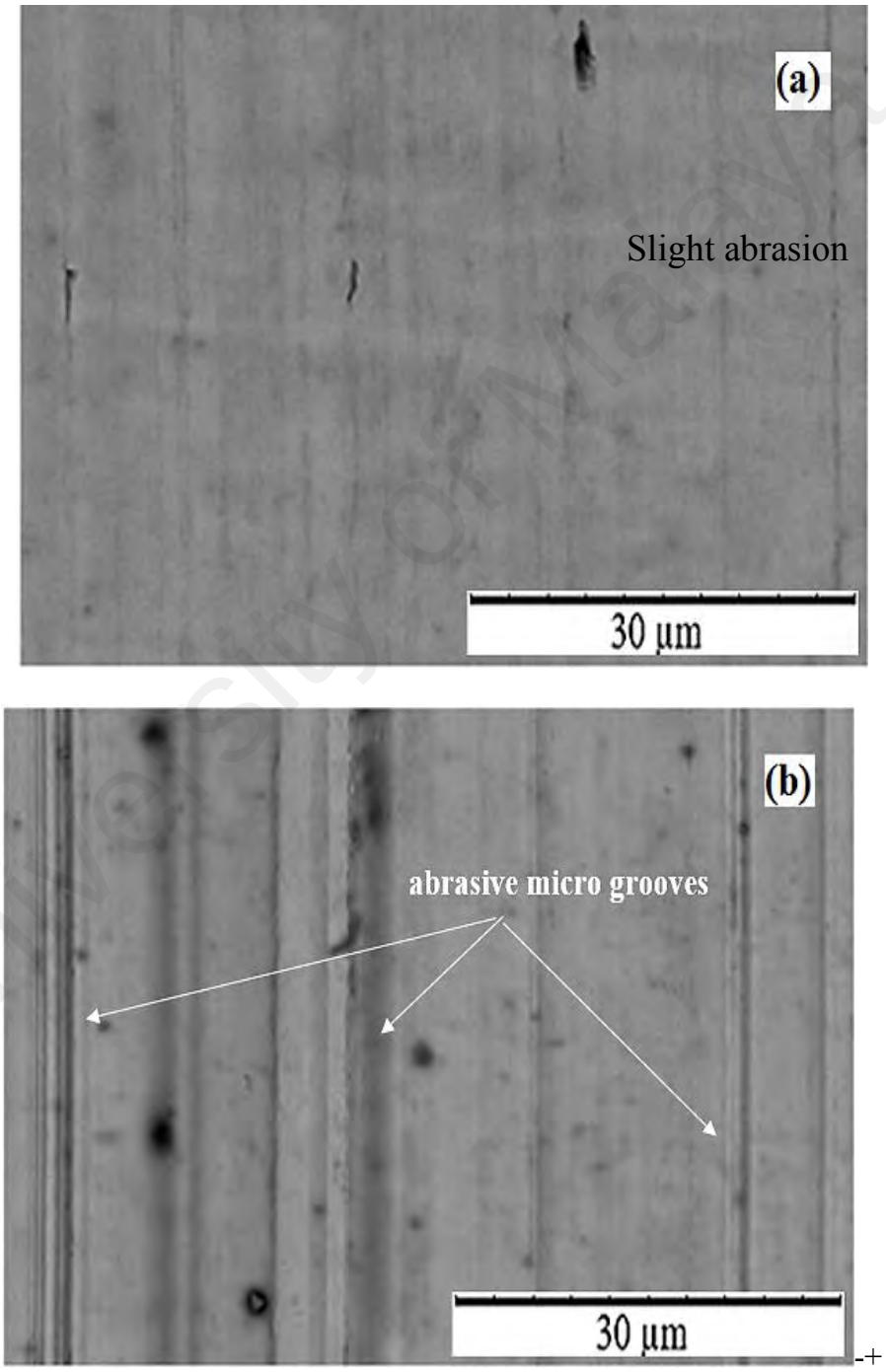

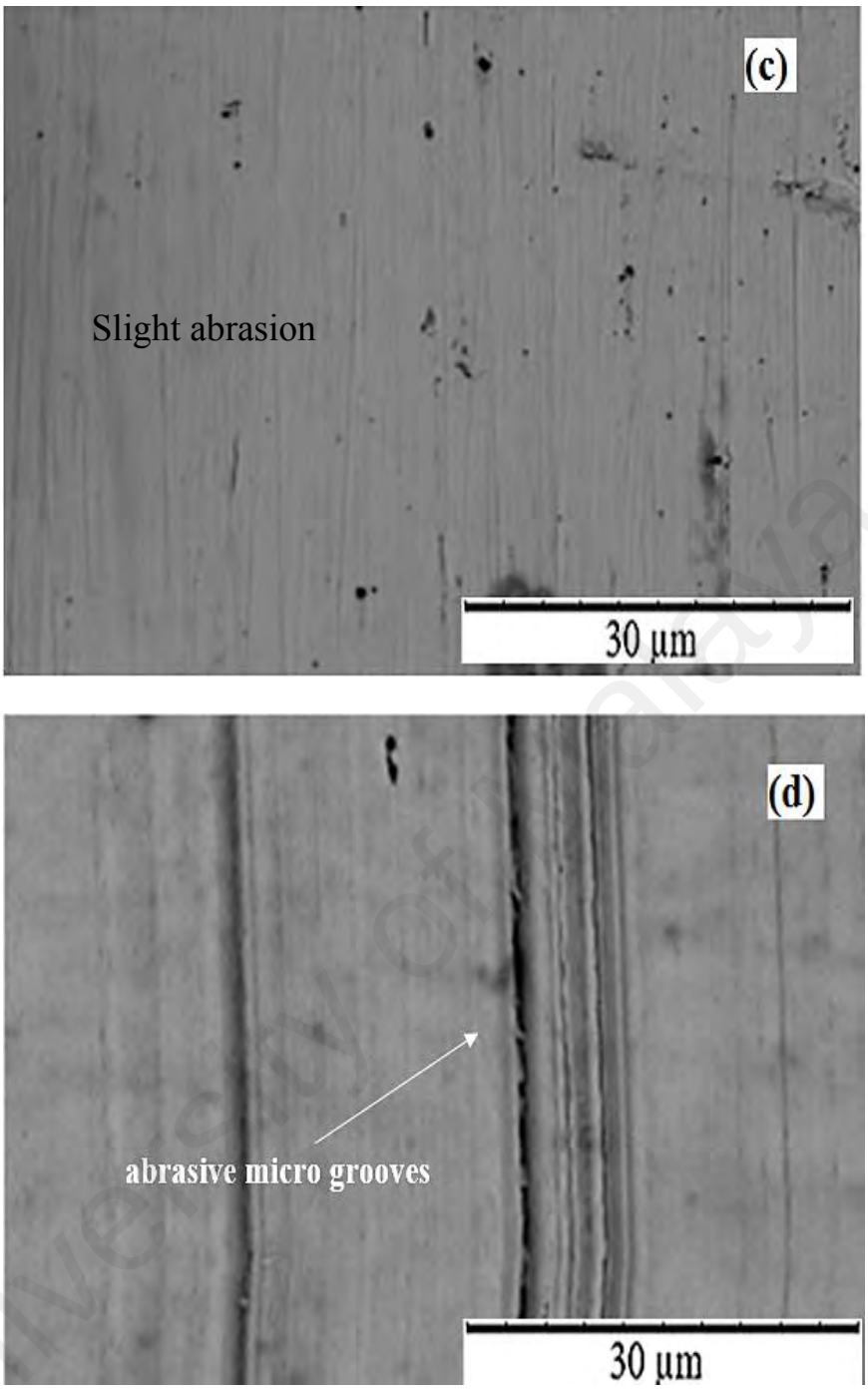

Figure 4.25 continued: SEM images of steel balls which rub against (a) ta-C.PAO-T125, (b) ta-C.PAO-C125, (c) ta-C.TMP-T125 and (d) ta-C.TMP-C125

Table 4.4: EDX analysis of un-textured/textured tetrahedral amorphous coated samples at various temperatures

Specimen	Elements (Atomic %)					
	C	O	Cr	Fe	Si	Mn
ta-C as deposited	97.93	0.08	-	1.99	-	-
ta-C.PAO-T40	94.85	2.01	0 .03	3.11	-	-
ta-C.PAO-C40	90.70	2.43	0.09	6.78	-	-
ta-C.TMP-T40	94.61	2.33	0.08	2.98	-	-
ta-C.TMP-C40	91.56	2.57	0.06	5.81	-	-
ta-C.PAO-T125	93.72	3.01	0.04	3.23	-	-
ta-C.PAO-C125	89.62	3.2	0.05	7.13	-	-
ta-C.TMP-T125	93.91	2.99	0.08	3.02	-	-
ta-C.TMP-C125	88.7	3.13	0.05	8.12	-	-

4.4.3 Comparison of tribological behavior of laser textured amorphous hydrogenated and tetrahedral amorphous carbon coatings at various temperatures

As observed in sections 4.3 and 4.4, laser micro texturing improved the tribological performance of amorphous hydrogenated and tetrahedral amorphous carbon coatings in PAO and palm based TMP lubrication. In this section, comparison is conducted between laser textured amorphous hydrogenated and tetrahedral amorphous carbon coatings for tribological performance. Figure 4.28 shows the average coefficient of friction of both textured coatings at temperatures 40, 80 and 125 ºC in PAO and palm based TMP lubricant. Samples ta-C.TMP-T40 and ta-C.PAO-T40 showed the lower average coefficient of friction values of 0.057 and 0.061 compared to 0.063 and 0.070 shown by samples TMP-T40 and PAO-T40. Figure 4.29 shows the wear coefficient of textured coating at 40, 80 and 125 ºC in PAO and palm based TMP lubricant. Lower wear coefficient can be observed in the case of samples ta-C.TMP-T40 and ta-C.PAO-T40 compared to samples TMP-T40 and PAO-T40.

At 80 ºC temperature, samples ta-C.TMP-T80 and ta-C.PAO-T80 showed lower average coefficient of friction of 0.077 and 0.078 compared to average coefficient of friction of 0.115 and 0.119 shown by samples TMP-T80 and PAO-T80. Wear coefficient was also lower for samples ta-C.TMP-T80 and ta-C.PAO-T80 compared to samples TMP-T80 and PAO-T80. Similar to tests conducted at 40 and 80 ºC, at 125 ºC the samples ta-C.TMP-T125 and ta-C.PAO-T125 showed lower coefficient of friction of 0.084 and 0.081 compared to average coefficient of friction of 0.14 and 0.13 shown by TMP-T125 and PAO-T125. Additionally, wear coefficient was also lower for samples ta-C.TMP-T125 and ta-C.PAO-T125 compared to samples TMP-T125 and PAO-T125.

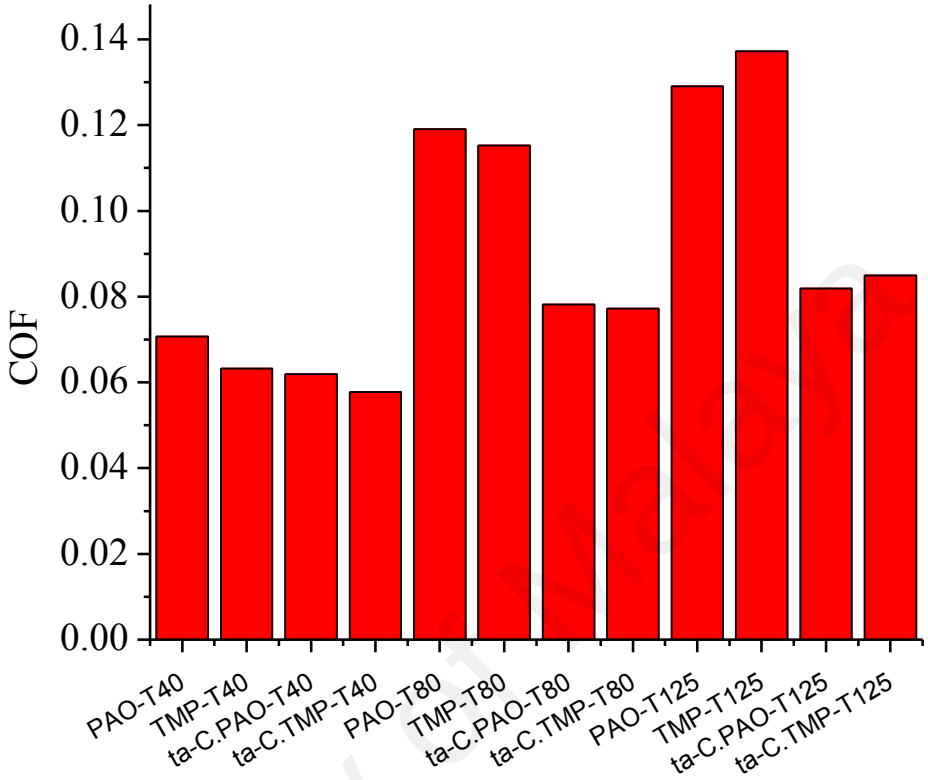

Figure 4.26: Average coefficient of friction of laser micro textured amorphous hydrogenated and tetrahedral amorphous carbon coated samples at temperature 40º C, 80º C and 125º C

Laser textured tetrahedral amorphous carbon coating showed lower average coefficient of friction and wear coefficient at 40, 80 and 125 ºC temperatures compared to laser textured amorphous hydrogenated carbon coating. Lower coefficient of friction of tetrahedral amorphous carbon coating compared to hydrogenated, carbon coating was reported earlier by Vengudusamy et al. (Vengudusamy et al., 2011) in base oil. Tasdemir et al. observed that lower hydrogen content and higher sp^3/sp^2 ratio can be responsible for the lower coefficient of friction of tetrahedral amorphous carbon coatings (Tasdemir et al., 2013).

Laser textured tetrahedral amorphous carbon coating showed the lower wear coefficient than laser textured hydrogenated amorphous carbon coating. Lower wear coefficient can be related to the higher H/E ratio of tetrahedral amorphous carbon coating. The H/E ratio of the coating is hypothesized to represent its wear behavior (Pintaude, 2013). The coating possesses maximum tensile elastic stress if H/E ratio is higher (Jiang et al., 1989), and therefore, can be related to high wear resistance. As tetrahedral amorphous carbon coating had higher H/E ratio compared to be amorphous hydrogenated carbon coating, higher wear resistance in case of laser textured tetrahedral amorphous carbon coating can be expected.

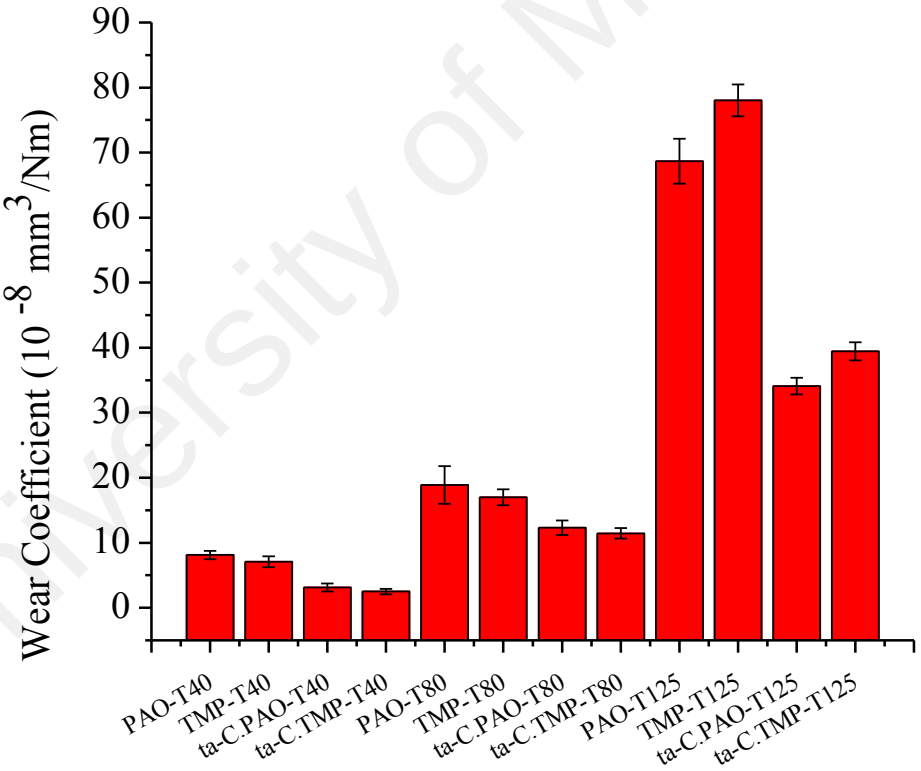

Figure 4.27: Wear coefficient of laser micro textured amorphous hydrogenated and tetrahedral amorphous carbon coated samples at temperature 40º C, 80º C and 125º C

CHAPTER 5: CONCLUSIONS AND RECOMMENDATIONS

5.1 Conclusions

Tribological effect of laser textured density, diameter and depth were evaluated on amorphous hydrogenated carbon coating. The tribological behavior of laser textured and un-textured amorphous hydrogenated carbon coating and tetrahedral carbon coating were evaluated at various temperatures in the presence of PAO, and palm based TMP lubrication. Based on the results of these studies following conclusions can be drawn.

1. Textured amorphous hydrogenated carbon coating showed the minimum coefficient of friction at 30 % dimple density compared to 10 % density for all combinations of diameters and depths. In the case of 20 % dimple density, dimple diameter of 100 μm and depth of 6 μm showed lowest coefficient of friction compared to all other samples.

   Sample Dn20Di100Dp6 yielded the lowest average coefficient of friction and wear coefficient among all the tested amorphous hydrogenated carbon coated samples. Dimple's diameter of 100 μm showed the lowest wear coefficient at all dimple densities tested. If the diameter exceeded 100 μm, wear resistance is reduced. The optimum dimple diameter depends on contact width-to-dimple diameter ratio. Contact load per unit area, coefficient of friction, and wear coefficient increase if dimple diameter and contact width are nearly similar.
2. Laser textured amorphous hydrogenated carbon showed higher wear resistance compared to un-textured coating at 40 ºC, 80 ºC and 125 ºC in the presence of PAO and palm based TMP lubrication.

   At 40 ºC temperature, lower coefficient of friction can be observed for laser textured amorphous hydrogenated carbon. However, coefficient of friction was higher as temperature was increased to 80 ºC and 125 ºC for both lubricants tested.

Coefficient of friction trends for laser textured amorphous hydrogenated carbon coating was stable at 40 ºC, 80 ºC and 125 ºC compared to un-textured coatings. The stability can be attributed to the fact that micro textures reduced the abrasive wearing by capturing the wear debris from the interface. This was confirmed with scanning electron microscope and atomic force microscope.

Palm based TMP lubricant showed lower coefficient of friction and wear coefficient compared to PAO lubricant for laser textured and un-textured amorphous hydrogenated carbon coatings at 40 ºC and 80 ºC temperature. As the temperature increased to 125 ºC, palm based TMP showed higher coefficient of friction and wear coefficient than PAO lubricant.

The lower coefficient of friction shown by un-textured amorphous hydrogenated carbon coatings at 80 ºC and 125 ºC can be attributed to graphitization phenomenon.

3. Tribological behavior of laser textured tetrahedral amorphous carbon coating was similar to that of laser textured amorphous hydrogenated carbon coating at 40 ºC, 80 ºC and 125 ºC. Laser textured tetrahedral amorphous carbon coating showed higher wear resistance compared to un-textured tetrahedral amorphous carbon coating at 40 ºC, 80 ºC and 125 ºC.

   As the temperature was increased from 40 ºC, coefficient of friction was higher in the case of laser textured tetrahedral carbon coating compared to un-textured coating, whereas wear coefficient remained lower throughout the temperature range. Lower coefficient of friction at 80 ºC and 125 ºC temperature in the case of un-textured tetrahedral amorphous carbon coating was due to graphitization phenomenon.

   At 40 ºC and 80 ºC temperature, Palm based TMP ester showed lower coefficient of friction and wear coefficient in the case of tetrahedral carbon

coating compared to PAO lubricant. However, at 125 ºC PAO showed better coefficient of friction and wear coefficient. This result was similar for both coatings tested.

Laser textured tetrahedral amorphous carbon coating showed lower coefficient of friction and wear coefficient at 40 ºC, 80 ºC and 125 ºC compared to laser textured amorphous hydrogenated carbon coating in both PAO and palm based TMP lubrication. Coefficient of friction and wear coefficient increased for both laser textured coatings with the increase in temperature.

Laser textured tetrahedral carbon coating (non-hydrogenated) can be used to improve friction and wear behavior of automotive components compared to laser textured amorphous hydrogenated carbon coating.

5.2 Recommendations for future work

1. Effect of various micro texture shapes on the tribological performance of tetrahedral amorphous carbon coating should be investigated. Until now most of the experimental work on surface texturing has been conducted using spherical shaped dimples. The reason for this research trend was that it is easier and less expensive to form spherical shaped dimples compared to other shapes. Theoretically, researchers have found that shape of textures effect the tribological performance (Nanbu, et al., 2008). Various shapes such as ellipse, rectangle etc. should also be experimentally investigated with tetrahedral amorphous carbon coating. Other shapes may enhance the tribological performance of coating.
2. Tribological performance of nano and micro textured tetrahedral amorphous carbon coating should be investigated and compared. Previously, in the case of cutting tool application, micro and nano textures have been found to show different tribological behavior (Enomoto et al., 2012; Kawasegi et al., 2009). In the case of automotive applications, this has to be investigated to find out whether

it is tribologically beneficial to use nano textured or micro textured tetrahedral amorphous carbon coating.

3. Tribological effect of solid lubricants such as tungsten disulfide and molybdenum disulfide filled micro and nano textured tetrahedral amorphous carbon coating should be investigated. Previously, researchers have found that solid lubricant filled textured steel show lower coefficient of friction and higher wear resistance than un-textured samples (Segu et al., 2013). They observed that textures provide solid lubricant at the interface and increase the adhesion of solid lubricant coating. As the properties of DLC coatings deteriorate with temperature, combination of surface texturing and solid lubricant can further enhance their tribological performance.

REFERENCES

Abboud, J. H., Benyounis, K. Y., Olabi, A. G., & Hashmi, M. S. J. (2007). Laser surface treatments of iron-based substrates for automotive application. *Journal of Materials Processing Technology, 182*(1-3), 427-431.

Al Mahmud, K., Kalam, M., Masjuki, H., Mobarak, H., & Zulkifli, N. (2015). An updated overview of diamond-like carbon coating in tribology. *Critical Reviews in Solid State and Materials Sciences, 40*(2), 90-118.

Al Mahmud, K. A. H., Varman, M., Kalam, M. A., Masjuki, H. H., Mobarak, H. M., & Zulkifli, N. W. M. (2014). Tribological characteristics of amorphous hydrogenated (a-C:H) and tetrahedral (ta-C) diamond-like carbon coating at different test temperatures in the presence of commercial lubricating oil. *Surface and Coatings Technology*.

Amanov, A., Cho, I. S., Pyoun, Y. S., Lee, C. S., & Park, I. G. (2012). Micro-dimpled surface by ultrasonic nanocrystal surface modification and its tribological effects. *Wear, 286–287*, 136-144.

Amanov, A., Tsuboi, R., Oe, H., & Sasaki, S. (2013). The influence of bulges produced by laser surface texturing on the sliding friction and wear behavior. *Tribology International, 60*, 216-223.

Amanov, A., Watabe, T., Tsuboi, R., & Sasaki, S. (2013). Improvement in the tribological characteristics of Si-DLC coating by laser surface texturing under oil-lubricated point contacts at various temperatures. *Surface and Coatings Technology, 232*, 549-560.

Arbain, N. H., & Salimon, J. (2010). Synthesis and characterization of ester trimethylolpropane based Jatropha curcas oil as biolubricant base stocks. *Journal of Science and Technology, 2*(2).

Austin, L. B. (2014). *Evaluation and optimisation of diamond-like carbon for tribological applications*: University of Leeds.

Aziz, N. A. M., Yunus, R., Rashid, U., & Zulkifli, N. W. M. (2016). Temperature effect on tribological properties of polyol ester-based environmentally adapted lubricant. *Tribology International, 93*, 43-49.

Bewilogua, K., & Hofmann, D. (2014). History of diamond-like carbon films—from first experiments to worldwide applications. *Surface and Coatings Technology, 242*, 214-225.

Bhushan, B. (2013). *Principles and applications of tribology*: John Wiley & Sons.

Bolander, N. W., & Sadeghi, F. (2006). *Surface modification for piston ring and liner* (Vol. 134).

Bremond, F., Fournier, P., & Platon, F. (2003). Test temperature effect on the tribological behavior of DLC-coated 100C6-steel couples in dry friction. *Wear, 254*(7–8), 774-783.

Brizmer, V., Kligerman, Y., & Etsion, I. (2003). A laser surface textured parallel thrust bearing. *Tribology Transactions, 46*(3), 397-403.

Caciu, C., Decenciere, E., & Jeulin, D. (2008). Parametric Optimization of Periodic Textured Surfaces for Friction Reduction in Combustion Engines. *Tribology Transactions, 51*(4), 533-541.

Cannon, A. H., & King, W. P. (2009). Casting metal microstructures from a flexible and reusable mold. *Journal of Micromechanics and Microengineering, 19*(9), 095016.

Canter, N. (2009). Special report: Boundary lubricity additives. *Tribology & Lubrication Technology, 65*(9), 10.

Casiraghi, C., Ferrari, A. C., & Robertson, J. (2005). Raman spectroscopy of hydrogenated amorphous carbons. *Physical Review B, 72*(8), 085401.

Chang, W., Sun, J., Luo, X., Ritchie, J. M., & Mack, C. (2011). Investigation of microstructured milling tool for deferring tool wear. *Wear, 271*(9-10), 2433-2437.

Checo, H. M., Ausas, R. F., Jai, M., Cadalen, J.-P., Choukroun, F., & Buscaglia, G. C. (2014). Moving textures: Simulation of a ring sliding on a textured liner. *Tribology International, 72*, 131-142.

Chen, C.-Y., Chung, C.-J., Wu, B.-H., Li, W.-L., Chien, C.-W., Wu, P.-H., & Cheng, C.-W. (2012). Microstructure and lubricating property of ultra-fast laser pulse textured silicon carbide seals. *Applied Physics a-Materials Science & Processing, 107*(2), 345-350.

Churi, N. (2010). *Rotary ultrasonic machining of hard-to-machine materials.* (Doctor of Philosophy), Kansas State University, Manhattan, Kansas.

Coblas, D. G., Fatu, A., Maoui, A., & Hajjam, M. (2014). Manufacturing textured surfaces: State of art and recent developments. *Proceedings of the Institution of Mechanical Engineers, Part J: Journal of Engineering Tribology, 229*(1), 3-29.

da Silva, W. M., Suarez, M. P., Machado, A. R., & Costa, H. L. (2013). Effect of laser surface modification on the micro-abrasive wear resistance of coated cemented carbide tools. *Wear, 302*(1-2), 1230-1240.

Davis, R. F. (1991). Diamond films and coatings: development, properties, and applications.

Demas, N. G., Polycarpou, A. A., & Conry, T. F. (2005). Tribological studies on scuffing due to the influence of carbon dioxide used as a refrigerant in compressors. *Tribology Transactions, 48*(3), 336-342.

Deng, J., Lian, Y., Wu, Z., & Xing, Y. (2013). Performance of femtosecond laser-textured cutting tools deposited with WS2 solid lubricant coatings. *Surface and Coatings Technology, 222*, 135-143.

Ding, Q., Wang, L., Hu, L., Hu, T., Wang, Y., & Zhang, Y. (2011). An explanation for laser-induced spallation effect in a-C:H films: Altered phase evolution route caused by hydrogen doping. *Journal of Applied Physics, 109*(1), 013501.

Ding, Q., Wang, L., Wang, Y., Wang, S. C., Hu, L., & Xue, Q. (2010). Improved Tribological Behavior of DLC Films Under Water Lubrication by Surface Texturing. *Tribology Letters, 41*(2), 439-449.

Dong, C., Gu, Y., Zhong, M., Li, L., Sezer, K., Ma, M., & Liu, W. (2011). Fabrication of superhydrophobic Cu surfaces with tunable regular micro and random nano-scale structures by hybrid laser texture and chemical etching. *Journal of Materials Processing Technology, 211*(7), 1234-1240.

Donnet, C. (1998). Recent progress on the tribology of doped diamond-like and carbon alloy coatings: a review. *Surface and Coatings Technology, 100–101*(0), 180-186.

Donnet, C., & Erdemir, A. (2007). *Tribology of diamond-like carbon films: fundamentals and applications*: Springer Science & Business Media.

Dowson, D., & Higginson, G. (1959). A numerical solution to the elasto-hydrodynamic problem. *Journal of mechanical engineering science, 1*(1), 6-15.

Dumitru, G., Romano, V., Weber, H. P., Pimenov, S., Kononenko, T., Hermann, J., . . . Shupegin, M. (2003). Laser treatment of tribological DLC films. *Diamond and Related Materials, 12*(3-7), 1034-1040.

Enomoto, T., & Sugihara, T. (2010). Improving anti-adhesive properties of cutting tool surfaces by nano-/micro-textures. *CIRP Annals - Manufacturing Technology, 59*(1), 597-600.

Enomoto, T., & Sugihara, T. (2011). Improvement of Anti-Adhesive Properties of Cutting Tool by Nano/Micro Textures and Its Mechanism. *Procedia Engineering, 19*, 100-105.

Enomoto, T., Sugihara, T., Yukinaga, S., Hirose, K., & Satake, U. (2012). Highly wear-resistant cutting tools with textured surfaces in steel cutting. *CIRP Annals - Manufacturing Technology, 61*(1), 571-574.

Erdemir, A. (2001). The role of hydrogen in tribological properties of diamond-like carbon films. *Surface and Coatings Technology, 146–147*, 292-297.

Erdemir, A., & Fenske, G. R. (1996). Tribological Performance of Diamond and Diamondlike Carbon Films at Elevated Temperatures. *Tribology Transactions, 39*(4), 787-794.

Etsion, I. (2004). Improving tribological performance of mechanical components by laser surface texturing. *Tribology Letters, 17*(4), 733-737.

Etsion, I. (2005). State of the Art in Laser Surface Texturing. *Journal of Tribology, 127*(1), 248.

Etsion, I., & Burstein, L. (1996). A Model for Mechanical Seals with Regular Microsurface Structure. *Tribology Transactions, 39*(3), 677-683.

Etsion, I., Halperin, G., & Becker, E. (2006). The effect of various surface treatments on piston pin scuffing resistance. *Wear, 261*(7-8), 785-791.

Etsion, I., & Sher, E. (2009). Improving fuel efficiency with laser surface textured piston rings. *Tribology International, 42*(4), 542-547.

Feldman, Y., Kligerman, Y., & Etsion, I. (2006). A Hydrostatic Laser Surface Textured Gas Seal. *Tribology Letters, 22*(1), 21-28.

Feldman, Y., Kligerman, Y., Etsion, I., & Haber, S. (2006). The Validity of the Reynolds Equation in Modeling Hydrostatic Effects in Gas Lubricated Textured Parallel Surfaces. *Journal of Tribology, 128*(2), 345.

Ferrari, A. C., & Robertson, J. (2000). Interpretation of Raman spectra of disordered and amorphous carbon. *Physical Review B, 61*(20), 14095-14107.

Ferraro, J. R. (2003). *Introductory raman spectroscopy*: Academic press.

Gadeschi, G. B., Backhaus, K., & Knoll, G. (2012). Numerical Analysis of Laser-Textured Piston-Rings in the Hydrodynamic Lubrication Regime. *Journal of Tribology, 134*(4), 041702.

Gao, F., Erdemir, A., & Tysoe, W. T. (2005). The Tribological Properties of Low-friction Hydrogenated Diamond-like Carbon Measured in Ultrahigh Vacuum. *Tribology Letters, 20*(3-4), 221-227.

Gao, Y., Wu, B., Zhou, Y., & Tao, S. (2011). A two-step nanosecond laser surface texturing process with smooth surface finish. *Applied Surface Science, 257*(23), 9960-9967.

Gellman, A. J., & Spencer, N. D. (2002). Surface chemistry in tribology. *Proceedings of the Institution of Mechanical Engineers, Part J: Journal of Engineering Tribology, 216*(6), 443-461.

Gharam, A. A., Lukitsch, M. J., Balogh, M. P., Irish, N., & Alpas, A. T. (2011). High temperature tribological behavior of W-DLC against aluminum. *Surface and Coatings Technology, 206*(7), 1905-1912.

Greco, A., Raphaelson, S., Ehmann, K., Wang, Q. J., & Lin, C. (2009). Surface Texturing of Tribological Interfaces Using the Vibromechanical Texturing Method. *Journal of Manufacturing Science and Engineering, 131*(6), 061005.

Grill, A. (1993). Review of the tribology of diamond-like carbon. *Wear, 168*(1), 143-153.

Grill, A. (1999). Diamond-like carbon: state of the art. *Diamond and Related Materials, 8*(2–5), 428-434.

Grill, A. (1999). Diamond-like carbon: state of the art. *Diamond and Related Materials, 8*(2), 428-434.

Hamilton, D. B., Walowit, J. A., & Allen, C. M. (1966). A Theory of Lubrication by Microirregularities. *Journal of Fluids Engineering, 88*(1), 177-185.

Handbook for Analytical Methods for Materials (2014). from http://www.mee-inc.com/

Hao, L., Meng, Y., & Chen, C. (2014). Experimental investigation on effects of surface texturing on lubrication of initial line contacts. *Lubrication Science, 26*(5), 363-373.

Haque, T., Morina, A., Neville, A., Kapadia, R., & Arrowsmith, S. (2009). Effect of oil additives on the durability of hydrogenated DLC coating under boundary lubrication conditions. *Wear, 266*(1-2), 147-157.

Hauert, R. (2004). An overview on the tribological behavior of diamond-like carbon in technical and medical applications. *Tribology International, 37*(11–12), 991-1003.

Heinke, W., Leyland, A., Matthews, A., Berg, G., Friedrich, C., & Broszeit, E. (1995). Evaluation of PVD nitride coatings, using impact, scratch and Rockwell-C adhesion tests. *Thin Solid Films, 270*(1-2), 431-438.

Hironaka, S. (1984). Boundary lubrication and lubricants. *Three bond technical news, 9*, 1-6.

Hsu, S. M., Jing, Y., Hua, D., & Zhang, H. (2014). Friction reduction using discrete surface textures: principle and design. *Journal of Physics D: Applied Physics, 47*(33), 335307.

Hu, T., Hu, L., & Ding, Q. (2012). Effective solution for the tribological problems of Ti-6Al-4V: Combination of laser surface texturing and solid lubricant film. *Surface and Coatings Technology, 206*(24), 5060-5066.

Hutchings, I. M. (1992). Tribology: friction and wear of engineering materials.

Ing, T. C., Mohammed Rafiq, A., Azli, Y., & Syahrullail, S. (2012). The effect of temperature on the tribological behavior of RBD palm stearin. *Tribology Transactions, 55*(5), 539-548.

Jiang, X., Reichelt, K., & Stritzker, B. (1989). The hardness and Young's modulus of amorphous hydrogenated carbon and silicon films measured with an ultralow load indenter. *Journal of Applied Physics, 66*(12), 5805-5808.

Jianxin, D., Ze, W., Yunsong, L., Ting, Q., & Jie, C. (2012). Performance of carbide tools with textured rake-face filled with solid lubricants in dry cutting processes. *International Journal of Refractory Metals and Hard Materials, 30*(1), 164-172.

Johnson, M., & Cote, P. (2006). Modeling Magnetron Sputter Deposition. *Materials and Manufacturing Processes, 21*(6), 628-633.

Kalin, M., Roman, E., Ožbolt, L., & Vižintin, J. (2010). Metal-doped (Ti, WC) diamond-like-carbon coatings: Reactions with extreme-pressure oil additives under tribological and static conditions. *Thin Solid Films, 518*(15), 4336-4344.

Kalin, M., Velkavrh, I., Vižintin, J., & Ožbolt, L. (2008). Review of boundary lubrication mechanisms of DLC coatings used in mechanical applications. *Meccanica, 43*(6), 623-637.

Kalin, M., & Vižintin, J. (2006). A comparison of the tribological behaviour of steel/steel, steel/DLC and DLC/DLC contacts when lubricated with mineral and biodegradable oils. *Wear, 261*(1), 22-31.

Kalish, R., Lifshitz, Y., Nugent, K., & Prawer, S. (1999). Thermal stability and relaxation in diamond-like-carbon. A Raman study of films with different sp3 fractions (ta-C to aC). *Applied physics letters, 74*, 2936.

Kato, K. (2000). Wear in relation to friction—a review. *Wear, 241*(2), 151-157.

Kawasegi, N., Sugimori, H., Morimoto, H., Morita, N., & Hori, I. (2009). Development of cutting tools with microscale and nanoscale textures to improve frictional behavior. *Precision Engineering, 33*(3), 248-254.

Kelly, P. J., & Arnell, R. D. (2000). Magnetron sputtering: a review of recent developments and applications. *Vacuum, 56*(3), 159-172.

Kligerman, Y., & Etsion, I. (2001). Analysis of the Hydrodynamic Effects in a Surface Textured Circumferential Gas Seal. *Tribology Transactions, 44*(3), 472-478.

Kligerman, Y., Etsion, I., & Shinkarenko, A. (2005). Improving tribological performance of piston rings by partial surface texturing. *Journal of Tribology-Transactions of the Asme, 127*(3), 632-638.

Kligerman, Y., & Shinkarenko, A. (2011). The effect of tapered edges on lubrication regimes in surface-textured elastomer seals. *Tribology International, 44*(12), 2059-2066.

Kodali, D. R. (2002). High performance ester lubricants from natural oils. *Industrial lubrication and tribology, 54*(4), 165-170.

Komlenok, M. S., Arutyunyan, N. R., Kononenko, V. V., Zavedeev, E. V., Frolov, V. D., Chouprik, A. A., . . . Pimenov, S. M. (2016). Structure and friction properties of laser-patterned amorphous carbon films. *Diamond and Related Materials, 65*, 69-74.

Kononenko, T. V., Garnov, S. V., Pimenov, S. M., Konov, V. I., Romano, V., Borsos, B., & Weber, H. P. (2000). Laser ablation and micropatterning of thin TiN coatings. *Applied Physics A, 71*(6), 627-631.

Koshy, P., & Tovey, J. (2011). Performance of electrical discharge textured cutting tools. *CIRP Annals - Manufacturing Technology, 60*(1), 153-156.

Koskinen, J., Tapper, U., Andersson, P., Varjus, S., Kolehmainen, J., Tervakangas, S., & Buss, W. (2010). Friction reduction by texturing of DLC coatings sliding against steel under oil lubrication. *Surface and Coatings Technology, 204*(23), 3794-3797.

Kovalchenko, A., Ajayi, O., Erdemir, A., & Fenske, G. (2011). Friction and wear behavior of laser textured surface under lubricated initial point contact. *Wear, 271*(9-10), 1719-1725.

Krumpiegl, T., Meerkamm, H., Fruth, W., Schaufler, C., Erkens, G., & Böhner, H. (1999). Amorphous carbon coatings and their tribological behaviour at high

temperatures and in high vacuum. *Surface and Coatings Technology, 120–121*, 555-560.

Kumar, A., & Sharma, S. (2011). Potential non-edible oil resources as biodiesel feedstock: An Indian perspective. *Renewable and Sustainable Energy Reviews, 15*(4), 1791-1800.

Kuršelis, K., Kiyan, R., & Chichkov, B. N. (2012). Formation of corrugated and porous steel surfaces by femtosecond laser irradiation. *Applied Surface Science, 258*(22), 8845-8852.

Lei, S., Devarajan, S., & Chang, Z. (2009). A study of micropool lubricated cutting tool in machining of mild steel. *Journal of Materials Processing Technology, 209*(3), 1612-1620.

Li, J., Xiong, D., Wu, H., Huang, Z., Dai, J., & Tyagi, R. (2010). Tribological Properties of Laser Surface Texturing and Molybdenizing Duplex-Treated Ni-Base Alloy. *Tribology Transactions, 53*(2), 195-202.

Li, Y., Deng, J., Chai, Y., & Fan, W. (2016). Surface textures on cemented carbide cutting tools by micro EDM assisted with high-frequency vibration. *The International Journal of Advanced Manufacturing Technology, 82*(9-12), 2157-2165.

Ling, T. D., Liu, P., Xiong, S., Grzina, D., Cao, J., Wang, Q. J., . . . Talwar, R. (2013). Surface Texturing of Drill Bits for Adhesion Reduction and Tool Life Enhancement. *Tribology Letters, 52*(1), 113-122.

Liu, H., Wan, D., & Hu, D. (2009). Microstructure and wear behavior of laser-textured and micro-alloyed Co-based WC and TiC composite sintered-carbide coating. *Journal of Materials Processing Technology, 209*(2), 805-810.

Liu, Y., Erdemir, A., & Meletis, E. I. (1996). An investigation of the relationship between graphitization and frictional behavior of DLC coatings. *Surface and Coatings Technology, 86–87, Part 2*(0), 564-568.

Liu, Y., & Meletis, E. (1997). Evidence of graphitization of diamond-like carbon films during sliding wear. *Journal of Materials Science, 32*(13), 3491-3495.

Lu, X., & Khonsari, M. M. (2007). An experimental investigation of dimple effect on the stribeck curve of journal bearings. *Tribology Letters, 27*(2), 169-176.

Marian, V. G., Gabriel, D., Knoll, G., & Filippone, S. (2011). Theoretical and Experimental Analysis of a Laser Textured Thrust Bearing. *Tribology Letters, 44*(3), 335-343.

Masuzawa, T. (2000). State of the Art of Micromachining. *CIRP Annals - Manufacturing Technology, 49*(2), 473-488.

Meijer, J. (2004). Laser beam machining (LBM), state of the art and new opportunities. *Journal of Materials Processing Technology, 149*(1-3), 2-17.

Mishra, S. P., & Polycarpou, A. A. (2011). Tribological studies of unpolished laser surface textures under starved lubrication conditions for use in air-conditioning and refrigeration compressors. *Tribology International, 44*(12), 1890-1901.

Mistry, K. K., Morina, A., & Neville, A. (2011). A tribochemical evaluation of a WC–DLC coating in EP lubrication conditions. *Wear, 271*(9-10), 1739-1744.

Mobarak, H., Masjuki, H., Mohamad, E. N., Kalam, M., Rashedul, H., Rashed, M., & Habibullah, M. (2014). Tribological properties of amorphous hydrogenated (aC: H) and hydrogen-free tetrahedral (ta-C) diamond-like carbon coatings under jatropha biodegradable lubricating oil at different temperatures. *Applied Surface Science, 317*, 581-592.

Mobarak, H. M., Niza Mohamad, E., Masjuki, H. H., Kalam, M. A., Al Mahmud, K. A. H., Habibullah, M., & Ashraful, A. M. (2014). The prospects of biolubricants as alternatives in automotive applications. *Renewable and Sustainable Energy Reviews, 33*, 34-43.

Mourier, L., Mazuyer, D., Lubrecht, A. A., & Donnet, C. (2006). Transient increase of film thickness in micro-textured EHL contacts. *Tribology International, 39*(12), 1745-1756.

Mourier, L., Mazuyer, D., Ninove, F. P., & Lubrecht, A. A. (2010). Lubrication mechanisms with laser-surface-textured surfaces in elastohydrodynamic regime. *Proceedings of the Institution of Mechanical Engineers Part J-Journal of Engineering Tribology, 224*(J8), 697-711.

Nakano, M., Korenaga, A., Korenaga, A., Miyake, K., Murakami, T., Ando, Y., . . . Sasaki, S. (2007). Applying micro-texture to cast iron surfaces to reduce the friction coefficient under lubricated conditions. *Tribology Letters, 28*(2), 131-137.

Nanbu, T., Ren, N., Yasuda, Y., Zhu, D., & Wang, Q. J. (2008). Micro-Textures in Concentrated Conformal-Contact Lubrication: Effects of Texture Bottom Shape and Surface Relative Motion. *Tribology Letters, 29*(3), 241-252.

Neves, D., Diniz, A. E., & de Lima, M. S. F. (2006). Efficiency of the laser texturing on the adhesion of the coated twist drills. *Journal of Materials Processing Technology, 179*(1-3), 139-145.

Neville, A., Morina, A., Haque, T., & Voong, M. (2007). Compatibility between tribological surfaces and lubricant additives—How friction and wear reduction can be controlled by surface/lube synergies. *Tribology International, 40*(10-12), 1680-1695.

Nguyen, T., & Butler, D. (2005). Simulation of precision grinding process, part 1: generation of the grinding wheel surface. *International Journal of Machine Tools and Manufacture, 45*(11), 1321-1328.

Obikawa, T., Kamio, A., Takaoka, H., & Osada, A. (2011). Micro-texture at the coated tool face for high performance cutting. *International Journal of Machine Tools and Manufacture, 51*(12), 966-972.

Oksanen, J., Hakala, T. J., Tervakangas, S., Laakso, P., Kilpi, L., Ronkainen, H., & Koskinen, J. (2014). Tribological properties of laser-textured and ta-C coated surfaces with burnished WS2 at elevated temperatures. *Tribology International, 70*, 94-103.

Peng, X. L., Barber, Z. H., & Clyne, T. W. (2001). Surface roughness of diamond-like carbon films prepared using various techniques. *Surface and Coatings Technology, 138*(1), 23-32.

Pettersson, U., & Jacobson, S. (2003). Influence of surface texture on boundary lubricated sliding contacts. *Tribology International, 36*(11), 857-864.

Pettersson, U., & Jacobson, S. (2004). Friction and Wear Properties of Micro Textured DLC Coated Surfaces in Boundary Lubricated Sliding. *Tribology Letters, 17*(3), 553-559.

Pettersson, U., & Jacobson, S. (2007). Textured surfaces for improved lubrication at high pressure and low sliding speed of roller/piston in hydraulic motors. *Tribology International, 40*(2), 355-359.

Pinkus, O., & Sternlicht, B. (1961). *Theory of hydrodynamic lubrication*: McGraw-Hill.

Pintaude, G. (2013). Introduction of the Ratio of the Hardness to the Reduced Elastic Modulus for Abrasion *Tribology - Fundamentals and Advancements* (pp. 217-230): InTech.

Puchi-Cabrera, E. S., Staia, M. H., Ochoa-Pérez, E. A., Teer, D. G., Santana-Méndez, Y. Y., La Barbera-Sosa, J. G., . . . Lesage, J. (2010). Fatigue behavior of a 316L stainless steel coated with a DLC film deposited by PVD magnetron sputter ion plating. *Materials Science and Engineering: A, 527*(3), 498-508.

Qiu, M., Bailey, B. N., Stoll, R., & Raeymaekers, B. (2014). The accuracy of the compressible Reynolds equation for predicting the local pressure in gas-lubricated textured parallel slider bearings. *Tribology International, 72*, 83-89.

Qiu, M., Delic, A., & Raeymaekers, B. (2012). The Effect of Texture Shape on the Load-Carrying Capacity of Gas-Lubricated Parallel Slider Bearings. *Tribology Letters, 48*(3), 315-327.

Qiu, M., Minson, B. R., & Raeymaekers, B. (2013). The effect of texture shape on the friction coefficient and stiffness of gas-lubricated parallel slider bearings. *Tribology International, 67*, 278-288.

Qiu, Y. K., M.M. (2011a). Experimental investigation of tribological performance of laser textured stainless steel rings. *Tribology International, 44*(5), 635-644.

Qiu, Y. K., M.M. (2011b). Performance Analysis of Full-Film Textured Surfaces With Consideration of Roughness Effects. *Journal of Tribology, 133*(2), 021704.

Rabinowicz, E. (1995). Adhesive wear. *Friction and Wear of Materials*, 143-190.

Rahmani, R., Mirzaee, I., Shirvani, A., & Shirvani, H. (2010). An analytical approach for analysis and optimisation of slider bearings with infinite width parallel textures. *Tribology International, 43*(8), 1551-1565.

Ramesh, A., Akram, W., Mishra, S. P., Cannon, A. H., Polycarpou, A. A., & King, W. P. (2013). Friction characteristics of microtextured surfaces under mixed and hydrodynamic lubrication. *Tribology International, 57*, 170-176.

Robertson, J. (1986). Amorphous carbon. *Advances in Physics, 35*(4), 317-374.

Robertson, J. (1991). Hard amorphous (diamond-like) carbons. *Progress in Solid State Chemistry, 21*(4), 199-333.

Robertson, J. (2002). Diamond-like amorphous carbon. *Materials Science and Engineering: R: Reports, 37*(4–6), 129-281.

Robiah, Y. l.-R., Ikuye, A., Indris, S., & A Ooi, T. (2003). Preparation and characterization of trimethylolpropane esters from palm kernel oil methyl esters.

Römer, G. R. B. E., Huis in't Veld, A. J., Meijer, J., & Groenendijk, M. N. W. (2009). On the formation of laser induced self-organizing nanostructures. *CIRP Annals - Manufacturing Technology, 58*(1), 201-204.

Ronen, A., Etsion, I., & Kligerman, Y. (2001). Friction-Reducing Surface-Texturing in Reciprocating Automotive Components. *Tribology Transactions, 44*(3), 359-366.

Ronkainen, H. (2001). Tribological properties of hydrogenated and hydrogen-free diamond-like carbon coatings. *Technical Research Centre of Finland. Publications(Finland), 434*, 3-52.

Ronkainen, H., & Holmberg, K. (2008). Environmental and thermal effects on the tribological performance of DLC coatings *Tribology of diamond-like carbon films* (pp. 155-200): Springer.

Ronkainen, H., Koskinen, J., Varjus, S., & Holmberg, K. (1999). Load-carrying capacity evaluation of coating/substrate systems for hydrogen-free and hydrogenated diamond-like carbon films. *Tribology Letters, 6*(2), 63-73.

Ronkainen, H., Varjus, S., Koskinen, J., & Holmberg, K. (2001). Differentiating the tribological performance of hydrogenated and hydrogen-free DLC coatings. *Wear, 249*(3–4), 260-266.

Roy, T., Choudhury, D., Bin Mamat, A., & Pingguan-Murphy, B. (2014). Fabrication and characterization of micro-dimple array on Al2O3 surfaces by using a micro-tooling. *Ceramics International, 40*(1), 2381-2388.

Rudnick, L. R., & Shubkin, R. L. (1999). *Synthetic lubricants and high-performance functional fluids, revised and expanded*: CRC Press.

Ryk, G., & Etsion, I. (2006). Testing piston rings with partial laser surface texturing for friction reduction. *Wear, 261*(7-8), 792-796.

Ryk, G., Kligerman, Y., & Etsion, I. (2002). Experimental Investigation of Laser Surface Texturing for Reciprocating Automotive Components. *Tribology Transactions, 45*(4), 444-449.

Ryk, G., Kligerman, Y., Etsion, I., & Shinkarenko, A. (2005). Experimental Investigation of Partial Laser Surface Texturing for Piston-Ring Friction Reduction. *Tribology Transactions, 48*(4), 583-588.

Sánchez-López, J. C., Erdemir, A., Donnet, C., & Rojas, T. C. (2003). Friction-induced structural transformations of diamondlike carbon coatings under various atmospheres. *Surface and Coatings Technology, 163–164*(0), 444-450.

Schreck, S., & Zum Gahr, K. H. (2005). Laser-assisted structuring of ceramic and steel surfaces for improving tribological properties. *Applied Surface Science, 247*(1-4), 616-622.

Segu, D. Z., Kim, J.-H., Choi, S. G., Jung, Y.-S., & Kim, S.-S. (2013). Application of Taguchi techniques to study friction and wear properties of MoS2 coatings deposited on laser textured surface. *Surface and Coatings Technology, 232*, 504-514.

Semenov, A. P., & Khrushchov, M. M. (2010). Influence of environment and temperature on tribological behavior of diamond and diamond-like coatings. *Journal of Friction and Wear, 31*(2), 142-158.

Shah, S., Moser, B., & Sharma, B. (2010). Glycerol Tri-Ester Derivatives as Diluent to Improve Low Temperature Properties of Vegetable Oils.

Shukla, P., Waugh, D., Lawrence, J., & Vilar, R. (2016). Laser surface structuring of ceramics, metals and polymers for biomedical applications: a review. *Laser Surface Modification of Biomaterials: Techniques and Applications*, 281.

Shum, P. W., Zhou, Z. F., & Li, K. Y. (2013). Investigation of the tribological properties of the different textured DLC coatings under reciprocating lubricated conditions. *Tribology International, 65*, 259-264.

Singh, D., & Singh, S. P. (2010). Low cost production of ester from non edible oil of Argemone mexicana. *Biomass and Bioenergy, 34*(4), 545-549.

Siripuram, R. B., & Stephens, L. S. (2004). Effect of Deterministic Asperity Geometry on Hydrodynamic Lubrication. *Journal of Tribology, 126*(3), 527-534.

So, H., & Chen, C. H. (2005). Effects of micro-wedges formed between parallel surfaces on mixed lubrication – Part II: modeling. *Tribology Letters, 19*(2), 83-91.

Song, H., Ji, L., Li, H., Liu, X., Zhou, H., Liu, L., & Chen, J. (2014). Improving the tribological performance of a-C:H film in a high vacuum by surface texture. *Journal of Physics D: Applied Physics, 47*(23), 235301.

Stachowiak, G., & Batchelor, A. W. (2013). *Engineering tribology*: Butterworth-Heinemann.

Sugihara, T., & Enomoto, T. (2009). Development of a cutting tool with a nano/micro-textured surface—Improvement of anti-adhesive effect by considering the texture patterns. *Precision Engineering, 33*(4), 425-429.

Sugihara, T., & Enomoto, T. (2012). Improving anti-adhesion in aluminum alloy cutting by micro stripe texture. *Precision Engineering, 36*(2), 229-237.

Sugihara, T., & Enomoto, T. (2013). Crater and flank wear resistance of cutting tools having micro textured surfaces. *Precision Engineering, 37*(4), 888-896.

Sutton, D. C., Limbert, G., Stewart, D., & Wood, R. J. K. (2013). The friction of diamond-like carbon coatings in a water environment. *Friction, 1*(3), 210-221.

Tanu Suryadi, K., Jian Huei, C., Hong Yee, L., & Sujeet, K. S. (2010). Texturing of UHMWPE surface via NIL for low friction and wear properties. *Journal of Physics D: Applied Physics, 43*(1), 015301.

Tasdemir, H. A., Wakayama, M., Tokoroyama, T., Kousaka, H., Umehara, N., Mabuchi, Y., & Higuchi, T. (2013). Ultra-low friction of tetrahedral amorphous diamond-like carbon (ta-C DLC) under boundary lubrication in poly alpha-olefin (PAO) with additives. *Tribology International, 65*, 286-294.

Taylor, C. M. (1993). *Engine tribology* (Vol. 26): Elsevier.

Tomanik, E. (2013). Modelling the hydrodynamic support of cylinder bore and piston rings with laser textured surfaces. *Tribology International, 59*, 90-96.

Tønder, K. (2010). Dimpled pivoted plane bearings: Modified coefficients. *Tribology International, 43*(12), 2303-2307.

Tseng, A. A. (2004). Recent developments in micromilling using focused ion beam technology. *Journal of Micromechanics and Microengineering, 14*(4), R15-R34.

Tung, S. C., & McMillan, M. L. (2004). Automotive tribology overview of current advances and challenges for the future. *Tribology International, 37*(7), 517-536.

Uhlmann, E., Piltz, S., & Doll, U. (2005). Machining of micro/miniature dies and moulds by electrical discharge machining—Recent development. *Journal of Materials Processing Technology, 167*(2-3), 488-493.

Usman, A., & Park, C. W. (2016). Optimizing the tribological performance of textured piston ring–liner contact for reduced frictional losses in SI engine: Warm operating conditions. *Tribology International, 99*, 224-236.

Vandoni, L., Demir, A., Previtali, B., Lecis, N., & Ugues, D. (2012). Wear Behavior of Fiber Laser Textured TiN Coatings in a Heavy Loaded Sliding Regime. *Materials, 5*(12), 2360-2382.

Vanhulsel, A., Blanpain, B., Celis, J.-P., Roos, J., Dekempeneer, E., & Smeets, J. (1998). Study of the wear behaviour of diamond-like coatings at elevated temperatures. *Surface and Coatings Technology, 98*(1), 1047-1052.

Velkavrh, I., Kalin, M., & Vizintin, J. (2008). The performance and mechanisms of DLC-coated surfaces in contact with steel in boundary-lubrication conditions: a review. *Strojniški vestnik, 54*(3), 189-206.

Vengudusamy, B., Mufti, R. A., Lamb, G. D., Green, J. H., & Spikes, H. A. (2011). Friction properties of DLC/DLC contacts in base oil. *Tribology International, 44*(7–8), 922-932.

Veverkova, J., & Hainsworth, S. V. (2008). Effect of temperature and counterface on the tribological performance of W-DLC on a steel substrate. *Wear, 264*(7–8), 518-525.

Vilhena, L. M., Sedlaček, M., Podgornik, B., Vižintin, J., Babnik, A., & Možina, J. (2009). Surface texturing by pulsed Nd:YAG laser. *Tribology International, 42*(10), 1496-1504.

Vincent, C., Monteil, G., Barriere, T., & Gelin, J. C. (2008). Control of the quality of laser surface texturing. *Microsystem Technologies, 14*(9-11), 1553-1557.

Volinsky, A. A., Moody, N. R., & Gerberich, W. W. (2002). Interfacial toughness measurements for thin films on substrates. *Acta Materialia, 50*(3), 441-466.

Wakuda, M., Yamauchi, Y., Kanzaki, S., & Yasuda, Y. (2003). Effect of surface texturing on friction reduction between ceramic and steel materials under lubricated sliding contact. *Wear, 254*(3-4), 356-363.

Wan, Y., & Xiong, D.-S. (2008). The effect of laser surface texturing on frictional performance of face seal. *Journal of Materials Processing Technology, 197*(1-3), 96-100.

Wang, D.-Y., Chang, C.-L., & Ho, W.-Y. (1999). Oxidation behavior of diamond-like carbon films. *Surface and Coatings Technology, 120–121*, 138-144.

Wang, T., Huang, W., Liu, X., Li, Y., & Wang, Y. (2014). Experimental study of two-phase mechanical face Seals with laser surface texturing. *Tribology International, 72*, 90-97.

Wang, X., Adachi, K., Otsuka, K., & Kato, K. (2006). Optimization of the surface texture for silicon carbide sliding in water. *Applied Surface Science, 253*(3), 1282-1286.

Wang, X., & Hsu, S. (2004). *An integrated surface technology for friction control: a new paradigm effects of geometric shapes on friction.* Paper presented at the The 4th China International Symposium on Tribology. Xi'an.

Wang, X., & Kato, K. (2003). Improving the anti-seizure ability of SiC seal in water with RIE texturing. *Tribology Letters, 14*(4), 275-280.

Wang, X., Kato, K., Adachi, K., & Aizawa, K. (2001). The effect of laser texturing of SiC surface on the critical load for the transition of water lubrication mode from hydrodynamic to mixed. *Tribology International, 34*(10), 703-711.

Wang, X., Kato, K., Adachi, K., & Aizawa, K. (2003). Loads carrying capacity map for the surface texture design of SiC thrust bearing sliding in water. *Tribology International, 36*(3), 189-197.

Wang, X., Liu, W., Zhou, F., & Zhu, D. (2009). Preliminary investigation of the effect of dimple size on friction in line contacts. *Tribology International, 42*(7), 1118-1123.

Willermet, P., Pieprzak, J., & Dailey, D. (1990). Tappet rotation and friction reduction in a center pivot rocker arm contact. *Journal of Tribology, 112*(4), 655-661.

Winer, W. O., & Peterson, M. B. (1980). *Wear Control Handbook*: American society of mechanical engineers.

Wos, P., & Michalski, J. (2011). Effect of Initial Cylinder Liner Honing Surface Roughness on Aircraft Piston Engine Performances. *Tribology Letters, 41*(3), 555-567.

Wu, W.-J., & Hon, M.-H. (1999). Thermal stability of diamond-like carbon films with added silicon. *Surface and Coatings Technology, 111*(2–3), 134-140.

Wu, W., Chen, G., Fan, B., & Liu, J. (2016). Effect of Groove Surface Texture on Tribological Characteristics and Energy Consumption under High Temperature Friction. *PLoS One, 11*(4), e0152100.

Wu, Z., Deng, J., Zhang, H., Lian, Y., & Zhao, J. (2012). Tribological behavior of textured cemented carbide filled with solid lubricants in dry sliding with titanium alloys. *Wear, 292-293*, 135-143.

Xiao, N., & Khonsari, M. M. (2012). Thermal performance of mechanical seals with textured side-wall. *Tribology International, 45*(1), 1-7.

Xie, J., Luo, M.-J., He, J.-L., Liu, X.-R., & Tan, T.-W. (2012). Micro-grinding of micro-groove array on tool rake surface for dry cutting of titanium alloy. *International Journal of Precision Engineering and Manufacturing, 13*(10), 1845-1852.

Xing, Y., Deng, J., Zhao, J., Zhang, G., & Zhang, K. (2014). Cutting performance and wear mechanism of nanoscale and microscale textured Al2O3/TiC ceramic tools in dry cutting of hardened steel. *International Journal of Refractory Metals and Hard Materials, 43*, 46-58.

Xing, Y. Q., Deng, J. X., Tan, Y. Q., & Zhou, H. M. (2012). Effect of surface textures on friction properties of Al2O3/TiC ceramics. *Surface Engineering, 28*(8), 605-611.

Yan, D., Qu, N., Li, H., & Wang, X. (2010). Significance of Dimple Parameters on the Friction of Sliding Surfaces Investigated by Orthogonal Experiments. *Tribology Transactions, 53*(5), 703-712.

Ze, W., Jianxin, D., Yang, C., Youqiang, X., & Jun, Z. (2012). Performance of the self-lubricating textured tools in dry cutting of Ti-6Al-4V. *The International Journal of Advanced Manufacturing Technology, 62*(9-12), 943-951.

Zhan, J., & Yang, M. (2012). Investigation on Dimples Distribution Angle in Laser Texturing of Cylinder-Piston Ring System. *Tribology Transactions, 55*(5), 693-697.

Zhang, B., Huang, W., Wang, J., & Wang, X. (2013). Comparison of the effects of surface texture on the surfaces of steel and UHMWPE. *Tribology International, 65*, 138-145.

Zhao, W., Wang, L., & Xue, Q. (2010). Influence of micro/nano-textures and chemical modification on the nanotribological property of Au surface. *Colloids and Surfaces A: Physicochemical and Engineering Aspects, 366*(1-3), 191-196.

Zulkifli, N. W. M. (2014). Lubricity and anti-wear characteristics of Trimethylolpropane ester derived from edible and non-edible resources

Zulkifli, N. W. M. (2014). Lubricity and anti-wear characterstics of trimethylolpropane ester derived from edible and non-edible resources.

Zulkifli, N. W. M., Azman, S. S. N., Kalam, M. A., Masjuki, H. H., Yunus, R., & Gulzar, M. (2016). Lubricity of bio-based lubricant derived from different chemically modified fatty acid methyl ester. *Tribology International, 93*, 555-562.

Zulkifli, N. W. M., Kalam, M. A., Masjuki, H. H., Al Mahmud, K. A. H., & Yunus, R. (2014). The Effect of Temperature on Tribological Properties of Chemically Modified Bio-Based Lubricant. *Tribology Transactions, 57*(3), 408-415.

Zulkifli, N. W. M., Kalam, M. A., Masjuki, H. H., Shahabuddin, M., & Yunus, R. (2013). Wear prevention characteristics of a palm oil-based TMP (trimethylolpropane) ester as an engine lubricant. *Energy, 54*, 167-173.

LIST OF PUBLICATIONS AND PAPERS PRESENTED

ISI Indexed Journal Articles (Accepted)

1. **Ahmed, A**., Masjuki, H., Varman, M., Kalam, M., Habibullah, M., & Al Mahmud, K. (2015). An overview of geometrical parameters of surface texturing for piston/cylinder assembly and mechanical seals. *Meccanica*, 1-15. **ISI indexed quartile 1**
2. **Arslan, A.**, Masjuki, H., Varman, M., Kalam, M., Quazi, M., Al Mahmud, K., . . . Habibullah, M. (2015). Effects of texture diameter and depth on the tribological performance of DLC coating under lubricated sliding condition. *Applied Surface Science, 356*, 1135-1149. **ISI indexed quartile 1**
3. **Arslan, A.**, Masjuki, H. H., Varman, M., Kalam, M. A., Quazi, M. M., & Mosarof, M. H. (2016). Effect of change in temperature on the tribological performance of micro surface textured DLC coating. *Journal of Materials Research*, 1-11. **ISI indexed quartile 2**

ISI Indexed Journal Articles (Under Preparation)

1. **Arslan, A**., Masjuki, H., Kalam, M., Varman, M., Mosarof, M., . . . Quazi, M. Investigating tribological performance of laser textured tetrahedral carbon coating at various temperatures in the presence of polyalphaolefin and palm based trimethylolpropane ester.
2. **Arslan, A**., Masjuki, H., Kalam, M., Varman, M., Mosarof, M., . . . Quazi, M. Investigating tribological performance of laser textured amorphous hydrogenated carbon coating at various temperatures in the presence of palm based trimethylolpropane ester.

Conference and Symposium

1. **Arslan, A**., Masjuki, H. H., Varman, M., Kalam, A., Mufti, R. A., Gulzar, M., & Quazi, M. M. (2015). *Effect of surface texture on the tribological performance of DLC coating.* Paper presented at the Malaysian International Tribology Conference (MITC).
2. **Arslan, A**., Masjuki, H., Kalam, M., Varman, M., Mufti, R., Mosarof, M., . . . Quazi, M. (2016). Tribological behaviour of surface textured hydrogenated amorphous carbon coating in the presence of PAO at various temperatures. 4th Malaysia-Japan Tribology Symposium 2016 (MJTS 2016).